Thèse préparée à l'Université de Bretagne Occidentale

pour obtenir le diplôme de DOCTEUR délivré de façon partagée par
L'Université de Bretagne Occidentale et l'Université de Bretagne Loire

Spécialité : Océanographie physique

École Doctorale Sciences de la Mer et du Littoral

présentée par

Tonia Astrid Capuano

Small-scale ocean dynamics in the Cape Basin and its impact on the regional circulation

Thèse soutenue le 04/12/2017
devant le jury composé de :

Bernard Barnier (rapporteur)
Ph.D, HDR,Directeur de Recherches CNRS, Institut des Géosciences de l'Environnement, IGE/MEOM, Grenoble.

Arne Biastoch (rapporteur)
Ph.D, Chercheur senior, GEOMAR Helmholtz Centre for Ocean Research, Kiel (Germany).

Laurent Memery (examinateur)
Ph,D, Directeur de Recherches CNRS, Laboratoire des Sciences de l'Environnement Marin (LEMAR), IUEM, Brest.

Bruno Deremble (examinateur)
Ph.D, Laboratoire de Météorologie Dynamique (LMD), Institut Pierre-Simon Laplace (IPSL), Paris.

Jonathan Gula (invite)
Ph.D, Laboratoire d'Océanographie Physique et Spatiale, LOPS-UBO, Brest.

Xavier Carton (co-directeur de these)
Professeur, Ph.D, HDR, Laboratoire d'Océanographie Physique et Spatiale, LOPS-UBO, Brest.

Sabrina Speich (co-directrice de these)
Professeur, Ph.D, HDR, Laboratoire de Météorologie Dynamique (LMD), Institut Pierre-Simon Laplace (IPSL), Paris.

ABSTRACT

This study addresses the role of the oceanic mesoscale and submesoscale processes on the formation and transformation of subsurface water masses that participate in the Indo-Atlantic interocean exchange. Our focus is on the Cape Basin dynamics. This is the southesearnmost basin of the Atlantic Ocean where Indian and Atlantic waters converge and mix. The ocean dynamics in this region is characterized by a highly non-linear, turbulent regime. Eddies of both polarities, meanders and filaments spawned by the Agulhas Current contribute to such an intense turbulence and strongly affect the local water masses dynamics and thermohaline structure. We provide qualitative and quantitative evidence of the direct impact that these meso- and submesoscale structures, their dynamical interactions and their seasonal variability have on the Cape Basin thermocline and intermediate waters. We used a sequence of numerical simulations, of increasing horizontal and vertical resolutions, and ranging from 'eddy-permitting' to fully 'submesoscale resolving'. In that respect, we underline the importance of an adequate vertical resolution of the model in order to correctly represent the water masses structure and variability.

We point out that Agulhas eddies are mainly generated through baroclinic instabilities and are marked by a clear seasonality. This temporal variability is directly linked to the seasonal occurrence of several types of meso-submesoscale instabilities in the Cape Basin upper layers. The analysis of the energy transfers between the different scales, in concert with other diagnostics, suggest that symmetric instabilities are mainly at play during summer, while mixed-layer instabilities prevail in winter. In addition, we found that Charney baroclinic instability connects these two different submesoscale regimes and plays a major role in the seasonal formation and subduction of a newly identified type of mode waters, that we defined as 'Agulhas Rings Mode Water'. Finally, we show that not only Agulhas rings but eddies of both polarity are involved in advecting and mixing Antarctic Intermediate Water. In particular we detail the processes that lead to such mixing. These are driven by the mesoscale strain field that produce submesoscale filaments and T-S fine-scale structures that, ultimately, generate intense lateral stirring and mixing.

Our results suggest the existence of two distinct dynamical regimes affecting the upper and intermediate layers of the Cape Basin. Near the surface, the submesoscale-driven frontogenesis and the enhanced energetics of the related divergent motions lead to a pre-

dominance of ageostrophic dynamics. The intermediate depths are, instead, characterised by a quasi-gesotrophic regime due to the prevailing effects of the mesoscale dynamics.

Contents

Chapter 1

Introduction

1.1 The Indo-Atlantic heat and tracer exchange

1.1.1 Nature, role and structure of the inter-ocean link

The inter-ocean leakage of heat and salt from the South Indian Ocean to the South Atlantic has important consequences for the global thermohaline circulation and in particular for the strength of overturning of the Atlantic Ocean as a whole [*Biastoch et al.*, 2008, *Blanke et al.*, 1999, *Gordon*, 2001, *Speich et al.*, 2001]. The leakage between these two subtropical gyres takes place south of Africa. The main mechanisms are the intermittent shedding of Agulhas rings from the retroflection of the Agulhas Current and the advection of Agulhas filaments from the border of the Agulhas Current, both of which move northwestward into the South Atlantic [*Boebel et al.*, 1998, *Bryden et al.*, 2005, *Gordon*, 2003, *Laxenaire et al.*, Submitted, *Lutjeharms*, 2001, 2006].

The wind-driven gyres of the South Indian and Atlantic Oceans are connected in the Agulhas Retroflection area. The southern boundary of the joint subtropical 'super gyre' of these two oceans is largely determined by the position of the zero wind stress curl, roughly at the Subtropical Convergence Zone ($\pm$ 45°S) [*De Ruijter*, 1982, *Gordon et al.*, 2010, *Speich et al.*, 2007]. From the above it should be clear that this inter-ocean connection is also a critical link in the global Meridional Overturning Circulation (MOC, Fig. 1.1). This is supported by paleoceanographic studies (e.g. see *Berger and Werfer* [1996], *Peeters et al.* [2004]) that indicate how a specific species of foraminifera became extinct in the South Atlantic during the last glacial period, probably owing to a decrease of the upper ocean temperatures. The same authors suggest that their more recent reappear-

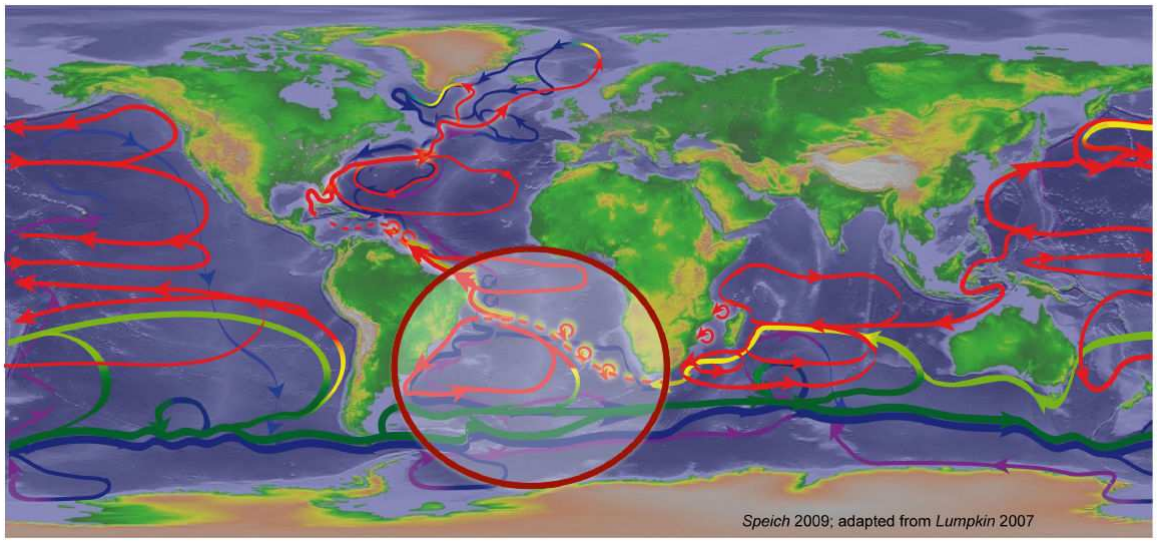

Figure 1.1: Diagram of the world ocean overturning circulation, where red is for surface flows, blue and purple are deep flows, and yellows and greens represent transition between depths (picture taken from: http://stockage.univ-brest.fr/∼speich/SAMOC/SAMOC_2009.ppt).

ance might be due to reopening of the Agulhas connection. There seems to have been a common start-up of North Atlantic Deep Water (NADW) formation, a reappearance of the species in the southeastern Atlantic and a poleward expansion of the wind-driven gyres some 10,000 years ago. If, indeed, this Agulhas leakage is one of the controlling factors of the Atlantic Ocean stratification and thermohaline overturning circulation [*Biastoch et al.*, 2009, *Biastoch and Boning*, 2013], then shutting it off during glacial times might have been a strong positive feedback mechanism to reduced NADW formation [*De Ruijter et al.*, 1999, *Lutjeharms*, 2007].

The probable importance of the inter-ocean exchange around South Africa for regional and global climate shifts has motivated many observational, theoretical, and modeling studies in the last three decades. Past descriptions of the link between the Indian and Atlantic Oceans at the Agulhas Retroflection suggested this transport to be dominated by the migration of Agulhas Rings from the Agulhas Retroflection through the Cape Basin, west of Cape Town (Fig. 1.2), into the western South Atlantic (see *Lutjeharms* [1996], for a summary of observational studies).

The shedding of Agulhas Rings was generally thought to follow a rather straightforward kinematic process and the rings merging out of this spawning process were believed to then move with the steadily flowing Benguela Drift into the interior Cape Basin and to veer successively westwards, pursuing a quasi-zonal path across the South Atlantic

[*Grutindlingh*, 1995]. While the Benguela Drift would be dominated by water from the South Atlantic [*Garzoli and Gordon*, 1996], "*isolated rings of Agulhas water west of the retroflection*" ([*Gordon*, 1986], p. 5043) would carry the bulk of Indian Ocean influence, which slowly would leak from the rings into the surrounding waters. Alternative inter-ocean exchange mechanisms, such as a possible direct inflow via narrow coast and shelf edge jet-like currents [*Stramma and Peterson*, 1989](also called filaments), were deemed intermittent [*Duncombe Rae et al.*, 1996] and to provide not more than 15% of the overall mass flux [*Lutjeharms and Cooper*, 1996].

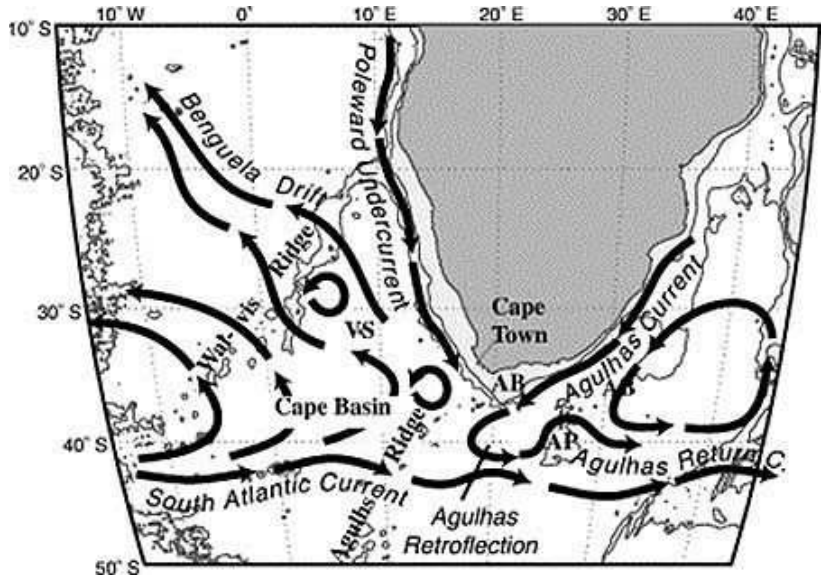

Figure 1.2: Schematic of the oceanic flow patterns around southern Africa for the upper and intermediate layers, where the Cape Basin is circumscribed by the Walvis Ridge, the African East coast and the Agulhas Ridge. Two Agulhas Rings are depicted at 29°S and 38°S. The Agulhas Bank is the shaded shelf region to the south of Cape Town (AB), the Agulhas Plateau (AP) is the shallow topographic feature near 40°S, 26°E. The Vema Seamount (VS) is indicated. Topography is delineated by the 0, 1000 and 3000 m isobaths (Source: *Boebel et al.* [2003]).

1.1.2 The zonal branches and the AAIW transport

Based on the previous concepts, researchers estimated the inter-ocean exchange by calculating the heat and salt anomaly contained within a ring relative to a suitably chosen reference station nearby, but outside of the ring [*Arhan et al.*, 2011]. The anomalies were then multiplied by the number of rings shed per year to estimate the annual mean transport [*Byrne et al.*, 1995, *Duncombe Rae et al.*, 1996, *Goni et al.*, 1997]. These studies described the Benguela Current and its vertical structure, involving the thermocline

and Antarctic Intermediate Water (AAIW) layers, while a southward flow was suggested below [*Garzoli and Gordon*, 1996]. The observed variability in the eastern part was predominantly assigned to the presence of energetic anticyclonic eddies (i.e. Agulhas Rings, Fig. 1.3), even though cyclonic eddies had also been identified, using satellite altimetry measurements [*Byrne et al.*, 1995, *Grutindlingh*, 1995]. And indeed, earlier works have already indicated that the Cape Basin dynamics was influenced by other effects that solely the inflow from the Indian Ocean [*Lutjeharms and Connel*, 1989, *Lutjeharms et al.*, 1992].

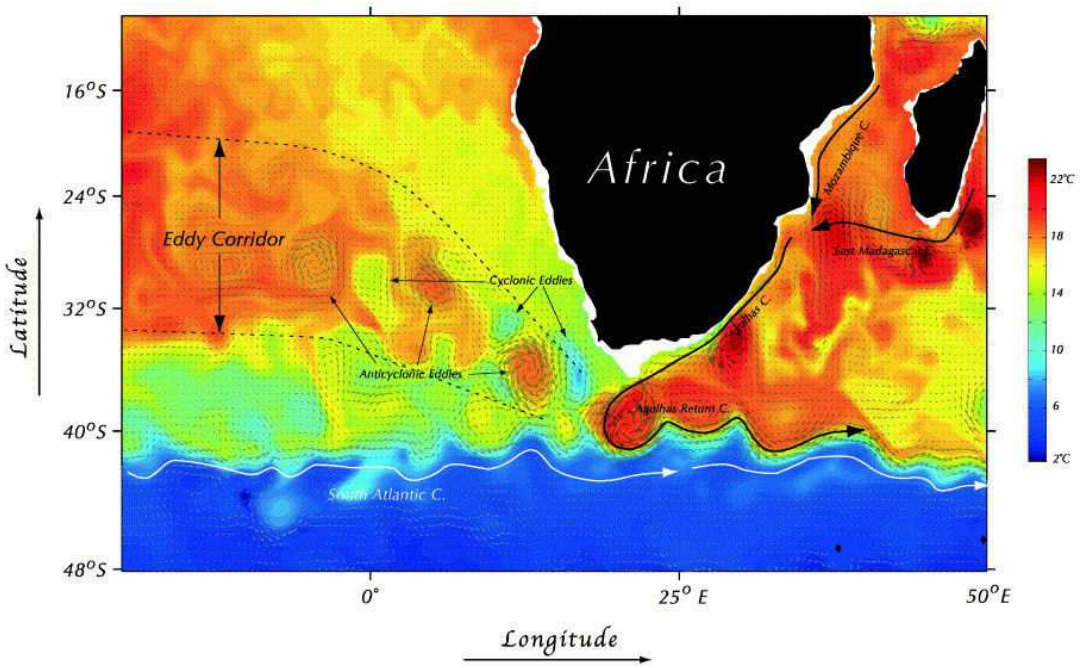

Figure 1.3: Snapshot of temperature (background color, °C) and velocities of the greater Agulhas Current System, as simulated in the numerical study of *Matano and Beier* [2003]. The superimposed schematic shows the path of the mean currents and eddies in the Cape Basin.

Later quasi-Lagrangian studies in the western South Atlantic from drifting deep floats [*Boebel et al.*, 1999] had showed two quasi-zonal branches of the subtropical gyre dominating the circulation at intermediate depth near the Mid-Atlantic Ridge. The South Atlantic Current brings fresh AAIW from the Brazil-Malvinas Confluence Zone into the southern Cape Basin, while to the north, at about 30°S, a westward flow band appears to drain the latter [*Schmid et al.*, 2000]. While the two limbs are joined in the west by the Brazil Current to form one half of the subtropical gyre, its closure in the East remained obscure [*Piola and Gordon*, 1989]. Several possibilities were proposed for the location of this missing link: a closure to the west of the Mid- Atlantic Ridge [*Siedler et al.*, 1996], a closure within the Cape Basin [*Stramma and England*, 1999], or a closure via a detour

through the Southwest Indian Ocean subtropical gyre [*Gordon et al.*, 1992]. With the AAIW salinity minimum changing only little over the entire width of the South Atlantic along the gyre southern and northern zonal branches, as displayed in the *You et al.* [2003] map of AAIW core salinity (their Fig. 1.3c), one is left wondering which processes are involved in their mixing and how the advected water is modified so significantly over a relatively short distance. *Boebel et al.* [2003] were the first in observationally demonstrating that the eastern closure of the subtropical 'supergyre' could actually take place within the Cape Basin. Later numerical [*Rimaud et al.*, 2012] and observational studies [*Rusciano et al.*, 2012] confirmed the oceanographic importance of this region; they called the attention on the role played by the high mesoscale variability of this area in the mixing and transformation of AAIW into different, local varieties. Thanks to these works, the 'Cape Cauldron' (as the Cape Basin was renamed by *Boebel et al.* [2003]) started to take on an essential, integral role as mixer and stirrer in the Indo-Atlantic inter-ocean exchange, with the interaction between cyclones and anticyclones resulting in a rapid homogenization of water mass anomalies introduced from the Indian Ocean into the Atlantic, particularly at intermediate depth.

1.2 The Agulhas and Atlantic subsurface water masses

As seen in the previous section, the present South Atlantic plays a unique role in the climate system in that it transports heat toward and across the equator, whereas all other oceans have poleward heat transports [*Stramma and Lutjeharms*, 1997]. The South Atlantic is a wide open basin and its thermohaline structure is determined largely in other areas of the World Ocean [*Rintoul*, 1991]. Water masses are continuously passing through, locally modified by air-sea buoyancy fluxes and mixing, and steered by topographic ridges, wind and thermohaline forcing [*De Ruijter et al.*, 1999, *Garzoli and Matano*, 2011]. To study the stratification of the Atlantic and its overturning circulation, one needs to know precisely the water mass characteristics and fluxes at the open boundaries with the surrounding oceans [*Thompson et al.*, 1997]. On its anticyclonic path through the warm and evaporative oceanic region, the subtropical gyre of the South Atlantic, driven by the meridional alternation of trades and west winds [*Durgadoo et al.*, 2013, *Loveday et al.*, 2014], picks up excess heat and gives back fresh water to the atmosphere [*Rouault and Lutjeharms*, 1994]. Consequently, the Brazil Current exports relatively warm and salty water poleward and much cooler and fresher water flows with the northward branch of

the South Atlantic Current and of the Benguela Current in the eastern part of the gyre [*Talley*, 1996]. So the wind-driven circulation acts according to intuition: it transports heat and salt poleward in the upper layers [*Rahmstorff*, 1996, *Weijer et al.*, 1999].

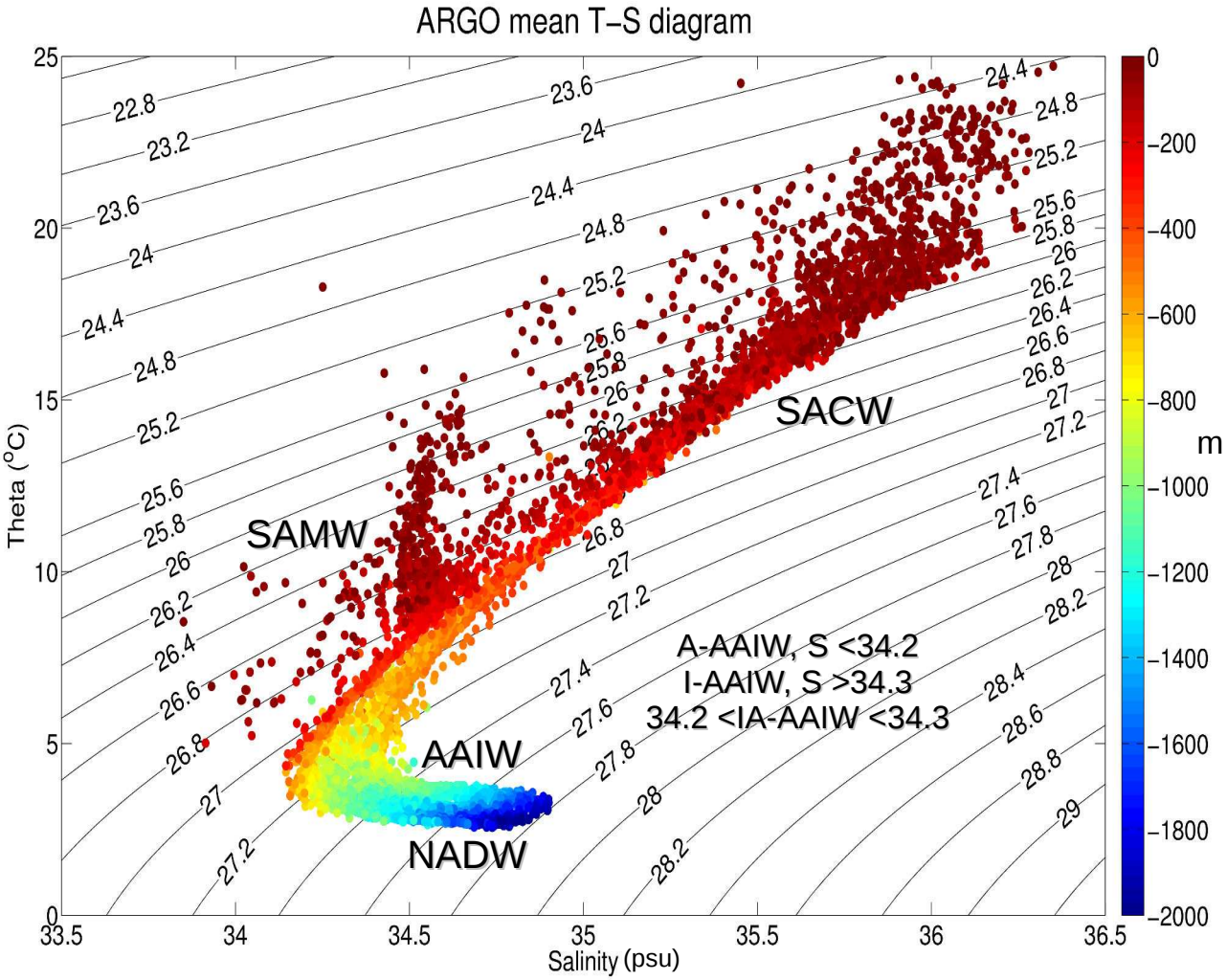

Figure 1.4: T-S diagram from the Argo climatology of *Rusciano et al.* [2012], showing the main thermocline and deep water masses circulating within the greater Agulhas Current System, and the depth ranges in which they can be localized.

The equatorward heat transport of the South Atlantic is therefore established by the global scale MOC, involving the deep southward flow of NADW and a compensating northward mixture of warm salty thermocline waters and cooler, fresher intermediate water masses [*Gordon et al.*, 1992]. These compensating water masses originate partly in the South Atlantic itself, as a result of water mass transformation processes in e.g. the Brazil-Malvinas confluence area and along the subtropical convergence zone [*Peterson and Stramma*, 1991, *Piola and Gordon*, 1989]. But a large part of the intermediate and

thermocline water masses originates in the Pacific and Indian Oceans, entering the South Atlantic via the Drake Passage and around the tip of South Africa, respectively [*Warner and Weiss*, 1992]. Here, isopycnally-compensated mixing of intermediate waters has been observed to take place within the Cape Basin, due to the intense mesoscale variability [*Boebel et al.*, 2003, *Rimaud et al.*, 2012, *Rusciano et al.*, 2012].

Although there is a great variety of water masses in the subsurface, the prevalent type in the Cape Basin is the South Atlantic Central Water (SACW, [*Mohrholz et al.*, 2001]), characterized by potential temperature and salinity in the range: 10°C, 34.5 psu and 18°C, 35.5 psu (Fig. 1.4). This water mass upwells to the surface along the South-African coast and thus constitutes the regional shelf water [*Shannon and Nelson*, 1996]. Because the central waters of the south Indian and south Atlantic have very similar θ-S structure, *Gordon et al.* [1992] used chlorofluoromethanes as tracers and suggested that as much as two-thirds of this thermocline water is drawn from the Indian Ocean. The same conclusion was reached by *Matano and Beier* [2003], who showed that not all the SACW was formed locally, but a substantial portion of it had its origin in the Indian Ocean and was introduced into the South Atlantic by Agulhas eddies and filaments.
Underneath the seasonal thermocline, Subantarctic Mode Water is found within the 12-13°C and the 34.5-34.6 psu (Fig. 1.4). This water is known to be formed at longitudes around 60°E in the south Indian Ocean [*McCartney*, 1977] and injected in the southern Indian Ocean subtropical circulation and conveyed to the retroflection area, where it may be pinched off in rings [*Gladyshev et al.*, 2008].

At greater depth, intermediate waters dominate the water mass structure of the subtropical gyre. The intermediate waters in the South Atlantic are forced from above by the wind-driven circulation and from below by the thermohaline-driven circulation [*Gordon et al.*, 1992]. One of the most striking differences between the upper and intermediate levels is that the northern limit of the subtropical gyre shifts from approximately 20°S in the near-surface layer, to 27°S in the intermediate layer [*Stramma and England*, 1999]. Another conspicuous difference between these levels is that while in the upper-level the westward flow is uniformly distributed across a wide band of latitudes, at the intermediate level it is restricted to a rather narrow latitudinal band (see Fig. 1c of *Matano and Beier* [2003]). Here AAIW moves with the Agulhas Current [*Shannon and Hunter*, 1988], exhibiting a temperature range of 2°-10°C and salinities between 33.8 and 34.8

psu (Fig. 1.4). This water mass is formed in the sub-polar and polar regions as surface low-salinity waters [*Talley*, 1996]; then it subducts under the seasonal thermocline and is no longer in contact with the atmospheric forcing. Hence, AAIW is known to retain the physical properties that were set at the sea surface, and it is a long-distance supplier of salt, heat, and nutrients typical of its formation regions [*Sarmiento*, 2004]. Based on temperature, salinity and oxygen concentrations, *Shannon and Hunter* [1988] were able to infer the general circulation of AAIW around southern Africa. It is nowadays assumed that a part of the AAIW flows eastward around 40°S and leaves the South Atlantic to flow into the southern Indian Ocean [*Boebel et al.*, 1998]. There it branches and mixes into the recirculation regime of the southwest Indian Ocean to reenter the South Atlantic via Agulhas leakage, embedded in the major rings that frequently pinch off from the retroflection [*Feron et al.*, 1992, *Gordon et al.*, 1992]. It is while crossing the turbulent Cape Basin that AAIW experiences a rapid transformation of its thermohaline properties, leading to their enhanced spreading along the 27.2 isopycnal (Fig. 1.4) and to the ultimate formation of AAIWs regional varieties [*Rimaud et al.*, 2012, *Rusciano et al.*, 2012].

Until the 1990s, little was known about the way the deeper waters interacted or were exchanged at the retroflection [*Gordon et al.*, 1992]. In the early 2000s, the pathways of the deeper waters south of Africa were the subject of a large international Lagrangian float campaign, the Cape of Good Hope Experiments (KAPEX), aiming at explaining the exchange of these waters between the two ocean basins. One of the main findings of this experiment was that floats in the intermediate layer of the Cape Basin usually did not remain trapped within the rings and cyclones for very long. This implies strong mixing between rings, cyclones and background water from the South Atlantic Current and Tropical Atlantic [*Richardson*, 2007, *Richardson and Garzoli*, 2003].

Beneath the AAIW layer, NADW flows poleward between 1000-3500 m and is relatively more saline and colder than the former, having temperature lower than 3°C and salinities above 34.8 psu [*Shannon and Nelson*, 1996]. *Arhan et al.* [2003] estimated an export of 11± 4 Sv of this water mass from the Atlantic near southern Africa inshore of the Subtropical Front. They showed that most of this flow could be traced back across the Cape Basin to passages south of 28°S in Walvis Ridge and further upstream to an entry in the eastern basin at 20-25°S.

At last, Antarctic Bottom Water (AABW, θ <0°C and S <34.8 psu) is situated at depths

exceeding the 3500 m and flows equatorward into the Cape Basin. Here this water mass turns back on itself creating a cyclonic loop that results in a deep poleward flow along the continental margin of western Africa [*Nelson*, 1989].

1.3 The Agulhas Current system

The Agulhas Current constitutes the western boundary current of the wind driven, anticyclonic gyre of the South Indian Ocean (Fig. 1.5 b). As described in the previous sections, it draws its water masses, and thermohaline characteristics, from this broad oceanic region [*Beal et al.*, 2006, *Bryden et al.*, 2005, *De Ruijter et al.*, 1999]. Conceivably, any interannual or decadal variability occuring in this subtropical gyre can influence the Agulhas Current [*Lutjeharms and de Ruijter*, 1996, *Reason et al.*, 1996a,b]. This current consists of a northern and a southern part with dissimilar characteristics [*Veitch et al.*, 2009]. The northern part starts approximately at the border between Mozambique and South Africa and stretches along the eastern seaboard of South Africa, down to the latitude of Port Elizabeth (Fig. 1.5 a). Its trajectory follows the continental shelf break quite closely, and, unlike any other western boundary current, the trajectory is quite stable [*Grutindlingh*, 1983]. The strong shelf slope most probably constrains the growth of lateral meanders in the current [*Jacobs and Georgi*, 1977], which is at least 2000 m deep. It carries a mass transport of about 84 Sv (1 Sv = $10^6 \mathrm{m}^3/\mathrm{s}$) [*Beal et al.*, 2015].

Farther downstream, the Agulhas Current, by contrast, flows past the broad continental shelf south of Africa, the Agulhas Bank, where the more gently inclined slope allows it to meander in the manner of most western boundary currents [*Beal and Bryden*, 1997]. As a result, many shear edge features common to such a current, namely eddies of both signs, filaments and plumes, are formed [*Lutjeharms et al.*, 1989]. These warm plumes move onto the Agulhas Bank to contribute to the very strong vertical stratification in temperature over the shelf, or they drift into the adjacent South Atlantic as Agulhas filaments [*Lutjeharms and Cooper*, 1996, *Whittle et al.*, 2008] (see Fig. 1.5 b). When the meandering southern Agulhas Current reaches a latitude of about 37°S it passes the southern tip of the African continental shelf and moves southwestward as a free jet into the South Atlantic [*Gordon et al.*, 1987]. Shortly after, it retroflects in a dramatic way and subsequently carries the bulk of its waters eastward (Fig. 1.5 b), back into the Indian Ocean. An Agulhas Undercurrent has been also measured directly near Port Ed-

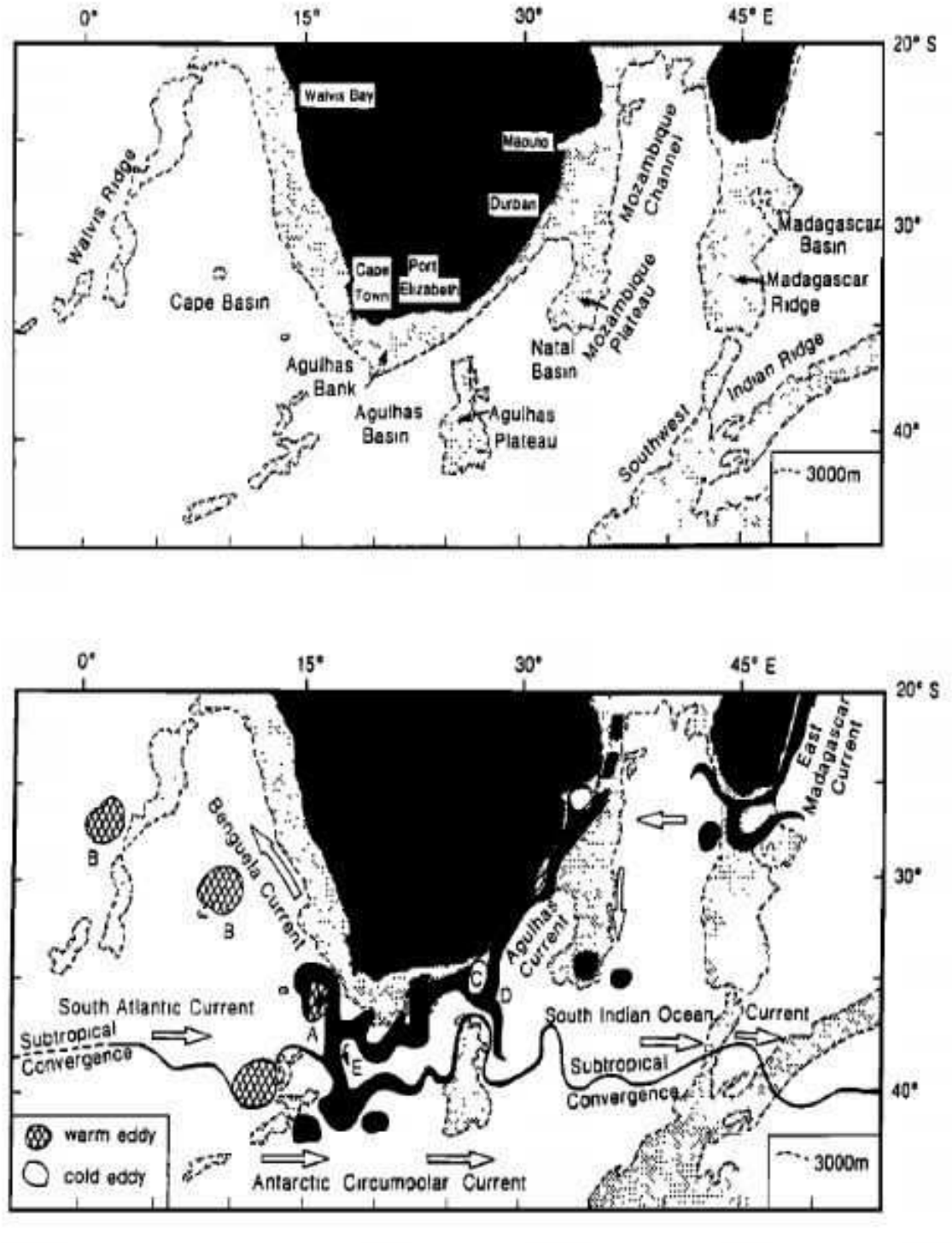

Figure 1.5: Main mesoscale and larger circulation features of the greater Agulhas Current System, superimposed on the bottom topography. Abbreviations are: A, Agulhas ring, recently shed from the Agulhas retroflection and encircled by an Agulhas filament; E, Agulhas retroflection; B, Agulhas rings drifting off into the South Atlantic; C, cyclonic eddy forming part of a well-developed Natal Pulse on the Agulhas Current preciding an upstream retroflection at the Agulhas Plateau, the shallow region south of Africa; and D upstream retroflection. The large-scale background circulations of the subtropical gyres are shown by open arrows; the shaded areas indicate where the bottom is shallower than 3000 m (after *De Ruijter et al.* [1999]).

ward (31°S) [*Beal*, 2009] and its core is centered around a depth of 1200 m and hugs the continental slope directly below the core of the Agulhas Current. It transports about 6 Sv north-eastward at maximum speeds of 30 cm/s.

The manner in which the Agulhas Current is supplied from different sources has been demonstrated to play a major factor in establishing how variations in its flow come about [*Beal et al.*, 2006, *De Ruijter et al.*, 1999]. Contrary to classical portrayals, the sources of the Agulhas are not dominated by the Mozambique Current [*Biastoch et al.*, 1999, *Halo et al.*, 2014, *Saetre and Da Silva*, 1984], or by the East Madagascar Current [*Lutjeharms*, 1988], but by the recirculation in the above mentioned South-West Indian Ocean subtropical gyre [*Harris*, 1972, *Stramma and Lutjeharms*, 1997]. Of the total volume flux of the upper 1000 m of the Agulhas Current (∼65 Sv) about 20 Sv comes from east of Madagascar, but not necessarily directly from the East Madagascar Current itself [see *Stramma and Lutjeharms* [1997] for a discussion of these fluxes]. In fact, it has been surmised [*Backeberg et al.*, 2012, *Lutjeharms*, 1988, *Penven et al.*, 2014] that water from this western boundary current may reach the Agulhas Current only intermittently and then predominantly in the form of mesoscale rings and filaments (Fig. 1.5 b). Estimates of the contribution through the Mozambique Channel range between 5 Sv [*Stramma and Lutjeharms*, 1997] and 21 Sv [*Di Marco et al.*, 1998]. South of Africa, the transport of the Agulhas Current was estimated at 95 Sv by *Gordon et al.* [1987], which is much larger than the transport upstream at about 32°S. From that they concluded the existence of a tight recirculation in which the Agulhas transport grows significantly. This was confirmed from analysis of satellite altimeter data [*Feron*, 1994, *Feron et al.*, 1998], as well as from later observational [*Boebel et al.*, 1998, 2003, *Garzoli and Goni*, 2000, *Lutjeharms and Ansorge*, 2001] and numerical studies [*Biastoch and Krauss*, 1999, *Lutjeharms et al.*, 2003a, *Matano*, 1996, *Weijer et al.*, 1999].

1.4 The regional meso and submesoscale dynamics

The fields of mesoscale variability of the Agulhas system from altimetry data (Fig. 1.6) from surface drifters observations (Fig. 1.7a, b) and from a high-resolution satellite product (Fig. 1.8) show a remarkable resemblance. The highest level of variability is found associated with the termination of the Agulhas Current south of Africa. From there an extensive tongue of increased variability outspreads eastward, along the Subtropical

Convergence and the trajectory of the Agulhas Return Current [*De Ruijter et al.*, 1999]. An unusual feature of the flow of the northern Agulhas Current is the intermittent occurrence of a solitary meandering in the trajectory of the current, called the Natal Pulse [*Lutjeharms and Roberts*, 1988]. This meander moves downstream at a rather steady rate of 20 km/day and grows in lateral dimensions on its journey. In cases of meanders with extreme amplitudes, early retroflection of the current even seemed to result [*Lutjeharms and van Ballegooyen*, 1988a]. On the other hand, the Agulhas Retroflection region exhibits rapidly and markedly changing flow patterns. In general, the sequence of events starts with the Agulhas Current propagating farther and farther westward until the retroflection loop occludes and a separate Agulhas ring is formed [*Gordon et al.*, 1987, *Lutjeharms and van Ballegooyen*, 1988b].

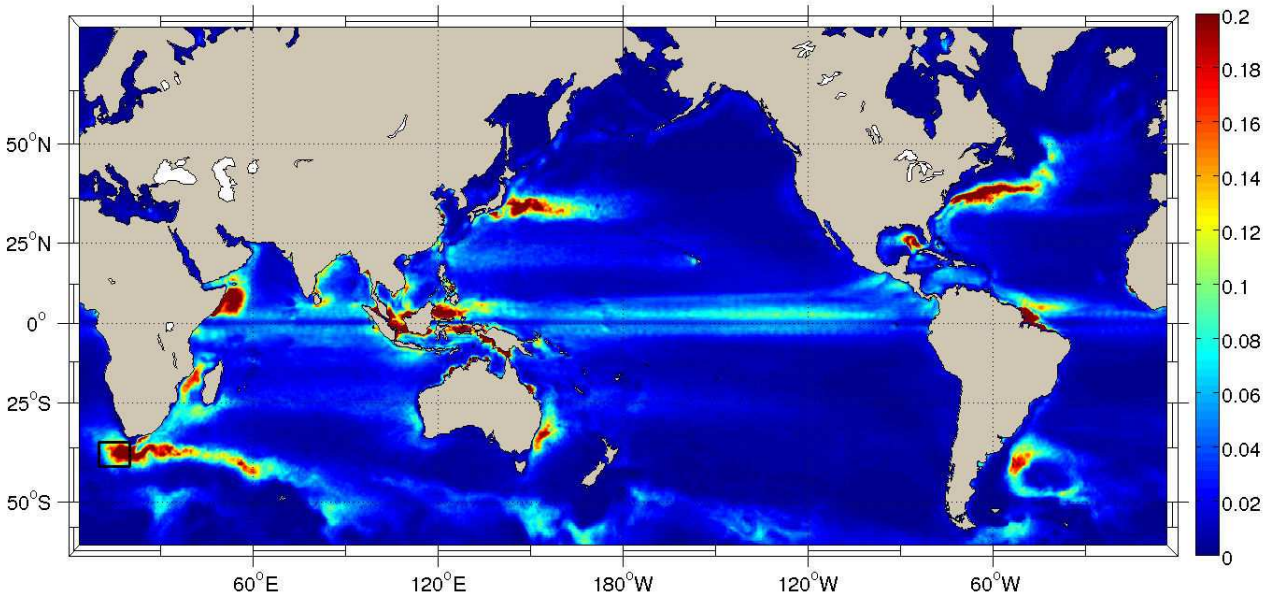

Figure 1.6: Global map of the root-mean-square of Sea Surface Hieght (SSH, in m^2/s^2), used as a proxy of Eddy Kinetic Energy (EKE), showing very high values within the Cape Basin (delimeted by the black box). The rms is calculated from 13 years of AVISO data (2000-2012) at 1/4° resolution.

The frequency of ring shedding is irregular [*Feron et al.*, 1992, *Goni et al.*, 1997] and has not yet been precisely determined. Past analyses of a variety of satellite data indicated that most Natal Pulses that reach the Agulhas retroflection precede a ring shedding event [*Van Leeuwen et al*, 2000], suggesting that these meanders might play a role in the timing of this process. But based on *Bleck and Boudra* [1986] reduced-gravity isopycnic model, *Pichevin et al.* [1999] simulated the Natal pulse and concluded that it does not create

Agulhas rings. According to the same authors, these pulses can, however, result in the shedding of a ring or accelerate the process. The model also underlined that the rings generation is intrinsically necessary, as without this production the flow force associated with the Agulhas Return Current would not be balanced. Other theoretical considerations indicated that the shelf-slope configuration along the northern Agulhas Current inhibits instabilities in the current trajectory, except at the Natal Bight (north of Durban, Fig. 1.5 a), at about 30°S [*De Ruijter et al.*, 1999]. Here the weaker gradient in the continental slope allows instabilities intermittently leading to the initiation of a pulse [*Beal and Bryden*, 1997]. The required intensification in the Agulhas Current transport may be due to inherent fluctuations in the recirculation gyre or to the entrapment of deep-sea eddies onto the outer border of the current [*Shannon*, 1979, *Shannon et al.*, 1989]. Such eddies have been observed in the region [*Grutindlingh*, 1988, 1995] and also interacting with the seaward border of the current [*Grutindlingh*, 1990]. Some of these eddies have been traced to east of Madagascar and they seem to substantially contribute to the high mesoscale variability in the southwest Indian Ocean (Fig. 1.3) [*Lutjeharms*, 1988a].

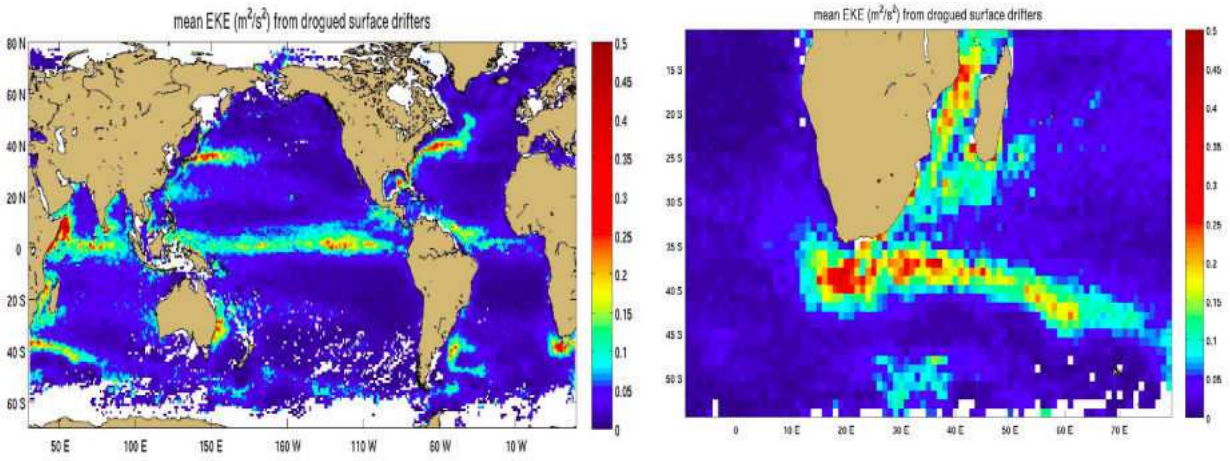

Figure 1.7: Maps kindly provided by Rick Lumpkin showing global mean Eddy Kinetic Energy (left) and a zoom of it in the area of the Agulhas Current (right) from in-situ observations of the Surface Velocity Program drifters. The Agulhas Current reaches values of 0.5 m^2/s^2 as elevated as other highly turbulent regions like the Gulf Stream, the Kuroshio extension and the Equatorial currents.

Overall, the warm-core Agulhas rings are the most energetic ones shed from a western boundary current in the world ocean [*Goni et al.*, 1997, *Olson and Evans*, 1986] being observed with diameters as large as 500 km [*Arhan et al.*, 1999, *Laxenaire et al.*, Submitted] and reaching 1000 m deep [*Arhan et al.*, 2011, *Doglioli et al.*, 2007, *Gordon et al.*,

1987, *McCartney and Woodgate-Jones*, 1991]. They propagate into the South Atlantic with speeds ranging between 5 and 10 km/day [*Byrne et al.*, 1995, *Laxenaire et al.*, Submitted, *Wakker et al.*, 1990] and the maximum anticyclonic surface currents are around 50 cms/s [*Arhan et al.*, 1999, *Duncombe Rae et al.*, 1992, *Laxenaire et al.*, Submitted], but can also reach speeds higher than 1 m/s [*Arhan et al.*, 2011]. A major part of the inter-ocean exchange at the Agulhas Retroflection is attributed to these rings; thus they have a considerable impact from the local to the global scale [*Beal et al.*, 2011, *Lutjeharms and Gordon*, 1987]. Even though the pinching-off of large rings at the Agulhas Retroflection leads to the major exchanges between the subtropical gyres of the South Indian and the South Atlantic Oceans [*Gordon et al.*, 1992, *Olson and Evans*, 1986], these are not the only vortices formed in this region. The portion of the Agulhas Current that does not get abstricted to form rings moves eastward as the Agulhas Return Current, usually along the Subtropical Convergence [*Lutjeharms and Valentine*, 1984] south of Africa. This produces intense horizontal shear and accompanying flow instabilities. A variety of eddy types is then generated [*Lutjeharms and Valentine*, 1988a], some of which have been observed to cross the front and enhance the cross-frontal exchange of water masses and heat [*Lutjeharms*, 1987]. The associated eddy stresses seem to also exert a net force and accelerate the mean flow considerably [*Feron*, 1994, *Feron et al.*, 1998].

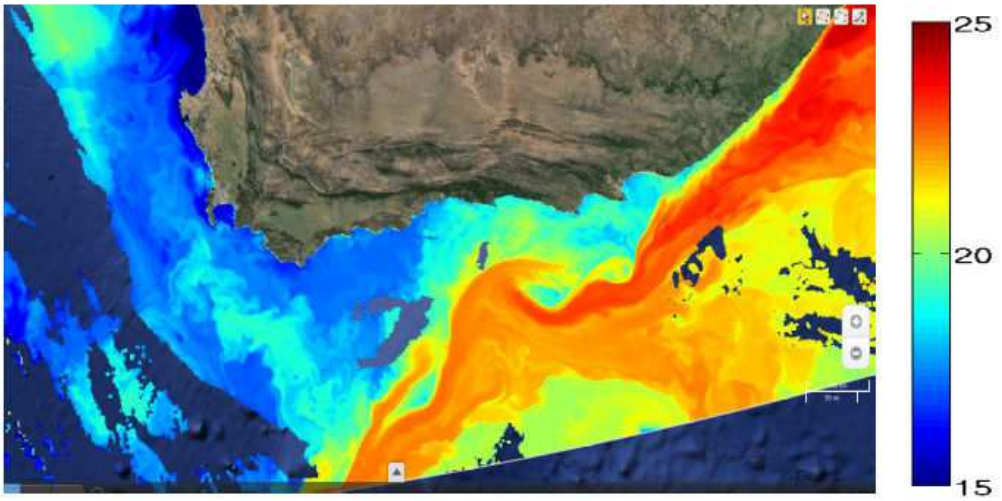

Figure 1.8: Istantaneous map of Sea Surface Temperature (in °C) at very high resolution ($\sim$ 5km), obtained from the merging of 3 satellite products of NASA: Chlorophyll-a MODIS, Chlorophyll-a VIIRS and SST MODIS denoised. Source: http://ovl.oceandatalab.com/.

For example, in Figure 1.8 we can clearly observe how cyclonic vortices detach from the

north wall of the Agulhas retroflection. They represent the cyclonic lee eddies studied by *Penven et al.* [2001] as generated through bartropic instabilities due to the flow detachment in the lee of the Agulhas Bank. On the other hand, *Lutjeharms et al.* [2003a] showed how cyclones associated with Natal Pulses and other shear-edge features are often instrumental in driving the occlusion of an Agulhas ring. Other papers [*Lutjeharms and Cooper*, 1996, *Whittle et al.*, 2008] reported on the behavior of Agulhas filaments interacting with a number of mesoscale features shortly after formation; they suggested that these filaments may result from many processes due to site-specific types of mixing. More recently, studies combining observational and modeling approaches(e.g. *Krug et al.* [2017]) investigated the formation of submesoscale cyclones, by horizontal shear instability in the Agulhas Current, south of 34°S; these cyclones trigger warm water plumes whose mean velocities exceed those observed in the frontal cyclones. Western boundary currents are indeed characterized by a rich submesoscale activity [*Gula et al.*, 2015], whose highly non-linear processes are expected to make an important contribution to the vertical flux of mass, buoyancy and tracers in the upper ocean [*Thomas and Ferrari*, 2008].

Recent review papers on the regime of these small scales[*Mahadevan*, 2016, *McWilliams*, 2016] have called the attention on the fact that the term 'submesoscale' does not merely indicate a length scale, but rather refers to processes characterized by O(1) Rossby and Richardson numbers, as a result of internal instabilities or surface forcing. Submesoscales indeed arise in localized regions of the surface ocean where the vertical component of the relative vorticity, ζ, attains a magnitude as large as (or larger than) the planetary vorticity f, making the local $\mathrm{Ro} = \zeta/\mathrm{f} = \mathrm{O}(1)$. Thei dynamics are associated with strong vorticity and strain rates occurring on lateral scales of 0.1-10 km, while buoyancy forcing and wind stress at the surface contribute to enhancing (or suppressing) such processes [*Thomas et al.*, 2008]. New insights into the submesoscale dynamics controlling the vertical exchange of properties near the surface have come from high-resolution satellite products (Fig. 1.8). However, submesoscale features can also arise at depth and influence the mesoscale dynamics and water masses exchanges in the subsurface, especially in regions where intermediate waters intrude and mix with deeper layers [*Smith and Ferrari*, 2009]. This could be the case of the Cape Basin, where AAIW is known to interact with deeper water masses, as NADW and AABW [*Talley*, 1996].

1.5 Summary

The inter-ocean exchange of heat and salt around South Africa is thought to be a key link in the maintenance of the global MOC of the ocean (Fig. 1.1) [*Gordon et al.*, 1992, *Lumpkin and Speer*, 2007, *Lutjeharms*, 1996]. It takes place at the Agulhas Retroflection, largely by the intermittent shedding of very large rings that penetrate into the South Atlantic Ocean (Fig. 1.3) [*Byrne et al.*, 1995]. This makes it extremely hard to estimate the inter-ocean fluxes [*Lutjeharms and van Ballegooyen*, 1988b]. At present, most of the Agulhas rings have been observed to cross the South Atlantic, even though they seem to decay exponentially to less than half their initial size (measured by their available potential energy) within 1000 km from the shedding region [*De Ruijter et al.*, 1999]. However, the majority of their thermohaline properties, resulting from the intense mixing happening in the southern Benguela region, have been observed to reach the Southeast Atlantic [*Laxenaire et al.*, Submitted], feeding directly into the upper (warm) limb of the global thermohaline circulation [*Sloyan and Rintoul*, 2001]. Most of the regional studies suggest that Agulhas water and AAIW are about equally important sources for the Benguela Current, so that variations in their strength may lead to anomalous stratification and stability of the Atlantic Ocean at decadal and longer timescales [*Lutjeharms*, 1996].

More recent, numerical works indicated that the Indo-Atlantic inter-ocean exchange is strongly related to the structure of the wind field over the South Indian Ocean [*Durgadoo et al.*, 2013, *Loveday et al.*, 2014, *Weijer et al.*, 2003]. This leads in the mean to a subtropical supergyre (Fig. 1.9) wrapping around the subtropical gyres of the South Indian and Atlantic Oceans [*Speich et al.*, 2007]. However, local dynamical processes, in the highly non-linear regime of the Cape Basin, have a crucial influence in inhibiting the connection between the two oceans [*Boebel et al.*, 2003]. The regional topography also seems to play an important role in locking the Agulhas Current retroflection [*Speich et al.*, 2006]. The interaction of rings with topography, in particular with the Verna Seamount, is shown frequently to cause their splitting, enhancing mixing of the rings Indian Ocean water into that of the southern Atlantic [*Goni et al.*, 1997, *Laxenaire et al.*, Submitted, *Schouten et al.*, 2000]. This localized mixing may well provide a considerable source of warm and salty Indian water into the Atlantic branch of the MOC [*Garzoli and Matano*, 2011].

Apart from mixing with ambient water masses, newly spawned Agulhas rings also undergo exchanges of heat and moisture with the atmosphere [*Arhan et al.*, 1999, 2011, *Faure*

et al., 2011]. The climatological heat flux to the atmosphere in this region is known to be the highest for the entire South Atlantic [*Bunker*, 1988]. *Hoflich* [1984] initially gave an average value of 200 W/m^2 with seasonal variations. However, these climatological estimates covered the whole region and did not make any distinction between Agulhas rings and other waters, underestimating for the heat loss from warm Agulhas rings [*Rouault et al.*, 2000]. In fact, *Mey et al.* [1990] have measured in-situ fluxes of between 400 and 840 W/m^2 over individual rings, whereas *Van Ballegooyen et al.* [1994] have estimated fluxes of between 300 and 400 W/m^2. These earlier observations are consistent with more recent measurements by *Rouault et al.* [2000, 2002] and *Rouault and Lutjeharms* [2003].

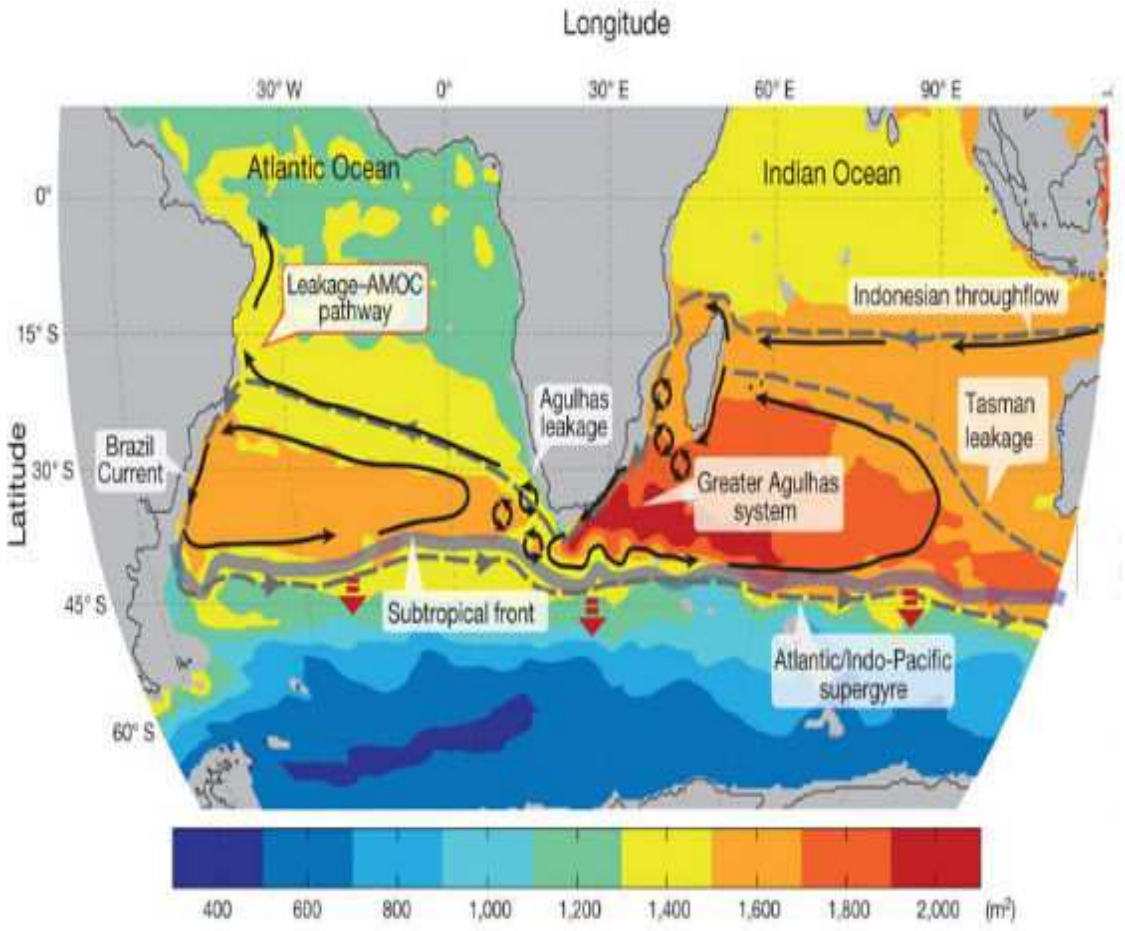

Figure 1.9: Schematic of the greater Agulhas system embedded in the Southern Hemisphere supergyre (outlined by the grey dashed line). Background colours show the mean subtropical gyre circulation, depicted by climatological dynamic height integrated between the surface and 2,000 dbar. Black arrows and labels illustrate significant features of the flow. Picture adapted from [*Beal et al.*, 2011].

Particularly noteworthy is the fact that, owing to its special synoptic weather condi-

tions, the net flux of heat in the retroflection region is from the ocean to the atmosphere throughout the year, although substantially reduced during the summer months [*Walker and Mey*, 1988]. This yearlong cooling leads to considerable modification in the upper layers of Agulhas rings in the retroflection [*Olson*, 1992]. Because of this strong air-sea interaction, the positive sea surface temperature (SST) anomalies of the rings tend to disappear quickly [*Olson*, 1992] so they can be identified from thermal infrared images only for a very limited part of their lifetime [*Schouten et al.*, 2000]. The rings signature in sea surface height (SSH) stay visible far longer, making satellite altimeter measurments very useful for monitoring the behavior of Agulhas rings over longer period [*Chelton et al.*, 2011, *Goni et al.*, 1997, *Gordon and Haxby*, 1990, *Grutindlingh*, 1995, *Laxenaire et al.*, Submitted, *Van Ballegooyen et al.*, 1994].
Nonetheless, since the rings decay is affected not only by exchanges with the overlying atmosphere, but also by interactions with the local bathymetry and with other turbulent structures (cyclones, filaments and submesoscale vortices), the numerical approach has proved to be the most appropriate tool to investigate this variety of non-linear interactions. State-of-the-art global and regional 'eddy-permitting' models show a reasonable representation of the mean Agulhas system; but the mesoscale variability and the local geometrical and topographic features, that determine largely the inter-ocean fluxes, still need considerable improvement [*Biastoch et al.*, 2008b, *De Ruijter et al.*, 1999, *Durgadoo et al.*, 2013].

As further explained in the next section, this work builds on the recent efforts of the international modelling community to refine our knowledge on the fine-scale mechanisms controlling the turbulent processes of key oceanic regions as the Cape Basin. Our goal is indeed to numerically explore the role played by meso- and submesoscale dynamics in the inter-ocean exchange around Southern Africa and the impact they have on the formation and advection of the watermasses participating in this transfer. In particular, we will show how increasing the horizontal and vertical resolutions of a regional model, from mesoscale-permitting to fully submesoscale-resolving, can highly improve the representation of the local turbulent processes and lead to a 'more-realistic' reproduction of this crucial inter-ocean exchange in terms of thermohaline properties and energy contents. This numerical approach has also allowed us to gain significant insight on the key physical mechanisms that regulate the Cape Basin meso-submesoscale interactions, on their seasonal variability and their impact on the formation, advection and transformation of the local watermasses.

Chapter 2

Scientific motivation

2.1 Thesis objectives

The main goal of the this study is to investigate the characteristics and effects on water-masses of mesoscale and submesoscale dynamics in the Cape Basin, south of Africa, as this oceanic region is considered a key nexus between the Atlantic MOC with the rest of the world ocean, possibly controlling such a connection. These turbulent processes should indeed play a capitol role in this region, characterised by the highest magnitude of Eddy Kinetic Energy in the world ocean. Therefore, the objectives we will attempt to tackle in this work are primarily directed towards the identification and analysis of meso- and submesoscale processes within a series of medium and high resolution, numerical simulations of the ocean circulation around Southern Africa. In particular, the scientific questions we are interested in will deal with:

1. Quantifying the turbulent field within the area of the Cape Basin, one of the world's greatest hotspot of mesoscale dynamics, being located at the eastern boundary of a mid-latitude basin (i.e., away from well defined, strong currents) and mainly constituted of eddies, interacting with the atmosphere and among themselves, within the upper and intermediate layers (i.e between 500 and 1000 m depth);

2. Understanding the characteristics of the regional mesoscale and submesoscale dynamics and their relations: energetics, scales, seasonality at different depths and at different locations in the Cape Basin, their effects on the Mixed Layer Depth and thermohaline

contents;

3. Diagnosing the distinct types of instabilities that arise from the interaction of the meso- and submesoscale processes and attempt to explain if their triggering mechanisms and short-term variability are related to local forcings or if more remote factors could be at play;

4. Analyzing the effects that these instabilities and transfers between scales and structures have on the advection and mixing of the local watermasses in terms of thermoaline properties and energetics;

5. Investigating the overall impact of the Cape Basin non-linear processes on the water masses exchanges and transformations, through the use of specific tools, as the algorithm for eddy detection and tracking, to capture and follow the evolution of eddies and finer-scales features, or the Ertel Potential Vorticity budget, to explore the seasonality of its anomaly and of its vertical (barotropic) terms. The latter will help us in evaluating the temporal variability of the mesoscale field.

2.2 Approach

In order to explore the above-mentioned topics we chose to run regional, numerical simulations at increasing vertical and horizontal resolutions (Figure 2.1). This has been proven to be a successful approach [*Capet et al.*, 2008a,b,c, *Molemaker et al.*, 2015] when studying meso- versus sub-mesoscale processes, once the spacing between grid points is reduced or even, in the case of the vertical levels, differently distributed. The output of our main numerical configurations were first validated against and quantitatively compared to observations (satellite retrieved and in-situ data), with the aim to highlight the model limitations, at different resolutions, in capturing the whole range of dynamical and thermohaline processes characterizing our oceanic region of interest. These simulations were then analyzed through diagnostics able to evaluate meso- and sub-mesocale structures and their properties, as well as to quantify the energy transfers typical of their interactions. Note that the definition of submesoscale adopted in the present work will be the one provided by *Capet et al.* [2008a], as "a spatial scale just smaller than the mesoscale: a horizontal scale of O(10) km, less than the first baroclinic deformation radius" (i.e., locally equal to about 30 km *Chelton et al.* [1998]); "a vertical scale of O(10) m, thinner

than the main pycnocline; and a time scale of O(1) day, comparable to a lateral advection time for submesoscale feature by a mesoscale velocity".

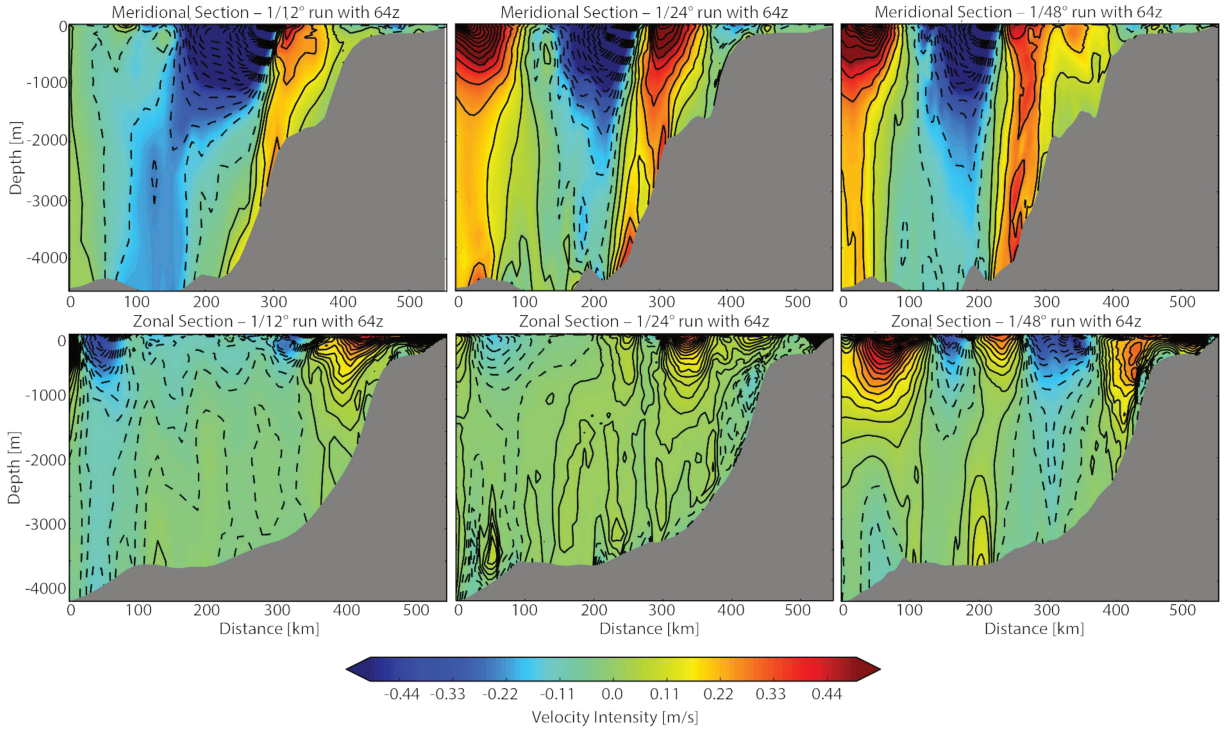

Figure 2.1: Sections of zonal (top) and meridional velocities (bottom) showing the vertical extension of eddies surface signatures for the 3 control runs of our model at different horizontal resolutions: at 1/12° (left plots), 1/24° (middle plots) and 1/48° (right).

2.3 Outline of the manuscript

This manuscript is organized as follows: Chapter 3 is devoted to a general description of the regional model, the runs setups and their outcome, as well as a brief overview of the datasets of satellite and in-situ measurements used to validate the numerical simulations. Chapter 4 deals with the results of the intercomparison between our 5 mesoscale-resolving simulations and the analysis of their validation against observations. The intent of this chapter is to draw the reader attention to the general role played by mesoscale dynamics on inter-ocean exchanges between the Southwest Indian and Southeast Atlantic basins not only within the upper layers of the water column, but down to, at least, the lower thermocline. This is why we focused our analyses on the water mass that, in the Southern Hemisphere, materializes the base of the thermocline, namely AAIW. We get to the principal finding that in order to correctly simulate the advection and mixing of the local

subsurface waters in a region of strong turbulence and importance for inter-ocean exchange, as the Cape Basin, both high horizontal and vertical resolutions of the model are necessary.

In Chapter 5 we present and discuss the analysis of the highest resolution simulations: the mesoscale-resolving solution at 1/24° with 100 vertical levels and the second child of a double-nested configuration at 1/108° resolution. Here, the main focus is to go through some of the possible instabilities that originate from the interactions of the meso- and submesoscale processes, and provide new insights on the mechanisms and factors responsible of their generation and variability. In parallel, we also examine the effects of these instabilities on the thermohaline structure of the local water masses and give evidence that symmetric and shear instabilities are active in the upper layers, likely involved in the formation and subduction of a local variety of mode waters (Agulhas Rings Mode Water, ARMW). At intermediate depths we show that the advection and transformation of AAIWs are driven by the lateral stirring and mixing of tracers from the predominant, mesoscale field.
This manuscript concludes with Chapter 6, where we provide final remarks on the major results we obtained and some perspectives aimed to signpost possible future work.

Chapter 3

Data and Methods

3.1 The Regional Ocean Modeling System (ROMS)

3.1.1 General Description

The numerical model used in this work is the Regional Ocean Modeling System (ROMS), that solves the free surface, hydrostatic, primitive equations over variable topography using stretched, terrain- following coordinates in the vertical and orthogonal curvilinear coordinates in the horizontal. We use the UCLA- IRD version of ROMS, which is an evolutionary descendent from the SCRUM model [*Song and Haidvogel*, 1994], featuring high order schemes and innovative parameterizations. For the embedded gridding of our nested configuration, we took advantage of the AGRIF (Adaptive Grid Refinement in Fortran) package for the inclusion of adaptive mesh refinement features within a finite-difference numerical model [*Blayo and Debreu*, 1999, *Debreu and Blayo*, 2003, *Debreu and Vouland*, 2003]. Even though we refer to *Shchepetkin and McWilliams* [2003, 2005] for a thorough description of the ROMS formulation and design, we will briefly describe in this section the main technical characteristics of this model.

ROMS makes the Boussinesq approximation, in which density variations are neglected except in their contribution to the buoyancy force in the vertical momentum equation, and the hydrostatic approximation, which assumes that the vertical pressure gradient balances the buoyancy force. Based on these assumptions, the model solves the primitive equations with a split-explicit free-surface, where short time steps are used to advance the surface elevation and barotropic momentum equation, and a larger time step is used for temperature and baroclinic momentum. It is coupled with advection/ diffusion schemes

for potential temperature and salinity and a non-linear equation of state. Thus, the primitive equations, explicitly solved by the model and expressed in cartesian coordinates, include: the horizontal momentum equation; the advective/diffusive equations for potential temperature and salinity; the hydrostatic balance; the continuity equation for an incompressible fluid and the equation of state. Its prognostic variables are the free-surface elevation, the barotropic and baroclinic horizontal velocity components and temperature and salinity. External forcing terms are introduced in the model through vertical viscosity and diffusivity via the surface and bottom boundary conditions. The absence of an ocean-atmosphere feedback term can lead to a drift in the model SST, but this is addressed in ROMS by formulating the surface heat flux term as a relaxation of the model to the Pathfinder 9 km climatological SST [*Barnier et al.*, 1995].
Due to the paucity of evaporation-precipitation forcing fields, a similar correction scheme is used also for sea surface salinity (SSS). At the domain edges, the model makes use of open-boundary conditions, which are a combination of outward oblique radiation and adaptive nudging toward prescribed, external boundary conditions [*Marchesiello et al.*, 2001]. The latter is necessary in order to maintain stability. Lateral viscosity is zero everywhere except in sponge layers at open boundaries, where it increases smoothly toward the edge of the domain in order to suppress model-data inconsistencies. Here, the amount of damping depend on the quality of the data at the lateral boundaries.

As regards the vertical structure, ROMS takes advantage of a sigma, terrain-following coordinate system, which allows a fair representation of bathymetry-flow interactions [*Marchesiello et al.*, 1998]. The use of sigma-coordinates requires the following transformation: z=z(x,y,σ), where z is the Cartesian height and σ is the distance from the free-surface, measured as a fraction of the water column at a particular location. That is, σ ranges between -1 and 0: at the free surface (z=ζ), it is equal to 0 and at the bottom (z=-h(x,y)) it is equal to -1 [*Shchepetkin and McWilliams*, 2005]. The transformation is performed following the method of *Song and Haidvogel* [1994] and can be stretched non-linearly according to the surface- and bottom-stretching parameters (Theta-S and Theta-B respectively). The approximation of the horizontal pressure gradient force in topographic-coordinate models has been a long-standing problem due to the hydrostatic inconsistencies that develop in the transformation of the horizontal pressure gradient terms in sigma-coordinate, hydrostatic primitive equation models. The error occurs when the discretized pressure gradient force fails to vanish with horizontal isopycnals,

thus resulting in spurious geostrophically- balanced currents. The issue was addressed by *Shchepetkin and McWilliams* [2003], who developed a new pressure-gradient algorithm. The latter reconstructs the density filed into z-coordinates as continuous functions of transformed coordinates and is then analytically integrated to compute the pressure gradient force. This ensured a reduction of the pressure-gradient error by achieving more accurate hydrostatic balance terms for the sigma-coordinate formulation.

In the horizontal, the discretization of ROMS is based on the Arakawa-C grid [*Arakawa and Lamb*, 1977] whose characteristic variable-placement scheme is particularly suited to model resolutions that are finer than the first Rossby radius of deformation. For computational efficiency, a mode-splitting technique is used to separate (fast) barotropic and (slow) baroclinic modes. Time discretization follows the third-order leap-frog predictor and the Adams-Moulton corrector scheme [*Shchepetkin and McWilliams*, 2005]. This was shown to be robust and stable and designed such that a number of barotropic time-steps are run within one baroclinic time-step in order to develop the free-surface and the depth-integrated momentum equations. The weighted temporal averaging procedure of the barotropic mode allows for accurate representation of barotropic motions resolved by the baroclinic time-step, thereby avoiding aliasing and ensuring that the stability of this scheme implies greater time-steps and enhanced computing efficiency.

In terms of advection, ROMS uses the third-order upstream biased which reduces dispersion errors, based on excessive dispersion rates necessary to maintain smoothness. This essentially increases the precision for a given grid resolution [*Shchepetkin and McWilliams*, 1998]. The recent implementation of higher-order diffusive advection schemes has lead to spurious diapycnal mixing in sigma-coordinates models. A solution to this problem was provided by *Marchesiello et al.* [2009] and involves the split of the advection and diffusion, the latter of which appears as a biharmonic operator. This split-up configuration was implemented in ours simulations in order to preserve the low dispersion and diffusivity capabilities of the original scheme, while conserving water masses characteristics.

Finally, the parametrization of unresolved, subgrid-scale vertical mixing processes is achieved by the non-local K-profile Parametrization (KPP) scheme [*Large et al.*, 1994], which employs distinct methods to parametrize subgrid mixing processes in the ocean interior and in the boundary layer. Mixing in the interior is represented by taking into

account shear instabilities (modeled as a function of the local, gradient Richardson number), internal waves and double diffusion. The depth of the boundary layer at each grid point is determined by a critical value of turbulent processes that are parametrized by the bulk Richardson number and depends on surface forcing, buoyancy and the vertical velocity gradient. Diffusion in the boundary layer is formulated based on the similarity theory of turbulence and is matched to diffusion within the ocean interior.

3.1.2 Main numerical configurations

Table 1 lists all the simulations analyzed in this manuscript. In the first 5 configurations and in the parent grid of our double-nested configuration (AGU12_36_108), the domain is based on a Mercator grid and encompasses the region spanning from 45°S to 22°S and from 9°W to 34°E (Fig. 3.1). This represents the extension of the original domain used in the reference 1/12° simulations of *Rimaud et al.* [2012] and *Rubio et al.* [2009]. For the sake of computational costs, an attempt to slightly reduce this domain, both zonally and meridionally, was performed at the beginning of this study in the first configuration run at high resolution (1/48°), where the eastern boundary was set at 30°E. This relatively small reduction of the domain extension showed to greatly and negatively affect a proper representation of the Agulhas Retroflection and its EKE transport. Therefore, in the following simulations, the eastern boundary was set back at 34°E.

The chosen domain presents an increasing horizontal resolution that goes from 7.5 km (at 1/12°) down to 3.8 km (1/24°) in the north and 7.2 km to 3.5 in the south. Since the first Rossby radius of deformation is locally about 30 km [*Chelton et al.*, 1998], all these simulations are fully eddy-resolving, and even submesoscale-permitting in the case of the 1/24° configurations. Hence, they are all able to satisfactorily capture the resolution of the local mesoscale processes; for example, Agulhas rings are thought to have a length scale of about 300 km [*Penven et al.*, 2006]. The vertical grid of these runs was initially defined by 32 levels, than 64 and finally 100 in the case of the highest simulation at 1/24°. These levels were in the first two simulations at 1/12° stretched toward the surface, since the surface- and bottom-stretching parameters (Theta-S and Theta-B) were set at the default values of 6 and 0, ensuring an enhanced resolution in the upper layers. Instead, in the following four simulations (labeled with a final 'H', for 'homogeneous'), being our interest mainly focused on the dynamics of thermocline and intermediate waters, we changed the values of these parameters to 5 and 1, in order to allow a more homogeneous

Table 3.1: List of the 6 simulations that will be presented in this manuscript, with the main technical features of their configurations.

Name of the simulation	Horizontal Resolution	Nb points in long/lat	Sigma levels	Stretching Terms (sigma-levels distribution)
AGU12_32	1/12°,~7.3km	530, 426	32	Theta-S=6, Theta-B=0
AGU12_64	1/12°,~7.3km	530, 426	64	Theta-S=6, Theta-B=0
AGU12_64_H	1/12°,~7.3km	530, 426	64	Theta-S=5, Theta-B=1
AGU24_64_H	1/24°,~3.6km	1059, 672	64	Theta-S=5, Theta-B=1
AGU24_100_H	1/24°,~3.6km	1059, 672	100	Theta-S=5, Theta-B=1
AGU12_36_108	1/12°,~7.3km+1/36°,~2.4km+1/108°,~0.8km	530, 426 671, 530 797, 836	100	Theta-S=5, Theta-B=1

distribution of the vertical levels along the water column and to acquire more resolution in the subsurface (Fig. 3.2). However, in all the simulations of Table 1 we also made use of the recently introduced function of the vertical levels, *Vtransform*, which was set at the value of 2 to enable a more uniform distribution of these levels, in respect to its original definition [*Lemarie et al.*, 2012]

In all the simulations, the ocean was initially at rest and the boundary conditions were supplied by the World Ocean Atlas (2009) [*Locarnini et al.*, 2010] temperature and salinity climatologies at 1° of resolution, from which the geostrophic velocities were calculated. For the Ekman transports we used a monthly climatological wind stress derived from daily QuikSCAT satellite scatterometer data gridded at 1/2° resolution [*Institut Français de Recherche Pour l' Exploitation de la Mer and Centre ERS d'Archivage et de Traitement, 2002*] [*Bentamy et al.*, 2003]. The bottom topography is derived from the ETOPO2 (2' resolution) data set [*Smith and Sandwell*, 1997], which, in a further attempt at avoiding pressure gradient errors, was smoothed in order to maintain a slope parameter 'r' ($r = \Delta h/h$) lower than 0.25 [*Armstrong and Vazquez-Cuervo* , 2001]. The area defined from 8°W to 30°E and from 25°S to 52°S displays a considerable relief with the Agulhas Bank, the Agulhas Plateau, and the Cape Basin, surrounded by the Walvis Ridge, the Agulhas

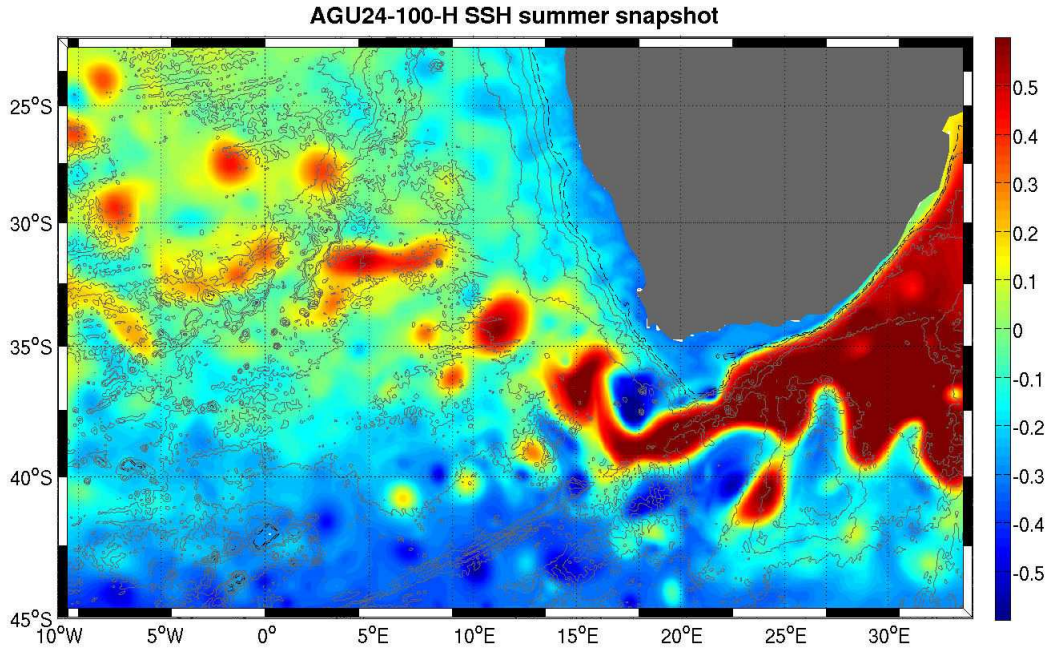

Figure 3.1: Summer instantaneous map of Sea Surface Height (SSH in m) from the 1/24° simulation with 100z (AGU24_100_H), showing the definitive domain extension that has been used in all the configurations whose output are discussed in this manuscript.

Ridge, the Republic of South Africa Seamounts and the Discovery Seamounts (Fig. 1.5 a). With these assumptions on the bathymetry, our simulations retain most of the sharp topographic features of the study region.

Due to our focus on intrinsic oceanic variability, the 1/2° QuikSCAT climatology of 2000-2007 wind data was used to force all our simulations, while surface radiative heat and fresh water fluxes were extracted from the Comprehensive Ocean-atmosphere Data Set (COADS) [*Da Silva et al.*, 1994] ocean surface monthly climatology, also at 1/2° resolution. The latent and sensible heat fluxes use satellite-derived atmospheric quantities (air temperature and QuikSCAT wind) in their bulk formulation [*Ayina et al.*, 2006, *Bentamy et al.*, 2003].

In the case of our last 5 simulations, we activated the diffusive component of the Rotated, Split, Upstream-biased, 3rd Order (RSUP3) tracer advection scheme. This scheme is rotated in order to follow geopotentials [*Marchesiello et al.*, 2009] and is designed to reduce artificial effects of spurious diapycnal mixing observed in the tracers fields of our first simulation at 1/12° with 32z (AGU12_32). All our simulations were run for 5 years and the model solution is considered stable after a spin-up period of about one year (see the diagnostic curves of Figure 3.3).

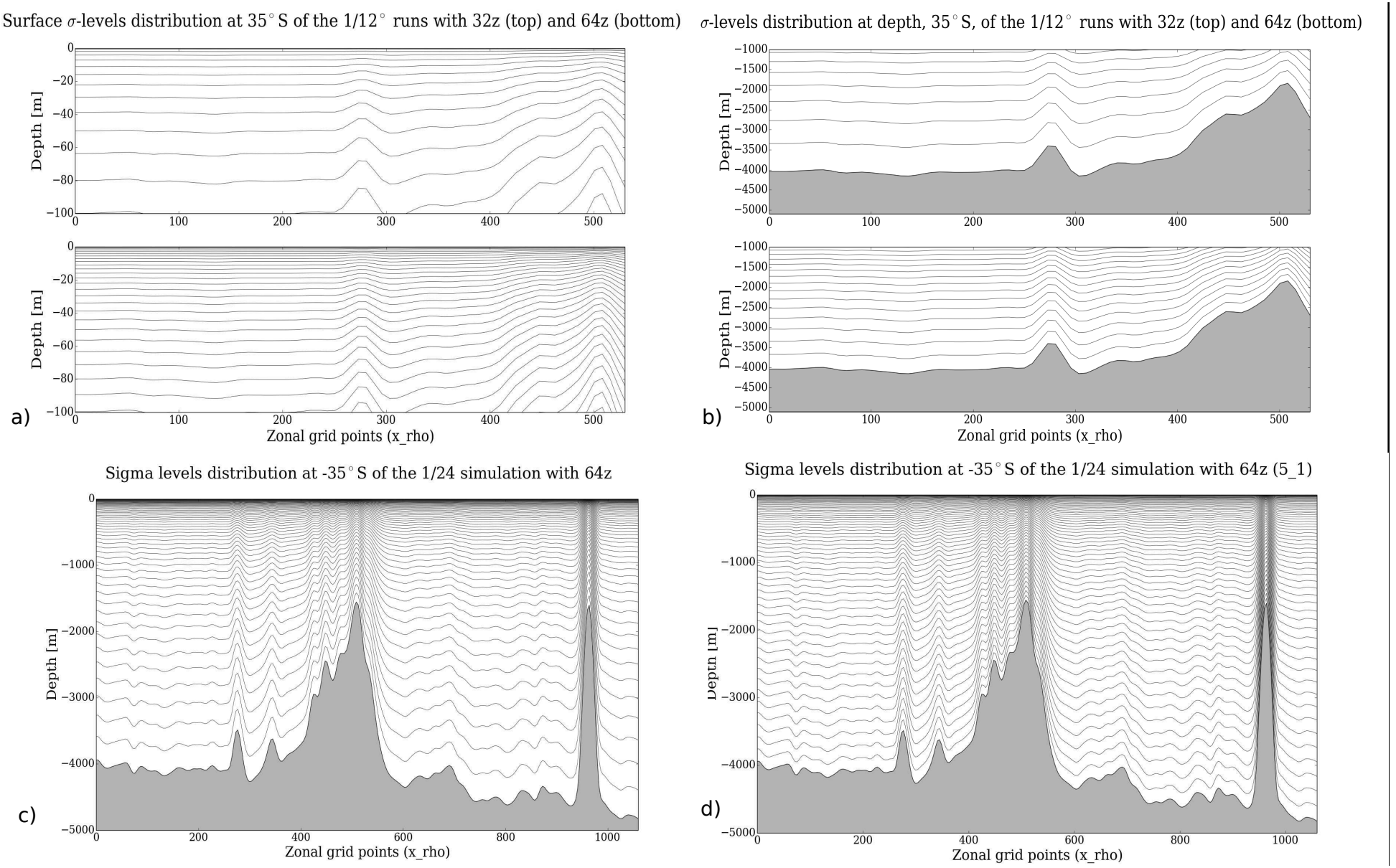

Figure 3.2: Sections showing the differences in the vertical distribution of the sigma levels between the simulations with 32z and 64z in the upper layers (a) and at depth (b), and between the ones having values of Theta-S and Theta-B at 6 and 0 (c) and those having them at 5 and 1 (d).

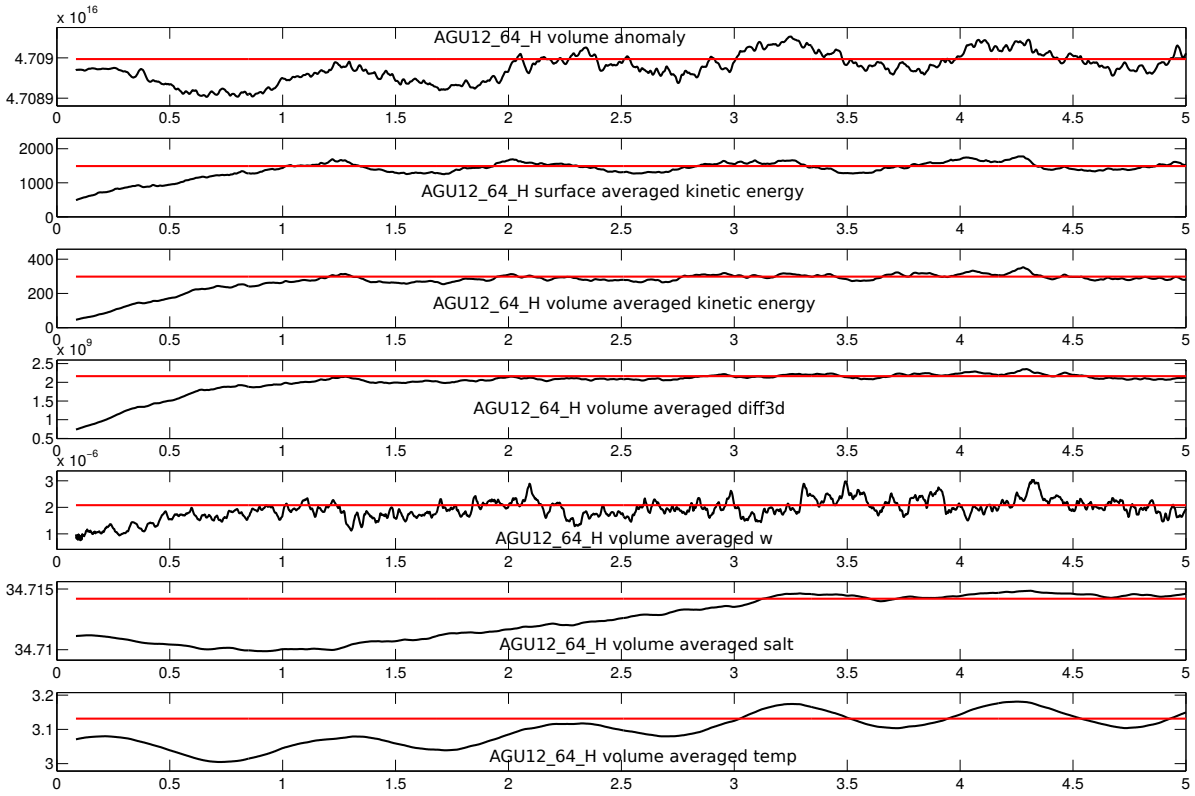

Figure 3.3: Diagnostic plots showing volume averages of the model prognostic variables (T and S), kinetic energy and horizontal diffusivity coefficient for the 1/12° simulation with 64z_H (AGU12_64_H), chosen here as two examples of the runs analyzed in this manuscript to show the time the model spends for the spin up, before reaching a steady-state.

Thus, our analysis will focus on the last 4 years of each simulation, in which the output have been averaged and stored on a daily basis.

With the aim to evaluate the impact of the domain extension, as already mentioned, but also of other background values, like the horizontal Laplacian diffusivity number or the bottom drag coefficient, as well as the topographically very influent slope parameter 'r', several simulations were run during the first phase of this study at very low resolution (1/4°). This allowed to test the sensitivity of the model to slight alterations in its initial parameters and to subsequently address our choice of the best configuration to use for running higher resolution configurations. All the simulations analyzed in this manuscript were then run on the Caparmor cluster at Ifremer in Brest, for the ones at 1/12°, and on the Ada cluster of 'Idris', for those at 1/24° and for the nested configuration. Pre- and post-processing of all these simulations used the Matlab ROMSTOOLS toolbox (http://www.romsagrif.org/) [*Penven et al.*, 2008].

3.1.3 The nested setup

In order to maximize computing efficiency of a submesoscale-resolving resolution simulation of the Cape Basin, the AGRIF nesting capability of ROMS [*Debreu and Mazauric*, 2006] was used to run a double-nested configuration. This nested approach is designed such that the boundary conditions of two high resolution 'child' domains are supplied by the lower resolution 'parent' domain within which they are embedded [*Debreu et al.*, 2012]. This allows for more consistent boundary conditions of the child domains than what could be obtained from, often sparsely available, in-situ data. *Penven et al.* [2006c] evaluated the use of the 1-way nesting approach described above for the central California upwelling system and found that it improved the fine resolution simulation, compared to the use of open boundaries at only a slightly higher computational cost. Our highest resolution simulation makes use of the latest implemented version of the ROMS-AGRIF package [see *Debreu and Blayo* [2008]] that authorizes a 2-way nesting procedure. The latter enables the child solutions to feed back into the parent domain and therefore allows for realistic simulation of coastal and ocean dynamics at multiple, interacting scales. Our parent domain consists of a $1/12°$(Δx$\simeq$ 8 km) run with 100, homogeneously distributed, vertical levels, forcing a first child domain at $1/36°$(Δx$\simeq$ 2.7 km), placed just after the Agulhas Retroflection and, embedded into it, a second child domain at $1/108°$ (Δx$\simeq$ 0.8 km), centred on the area of the Cape Basin. Figure 3.4 shows the geographical extensions of the three domains making up our nested simulation.

In terms of forcing at the open, lateral boundaries of the parent grid, initial state and advection/ diffusion schemes, we used in this nested solution the same datasets and conditions employed in the previous 5, mesoscale-resolving simulations we run, as described in section 3.1.2. Also this nested configuration was integrated for 5 years in total and during this time a robust seasonal signal approximately repeats itself from approximately the first year. The spin-up time is estimated from surface and volume averaged kinetic energy (KE), as well as other volume integrated quantities, which are shown for the parent domain in Figure 3.5. After the rapid adjustment of $\sim$1 year, a statistical steady-state is reached and the system does not exhibit any temporal drift. The results of this manuscript are then based, as for the previous simulations, on the output from the last 4 model years and the snapshots used for the analysis of some instantaneous fields (tracers and velocities) are taken from the last year (year 5).

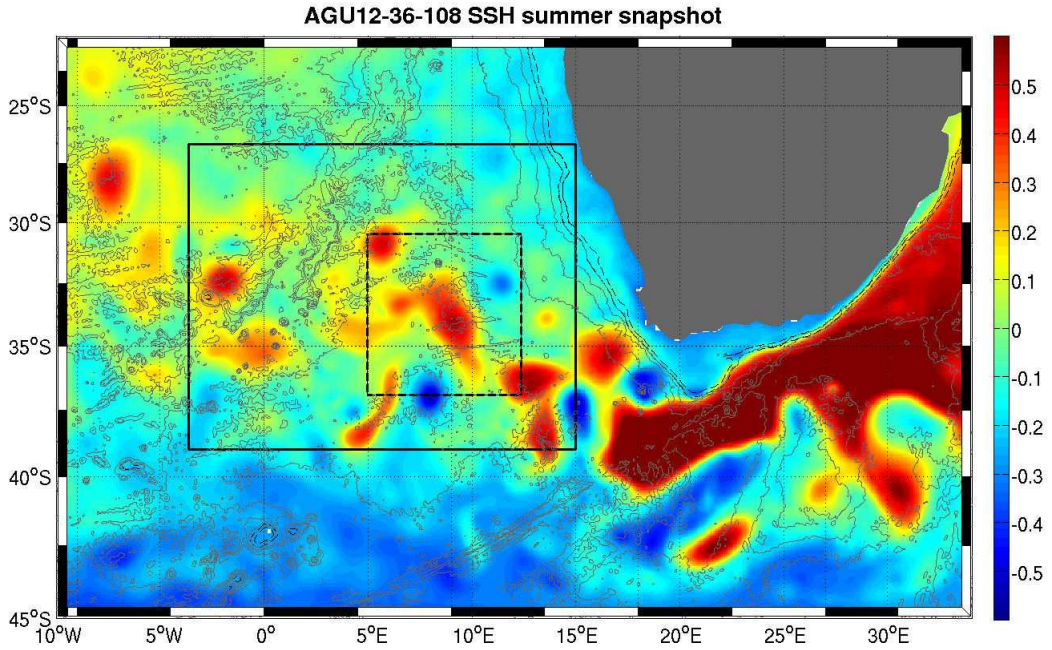

Figure 3.4: Same as Figure 3.1 but for the nested configuration (AGU12_36_108), showing as well the geographical extensions of the three domains of this simulation.

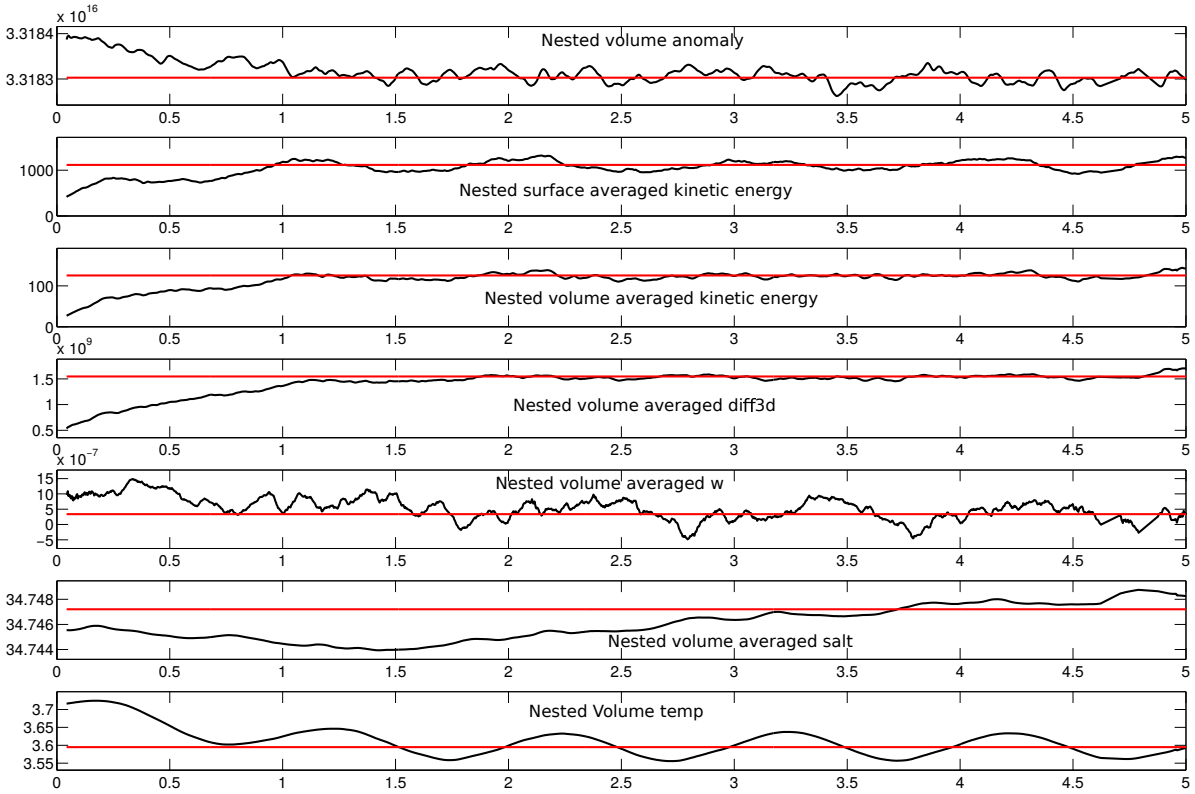

Figure 3.5: Same diagnostic time series of Figure 3.3 but for the parent domain of our nested configuration (AGU12_36_108).

3.2 Data sources for the model validation

This section describes the datasets of observations used to validate the output of our numerical simulations and introduce the specificities of each of these datasets, in order to better understand the differences in the comparisons. To make the latter as meaningful as possible, the resolutions of the finest simulations (i.e. at 1/24° and the ones of the nested solution, at 1/36° and 1/108° of the child domains) have been degraded to approximate the lower resolution of the observational products. For this aim, a simple spatial collocation technique is employed in order for higher resolution data to approximate the lower resolution of the observations. In this manner, a new, lower-resolution grid is defined for the higher resolution model output by creating a new point at the center of four points of the original grid and the variable is here calculated by taking the average of the four surrounding points. This simple procedure allows to halve the resolution of the higher resolution grid (e.g. a 4 km grid becomes an 8 km grid and so on).

3.2.1 Satellite-retrieved observations: AVISO altimetry and OSTIA SST data

For the validation of the surface energy contents reproduced in each of our simulations, we took advantage of 20 years of altimetric observations (from January 1993 to December 2012), produced by Ssalto/Duacs and distributed by AVISO, with support from Cnes (url: http://www.AVISO.altimetry.fr/duacs/). Multi-mission products refer to the combination of all satellite data available at one time: Jason-1, Envisat, GFO, ERS-1, ERS-2 and Topex/Poseidon. The new version of the altimetric product used in this work was released in April 2014 [*Duacs/AVISO*, 2014], filtering out fewer data than the former version. All daily along-track satellite data available each day are filtered, subsampled and then merged. Two algorithms are daily applied to reduce orbit errors and interpolate data on a homogeneous 1/4° grid. The final products are daily gridded maps of Sea Surface Height (SSH), that we have extracted for our region of interest (Figure 3.1).

Instead, for validating the temperature field at the surface, we used 4 years of the SST reanalysis product from the Operational Sea Surface Temperature and Sea Ice Analysis (OSTIA, from 2007 to 2010), downloadable at the url: http://ghrsst- pp.metoffice.com/pages/latest analysis/ostia.html. This platform produces a high resolution analysis of the sea surface temperature for the global ocean, using satellite data provided by the GHRSST project,

together with in-situ observations. The analysis is performed using a variant of optimal interpolation (as described by *Martin et al.* [2007]) and is determined daily at a resolution of 1/20° (approx. 5km). OSTIA data is provided in GHRSST netCDF format every day.

3.2.2 In-situ observations from Argo profiles

A total of about 92700 individual profiles of temperature and salinity located in a quadrant at 10°W-40°E and 20°S -60°S between 2004 and 2011 were interpolated, in time and space, to produce the climatology of *Rusciano et al.* [2012]. We used these observations to validate our simulations output in terms of water masses characteristics, especially within the thermocline and the AAIWs layer. The main ARGO projects contributing to this dataset are: GoodHope (Coriolis, France), U.S. Argo (AOML, USA), Argo UK (BODC, UK), J-ARGO (Jamstec, Japan), Argo AUSTRALIA (CSIRO, AUS) and some others, making a total of 309 floats. Argo data were downloaded from the Coriolis Operational Oceanography Centre, which is one of the two Argo Global Data Assembly Centres (GDAC) worldwide. Profiles from Argo floats pass through various quality control procedures. The real-time tests are automatic and standardized (for more details refer to the document available at http://www.argodatamgt.org/). Additionally, an extensive quality control procedure has been performed on the data, under the auspices of the CLIVAR International observing program [*Cabanes et al.*, 2013, *Owens and Wong*, 2009]. The accuracy of the pressure, conductivity and temperature sensors used by the profiling floats during the GoodHope program are 3 dbar for the pressure accuracy, +/-0.03 mS/cm for the conductivity and +/-0.03 °C for the temperature.

3.3 Algorithm for eddy identification and tracking

To statistically quantify the mesoscale field simulated in each of our simulations we applied to their output the detection and tracking methodology of *Chaigneau et al.* [2008, 2011], further developed by *Pegliasco et al.* [2015] and recently extended by *Laxenaire et al.* [Submitted]. We refer to the latter for a detailed description of the algorithm formulation, even though we will provide here some information on its main technical features. This method, based on geomtric criteria, has been shown to detect fewer false eddies than other classically used methods [*Chaigneau et al.*, 2008, *Souza et al.*, 2011, *Yi et al.*, 2014] and is similar to the one designed by *Chelton et al.* [2011] to study the main eddy characteristics at global scale.

The eddy detection algorithm characterizes an eddy structure by a point that defines its center and by a closed streamline contour corresponding to the eddy edge. The inner points bordered by this contour line belong to the eddy and determine its surface area. For each SSH map, possible cyclonic (or anticyclonic) eddy centers are identified finding local SSH minima (or maxima) in an arbitrary chosen 1°x 1° latitude-longitude moving window. Streamlines are computed following the trajectories of virtual particles released in the geostrophic current field from every 0.25° x 0.25° grid point. The step size and the number of steps for the integration of the streamlines are carefully chosen to get a step size as small as possible to achieve the highest accuracy, while the number of steps should be as high as possible to ensure that paths are long enough, particularly in regions of low velocity magnitude. The eddy identification process consists of two main stages: the selection of streamlines associated with eddies and the clustering of distinct streamlines corresponding to the same vortex. Each cluster consists of closed streamlines rotating around the same vortex center and the outer streamline corresponds to the eddy edge.

After a vortex edge is identified, several eddy properties are computed. The position of the vortex center is determined as the position of the maximum absolute value of SSH inside the eddy. Henceforth other characteristics related to the vortex geometry, as the vortex area, its amplitude, its apparent radius, are defined. And also properties more related to the eddy kinematics- like the eddy intensity or density, swirl velocity, EKE, divergence, vorticity, straining and shearing deformation rates- are estimated for each detected vortex. In addition to these various properties, the detection algorithm allows to analyze the eddy occurrence frequency, polarity (see examples in Fig. 3.6) and distribution, as well as the eddy life span and eddies mean characteristics along their tracks. Since in this work, our major focus is on the impact that mesoscale eddies have on the water masses mixing and transformation, we mainly looked at the distributions and modifications of the thermohaline properties within the detected eddy cores.

A tracking method is applied in a second step of the algorithm to follow eddies between successive SSH maps, which allows to recover a complete and continuous set of eddy trajectories and how eddies evolve over time. Here the main assumption is that mesoscale eddies move slowly (displacements of less than 10 km/day, see also *Chelton et al.* [2011]) compared to their typical radii that span from 20 to 200 km [*Carton*, 2001]. This en-

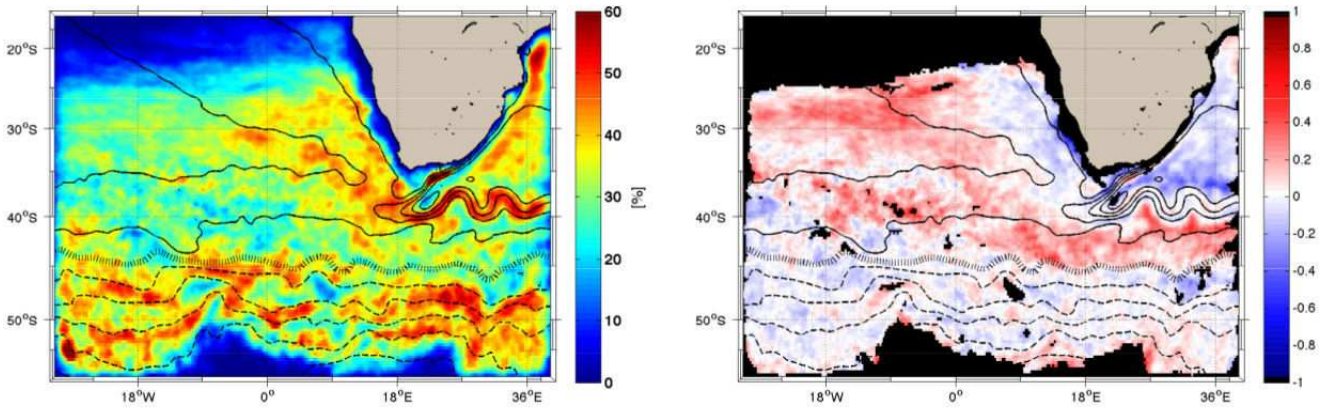

(a) Frequency of eddy presence

(b) Polarity

Figure 3.6: Frequency of the eddy presence (a) and polarity (b) from the eddy detection algorithm applied to the outptut of the AGU12_64 simulation.

sures that the areas covered by the same eddy on two consecutive days overlap, and such an overlapping can be used to track eddies [*Pegliasco et al.*, 2015]. Here, we imposed that the percentage of the surface overlapping between two consecutive identifications of an eddy is larger or equal to 25% (for our simulations output) and 75% (for AVISO data) of the extent of the smallest of the two areas. However, eddies can also disappear from the altimetric signal during few time steps [*Chaigneau et al.*, 2008, *Chelton et al.*, 2011]. To reduce this effect, the algorithm allows the association of eddies when they are lost up to 5 days if their intersection area fulfill the surface overlapping criterion.

Furthermore, eddy-merging or separation events frequently occur in the ocean. The tracking algorithm used here takes into account both processes: it associates the separation of a large eddy with two or more smaller eddies in the splitting case, and it relates the coalescence of two or more small eddies into a larger eddy in the merging case. In this study, we only retain 'long-lived eddies' lasting more than 7 days, meaning that all the eddies who last less than 7 days, before a merging or after a splitting event, are removed. Apart the temporal filter of 7 days, a restriction is also applied on the amplitude of the detected eddies which will be then tracked along their path: eddies whose median amplitude was lower than 2 cm along their lifetime were discarded. Thanks to these two criteria, we get rid of all the suspicious detections and the remaining structures are classified by their nature (cyclone vs anticyclone). Their contours and properties have then been used for the analysis of different diagnostics, whose results will be the subject of the following sections.

Chapter 4

Mesoscale Variability and Impact on the AAIW advection

4.1 Introductory Remarks

4.1.1 Challenges in modelling the Agulhas Current

This chapter constitutes the synthesis of the work devoted to study the impact of different numerical configurations, at increasing horizontal and vertical resolutions, on simulating the Cape Basin circulation and water masses. The aim was to identify the best combination of both which would allow us to more 'realistically' (i.e. in comparison with the observations available over the study region) reproduce the local thermoaline structure and turbulent processes. A realistic simulation of the Indo-Atlantic inter-ocean exchange is a formidable challenge due to the highly non-linear dynamics of the Agulhas retroflection regime and leakage, including its little known dependence on mesoscale flow perturbations further upstream [*Biastoch et al.*, 2008b]. Previous modelling experiments have begun to capture these intricacies of the Agulhas system, however, at the expense of the modelled frequency and dimensions of rings being shed in the retroflection region due to compromises between resolution [*Biastoch and Krauss*, 1999] and domain sizes [*Speich et al.*, 2006].

In fact, to simulate the inter-ocean exchange south of Africa, numerical models must describe the Agulhas Current and its retroflection, ring shedding, and drift (i.e., the leakage of warm and salty water into the Atlantic), in a qualitatively and quantitatively correct

way [*Biastoch and Krauss*, 1999, *De Ruijter et al.*, 1999]. Successful simulations of the formation and drill of Agulhas rings and other Cape Basin eddies depend on parameters such as grid resolution and viscosity [*Chassignet et al.*, 1989], topography, diffusion and vertical mixing [*Gula et al.*, 2015]. In addition, the vertical coordinate system, governing equations, boundary conditions and details of geometry, all have direct impacts on the number of model rings formed, their lifetime, and propagation speeds [*Chassignet*, 1992, *Durgadoo et al.*, 2013, *Penven et al.*, 2006]. Previous comparisons of models with different resolution [*Thompson et al.*, 1997] have shown that only configurations with horizontal grid spacing finer than 1/8° have the potential ability to generate Agulhas rings and to fulfill the above requirements. So we started from a fully 'eddy-permitting' resolution of 1/12° (with 32 vertical levels) to gradually reach the fully 'mesoscale-resolving' resolution at 1/24°(with 100z) in order to verify our model capability to increasingly capture a broader spectrum of the Cape Basin turbulent dynamics.

The results of this intercomparison between mesoscale-permitting and mesoscale-resolving simulations are discussed in a manucript under revision at JGR and enclosed in section 4.2. In general, we found that in our simulations at 1/12° a much higher fraction of the Agulhas water enters the Atlantic in comparison to the 1/24° simulations and to observations (Fig. 4 of the submitted manuscript presented in section 4.2 and Supplemental Figs. 1 and 2 of the same manuscript). The pronounced contrast between these two resolutions with identical set-up conditions (forcing, open boundaries, advection scheme, smoothing of the topography, etc) demonstrates that the supply of Indian Ocean water to the South Atlantic, and thus, the warm water path of the Atlantic MOC, is not determined by large-scale dynamics alone, but significantly influenced by the regional, mesoscale dynamics of the Agulhas regime.

The numerical work of *Biastoch et al.* [2008b] had indeed underlined how the upstream retroflections of the Agulhas Current represent a prominent feature of the Agulhas dynamics and further downstream [*Durgadoo et al.*, 2013]. The generation of Agulhas eddies depends on local processes such as baroclinic or barotropic instability [*Biastoch and Krauss*, 1999, *Pichevin et al.*, 1999], and remote processes, as the downstream propagation of smaller eddies originated in the Mozambique Channel [*Biastoch et al.*, 1999] or at the retroflection of the East Madagascar Current [*Schouten et al.*, 2000], as well as the formation of cyclonic lee eddies along the Agulhas Bank [*Penven et al.*, 2001]. After shedding, the eddies propagate in a northwestward direction leading to the Walvis Ridge

where they veer to the west and merge with the circulation of the subtropical gyre.

4.1.2 On the model vertical resolution

We believe that one of the main finding we obtained from the aforementioned intercomparison of our numerical simulations is the evidence that both the horizontal and the vertical resolutions of the model highly impact the surface and subsurface thermohaline properties of the Cape Basin water masses. In fact, by increasing the number of vertical levels and by homogenizing their distribution along the water column we were able to enhance the vertical resolution in the subsurface and deep layers. This induced a significant improvement in the reproduction of the temperature and salinity fields. In particular, the refinement of the vertical resolution has generated the highest gain in simulating the thermohaline distribution of thermocline and intermediate water masses.
At present, in the standard design of an ocean model the vertical grid spacing is a function of depth, with fine spacing of O(1-10 m) at the ocean surface and coarser spacing below. Such a refinement implies, moreover, that some unresolved vertical processes are parametrized (as, for example, through enhanced vertical eddy viscosities and diffusivities), highly impacting the water masses transport and their thermohaline properties. Our results clearly suggest that this vertical levels distribution is not adequate for resolving the dominant dynamics of both the surface and subsurface layers, and that it is instead crucial to correctly solve the vertical structure of the horizontal motions.

Indeed, only when we homogeneously increased the vertical spacing of the model to, at least, 80m (experiment AGU12_64_H) we are able to reproduce the observed distinct stratification of Indian and Atlantic waters. This is shown for the lower thermocline levels in Figure 4 of the submitted manuscript presented in Section 4.2. The comparison of the stratification simulated in the standard vertical level distribution (experiments AGU_12_32 and AGU_12_64, Figs. 4b and 4c), with that at higher vertical resolution (Fig. 4d) is striking. In addition, such a vertical distribution highly influences also the upper-layer dynamics. In Figure 5 of the submitted manuscript presented in Section 4.2, the simulated eddy variability gains in realism when, at equal horizontal resolution, the vertical levels are homogeneously distributed along the vertical instead of being refined in the upper layers only (Figs. 5b and 5c to be compared with 5d). A higher vertical and horizontal refinement further improves the realism of the simulated dynamics (experiments AGU24_64_H and AGU24_100_H, Figs. 4e-5e and 4f-5f respectively).

4.1.3 Cape Basin eddy variability

A distinct characteristic of the simulated eddy variability within the Cape Basin is the co-existence of cyclonic and anticyclonic vortices, as already mentioned in the Introduction of this manuscript. Although there are abundant descriptions of the larger rings (e.g., *Lutjeharms* [1996] and references therein), the less conspicuous, cyclonic vortices have received recognition only during the last two decades [*Boebel et al.*, 2003, *Doglioli et al.*, 2006, *Garzoli et al.*, 1996, *Giulivi and Gordon*, 2006]. The Cape Basin anticyclones and cyclones tend to form dipole structures that resemble the Heton model of *Hogg and Stommel* [1985]; the name deriving from the high efficiency with which these dipoles transport heat, particularly across frontal structures [*Spall*, 1995]. While most theoretical studies of Hetons have been focused on the dynamics of dipoles, the structures observed in the Cape Basin are far more complex, consisting of several cyclones and anticyclones [*Laxenaire et al.*, Submitted], although it is frequently possible to identify a dominant pair.

Most of the Agulhas anticyclones appear to be confined within a well-defined region, or "eddy corridor", that pass through the portion of the Walvis Ridge located between 24° and 33°S (Fig. 3.7a). We will see that the mean path of the rings simulated in our highest resolutions simulation is in close agreement with that inferred from altimetry (Fig. 9 of the submitted manuscript presented in section 4.2). On the other hand, a good portion of the Agulhas cyclones seem to never leave the Cape Basin (Fig. 3.7b). Noteworthy is that the path of the eddy corridor changes abruptly from a northwest to a more westward direction at approximately 9°E, before any eddy can actually interact with the ridge. The region where the eddies veer coincides with the location of the Vema Seamount ($\simeq$31°S, 8°E), a very shallow peak reaching to near-surface depths ($\simeq$60 m of the surface). *Arhan et al.* [1999], *Schouten et al.* [2002] and, lately, *Laxenaire et al.* [Submitted] reported the splitting of the Agulhas eddies trajectories after passing this peak.

Previous numerical studies [*Matano and Beier*, 2003] and more recent observational findings [*Laxenaire et al.*, Submitted] indicated a marked decrease of the anticyclones upper layer velocities after crossing this ridge (Fig. 4.1), resulting in a reduction of their kinetic energy content of approximately 30%. One of the possible reasons of why the topographic effect does not show more prominently in the SSH signal (Fig. 5 of section 4.2 for its RMS and Supplemental Fig. S2 for its mean) is that it appears to affect more the barotropic component of the flow. However, the energy losses caused by the topographic interaction is likely responsible of weakening the meridional component of the eddy propagation,

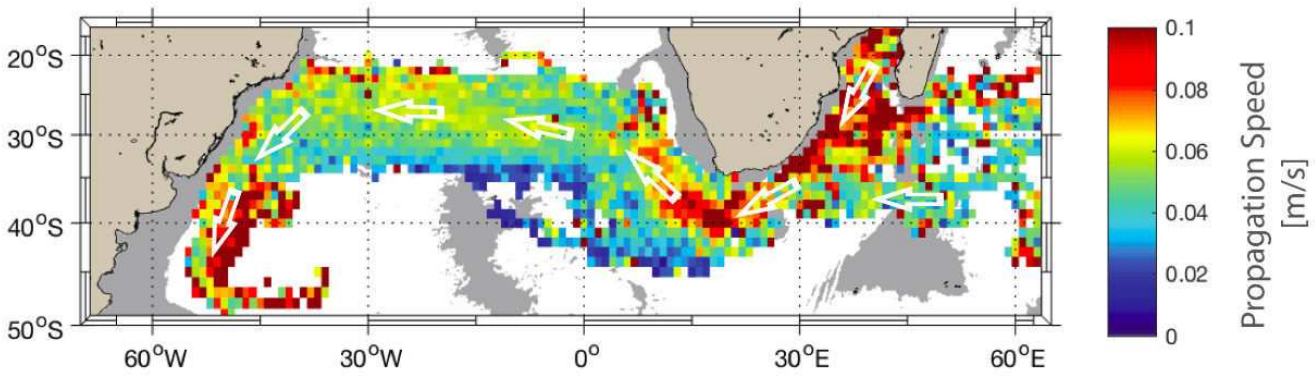

Figure 4.1: Figure adapted from *Laxenaire et al.* [Submitted], showing the median propogation speed of Agulhas Rings detected in 16 years of AVISO gridded data. The gray shading represents water depth shallower than 3500 m in the ETOPO2 data set [*Smith and Sandwell*, 1997].

which is mostly driven by the non-linearity of the flow, and forcing the eddy path into a predominantly westward direction [*Treguier et al.*, 2003].
If so, this may be a plausible explanation to the observed shrinking of the meridional extent of the subtropical gyre with depth, given that the Cape Basin geometry only allows the export of zonal momentum fluxes in a very restricted range of latitudes [*Garzoli and Matano*, 2011]. At the upper level the wind-stress curl is the dominant forcing for the large-scale circulation and therefore sets the meridional scale of the gyre. At intermediate depths, wind effects are much reduced and the structure of the gyre is largely dominated by momentum and thermoaline fluxes from the Cape Basin [*Schmid and Garzoli*, 2009].

4.1.4 Statistical properties of the mesoscale field

Hence, in our submitted manuscript (section 4.2) we firstly qualify the eddy component of these fluxes by statistically describing the mesoscale field, as simulated in each of our numerical configurations, and then evaluate their role on the advection of AAIWs T-S properties through the Cape Basin. An algorithm of eddy detection and tracking was the tool used to identify the mesoscale eddies [*Laxenaire et al.*, Submitted], to separate them according to polarity and to compute a bunch of statistical metrics (number, mean radius, amplitude), in comparison to the same analysis performed on satellite data. The highest resolution simulations (at 1/24°) exhibited the most abundant presence of eddies, whose mean radius ranged from 50 to 100 km. Their eddies were thus higher in number and smaller in size than those detected in AVISO and in the 1/12° simulations, as qualitatively shown in Figure 4.2 and more quantitatively in Supplement Figure S4 of section

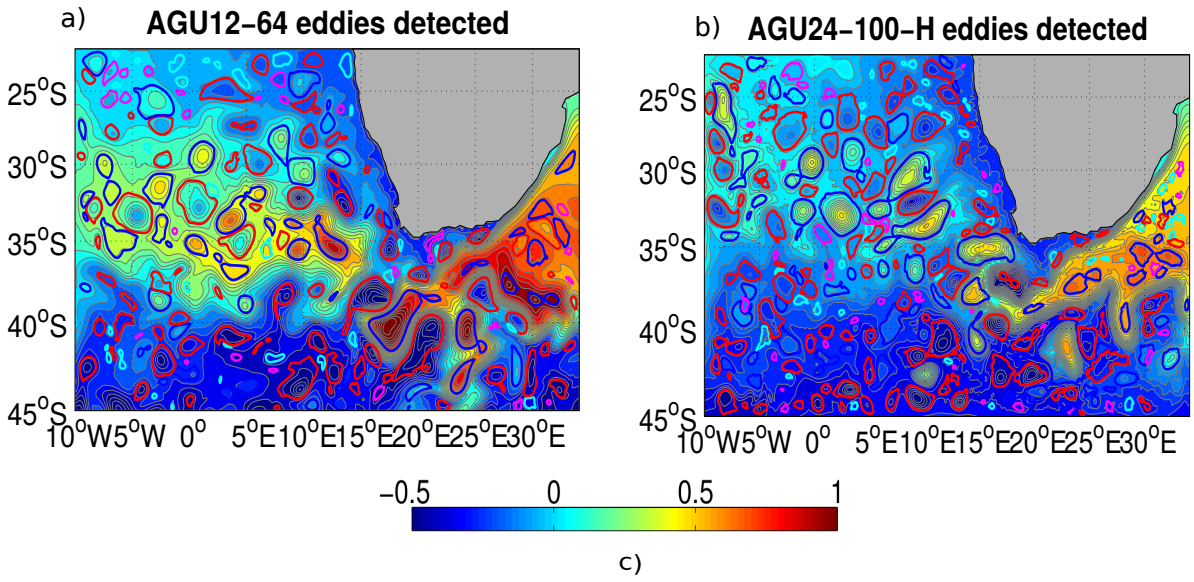

Figure 4.2: Instantaneous maps (model Y5M1) of SSH [m] showing the distribution of detected eddies for the 1/12° run with 64z (a) and the 1/24° run with 100z-H (b). c displays the colorbar for the SSH intensity, while colours legend for the contours of the eddies is the following: the contours of the cyclones kept, after the filtering step of the detection algorithm, are in red and in magenta those removed; in blue are the anticyclones retained and in cyan those filtered out.

4.2. In both the simulated and observed eddy distributions, more cyclones were detected than anticyclones (in a ratio of 3/2), being on average slightly smaller (50 vs 60 km). Taking into account the limited resolution of the interpolated AVISO product, we filtered out, in our simulations, all the structures having a radius equal or greater than 30 km, with the aim to more precisely compare the distributions of our eddies number and radius with the observed ones. After this filtering process, the highest resolution results became much more comparable to the AVISO estimates (see Fig. 7 of section 4.2 and Fig. 4.3 below), above all in terms of the number of cyclones and anticyclones.

For the anticyclonic vortices detected in AGU24_100_H, we also examined their geometry and found that most of the rings crossing the Cape Basin have a quasi-Gaussian profile (Fig. 10a of section 4.2). By computing their geometrical moments, we showed that these rings are averagely interested by several modes of deformation (Fig. 10b of section 4.2). The angular mode 2 was predominant, but modes 3 and 4 had close amplitudes, confirming that these rings undergo complex interactions with topography, with the surrounding currents and with several, neighbouring eddies entrained in the Cape Basin.

Thanks to the tracking methodology of the eddy algorithm, we followed anticyclonic and

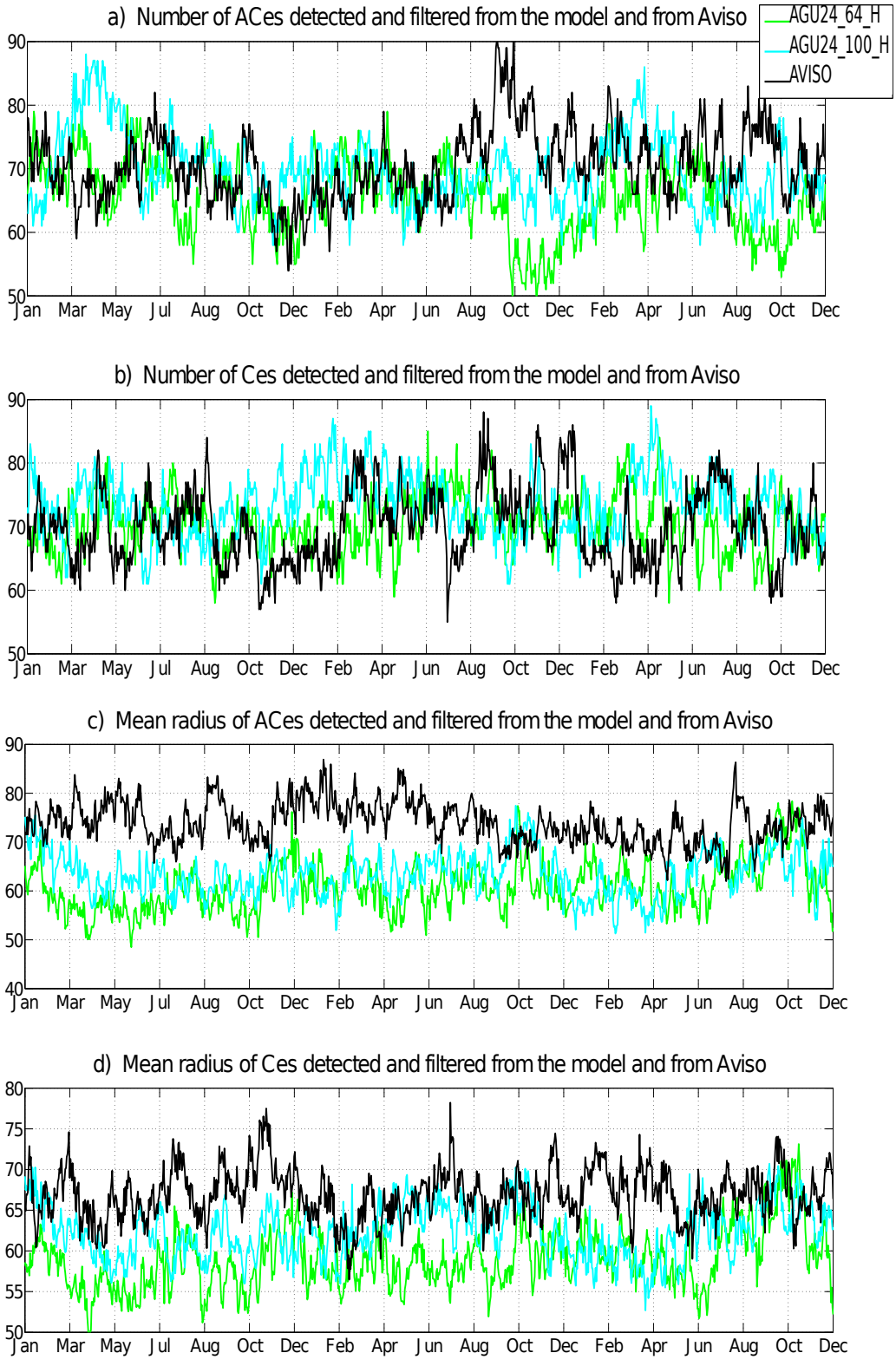

Figure 4.3: Time series of the number of anticyclones (a) and cyclones (b) detected in the highest resolution simulations of the first article (AGU24_64_H and AGU24_100_H) and from AVISO data. The simulated eddies have been filtered as explained in the text. c and d display the same as a and b but for the eddy mean radius.

cyclonic trajectories over the three years of detection, as shown in Figure 4.4, where the trapezoidal sector, used as the formation zone of the tracked eddies, is also displayed. Here we can observe how in our highest resolution simulation we were able to capture the progression of large cyclonic, trapped lee eddies, that propagate downstream, with the Agulhas Current, along the east coast of South-Africa, between 32-22°E and 35-40°S. As concerns the Agulhas Rings, their mean lifetime and pathways in the Southeast Atlantic compare well, for the highest resolution simulation, with the same estimates from AVISO (Figs. 8 and 9 of section 4.2). The slight discrepancies that persist among the two have been explained in the article by a series of limitations due, on one hand, to the coarse resolution of the satellite product, and, on the other, to our numerical setting (forcing at the surface and at the lateral boundaries, the positioning of the open boundaries, etc.).

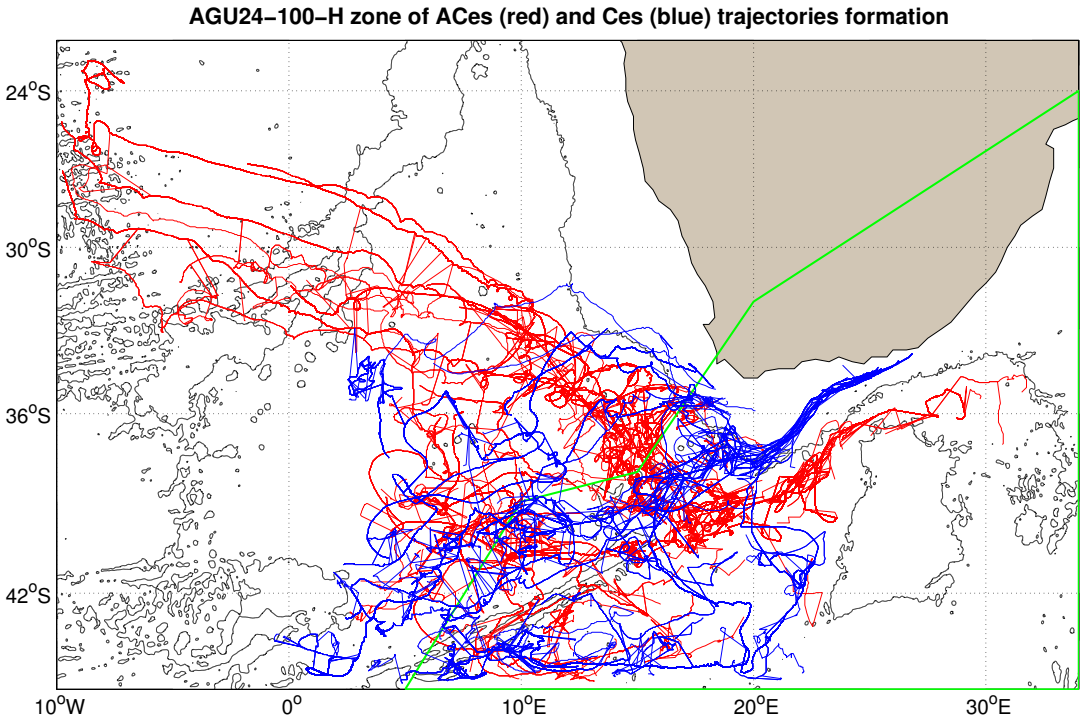

Figure 4.4: Trajectories of the anticyclones (red) and cyclones (blue) detected in AGU24_100_H, whose formation zone is the trapezoidal area delimeted by the green line.

Despite the use of climatological surface forcing in our simulations, the time series of the number of detected eddies and their mean radius show a temporal-dependent behaviour, for both the simulated and observed distributions. However, this seasonal variability differs between the simulations, being more pronounced for the higher horizontal resolution runs (Fig. 11 of section 4.2). For AGU24_100_H, this seasonality is clearly related to

the one of the Ertel potential vorticy anomaly and its vertical terms, as well as to the one of the mixed layer depth and to the first Rossby radius of deformation. Moreover, a seasonal cycle was retrieved also in the spectral curves of the diffusion coefficients of temperature and salinity (Fig. 13 of section 4.2), both at the surface and along the AAWIs layer. Several hypothesis were mentioned in the article in order to explain the seasonal variability of the mesoscale field, but, due to limitations of our current numerical configurations (resolution, forcing, boundaries, etc.), we were not able to thoroughly verify any of them. The results of our submesoscale-resolving, nested solution (presented in Chapter 5 of this manuscript) will highlight how the eddy temporal-dependance is directly linked to the different types of instabilities that develop, in the upper and intermediate layers of the Cape Basin, from the meso-submesoscale interactions according to the analyzed season.

4.1.5 Eddies role in the AAIWs dynamics

In this chapter we will rather focus on the role played by the mesoscale field, as reproduced in our eddy-permitting and -resolving simulations, in the transport and mixing of the local varieties of AAIWs. Observational studies [*You*, 1998, 2002] in the Indian and South-Atlantic oceans have identified a total of four sources of intermediate water masses: AAIW from the Drake Passage (dAAIW); a component of AAIW from the south-Indian Ocean; intermediate water from the Indonesian Seas and from the Red Sea; and a transformation end member of these sources. A later analysis of *You et al.* [2003], performed using a source-water mass mixing scheme, showed that dAAIW was the dominant water mass, even though a significant contribution was given also by the two Indian Ocean sources, via the southern tip of South-Africa.

Here, AAIWs of both Atlantic and Indian origins undergo fairly important changes in water mass characteristics while entering, progressing across and exiting the Cape Basin. These changes occur where the waters flow over strong topographic features, and particularly inside the Cape Basin, where the highly energetic mesoscale and submesoscale dynamics favour an important mixing between the two varieties of intermediate water. The latter statement is supported by in-situ observations that show vertical fine-scale structures along the AAIW depth on profiles located at the edge of eddies [*Arhan et al.*, 2011, *Gladyshev et al.*, 2008, *Piola and Georgi*, 1982]. This suggests that lateral isopycnal mixing develops in the region due to highly non-linear local dynamics, as we will demonstrate in the following chapter. The effect of the regional topography on eddies

and more generally on vertical mixing has not yet been clearly diagnosed and precisely quantified from observations or theoretical process studies, even if it is thought to be important (e.g., [*Jayne et al.*, 2004, *Mauritzen et al.*, 2002, *Sutyrin et al.*, 2011]).

The Cape Basin turbulent mixing of AAIW ultimately results in the distinction of three regional varieties of this water mass: the Atlantic AAIW (A-AAIW), characterized by S $\leq$ 34.2; the Indian AAIW (I-AAIW) with S $\geq$ 34.3 and the Indo-Atlantic intermediate water (IA-AAIW, 34.2 <S <34.3) [*Rusciano et al.*, 2012]. Through the analysis of a sizable Argo database [*Speich et al.*, 2012], *Rusciano et al.* [2012] suggested that different routes are followed in the Cape Basin by these three varieties of AAIWs, all later converging in the Southeast Atlantic. In particular, the numerical Lagrangian analyses of *Rimaud et al.* [2012] showed that I-AAIW flows into the Cape Basin more within eddies, especially within cyclones, than A-AAIW. Their Lagrangian tracking of particles of I-AAIW and A-AAIW showed that changes in the physical properties of both AAIW varieties combine with variability in the Okubo-Weiss parameter, and that the transformations occur mostly in the Cape Basin, where mesoscale activity is known to be strong.

Therefore, even if these studies agree with *You et al.* [2003] that the dominating variety of AAIW in the inter-ocean exchange is the Atlantic one, they underline that its physical properties are highly changed during its journey across the Cape Basin. This confirms *Boebel et al.* [2003] suggestion on considering this basin as an active region with regard to water mass transformation. The same conclusion was reached by *Garzoli and Matano* [2011] in pointing out that, albeit water mass transformation occurs everywhere in the South Atlantic, it is especially intensified in the regions of significant mesoscale activity. The erosion of the thick A-AAIW observed east of 12°E is very likely due to a strong lateral mixing characterizing the Cape Basin, and to the topography that somewhat blocks the passage of the A-AAIW eastward of 12°E [*Arhan et al.*, 2011, *Dencausse et al.*, 2010, 2011, *Faure et al.*, 2011, *Piola and Georgi*, 1982]. Here the turbulent mesoscale and submesoscale dynamic processes allow the Atlantic and Indian varieties to meet, mix with each other, and consequently form the Indo-Atlantic AAIW variety [*Rusciano et al.*, 2012].

In the submitted manuscript presented in section 4.2, we corroborate these findings, providing qualitative evidence that eddies of both signs equally contribute to the mixing and advection of the different varieties of AAIWs in the Southeast Atlantic. By tracing

the T-S profiles, in the AAIWs range, at the centres of all the detected cyclones and anticyclones, we show that, despite differences between the distributions of the various numerical resolutions and in comparison to Argo data, these properties are, in the Cape Basin, relatively homogeneous. Therefore, in line with previous studies [*Boebel et al.*, 2003, *Doglioli et al.*, 2006] we point out that cyclones play an active and significant role as anticyclones in the regional transformation and transport of AAIWs.

The turbulent activity, that distinguishes the Cape Basin at different dynamical scales, explains the complexity involved in producing an accurate quantification of their relative contributions in the inter-ocean exchanges and spreading of the AAIW varieties, as their physical proprieties are rapidly mixed and deviate from the original characteristics [*Boebel et al.*, 2003, *Richardson and Garzoli*, 2003]. A Lagrangian approach, similar to *Rimaud et al.* [2012] and *Doglioli et al.* [2006], but applied to a higher numerical simulation than 1/12°, would help determining to which extent the advection and mixing of the AAIWs varieties are in the Cape Basin related to the passage of the bigger mesoscale eddies or/and to the action of smaller scale features. In this regard, complementary study processes would be recommended to theoretically investigate how the interactions between the various turbulent scales impact the intermediate waters structure and spreading.

4.2 Article "Indo-Atlantic exchange, mesoscale dynamics and Antarctic Intermediate Water"

Indo-Atlantic exchange, mesoscale dynamics and Antarctic Intermediate Water.

Tonia Astrid Capuano[1], Sabrina Speich[2], Xavier Carton[1], Remi Laxenaire[3]

[1]Laboratoire d'Ocanographie Physique et Spatiale, LOPS-UBO, Brest, France

[2]Laboratoire de Meteorologie Dynamique, LMD-IPSL, Ecole Normale Superieure, Paris, France

[3]Laboratoire de Meteorologie Dynamique, UMR 8539 Ecole Polytechnique, ENS, CNRS, Paris, France

Key Points:

- High horizontal and vertical numerical resolutions required to depict the Cape Basin turbulent dynamics
- Key role of the Agulhas eddies in the advection of AAIW properties and associated thermohaline transport.
- The regional mesoscale processes are characterized by a strong seasonality.

Corresponding author: Sabrina Speich, speich@lmd.ens.fr

Abstract

This study evaluates the capability of eddy-permitting regional ocean models to reproduce the interocean exchange south of Africa. In this highly turbulent region, we show that the vertical structure of the horizontal flows need to be appropriately resolved to realistically advect thermocline water-masses into the South Atlantic. Our results point out that a grid-spacing of 1/24° on the horizontal and 50 m on the vertical are required to account for a correct transport of surface and subsurface water-masses properties and their in-route transformation by mixing. Preliminary Lagrangian analyses highlight the primary role of the upper-ocean mesoscale eddies on their transport and fate, with a particular focus on the Antarctic Intermediate Waters (AAIWs) layer dynamics and characteristics. We evaluate the numerical results against observations (AVISO data and Argo floats profiles). Modelled and observed eddies were examined in number, polarity, size, trajectory and for their contribution to AAIW properties. A clear asymmetry, in number and radius, emerges between cyclones and anticyclones. The high resolution simulation was the most energetic, with more abundant and smaller structures than those detected in AVISO. However, eddy statistics compare reasonably well in terms of mean pathways when restricted to Agulhas Rings, which are on average quasi-Gaussian in shape. Regionally, the Ertel potential vorticity anomaly is marked at the surface by a temporal variability with winter intensification, directly reflected in the seasonal cycle of the eddies number. Noting the growth of the baroclinic Rossby radius in winter, this suggests baroclinic processes as essential for these eddies generation.

1 INTRODUCTION

South of Africa is the open gateway for the global Meridional Overturning Circulation (MOC) that provides the export channel for the North Atlantic Deep Water (NADW) to the global ocean and the counterbalancing water transport to the North Atlantic importing heat and salt from the Indian and Pacific Oceans [*Gordon et al.*, 1992; *Speich et al.*, 2007]. This region is influenced by the largest levels of turbulence observed in the world ocean, being the confluence area of intense large-scale currents: the eastward flowing Antarctic Circumpolar Current (ACC), the South-Atlantic Current (SAC) and the Agulhas Current (AC), all later converging through the Cape Basin into the Benguela Current [*Gordon et al.*, 1992, 2010].

The AC flows south and then westward around the southern-east rim of Africa, with an annual mean volume flux to the sea bottom at 30°E of 75 Sv [*Bryden and Beal*, 2001]. South of Africa (15-20°E) the Agulhas waters curl back to the Indian Ocean, forming the Agulhas

Retroflection, whose significant role does not end with its momentary loop into the southeast corner of the South Atlantic: there is considerable transfer of Indian Ocean water into the upper kilometer of the Atlantic, often referred to as the Agulhas leakage [*Lutjeharms*, 2006].

Pioneering modeling studies have revealed the potential impact of this leakage on the strength and stability of the Atlantic MOC (AMOC) [*Weijer et al.*, 1999; *Biastoch et al.*, 2008] and the global-scale oceanic circulation associated to it. This impact is strongly dependent on how the characteristics (temperature, salinity and potential vorticity) of the various waters, leaking from the Indian Ocean to the Atlantic, mix and blend in the Cape Basin through jets, meanders, eddies and filaments, determining the contribution of the leakage in the broader scale MOC. There is mounting, scientific evidence that these local, meso- and submesoscale interactions could actually constitute the major link between the South-Atlantic Ocean and the global MOC [*Biastoch et al.*, 2008]. In particular, a highly energetic field of coexisting anticyclonic and cyclonic eddies has been documented: Agulhas Rings of typically 70-200 km diameter have been observed to merge, split, deform, and to reconnect to the Agulhas Retroflection [*Boebel et al.*, 2003]. Concomitant, slightly smaller cyclones seem to drift across the northwestward migration path of the Agulhas Rings [*Boebel et al.*, 2003; *Morrow et al.*, 2004; *Chelton et al.*, 2011]. These cyclones, with typical diameters of 60-120 km, are formed within the Cape Basin along the African shelf, inshore of the AC, and in the subantarctic region south of Africa [*Boebel et al.*, 2003]. Oceanographers have for long time looked at this region as an area where *"...isolated Agulhas Rings embedded in a sluggish Benguela Drift..."*. This concept has been recently revisited by *Boebel et al.* [2003], who proposed to rename the Cape Basin as Cape Cauldron to indicate the highly energetic field of coexisting anticyclonic and cyclonic eddies, which continuously interact with each other, in a general environment of vigorous stirring and mixing. In addition, *Matano and Beier* [2003] have suggested a subsurface intensification of both cyclones and anticyclones in this region, meaning that their dynamical signature would be able to influence also the thermohaline properties of water masses at depth [*Schmid et al.*, 2003].

The Cape Basin is actually so efficient in terms of mixing that Antarctic Intermediate Water (AAIW), inflowing from the Indian and South-Atlantic oceans, gets locally modified in three regional varieties: Atlantic AAIW (A-AAIW, characterized by $S \leq 34.2$), Indian AAIW (I-AAIW, $S \geq 34.3$), and Indo-Atlantic intermediate water (IA-AAIW, $34.2 < S < 34.3$) [*Rusciano et al.*, 2012]. Modeling results associated to Lagrangian diagnostics confirmed that local dynamics induce an important mixing of remote AAIW varieties within the Cape Basin [*Rimaud et al.*, 2012]. However, this numerical study, as well as any other focusing on this re-

gion, were performed at a maximum horizontal grid spacing of 1/12°, that is at about 7.3 km, an insufficient resolution to correctly reproduce the mesoscale dynamics [*Levy et al.*, 2010]. Indeed, the recent work of *Soufflet et al.* [2016] showed that, in the case of the Regional Ocean Model System (ROMS) used here, the effective resolution is approximately equal to $7\Delta x$ (being Δx the horizontal gridpoint spacing of the model), since dynamics of smaller lengthscales appear to be unsupported by the model simulations. This means that for numerical simulations at 1/12°, the effective horizontal resolution is closed to 50 km rather than 8. Given that the local internal radius of deformation is about 30 km [*Chelton et al.*, 1998], a model resolution two or three times higher than 1/12° is required to improve the reliability of the simulated mesoscale field, even if the simulation of a realistic energy cascade and processes spectrum would require a much higher resolution to resolve the submesoscale dynamics [*Capet et al.*, 2008].

In this manuscript we focus on how the Indo-Atlantic interocean exchange and the Cape Basin dynamics improve in a regional simulation by including smaller spatial scales, in order to better resolve the strongly non-linear processes and qualify their impact on the thermohaline structure of AAIW. Given that the Cape Basin mesoscale eddies represent the principal means of transport of thermocline and intermediate waters between the Indian and Atlantic ocean, our main scientific objectives will be: 1) to quantitavely assess how much the representation of the local thermohaline distribution and energetics improves, at the surface and in the subsurface, when increasing the model resolution, both vertically and horizontally; 2) to statistically characterize the modelled mesoscale field in comparison to altimetric gridded product; 3) to investigate if a specific temporal variability distinguishes the regional mesoscale field and 4) evaluate their contribution to the advection of the AAIW T-S properties in our study region. Each of these questions will be discussed in a dedicated subsection of this article.

In the following, we will first introduce, in section 2, the methods we have implemented for addressing our study objectives, as well as the dataset of in-situ and satellite observations used in conjunction with our model output. In section 3 we will first present an extensive comparison of the numerical simulations, in terms of their skill in reproducing both the observed thermohaline properties and dynamics. We will then describe the analyses of the mesoscale eddies sensitivity to changes in the model resolution, providing evidence of a temporal-dependent behavior and assessing their impact on the watermass properties, mixing and transport. In the last section, we will summarize the results and draw the major conclusions of this study.

2 DATA AND METHODS

2.1 The Ocean Model

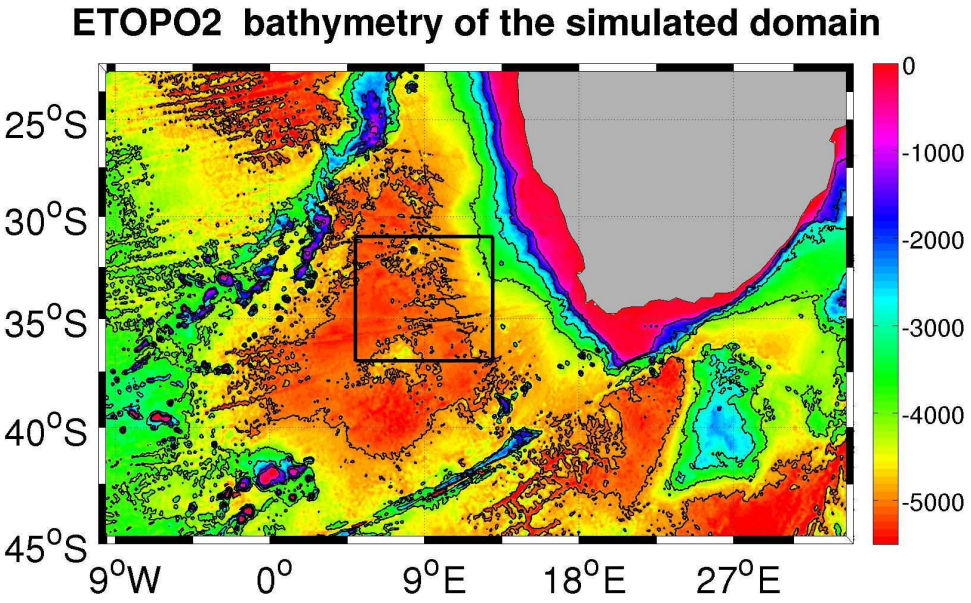

Figure 1. The geographical domain we used to implement the ROMS regional simulations. The color shading displays the bottom topography [m] from the Etopo2 dataset [*Smith and Sandwell*, 1997]. The square represents the box in the Cape Basin where several analysis were carried out.

The methodology chosen in this work was to run realistic numerical simulations of the ocean circulation around Southern Africa, using the UCLA-IRD version of ROMS (url: http://www.romsagrif.org/), which is a free surface, primitive-equation ocean model. We refer to *Shchepetkin and McWilliams* [2005], for a detailed description of the numerical model, even though it is worth mentioning here a few technical characteristics that have important effects on the model capability of properly reproducing coastal dynamics. ROMS uses a terrain-following vertical coordinate system that allows a more realistic representation of the local bathymetry, compared to z-levels models. This is a key factor when studying an oceanic region like the Cape Basin, where the ocean topography has been shown to be very influential on the interocean exchanges [*Speich et al.*, 2006]. The bathymetry (h) used in this model has been filtered in order to keep a slope parameter 'r' (= $\Delta h/2h$, ratio of the difference in depth to twice the depth) smaller than a given value (0.25 in our case). This topographic filtering ensures the avoidance of eventual incon-

sistencies which could occur in the approximation of the horizontal pressure gradient terms, when these are transformed in sigma-coordinates [*Shchepetkin and McWilliams*, 2003]. In addition, the ROMS grid is isotropic and does not introduce any asymmetry in the horizontal dissipation of turbulence, allowing a fair representation of mesoscale dynamics [*Speich et al.*, 2006].

Our simulated domain extends from 10°W to 34°E and from 22°S to 45°S (Figure 1). The five simulations under examination in this paper are listed in Table 1 and were designed using different horizontal and vertical resolutions: from 1/12° to 1/24°, against 32, 64 and 100 vertical levels, in order to increasingly better resolve the baroclinic modes of the study region, not only in the horizontal but also along the water column [*Stewart et al.*, 2017]. To better depict the characteristics of the local water masses at depth, we performed changes in the model vertical stretching parameters, that control the distribution of sigma-levels, in our last three simulations (namely AGU_12_64_H, AGU_24_64_H and AGU_24_100_H, dubbed with 'H' for homogeneous). This allows the vertical levels to be more uniformly spaced, instead of being concentrated in the upper layers (default model version). Moreover, in the highest resolution simulation (AGU24_100_H) we also made use of a recently-introduced function optimizing the sigma-levels, designed to impose a more homogeneous distribution of these levels, in respect to its original definition [*Lemarie et al.*, 2012]. This new function acts to smooth the tracer fields (T and S) and to filter out the slight, spurious numerical noise that we experimented in our first four runs, due to the use of the advection scheme rotated along the isopycnals (RSUP3) [*Marchesiello et al.*, 2009]. The choice of these numerical options in the vertical distribution of the sigma-levels, enabled us to gain a significant improvement in the representation of the isopycnal interfaces within the water masses, as we will further discuss in section 3.

To easily compare the different configurations of Table 1, we used the following datasets and conditions to create the mesh grid, the forcings at the open boundaries and the initial state:

-Bathymetry (h) is derived from the ETOPO2 dataset [*Smith and Sandwell*, 1997] and smoothed under the constraint that 'r' <0.25 with the minimum depth represented at 10m;

-At the surface, wind forcing, heat and fresh waters sources were extracted from the COADS climatology [*Da Silva et al.*, 1994], in accordance with our focus on the investigation of intrinsic, oceanic variability;

-At the lateral open boundaries, an active, implicit, upstream biased radiation condition connected the model solution to the surrounding ocean [*Marchesiello et al.*, 2001];

-The ocean was set initially at rest, with temperature and salinity fields taken from the World Ocean Atlas 2009 dataset (WOA09) [*Locarnini et al.*, 2010] at 1° of resolution.

All the simulations were run for five years and the steady state was statistically achieved after a spin-up period of roughly one year, after which the surface-averaged kinetic energy approached a stable level and started to exhibit fluctuations. At the end of this short spin-up, the volume integrated temperature and salinity did not present any significant temporal drift.

In order to evaluate the effect of other background values, like the horizontal diffusion or the bottom drag coefficient, as well as the topographically influent slope parameter 'r', several simulations were run at very low resolution (1/4°). This allowed us to test the sensitivity of the model to slight alterations in its initial parameters and to subsequently address the choice of the best configuration to use for running higher resolution simulations. It will be on these latter runs that our presentation of results and discussion will focus hereafter. The rest of this section will describe the observations datasets used to validate our numerical configurations, the eddy detection and tracking algorithm used to assess the simulated mesoscale eddies and the potential vorticity budget applied to investigate the mesoscale dynamics.

Table 1. Table summarising the technical features of the five simulations here presented. The 5^{th} and 7^{th} columns show the RMSE values of the difference between each simulation and Argo data in terms of the salinity distribution of Figure 3 and the Q estimate of Figure 4. The values of the 6^{th} column represent the difference in potential density (Σ) between its mean value at a given level and the following one for each run.

Name of the simulation	Horizontal Resolution	Sigma levels	Sigma levels Distribution	S rmse	Σ difference	Q rmse
1/12_32z	1/12°,~7.3km	32	Surface-stretched	0.065	0.046	0.074
1/12_64z	1/12°,~7.3km	64	Surface-stretched	0.064	0.038	0.062
1/12_64_H	1/12°,~7.3km	64	Homogeneously stretched	0.053	0.026	0.055
1/24_64_H	1/24°,~3.6km	64	Homogeneously stretched	0.037	0.021	0.048
1/24_100_H	1/24°,~3.6km	100	Homogeneously stretched	0.032	0.016	0.041

2.2 Observational data sets for model comparison

12 years of in-situ observations (from the beginning of December 2000 to the end of December 2012) from the Argo program- a global array of free-drifting profiling floats that measure temperature and salinity within the upper 2000 m of the ocean- were retrieved from the Coriolis Data Center (url: http://www.coriolis.eu.org). For the comparison with the model reproduction of AAIW, we used the gridded version of this dataset as created by *Rusciano et al.* [2012], where data were grouped and averaged in 1° longitude by 1° latitude boxes within the simulated domain. While, for the comparison of the modelled θ-S and available potential energy distributions at depth, the raw data of the profilers were employed, using exclusively those in the delayed mode as their salinity has been adjusted by comparison with other measurements. Only data with control quality flags 1 and 2, that refer to 'good observation' and 'probably good observation', were kept.

We also took advantage of the daily gridded, altimetry data, produced by Ssalto/Duacs and distributed by Aviso, with support from CNES, after being interpolated over a homogeneous 1/4° grid. These data were used to validate the energy content of our simulations at the surface and compare the results of the eddy detection of our model output with the same results from the Aviso product. The latter consists of 16 years (from January 2000 to December 2015) of altimetric retrieved observations and represents a multimission product, deriving from the combination of all satellite data available at one time (Jason-1, Envisat, GFO, ERS-1, ERS-2 and Topex/Poseidon). We made use of the latest version of the AVISO Ssalto-Duacs altimetric product [*Duacs/AVISO*, 2014].

2.3 Algorithm of eddy detection and tracking

For localizing eddies at the surface and exploring the differences in shape, number and size between the five simulations, along with those in the characteristics of the intermediate waters trapped within these structures, we applied to our model outputs the detection and tracking methodology of *Chaigneau et al.* [2008, 2011], further developed by *Pegliasco et al.* [2015] and more recently extended by *Laxenaire et al.* [Submitted]. Their approach is similar to the one of *Chelton et al.* [2011] for identifying and extracting eddies from the geophysical turbulent flow, since they are both based on geometric criteria, in opposition to other methods based on physical properties. The original method of *Chaigneau et al.* [2008] hinges on the search of the outermost closed contour of Sea Level Anomaly (SLA) around extremes of AVISO Ssalto-Duacs Mapped SLA [*Ducet et al.*, 2000; *Pascual et al.*, 2006]. In the case of our simulations,

we used a set of Sea Surface Height (SSH) maps, taken as daily snapshots from the last three years of each of our simulations, in order to allow them to reach a full statistical adjustment.

The first step of the analysis consists in the detection of possible centers of cyclones (anticyclones) that are associated with local minima (maxima) of SSH. The detection of the extrema is done separately for the minima and maxima, with a moving window set to 1°x 1° width in this study. In a second step, extrema centered in 6°x 6° squares, where closed contours of SSH have been identified, are individually studied. The outermost contours around minima (maxima), containing only one local extremum, are classified as the outer limit of each eddy. This limit is used to define the eddy amplitude, which corresponds to the modulus of the SSH difference between the center and the outermost contours. Identified extrema associated with amplitude lower than 1 cm are rejected. This allows to prevent the separation of one large eddy into two or more smaller features at one given time step.

Another particularity of this technique worth mentioning is that the detected contours of all the eddies are stored and can be used later to define their trajectories. Some basic properties for each eddy are computed such as their amplitude, area and equivalent radius for a circle. Beside the restriction applied on the eddies amplitude, a temporal filter is used after the completion of the eddies tracking. The latter is based on the superimposition of contours between 2 successive days and enables us to define trajectories of both cyclones and anticyclones. Here a minimum lifetime of 7 days is set for all trajectories, thus all the eddies which last less than 7 days before a merging or after a splitting event are also removed. By these two criteria, we avoid spurious detections and the remaining structures are classified as either cyclonic or anticyclonic. For the latter, we have estimated some of their statistical properties (eg., number, radius, shape and trajectory) and looked at the AAIW's characteristics within the eddies crossing the Cape Basin.

2.4 Potential Vorticity

The Ertel Potential Vorticity [*Ertel*, 1942] has the following mathematical form:

$$EPV = -\frac{1}{\rho}\left((f+\omega)\frac{\partial\rho}{\partial z} - (\frac{\partial v}{\partial z}\frac{\partial\rho}{\partial x}) + (\frac{\partial u}{\partial z}\frac{\partial\rho}{\partial y})\right) \quad (1)$$

where ρ is the potential density, f is the Coriolis parameter (f= $2\Omega\sin\phi$), ω is the vertical component of the relative vorticity ($\partial v/\partial x$-$\partial u/\partial y$), $\partial\rho/\partial$z represents the stratification, which combined all together constitute the vertical components of the Ertel PV, namely the sum of the relative vorticity (ω) and the vortex stretching (f*$\partial\rho/\partial z$) terms. The last two terms

of the RHS are the sum of the horizontal components of the Ertel PV in the x- and y-directions, where the terms of the zonal and meridional shear ($\partial u/\partial z$ and $\partial v/\partial z$) are multiplied by the lateral gradients of density ($\partial\rho/\partial x$ and $\partial\rho/\partial y$).

Potential vorticity (PV) analyses provide essential information on mesoscale flows. *Marchesiello et al.* [2003] showed that significant departures from the Sverdrup balance occur in the California Current System and are mainly due to the effect of the PV vertical terms. In our area of interest, given the regional high level of turbulence characterizing the Agulhas System, we expect the PV vertical terms to be important. Moreover, PV analyses can help distinguish the origin of water masses within the Agulhas System (e.g. AAIW is characterized by a relative PV maximum, [*Talley*, 1996]).

The Ertel PV (EPV hereafter) is adiabatically conserved along isopycnals in a Lagrangian sense, meaning that it can only be changed by diabatic or frictional processes. The EPV is thus an useful tracer for the identification of filaments, meanders, smaller vortices and fronts and looking separately at each of its components allows to better apprehend their scales and intensity. At large scale, these terms are quite negligible, if taken separately, but at mesoscale or smaller scales, their magnitude becomes relevant, above all in presence of fronts. Since they are also related to the development of instabilities, quantifying their respective intensity and spatio-temporal distribution could help shedding some light on these non-linear processes.

In the following section, we will describe the horizontal distributions of the vortex stretching (Q hereafter) and the relative vorticity (ω) terms, as means of further validating and discriminating our simulations; time series of the EPV anomaly and its vertical components will be discussed in relation to eddies temporal trends.

3 RESULTS

To evaluate the realism of our ROMS simulations and to qualify the impact of the mesoscale processes on the regional dynamics, we have undertaken various comparisons with different data sets. Even though the focus of our study is on the dynamics of intermediate waters, we have first validated our numerical simulations against surface observations (satellite and in-situ data); indeed, subsurface observations are still very sparse.

3.1 Surface dynamics and thermohaline structure

As expected from previous high-resolution numerical studies [*Capet et al.*, 2008; *Molemaker et al.*, 2015; *Rosso et al.*, 2014], we observe a gradual improvement in the way our model

reproduces the main features and characteristics of the surface circulation, in terms of the T-S variables and modelled dynamics, as we increase the vertical and horizontal resolutions (Supplement Figures 1 and 2). All the simulations are able to capture the large-scale features of the greater Agulhas System. However, the two higher resolution runs (at 1/24°) exhibit surface temperature and height fields with closer agreement to the observations, capturing in particular the higher values shown in the observations over the Agulhas Plateau. Concerning the alongshore Agulhas Current temperature, salinity and energy inflow from the Indian Ocean into the Southeast Atlantic, the lowest horizontal resolution simulations (AGU12_32, AGU12_64 and AGU12_64_H) tend to overestimate the averages of the analyzed surface variables, especially in areas close to the South-African west coast and around the Agulhas Retroflection.

Noteworthy are also the differences discernible between the numerical experiments having a homogeneous distribution of the vertical levels (AGU12_64_H, AGU24_64_H, and _100_H) with those characterized by a higher vertical resolution in the upper layers (AGU12_32 and AGU12_64). The homogeneous distribution of vertical levels increases the vertical resolution at depth. This induces a reduction in the discrepancies between the model surface fields and the observational products, attenuating those warm biases event at the lowest horizontal resolution. While this improvement is not major if only the number of vertical levels is increased (e.g., AGU12_32 versus AGU12_64), as this increase concerns only the upper 200m of the ocean, it indicates that the vertical resolution of the model is as important as the horizontal one to reproduce more realistic surface dynamics and thermohaline distributions.

3.2 Water masses properties at depth

Figure 2 shows the Potential Temperature-Salinity (θ-S) diagrams for the whole domain and for waters at intermediate and deep levels (i.e., θ <10°C), where every dot represents the θ-S values extracted at each grid point of the model. The values are scattered in red colour for the lowest resolution simulation (AGU12_32, Fig. 2a) and in cyan for the highest resolution one (AGU24_100_H, Fig. 2b). The overlaid blue curves represent the mean (continuous line) and standard deviation (dotted lines) values from Argo data.

These diagrams show the main water masses circulating, at depth, within the greater Agulhas Current System and Cape Basin. The highest values of θ and S correspond to the warmer and more saline waters inflowing from the Indian Ocean; the centre of the diagram is occupied by intermediate waters (AAIW of both Indian and Atlantic origins, see *Rusciano et al.* [2012]), while the lowest part of the plot indicates the presence of deep and bottom waters (NADW,

CDW and modified AABW; these waters appear only in the model data as Argo profiles do not exceed 2000 dbar), characterized by higher values of S and lower θ than AAIW.

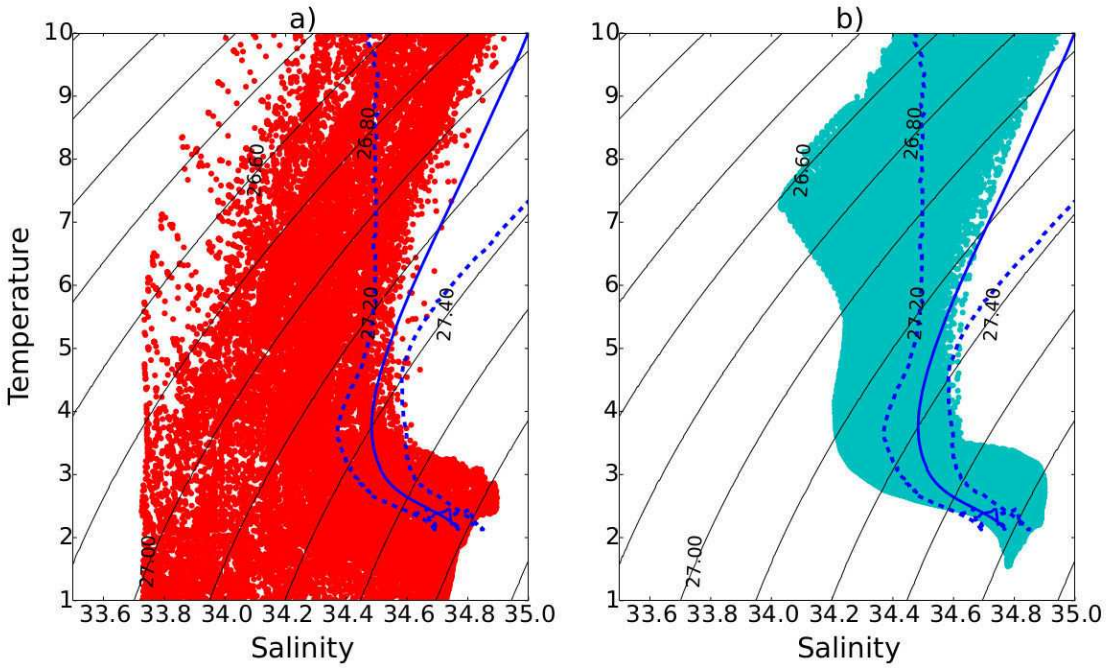

Figure 2. The panel shows the θ-S distribution for (a) the lowest resolution simulation (AGU12_32) and for (b) the highest resoultion (AGU24_100_H). In both diagrams, are also presented the θ-S mean and standard deviation (in blue, continuous and dotted lines) from Argo data for the whole simulated domain for subsurface and deep waters (defined as those having a value of θ <10°C).

The simulations with the lowest horizontal and vertical resolutions (AGU12_32, in Fig. 2a, and AGU12_64) show, for all the water masses, a wider θ-S range than the higher resolution solutions and observations. The simulation with increased vertical resolution in the subsurface and deep layers (AGU12_64_H, not shown here) presents a behavior closer to observations than the two previous experiments. In fact, the differences between AGU12_64 and AGU12_64_H is larger compared to that between AGU12_32 and AGU12_64, which almost completely overlap (not shown). The latter are more diffusive, leading to values of θ and S very different from those measured by Argo or found in the higher vertical resolution simulations. In particular, their salinity minimum, intersecting the 27.05 isopycnal, is of ∼33.7 psu.

These values differ from the regional observed AAIW minimum of salinity (around 34.3 psu) and from the typical range of potential density anomaly (27.2-27.6 kg/m^3) of Argo data.

The water masses properties in the whole set of simulations with homogeneous vertical levels distribution are better preserved, even though a discrepancy persists between the thermohaline distributions of these numerical experiments and the one from Argo, especially at the level of the central waters (Fig. 2b). This shift in θ-S is probably to ascribe to the lack of more realistic, synoptic forcings at the lateral and surface boundaries of our simulations. However, since the focus of our study is on the full range of watermasses accomplishing the Indo-Atlantic exchange, and particularly on AAIW, we can affirm that a reasonable agreement between water masses properties in AGU24_100_H and in observations has been achieved for these layers. Such a modeling improvement is confirmed by the estimation of the root mean squared error (RMSE) of the difference in mean salinity between each simulation output and Argo, whose value slowly reduces from AGU12_32 to AGU24_100_H (see fifth column of Table 1).

By augmenting the number of sigma levels and by homogenizing their vertical distribution, also the difference in potential density between its mean value at a given level and the following one substantially decreased from the lowest to the highest resolution simulation (see sixth column of Table 1). Thus, the model improves in reproducing the vertical thermohaline structure of the water column. This is true for the simulation at the lowest horizontal resolution (AGU12_64_H) and it is even more remarkable at higher, horizontal and vertical resolutions (AGU24_64_H and AGU24_100_H). Both aspects are therefore essential for a correct representation of thermocline water masses, and, in particular of AAIW.

3.3 Agulhas leakage and related AAIW characteristics

To acquire a more quantitative insight on the model capability of capturing the AAIW characteristics and dynamics, we carried out various analyses along the 27.2 isopycnal. The latter constitutes the typical potential density surface for this watermass in the Southwest Indian and Southeast Atlantic oceans [*Reid*, 1989; *Piola and Gordon*, 1989; *Talley*, 1996].

Figure 4 displays the linear vortex stretching term (Q) in the EPV (first term on the RHS of Eq.1), computed from Argo data (Fig. 3a) and estimated averaging daily means over the last three years of each simulation (Figs. 3b-f). The Argo climatology shows the already documented regional pattern for the AAIW Q: a maximum characterizing the Agulhas Current system and a high-Q tongue originating from the Agulhas Retroflection and progressing northwestward across the Cape Basin, after undergoing a sharp transition due to the local intense mixing of I-AAIW with A-AAIW [*Talley*, 1996; *Rusciano et al.*, 2012]. Only the simulations at 1/24° (Figs. 3e and 3f) correctly represent such a behaviour, while the lower resolution

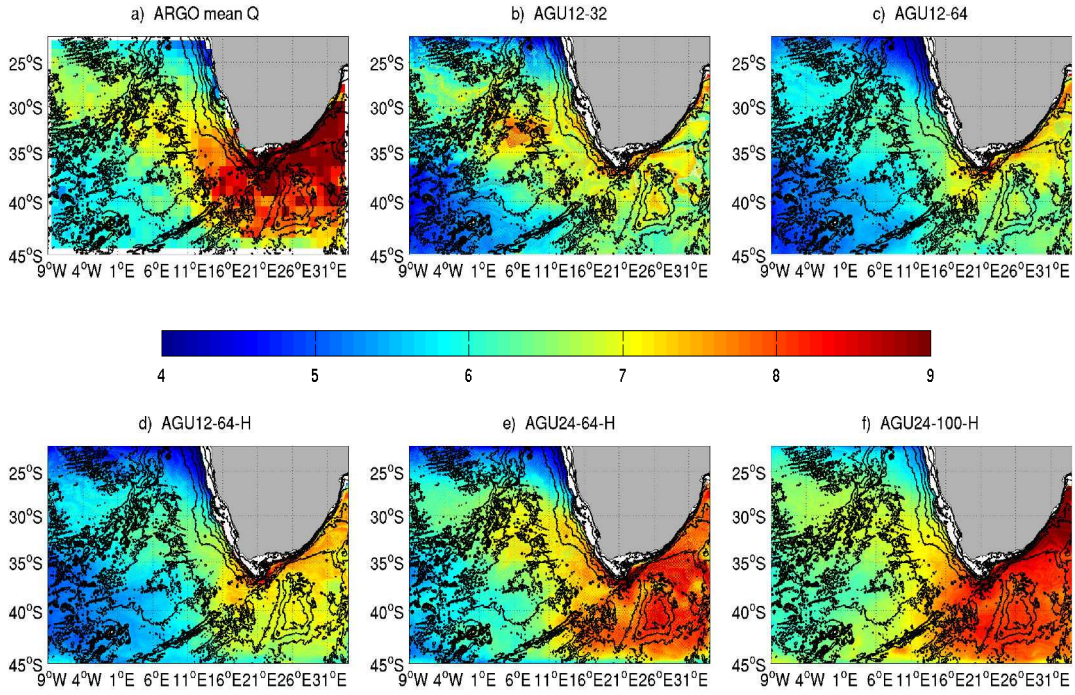

Figure 3. The panel shows the average of the linear vortex stretching term (Q, [$m^{-1}s^{-1}$ x 10^{-11}]) extracted along the 27.2 isopycnal for (a) the Argo climatology and the model simulations (b-f). Black contours represent the -5000, -4000, -3000, -2000, -1000, -500, -200, -100 m isobaths from the Etopo2 dataset [*Smith and Sandwell*, 1997].

Confidential manuscript submitted to *JGR-Oceans*

simulations (AGU12_32 and AGU_12_64, Fig. 3b and c) do not show a contrast in Q between the two oceans nor a maximum for the Agulhas Current system AAIW. The transition in Q starts to appear in AGU12_64_H (Fig. 3d) and it gains in realism in AGU24_64_H and AGU24_100_H. This improvement with resolution has been quantified through the RMSE of the difference in Q between the model estimates and Argo for each run (see seventh column of Table 1).

These results emphasize the model capability at the highest resolutions to correctly reproduce the regional stratification of AAIW, as well as their advection and mixing. In this regard, a sufficient vertical resolution at depth is mandatory to resolve the non-linear dynamics of the Agulhas Retroflection and leakage. The more viscous dynamical behavior of the lowest resolution simulations and their vertical inadequacy to realistically depict the watermasses characteristics lead to the incorrect representation, transport and mixing of T-S properties between the Indian and the Atlantic oceans. In fact, an appropriate increase of the vertical resolution complements the resolution capabilities of the horizontal grid [*Stewart et al.*, 2017]. *Barnier et al.* [1991] have indeed demonstrated that models at coarse vertical resolutions fail to reproduce baroclinic modes higher than the first two; albeit these high modes have low kinetic energy content, they play a catalytic role in the eddy-driven circulation. In the next we will thus analyse the effects of our model resolutions on the simulated mesoscale dynamics.

3.4 Energy content of the mesoscale eddy field

Here we focus on eddy energy budgets to quantitatively assess the way in which our simulations picture the regional mesoscale processes, as they play a leading role in regulating the Indo-Atlantic exchange. The eddy kinetic energy (EKE) filed has been widely observed with the global coverage of satellite altimetry measurements and we use the root-mean-square (RMS) of the SSH as a proxy of its surface distribution. Figure 4 displays the time-mean value of EKE from satellite data (Fig. 4a) and from our 5 simulations (Figs. 4b to 4f), computed by subtracting to its value at each grid point the spatio-temporal average over the whole domain. Both, AVISO and the modelled distributions of SSH RMS show low values (about 0.05-0.1 $m^2 s^{-1}$) offshore and along the northwestern coast of southern Africa, and high values (0.15-0.3 $m^2 s^{-1}$) at the Agulhas Retroflection and in the southern Cape Basin (roughly west of 10°E). This corresponds to the intense mesoscale activity driven by Agulhas eddies shed by the Agulhas Current system and found along the South African continental slope. While the spatial pattern of the modelled EKE agrees well with AVISO, its magnitude is generally higher than the

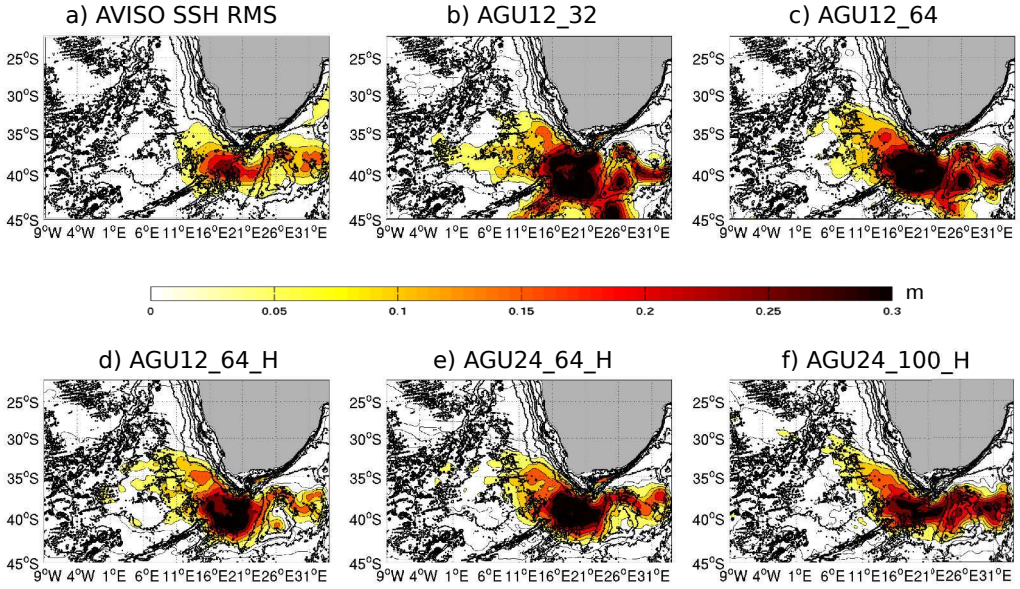

Figure 4. The root-mean square of the mean Sea Surface Height [m] for (a) the AVISO satellite altimetry gridded product and for the model simulations (b-f). The bottom topography is shown by the black lines tracing the -5000, -4000, -3000, -2000, -1000, -500, -200, -100 m isobaths from the Etopo2 dataset [*Smith and Sandwell*, 1997].

Confidential manuscript submitted to *JGR-Oceans*

one observed. This bias is greatest near the Agulhas Retroflection and along the shelf downstream; it could be ascribed, on one hand, to the satellite inability to capture near-shore dynamics and to its coarse resolution, preventing the observation of the smallest mesoscale structures. On the other hand, the model bias in EKE could be due to its tendency to overestimate the Agulhas leakage, causing an enhanced horizontal gradient of density structure between the shelf and offshore, and increasing local instabilities near the shelf-edge [*Rubio et al.*, 2009].

The high degree of turbulence in all the simulations extends from the surface down to intermediate layers. Indeed, most eddies have a deep, dynamical influence in the ocean interior. Therefore, changes in their surface structure have been observed to regionally affect also the energetics and thermohaline properties of waters at intermediate depths [*Schmid et al.*, 2003]. The snapshots of the vertical component of relative vorticity (ω), computed along the 27.2 isopycnal, reveal the scales that spontaneously develop at the AAIW level (Supplement Figure 3). Every simulation shows the main features of the regional turbulence and its characteristic scales: mesoscale eddies of both signs, meanders and filaments form in all runs, spatially concentrating around the Agulhas Retroflection area, in the Cape Basin and along the main topographic features of the central and south-western parts of the domain. Even though all the simulations show similar patterns of ω, their spatial scales decrease, they become more localised and finer structures are more recurrent, as the model resolution increases both horizontally and vertically. This clearly appears also in Figure 4.

To gain more insight on the level of simulated eddy energy in comparison with observations, we have quantified the Eddy Avalaible Potential Energy ($EAPE = -\frac{g}{2\rho_0}\overline{\zeta'\rho'}$, where ζ' is the isopycnal displacement and ρ' is the associated density anomaly) [*Roullet et al.*, 2014] along the 27.2 isopycnal. Here we have slightly modified the EAPE formulation from the original version of *Roullet et al.* [2014] by replacing the virtual density with potential density and including more recent Argo vertical profiles (up to July 2015). EAPE can be considered a proxy of the turbulent state of the ocean interior since its variations are due to the vertical displacement and tilting of the isopycnals [*Roullet et al.*, 2014]. The EAPE distribution and magnitude are comparable to those of EKE as, in the quasi-geostrophic framework, an equivalence between EAPE and EKE stems from the hypothesis of 3D isotropy of developed turbulence (comparable magnitudes of ω and Q) [*Roullet et al.*, 2014]. Hence, EAPE can be usefully computed in models and compared to observations in order to validate the energy content of the ocean also at depth, complementing the surface information provided by EKE estimates.

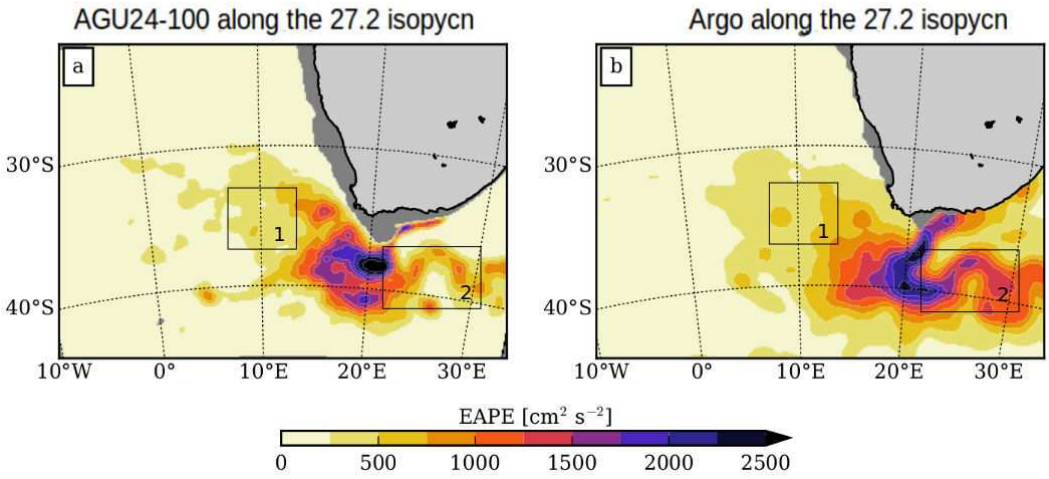

Figure 5. Distributions of Eddy Avalaible Potential Energy along the 27.2 isopycnal, comparing the mean estimate from our highest resolutions simulation (AGU24_100_H, a) and the one from Argo data (b). The black boxes (1 and 2) represent particular areas discussed in the text.

In Figure 5 are presented the 27.2 isopycnal EAPE distributions for (a) the highest resolution simulation (AGU24_100_H), and (b) for Argo data. The modelled EAPE distribution compares relatively well with Argo estimate at the AAIW level, particularly within the region of the Cape Basin (box 1 of Figure 5) and less so east of the Retroflection (box 2 of Figure 5). This difference could be partly due to the absence of synoptic variability in the model boundary conditions (at the surface and lateral boundaries). It could also be explained by the position of the easternmost boundary of the domain, likely positioned too close to the Retroflection area to correctly reproduce the energetics and dynamics of the AC System that depend on the Agulhas upstream mesoscale dynamics [*Biastoch et al.*, 2008]. Instead, west of the Retroflection, within the Agulhas rings corridor, the modelled EAPE values and shape better agree with observations, allowing us to validate the energy content of this simulation also at depth and to adquire a hint on the turbulence level characterising the Cape Basin intermediate layers.

3.5 Mesoscale Eddies Statistics

This subsection aims to statistically describe the geometrical and dynamical characteristics of the simulated eddies. In order to do so, we implemented in our different simulations the eddy-detection algorithm of *Laxenaire et al.* [Submitted]. This enabled us to estimate the number, sign, size, amplitude and mean trajectory of all the simulated mesoscale eddies and

to compare them to the equivalent estimates from altimetry. It is nowadays known that due to the limited resolution and coarse interpolation processing of the satellite products, these observations are only able to capture the largest mesoscale structures. In fact, as recently shown by *Keating and Smith* [2015], extant satellite altimetry products struggle to resolve scales within the 10-50 km range and below. Therefore, in order to render our eddy detection results as comparable as possible to the ones from AVISO, we have filtered out all the modelled mesoscale structures whose radius was equal or smaller than 30 km.

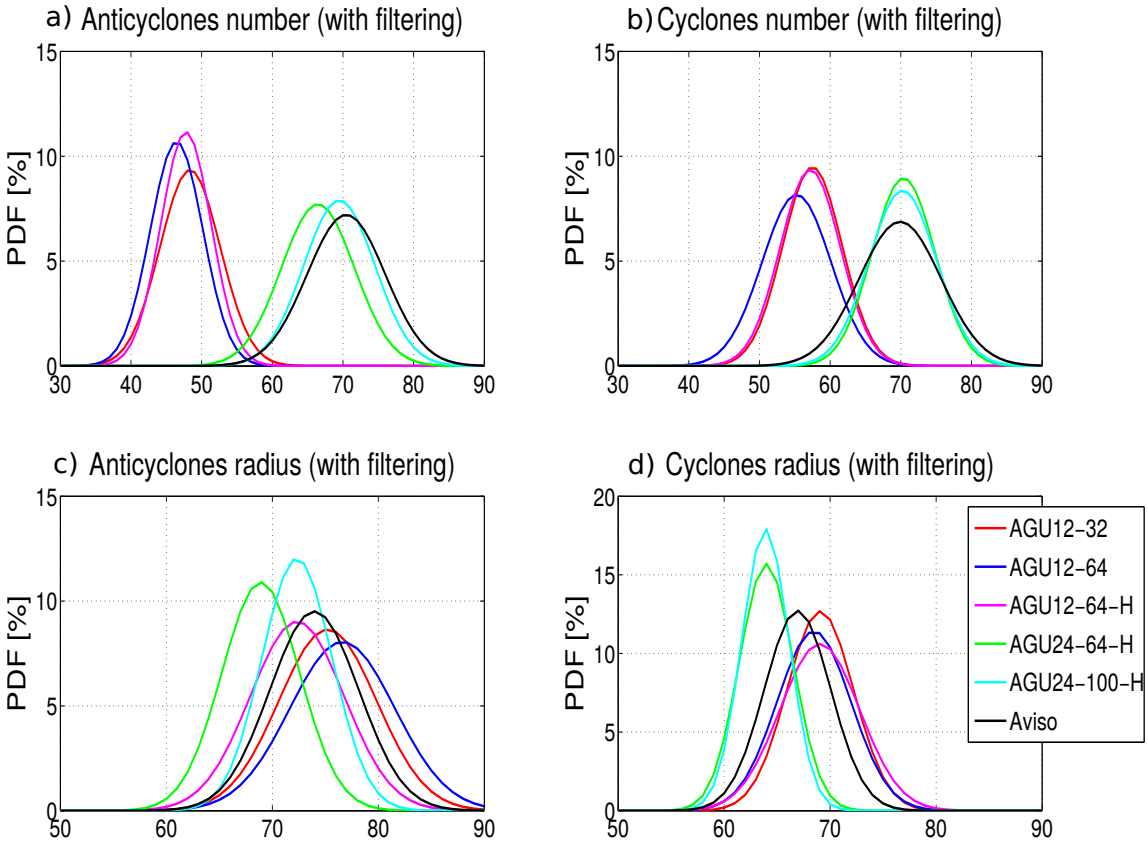

Figure 6. Probability density functions fitted to the time series of the number of (a) anticyclones and (b) cyclones and the mean radius of (c) anticyclones and (d) cyclones detected in each of the five numerical simulations (colored lines) and from AVISO data (black line). Here the modelled eddies whose radius was equal or smaller than 30 km have been filtered out, in order to render them more comparable to the AVISO resolution.

Figure 6 (a-d) shows the mean number and radius of the detected anticyclones and cyclones in our simulations after the filtering process (see Supplement Figure 4 for the non-filtered

results), along with the ones from AVISO. Here the normal probability density functions (PDFs) have been fitted to their distributions, which do not substantially differ from the non-filtered version of these results in terms of simulations intercomparison. The number of detected cyclones is always slightly higher than that of anticyclones (in a ratio of 3/2, Figs. 6a and b) for all the simulations, as originally proposed by *Boebel et al.* [2003] from quasi-Lagrangian observations achieved with deep floats south of Africa. This asymmetry in the eddies number is also suggested from numerical studies of geophysical turbulence in idealized frameworks [*Roullet and Klein*, 2010]. The mean radius is usually larger for the anticyclones than for the cyclones ($\sim$75 vs 65 km, Figs. 6c and d), as observed in geophysical stratified flows [*Lapeyre and Klein*, 2006] and for the region of study [*Boebel et al.*, 2003; *Richardson and Garzoli*, 2003].

Looking at the differences between the unfiltered distributions of the various simulations (Supplement Figure 4), those at the highest resolutions (AGU24_64_H and AGU24_100_H) show the most bountiful presence of eddies, reaching a mean value of 110 for cyclones and 90 for anticyclones, versus mean values of respectively 90 and 70 identified in the 1/12° runs. The situation is reversed in terms of their mean radius: smaller values are found for the highest resolution simulations (about 50 km) than for the lowest resolution counterparts ($\sim$60 km).

Once filtered, the results of our highest resolutions (AGU24_64_H and AGU24_100_H) agree particularly well with those from altimetry, in terms of the number of both antyclones and cyclones (Figs. 6a and b). Less comparability is instead evident for the their mean radius (Figs. 6c and d), as the mesoscale eddies captured in AVISO are slighlty larger than those of our 1/24° simulations and are closer to the ones of the lower resolutions. We believe that this is due to the fact that at finer resolutions eddy baroclinic modes higher than the first two (barotropic and first baroclinic), when properly resolved (as in our 1/24° simulations), enrich the scales and energetics of the first two modes, increasing the presence of smaller structures [*Barnier et al.*, 1991]. Another possible explanation would be that when fine horizontal scales are resolved, they can interact among each other and lead to the formation of additional mesoscale structures [*Aguiar et al.*, 2013]. This phenomenon is obviously missing if these scales are not captured by a limited resolution of the model.

The discrepancy between the number of eddies detected in the non-filtered distribution of our highest resolution simulation (AGU24_100_H, Supplement Figure 4) and AVISO is evident also in Figure 7, showing the estimates of the mean pathways followed by Agulhas Rings in the Cape Basin from AGU24_100_H and AVISO. Rings are defined in this analysis as anticyclones initially detected in the Southwest Indian sector within a trapezoidal area extend-

ing between 12°-34°E and 34°-44°S. Here, the number of anticyclonic trajectories that are formed or disappear in each grid cell of the model are computed taking into account that a trajectory only starts when an eddy splits and similarly ends when two eddies merge. The coloured cloud of AGU24_100_H, representing the mean percentage of rings per grid-box along their trajectories, is slightly shifted north-westward compared to the AVISO envelope represented with a black contour.

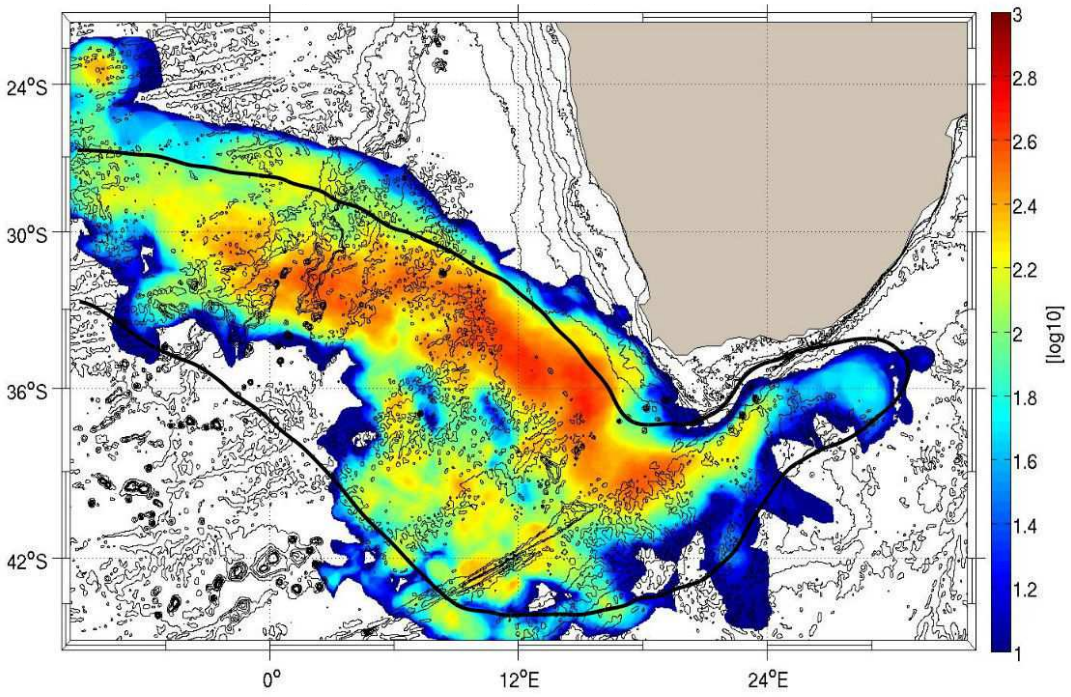

Figure 7. The mean presence of Agulhas Rings, as detected in AGU24_100_H, in colour shading and expressed with a logarithmic decimal scale. The thick, black line delimit the same estimate from AVISO. The underneath black contours are for the -5000, -4000, -3000, -2000, -1000, -500, -200, -100 m isobaths from the Etopo2 dataset [*Smith and Sandwell*, 1997].

This difference in the directions of Agulhas Rings mean path could be explained by: 1) smaller or more intense simulated rings than those detected in AVISO, and thus anticyclones less sensitive to the β-effect; 2) a (westward) shift in the position of the simulated Agulhas Retroflection, where the process of rings shedding is known to take place; 3) an enhancement

in the intensity or a more northward location of the simulated subtropical gyre than in observations, leading to an advection of more rings northward; 4) a discrepancy either in the vertical size of the rings or in their intensity at depth, resulting in a different bathymetric deflection. In this study, the first condition was verified: the anticyclones surface signature in EKE was shown to be higher than what observed in the altimetric product (Fig. 5) and their radius is averagely smaller than the rings detected in AVISO (Fig. 7c). The second condition was also partially verified by running some sensitivity tests (not shown), where the eastern boundary of our simulated domain was placed slightly more westward than presently (30°E instead of 34°E), inducing a substantial reduction in the mean EKE content of the test runs. We expect that placing this boundary even further east then 34°E, altough highly augmenting the computational costs of the run, would allow us to reproduce a more realistic Agulhas Retroflection. An even larger domain and a longer simulation would be required to test the third condition on the subtropical gyre position and intensity, whereas a three-dimensional reconstruction of the eddies from AVISO would be necessary to investigate the fourth condition.

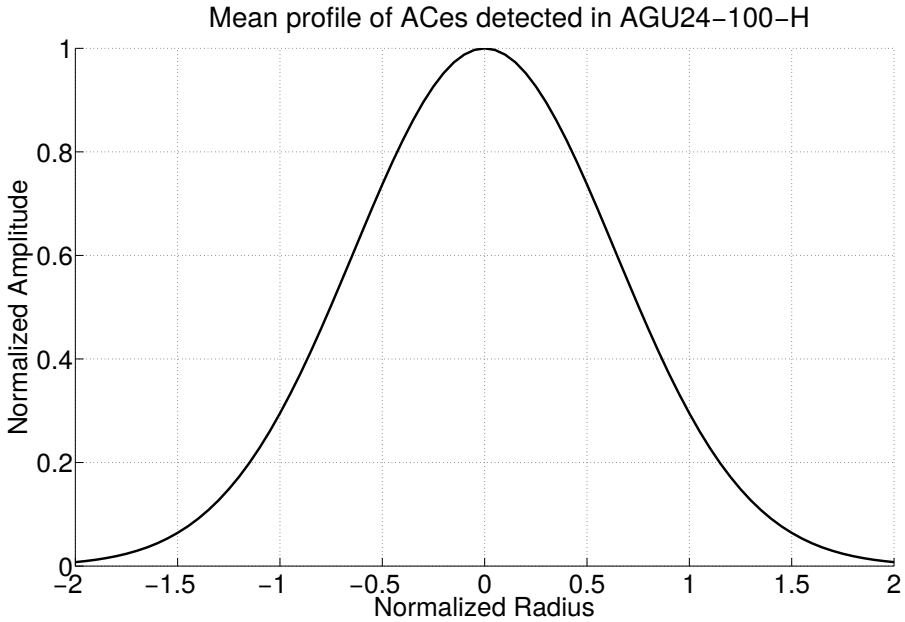

Figure 8. Mean profile of all the anticyclones detected in AGU24_100_H, plotted as their mean amplitude, normalized by their mean number, against their normalized radius.

In general, the displacement of coherent mesoscale structures in the ocean is attributed, in addition to the influence of the β-effect and of topography, also to the influences of neighboring currents and to the interactions with other eddies, which account for the loops and cusps

in their trajectories [*Carton*, 2001]. Since the Cape Basin is characterised by the co-existence of cyclonic and anticyclonic vortices, generated in proximity of the continental slope and of the Agulhas retroflection, eddy merging and splitting events, as well as absorption and detachment from the main current, are expected to highly impact the Agulhas rings trajectories [*Laxenaire et al.*, Submitted] and also their geometry. Therefore, we statistically examined their two-dimensional structure, by tracing their mean amplitude, normalized by their mean number, against their normalized radius. Figure 8 shows that the anticyclones mean profile (given by the mean SSH eddy-amplitude versus the eddy-radius) in AGU24_100_H has a quasi-Gaussian shape, in line with previous results on global scale [*Chelton et al.*, 2011]. Since investigating the relation between the eddy horizontal geometry and the different mechanisms of eddy deformation goes beyond the scopes of this paper, in the following we will examine the temporal variability of the simulated eddies and its driving factors.

3.6 Temporal Variability of the Mesoscale Dynamics

The monthly time series of the number of eddies detected in each numerical experiment (not shown here), from which we computed the eddy-PDF distributions of Figure 6, disclose a temporal-dependent behavior. In particular, these time series are characterized by a strong seasonal cycle, more pronounced for the higher resolutions simulations (AGU24_64_H and AGU24_100_H).

This seasonality could be further investigated through the analysis of a longer simulation in order to test its statistical significance over a more extended time series. However, in order to ascertain this seasonal variability with observations, we plotted the mean monthly time series of the number of eddies for AVISO and for our highest resolution simulation (Fig. 9) and we undertook preliminary analyses to investigate possible processes responsible of such variations. We observe that in both time series the seasonal cycle is distinguishable (Fig. 9a and b); it is particularly marked in the model distribution, where the winter maximum (July to September) clearly appears for eddies of both polarities. This temporal variability was further explored, performing a discrete Fourier transform on these two time series (Figs. 9c and d); it suggests that an annual cycle is dominant for both observed and modelled eddies.

Multiple factors could be responsible of this time-dependence of the mesoscale field. Among these are the variability of the atmospheric forcing, the seasonality of the regional upwelling or the local influence of intermittent Natal Pulses [*Schouten et al.*, 2003; *van Leeuwen et al*, 2000; *de Ruijter et al.*, 1999]. Given that the surface forcings and boundary conditions of our simulations are based on interannual, smoothed climatologies, our simulations do not allow

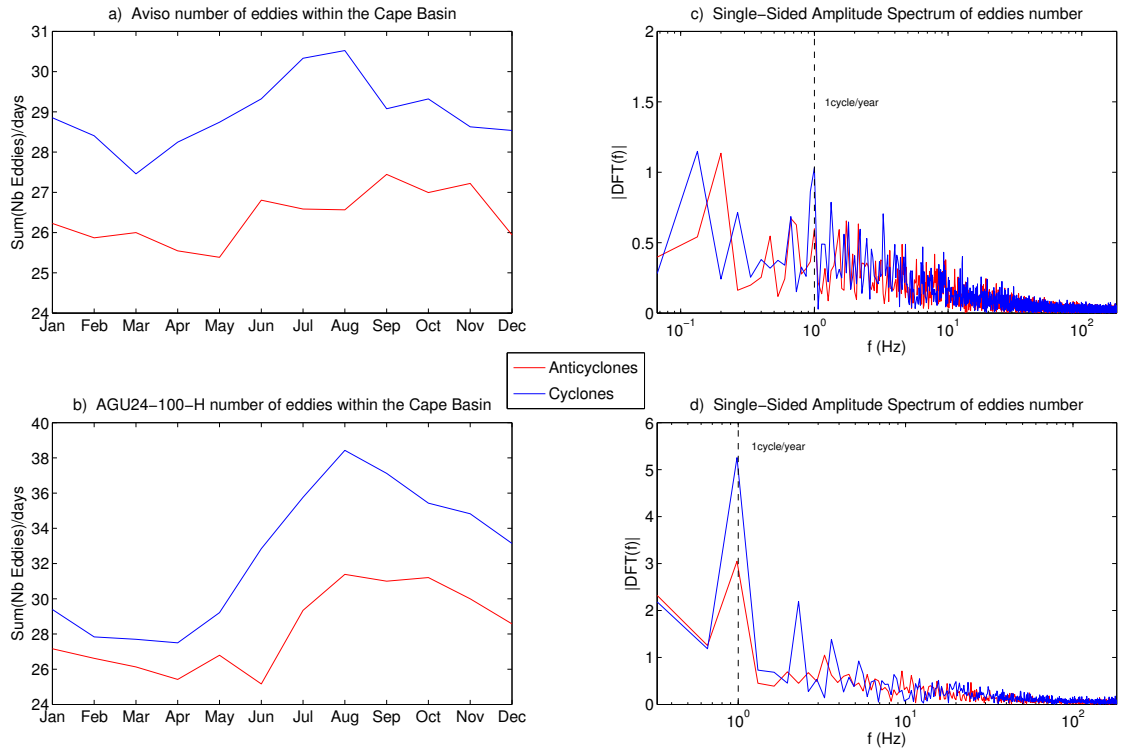

530 **Figure 9.** Seasonal time series of the mean number of anticyclones (red) and cyclones (blue) for (a) AVISO
531 and (b) AGU24_100_H. Single-Sided Amplitude Spectrum from the discrete Fourier tranform of these distri-
532 butions for (c) AVISO and (d) AGU24_100_H.

us to explore these factors. But, we can analyse three oceanic metrics that relate mesoscale eddies to their generation processes: the EPV [*Marchesiello et al.*, 2003; *Peliz et al.*, 2014]; the first baroclinic Rossby radius of deformation (computed along the pycnocline, as in *Chelton et al.* [1998]), relating the eddies size and temporal distribution to their formation mechanism [*Smith*, 2007; *Chelton et al.*, 2011]; and the mixed-layer depth (MLD, calculated as the depth where the density difference with respect to the surface is equivalent to a 0.03 density change), whose seasonality, in relation to that of eddy dynamics, has been recently explained by meso-submesoscale interactions [*Brannigan*, 2016; *Callies et al.*, 2015].

In this framework, we will consider the EPV anomaly (EPVA), quantifying the EPV difference with the background ocean, and its vertical components (i.e., the first RHS term of Equation 1). These terms, as well as the Rossby radius and the MLD, are averaged over the geographical domain during the last year of each simulation (year 5). The results are presented for AGU12_64 and AGU24_100_H. Figure 10a shows the time series of the EPVA, obtained by subtracting from each instantaneous value of EPV the interannual mean over the last 3 years of integration (this was the period used for the the eddy detection). Figure 10b displays the EPV vertical components (i.e., the relative vorticity and the vortex stretching terms). The EPVA for the highest resolution simulation (AGU24_100_H, black continuous line in Fig. 10a) is characterized by a marked seasonality, in which negative and positive values alternate, reaching a maximum during the austral winter. This maximum corresponds to those of the vortex stretching and relative vorticity terms (respectively blue and red continuous lines in Fig. 10b). The vortex stretching is directly linked to the stratification, which is indeed higher in summer as a consequence of the seasonal warming, and declines in winter by cooling and under the action of stronger winds. These conditions favor higher values in the temporal distribution of relative vorticity (red, continuous line in Fig. 10b) in winter, when more ageostrophic, turbulent dynamics are at play, increasing the seasonal values of the EPV anomaly.

A clear seasonality is also distinguishable in the time series of the first baroclinic Rossby radius of deformation and in that of the MLD (Fig. 10c) for both model resolutions (AGU12_64 and AGU24_100_H, respectively dashed and continuous lines in Fig. 10c). Because the first Rossby radius is the scale of the fastest growing mode for the baroclinic instability [*Rhines*, 1975], its winter maximum corresponds to a seasonal peak in the time series of the mean eddy radius of the eddies detected. We can retrieve these winter peaks in the three-years time series of the mean radius of both cyclones and anticyclones (not shown here). These peaks are well marked in the higher resolution simulations (AGU24_64_H and AGU24_100_H); this con-

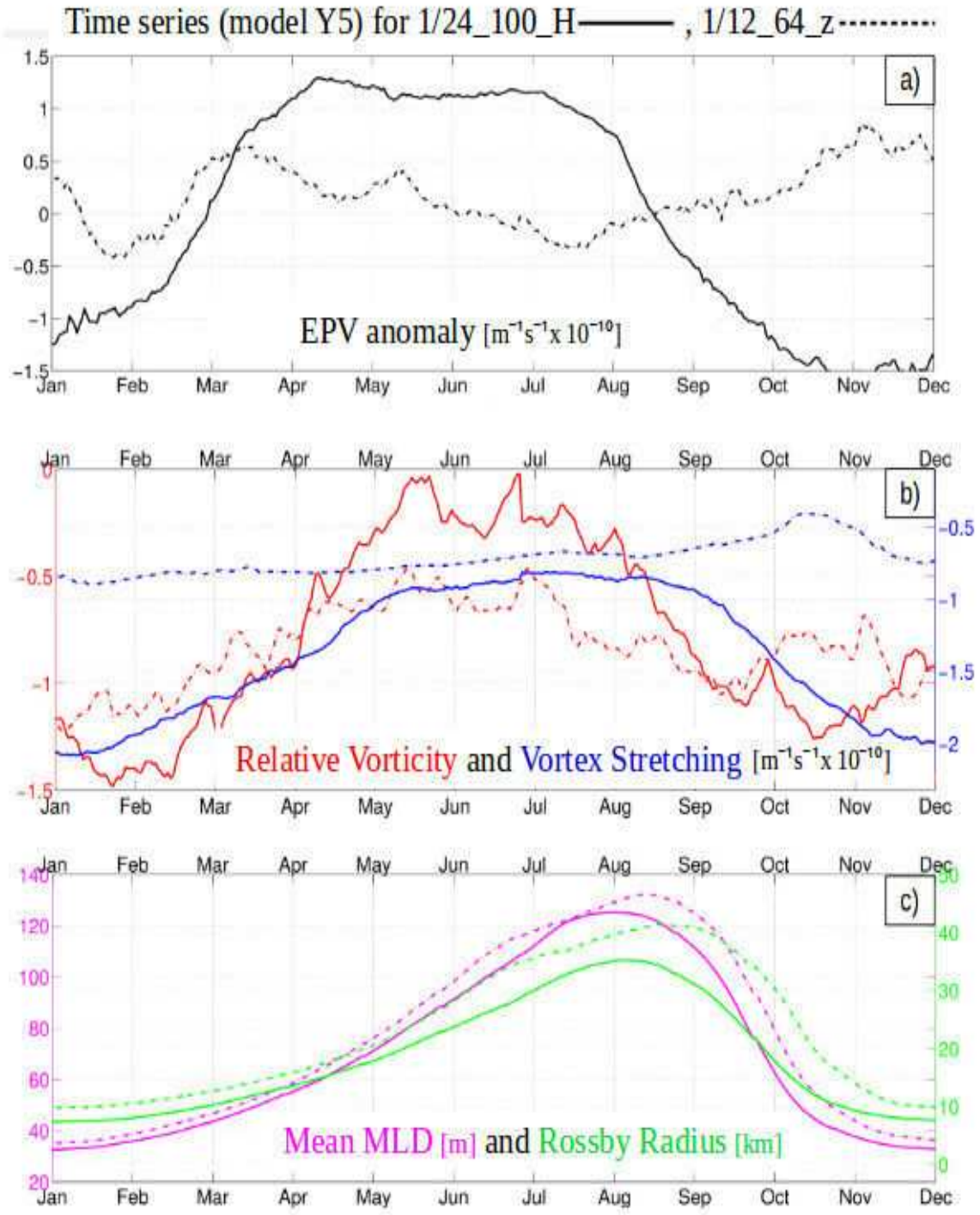

577 **Figure 10.** Time series of the surface spatially averaged (a) Ertel PV anomaly, (b) its vertical components,
578 (c) Rossby radius and mixed-layer depth, for AGU12_64 (dashed line for all the curves) and AGU24_100_H
579 (continuous line for all the curves).

firms the relationship existing between the eddy size and the local Rossby radius of deformation, suggested by several studies [*McWilliams*, 1991; *Carton*, 2001; *Aubert et al.*, 2012]. Upper-ocean eddies often form from the development of baroclinic instability, essentially projecting on the barotropic and on the first baroclinic modes. Consequently, their size is close to the first baroclinic Rossby radius of deformation. A winter increase of the eddies mean radius also occurs in the lower resolution simulations (not shown), corresponding to the winter peak of the Rossby radius of deformation (dashed line in Fig. 10c, displaying these values for AGU12_64).

On the other hand, the time series of the EPV anomaly for AGU12_64 (black, dashed line in Fig. 10a), does not show a well defined seasonal cycle, in relation with limited seasonal variation of the vortex stretching term (blue, dashed line in Fig. 10b). This suggests that the lower resolution simulations (at 1/12°) are not able to correctly reproduce the seasonal cycle of baroclinic instabilities. They capture the seasonal evolution of relative vorticity (red, dashed line in Fig. 10b), driven by the largest mesoscale structures, but they cannot recover the variability in the vortex stretching, highly affected by finer scales dynamics [*Capuano et al.*, Submitted; *Brannigan*, 2016; *Callies et al.*, 2015].

To conclude this subsection on eddy seasonality, we estimate its impact on thermohaline fluxes, computing the diffusion coefficients of temperature and salinity, Kv_T and Kv_S, defined as in *Joyce* [1977]:

$$<w'T'> = Kv\_T \frac{\partial \overline{T}}{\partial z}$$

$$<w'S'> = Kv\_S \frac{\partial \overline{S}}{\partial z},$$

where w is the vertical velocity; brackets and prime respectively denote a time average and fluctuations relative to it, and the bar represents a spatio-temporal mean.

The strongest heat and salt fluxes coincide with the presence of eddies of both polarities, with a clear seasonality. Their summer distribution (not shown here) is characterised by enhanced values of these fluxes in correspondance of the largest mesoscale structures, while in winter we observe an abundance of finer scales, locally leading to higher values for both diffusion coefficients. To better quantify this seasonality we computed the horizontal spectra of the diffusivities (Fig. 11) at the surface and along the 27.2 isopycnal in the Cape Basin box of Figure 1, during summer and winter. At the surface, the seasonal contrast is very pronounced at small scales, which present similar values of diffusivity as the larger scales. Instead, at depth, the seasonal difference does not seem to depend on the horizontal scales; also here we observe a winter increase in the values of diffusivities. These processes have been investigated in more detail in *Capuano et al.* [Submitted] where it has been suggested that submesoscale instabil-

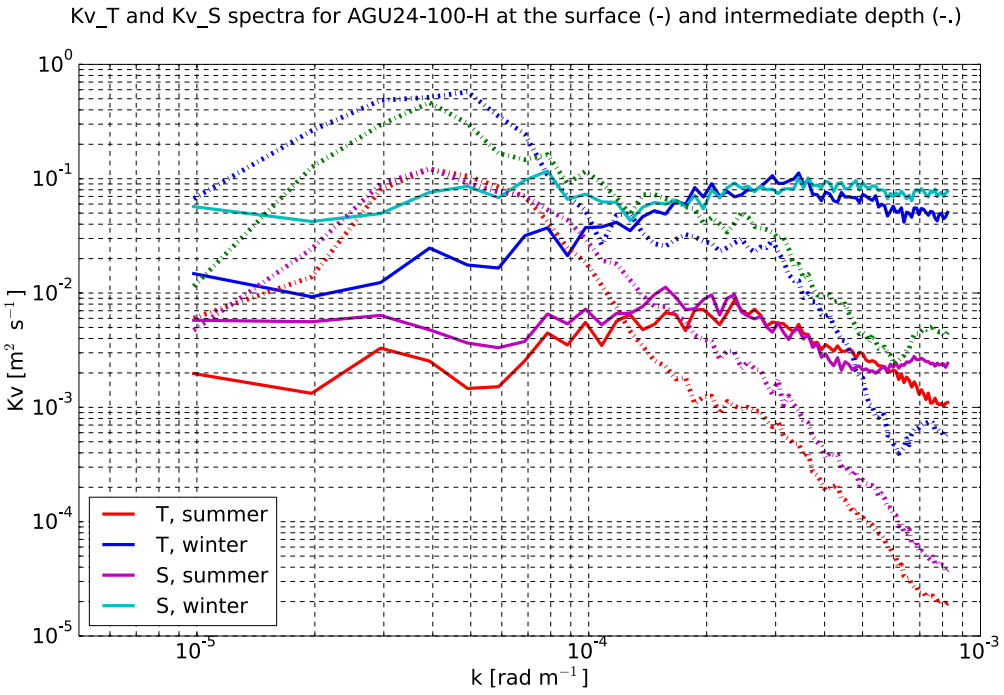

Figure 11. Horizontal spectra of the diffusion coefficients of temperature and salintiy, computed for AGU24_100_H at the surface (continuous line) and at intermediate depth (dashed) in summer and winter.

ities of the mesoscale field play a role on the vertical thermohaline structure of the local watermasses. Such processes are partially represented by AGU24_100_H.

3.7 Eddies signature on AAIW advection

Since this work is centered on the impact of the mesoscale dynamics on the Indo-Atlantic exchange and regional mixing of AAIW, we focus here on the properties of water masses advected in the Cape Basin by the simulated mesoscale features. To assess subsurface water mass properties within the eddies, we have estimated the θ-S diagram corresponding to the center of every eddy detected in each simulation within the the Cape Basin box lying on the principal route of the Agulhas leakage (box drawn in Figure 1). All these θ-S profiles are shown for anticyclones and for every simulation in Figure 11a, and for cyclones in Figure 11b.

These diagrams illustrate how the vertical thermohaline properties in the AAIW layer of the eddies change with the model resolutions. At lower vertical and horizontal resolutions, the eddy-core AAIW θ-S properties diverge from those of Argo profiles (light green dots in Figure 11c and d). AAIW as measured by Argo floats is fresher than that advected within the

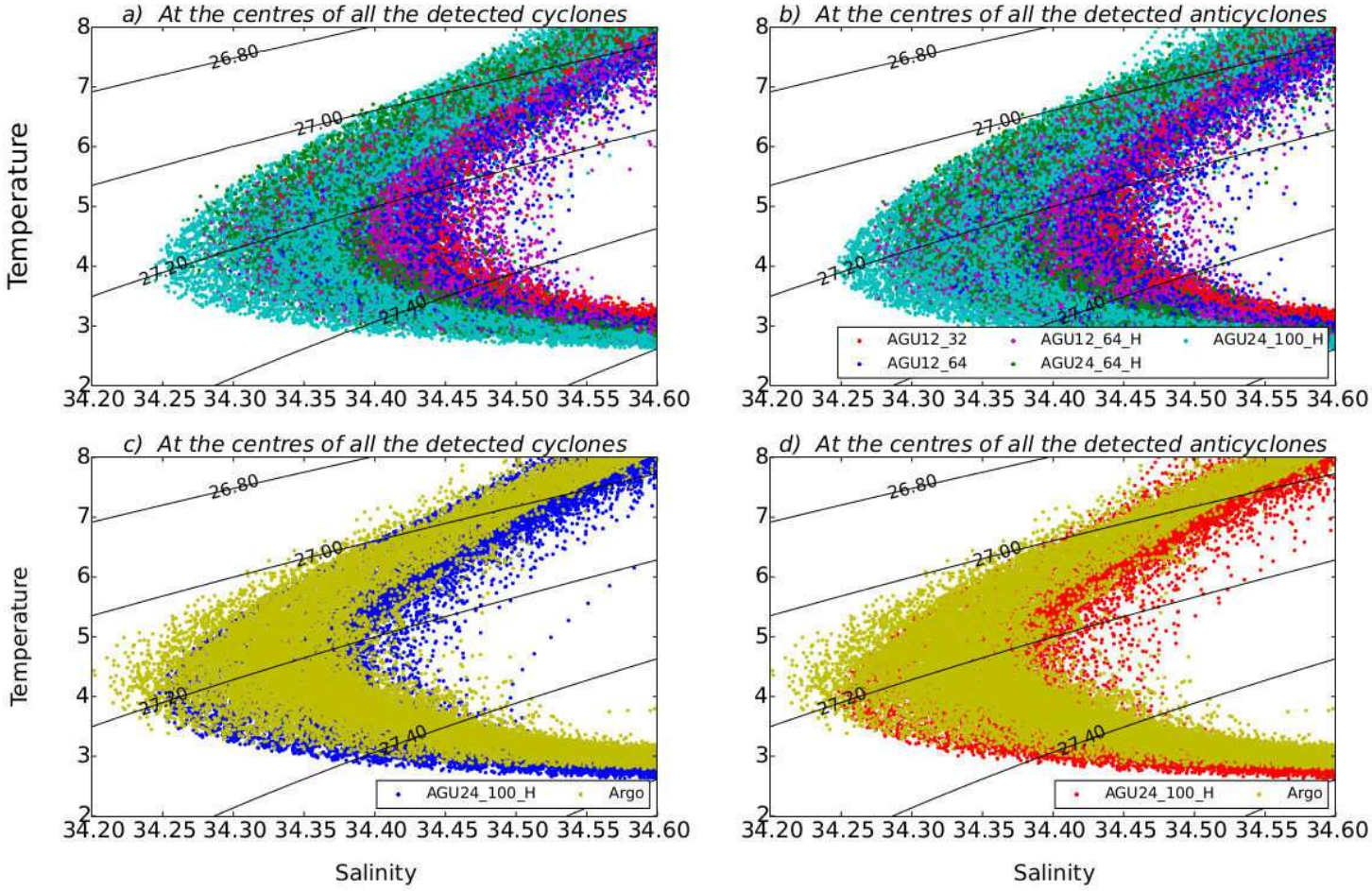

626 **Figure 12.** θ-S diagrams plotted at the centre of all the anticyclones (a) and of all the cyclones (b) detected
627 in each of our 5 simulations for the AAIW thermohaline range (8-2°C of θ and 34.2-34.6 psu of S). c and d
628 are identical to a and b, except the comparison is between the θ-S distribution of AGU24_100_H and Argo.

simulated eddies, with the exception of the highest resolution simulation (AGU24_100_H) that well compares with the observations (light blue dots in Figure 11a and b, and red and blue dots in Figure 11c and d). Thus, advection and mixing of water masses in the Cape Basin, and in particular within the AAIW layer, are represented in models with a horizontal resolution of 1/24° and a vertical resolution of about 50 m or higher.

However, despite the differences in AAIW properties within the core of eddies among the various simulations and in comparison to Argo data, it appears that these properties are, in the Cape Basin, relatively homogeneous. Both cyclones and anticyclones show indeed salinities values in the AAIW layer ranging from 34.25 and 34.4 psu (in the AGU24_100_H simulation) in accordance with the Argo sampled properties and with historical hydrographic cruises [*Richardson and Garzoli*, 2003; *Giulivi and Gordon*, 2006; *Arhan et al.*, 2011]. This implies that both types of eddies are involved in the advection of the same AAIW varieties, namely the Indian (I-AAIW: S $\geq$ 34.3) and the Indo-Atlantic (IA-AAIW: 34.2 <S <34.3) ones [*Rusciano et al.*, 2012]. This is also in agreement with the findings of *Arhan et al.* [2011] from in-situ observations of an Agulhas Ring and an Agulhas Bank cyclone in the southern Cape Basin, along the GoodHope line. Thus, in line with the results of *Rimaud et al.* [2012], cyclones are as fundamental as anticyclones for the transport, mixing and transformation of I-AAIW with AAIW of Atlantic origin (S $\leq$ 34.2) within the Cape Basin, before entering the South Atlantic.

The significant improvement that we gained, with the highest resolutions simulation, in the reproduction of the modelled thermohaline structure is reflected also in the interocean exchange of upper and lower thermocline waters. Here we used the offline mass-preserving algorithm ARIANE [*Blanke et Raynaud*, 1997; *Blanke et al.*, 1999] to perform in each simulation a Lagrangian integration, backward in time, of particles selected as those having density values (25-27.6σ) typical of thermocline waters in the Cape Basin. These particles were initialised at the east section (in red) and intercepted at the north and western sections (in black) of the control domain shown in the map of Figure 14b, where the coloured curves represent the transport streamfunction (PSI). The latter is estimated in AGU24_100_H by algebrically summing every particle transport at each velocity point of the three-dimensional grid, before vertical integration and derivation of the Lagrangian streamfunction, showing a max value of 8 Sv (1 Sv = $10^6 m^3 s^{-1}$). This value is comparable with previous estimates of the Indo-Atlantic transfer (9 Sv of [*Boebel et al.*, 2003], 12 SV of [*Biastoch et al.*, 2008]).

We then plotted histogram bars of the difference between the final and the initial transports, computed as the number of particles normalised by their total transport and binned by

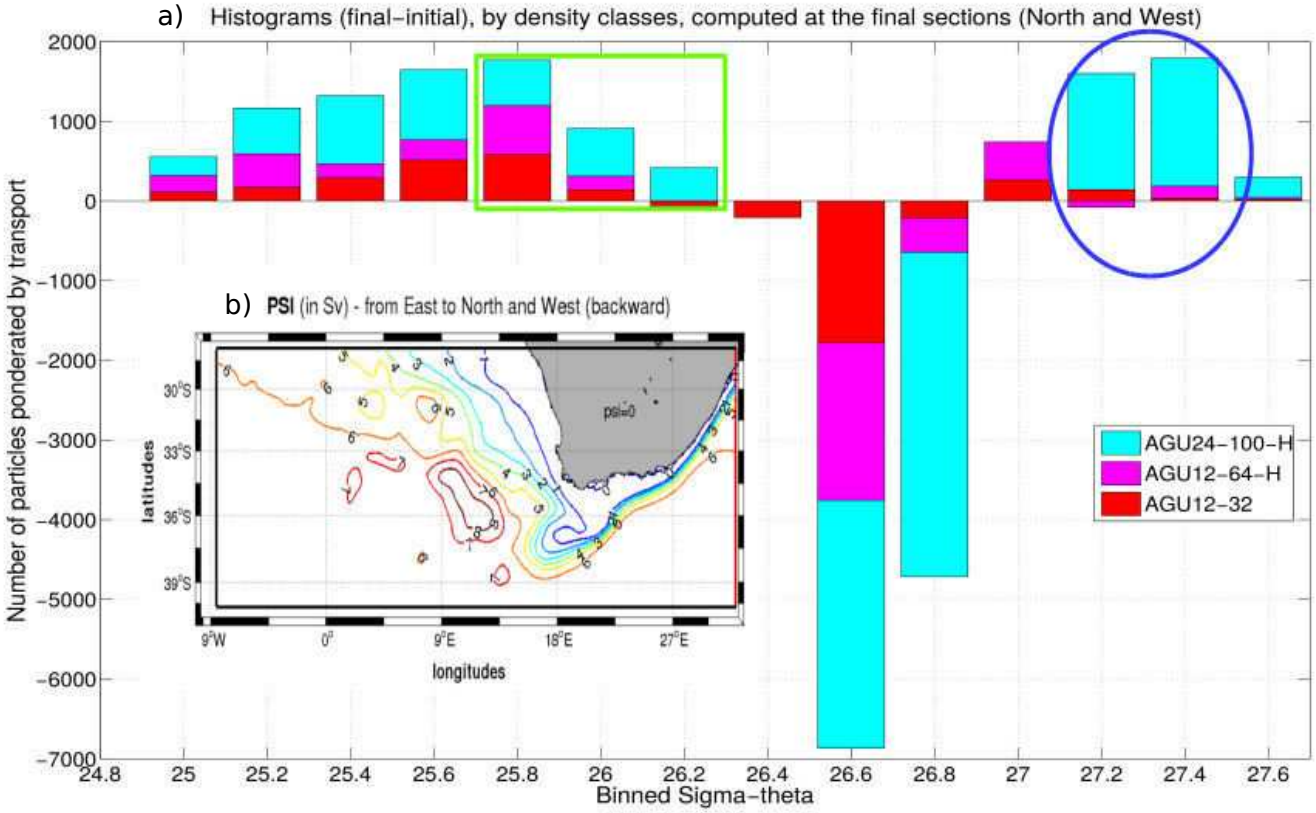

671 **Figure 13.** (a) Histograms of the differences between the final and initial Lagrangian transports [Sv],
672 binned by density classes, for AGU12_32 (red), AGU12_64_H (magenta) and AGU24_100_H (cyan), com-
673 puted within the domain control shown in the transport streamfunction map (b). In (a), highlighted in green
674 are the lighter varieties of mode waters and in blue the Atlantic and Indo-Atlantic varieties of AAIWs.

potential density classes (Fig. 14a) for AGU12_32 (red), AGU12_64_H (magenta) and AGU24_100_H (cyan). For this calculation, the potential density changes are estimated between successive positions (archived everyday) and by algebrically summing the individual and local density changes weighted by the transports allotted to the corresponding particles. The spatial integration of this field is roughly equal to the magnitude of the transfer multiplied by the mean difference in density between the final and initial sections. This diagnostic allowed us to verify that the highest resolutions simulation is the only one able to capture a net transport, from the Indian to the Atlantic oceans, of thermocline waters, consisting of the lighter variety of mode waters and of intermediate waters (highlighted respectively in green and blue in Fig. 14a). The model inability, at lower resolution, to capture a part of the local mesoscale processes implies a prominent reduction in the quantity of transport of thermocline waters from the Indian to the Atlantic oceans. These preliminary results indicate that the Cape Basin turbulent dynamics have a direct effect on the characteristics and transfer of the water masses participating in the AMOC, and confirm that this region is essential in connecting the ocean basins and making possible a global circulation [*Garzoli and Matano*, 2011].

4 SUMMARY AND CONCLUSIONS

The Indo-Atlantic exchange of thermocline waters south of Africa strongly depends on highly energetic mechanisms, affecting subsurface water masses advection and mixing. By improving the simulation of the non-linear dynamics that drives this exchange, we were able to capture a realistic part of the ocean mesoscale processes that transport and stir the local water masses. In particular, we demonstrate how a satisfactory representation of the surface dynamics is not sufficient to ensure a realistic upper and intermediate watermasses advection and transformation. We obtained the most prominent improvements in simulating these processes by augmenting and homogenizing the vertical resolution of the model to reach a 50 m spacing between the levels. This increase in the vertical resolution of the water column positively impacts also the surface ocean dynamics. A doubling of the horizontal grid-spacing (from 8 km in the 1/12° to 4 km for the 1/24°) improves even further the realism of the simulations.

By increasing the model resolution both vertically and horizontally, we show that:

-The contrast between the southwest Indian and the southeast Atlantic waters becomes sharper, with distinct structures of the thermocline observed. Watermasses in the subsurface layers compare particularly well to observations from classical hydrography and Argo profiles.

- In finer resolutions simulations mesoscale dynamics and energetics are generally in better agreement with the available observations. The highest resolutions configuration clearly shows a dynamical behavior change, with a richer spectrum of spatio-temporal scales and more non-linear processes than classical eddy permitting (at 1/12°) simulations, as seen in the diffusivities spectra, where smaller length scales are reached, both at the surface and at depth.

- A precise estimate of the distribution, size and properties of the simulated upper-ocean eddies of both signs can be achieved by applying the detection algorithm of *Laxenaire et al.* [Submitted] to the output of each of our simulations. Remarkably all the runs are characterized by an asymmetry among cyclones and anticyclones, the former being always more abundant (in a ratio of 3/2) and smaller in radius (about 65 vs 75 km), as already suggested in previous, observational and theoretical, studies.

-The structure and mean pathways of the modelled Agulhas rings compare well with their counterparts estimated from altimetry, once the simulated eddies having radius equal or higher than 30 km are filtered out. Considering the limitations in the resolution of the satellite products, results of the 1/24° simulations better agree with these data after the filtering process, even though a slight discrepancy persists in terms of the mean radius. However, in AGU24_100_H, Indian-water anticyclones can be clearly retrieved within the migration drift path of the observed Agulhas Rings into the South-Atlantic [*Boebel et al.*, 2003; *Dencausse et al.*, 2010] (see the SSH-RMS map of Fig. 4f or their mean trajectories in Fig. 7).

- Both types of eddies contain the Indian variety of AAIW (I-AAIW) as suggested by *Richardson and Garzoli* [2003]; *Giulivi and Gordon* [2006]; *Arhan et al.* [2011] from sparse hydrographic observations. We also corroborate the finding that in the Cape Basin, the eddies advected I-AAIW experiences mixing with the Atlantic variety of AAIW (A-AAIW) producing a new variety, the Indo-Atlantic AAIW (IA-AAIW), whose properties are intermediate between the two AAIWs, as observed by *Rusciano et al.* [2012] and *Rimaud et al.* [2012].

- The number and radius of eddies (of both signs) show a seasonal cycle. The latter is largest for the highest resolutions simulations displaying a maximum in the eddies number and radius during winter, when the first baroclinic Rossby radius of deformation is also maximum. This supports baroclinic processes as key mechanisms for the generation of these eddies, while undoubtedly linked with the seasonality of the EPV anomaly, of its vertical components and with the one of the MLD.

- The diagnostic tool ARIANE provided a Lagrangian interpretation of the modelled Indo-Atlantic exchange. This allowed us to quantify the intensity of thermocline waters transfers and to illustrate that at least a fully mesoscale-resolving resolution of the model is required to depict the Cape Basin dynamics and transformations inherent to these transfers.

The last two points underline the need for numerical experiments at higher horizontal resolution than 1/24°, which would allow the representation of an even broader range of scales (including submesocale filaments, fronts, meanders), whose spatio-temporal variability could explain the seasonal correlation between the eddy statistics and the dynamical metrics obtained here. Also, we expect the use of synoptic surface forcing and more realistic boundary conditions, in a fully submesoscale-resolving configuration, to further improve the reproduction of the flow instabilities seasonality and their effect on the thermohaline properties and spreading of the Indo-Atlantic waters into the AMOC.

The challenges presented by high-resolution requirements to solve the realism of the ocean circulation will accompany global ocean modeling efforts. In this respect, ocean models must have consistently high resolution, both horizontally and vertically, and particular attention must be paid to correctly simulate the baroclinic structure of the subsurface and deep water masses.

Acknowledgments

The authors greatly appreciate discussions with Xavier Capet, Gildas Cambon, Guillaume Lapeyre, Guillaume Roullet, Bernard Barnier, Arne Biastoch and Jeroen Molemaker. This work was supported by the ”Laboratoire d’Excellence” LabexMER (ANR-10-LABX-19) and co-funded by a grant from the French government under the program ”Investissements d’Avenir”, and by a grant from the Regional Council of Brittany. We also acknowledge funding from the ANR/DGA program DYNED ATLAS and the national computer centre IDRIS for technical and computational support.. We sincerely thank Xavier Capet (LOCEAN, Paris), Gildas Cambon (LOPS, Brest) and Clement Vic (SOTON, UK) for their precious help and technical support on different aspects of the model. This study is part of the CLIVAR-SAMOC international initiative and was also supported by the European Union Horizon 2020 research and innovation programme under grant agreement no. 633211 (AtlantOS), a by the French CNES-TOSCA research funding and the 11-ANR-56-004 SAMOC research grant. We thank both reviewers who helped us to improve this manuscript.

References

Aguiar Barbosa, A. C., Peliz, ., and Carton, X. (2013). A census of meddies in a long-term high-resolution simulation. *Progress in Oceanography, 116:8094*.

Arhan, M., S. Speich, C. Messager, G. Dencausse, R. Fine, and M. Boye (2011), Anticyclonic and cyclonic eddies of subtropical origin in the subantarctic zone south of Africa. *J. Geophys. Res.* 116, C11004, doi:10.1029/2011JC007140.

Aubert O., Le Bars M., Le Gal P. and Marcus P. S. (2012), The universal aspect ratio of vortices in rotating stratified flows: experiments and observations. *Journal of Fluid Mechanics* 706, pp 3445 doi:10.1017/jfm.2012.176.

Barnier, B., C. Le Provost, and B.L. Hua, (1991). On the Catalytic Role of High Baroclinic Modes in Eddy-driven Large-Scale Circulations.*J. Phys. Oceanogr., 21, 976997*, https://doi.org/10.1175/1520-0485(1991)021¡0976:OTCROH¿2.0.CO;2.

Blanke, B., and S. Raynaud (1997), Kinematics of the Pacific Equatorial Undercurrent: An Eulerian and Lagrangian approach from GCM results, *J. Phys. Oceanogr., 27, 10381053*, doi:10.1175/1520-0485(1997) 027¡1038:KOTPEU¿2.0.CO;2.

Blanke, B., M. Arhan, G. Madec, and S. Roche (1999), Warm water paths in the Equatorial Atlantic as diagnosed with a general circulation model, *J. Phys. Oceanogr., 29, 27532768*, doi:10.1175/1520-0485(1999) 029¡2753:WWPITE¿2.0.CO;2.

Biastoch, A., C. W. Boning, and J. R. E. Lutjeharms (2008), Agulhas leakage dynamics affects decadal variability in Atlantic overturning circulation. *Nature* 456, 489 492 doi:10.1038/nature07426.

Biastoch, A., J. R. E. Lutjeharms, C. W. Bning, and M. Scheinert (2008), Mesoscale perturbations control inter-ocean exchange south of Africa,*Geophys. Res. Lett., 35, L20602*, doi:10.1029/2008GL035132.

Boebel, O., J. R. E. Lutjeharms, C. Schmid, C. Zenk, T. Rossby, and C. Barron (2003), The Cape Cauldron: A regime of turbulent inter-ocean exchange. *Deep Sea Res., Part I, 50, 5786* doi:10.1016/S0967-0645.

Brannigan L. (2016), Intense submesoscale upwelling in anticyclonic eddies. *Geophys. Res. Lett., 43, 33603369* doi:10.1002/2016GL067926.

Bryden, H.L., Beal, L.M., (2001), Role of the Agulhas Current in the Indian Ocean circulation and associated heat and freshwater fluxes. *Deep-Sea Research* I 48, 18211845.

Callies J., Ferrari R., Klymak J. M., and Gula J. (2015), Seasonality in submesoscale turbulence, *Nat. Commun., 6*.

Capet X, McWilliams JC, Molemaker MJ, Shchepetkin AF (2008), Mesoscale to submesoscale transition in the California Current System. Part I: Flow structure, eddy flux, and observational tests. *J. Phys. Oceanogr.* 38, 2943.

Capuano T. A., Speich S., Carton X., Mesoscale and submesoscale processes in the southeast Atlantic and their impact on the regional thermohaline structure. Submitted.

Carton X., (2001), Hydrodynamical modeling of oceanic vortices. *Surveys in Geophysics* 22(3), 179-263.

Chaigneau, A., Gizolme, A., Grados, C., (2008), Mesoscale eddies off peru in altimeter records: Identification algorithms and eddy spatio-temporal patterns. *Progress in Oceanography.* 79 (2), 106119.

Chaigneau, A., Marie, L. T., Grard, E., Carmen, G., Oscar, P., (2011). Vertical structure of mesoscale eddies in the eastern south pacific ocean: A composite analysis from altimetry and argo profiling floats. *Journal of Geophysical Research: Oceans.* 116 (C11).

Chelton, D. B., R. A. deSzoeke, M. G. Schlax, K. E. Naggar, and N. Siwertz (1998), Geographical variability of the first-baroclinic rossby radius of deformation. *J. Phys. Oceanogr.* 28, 433 460.

Chelton, D. B., Schlax, M. G., Samelson, R. M., (2011), Global observations of non-linear mesoscale eddies. *Progress in Oceanography.* 91 (2), 167216.

Da Silva, A.M., Young-Molling, C.C., Levitus, S. (1994), Atlas of Surface Marine Data 1994, vol. 1. *Algorithms and Procedures, NOAA Atlas NESDIS, vol. 6, NOAA, Silver Spring.*

Dencausse, G., M. Arhan, and S. Speich (2010), Routes of Agulhas rings in the southeastern Cape Basin. *Deep Sea Res.* Part I, 57, 14061421, doi:10.1016/j.dsr.2010.07.008.

de Ruijter, W. P. M., van Leeuwen, P. J. and Lutjeharms, J. R. E. (1999). Generation and evolution of Natal Pulses: solitary meanders in the Agulhas Current.*Journal Physical Oceanography, 29, 3043-3055.*

A new version of ssalto/duacs products available in April 2014. version 1.1, CNES,*http://www.aviso.altimetry.fr/fileadmin/documents/data/duacs/Duacs2014.pdf*.

Ducet, N., P.-Y. Le Traon, and G. Reverdin, (2000), Global high resolution mapping of ocean circulation from TOPEX/Poseidon and ERS-1 and -2. J.*Geophys. Res.*, 105, 19477- 19498.

833 Ertel, H., 1942a: Ein neuer hydrodynamischer Erhaltungssatz. *Naturwiss.* 30, 543544.

834 Garzoli, S. L., and R. Matano (2011), The South Atlantic and the Atlantic merid-
835 ional overturning circulation,*Deep Sea Res., Part II, 58 (1718), 18371847*,
836 doi:10.1016/j.dsr2.2010.10.063

837 Giulivi, C. F. and A. L. Gordon, (2006), Isopycnal displacements within the Cape Basin
838 thermocline as revealed by the Hydrographic Data Archive. *Deep-Sea Research Part*
839 *I-Oceanographic Research Papers.* 53(8): 1285-1300.

840 Gordon, A. L., R. F. Weiss, W. M. Smethie Jr., and M. J. Warner (1992),Thermo-cline and
841 intermediate water communication between the South Atlantic and Indian Oceans. *J.*
842 *Geophys. Res.* 97, 72237240, doi:10.1029/92JC00485.

843 Gordon, A.L., Sprintall, J., Wijffels, S., Susanto, D., Molcard, R., Van Aken, H., Ffield,
844 A.L., de Ruijter, W., Lutjeharms, J., Speich, S., Beal, L. (2010), Interocean exchange
845 of thermocline water: Indonesian Throughflow; 'Tassie' Lekage; Agulhas Leakage.
846 *Proceedings of OceanObs09: Sustained Ocean Observations and Information for Society.*
847 (Vol. 2).

848 Joyce, T.M., (1977). A Note on the Lateral Mixing of Water Masses.*J. Phys. Oceanogr., 7,*
849 *626629*, https://doi.org/10.1175/1520-0485(1977)007¡0626:ANOTLM¿2.0.CO;2

850 Keating, S. R., and K. S. Smith (2015), Upper ocean flow statistics esti- mated from su-
851 perresolved sea-surface temperature images.*J. Geophys. Res. Oceans, 120, 11971214,*
852 doi:10.1002/2014JC010357.

853 Lapeyre G. and Klein P. (2006). Impact of the small-scale elongated filaments on the
854 oceanic vertical pump. *Journal of Marine Research.* 64, 835851.

855 Laxenaire R., Speich S., Blanke B., Chaigneau A. and Pegliasco C. (Accepted), New
856 insights on Agulhas rings dynamics as inferred from altimetry.

857 Lemarie F., Kurian, J., Shchepetkin, A.F., Molemaker, M.J., Colas, F., McWilliams, J.C.
858 (2012), Are There Inescapable Issues Prohibiting the use of Terrain-Following Coordi-
859 nates in Climate Models ? *Ocean Modell.* doi:10.1016/j.ocemod.2011.11.007.

860 Levy, M., P. Klein, A.-M. Trguier, D. Iovino, G. Madec, S. Masson and K. Takahashi
861 (2010), Modifications of gyre circulation by sub-mesoscale physics. *Ocean modeling.*
862 doi:10.1016/j.ocemod.2010.04.001, 34, 1-15.

863 Locarnini, R., A. Mishonov, J. Antonov, T. Boyer, H. Garcia, O. Baranova, M. Zweng,
864 and D. Johnson (2010), World Ocean Atlas 2009. *vol. 1, Temperature, US Gov. Print.*
865 *Off., Washington, DC.*

Lutjeharms, J. R. E. The Agulhas Current. *Springer, 2006.*

Marchesiello P., McWilliams J.C., Shchepetkin A.F., (2001), Open boundary conditions for long-term integration of regional oceanic models. *Ocean modeling.* 3, 121.10.1016/S1463-5003(00)00013-5.

Marchesiello, P., McWilliams, J., Schepetkin, A. (2003), Equilibrium structure and dynamics of the California Current System. *Journal of Physical Oceanography.* 33, 753783.

Marchesiello P., Debreu L., and Couvelard X. (2009), Spurious diapycnal mixing in terrain-following coordinate models: The problem and a solution. *Ocean Modell.* 26,156169, doi:10.1016/j.ocemod.2008.09.004.

Matano, R., Beier, E.J. (2003), A kinematic analysis of the Indian/Atlantic interocean exchange. *Deep Sea Res. II, this issue (PII:S0967-0645(02)00395-8).*

McWilliams, J.C.: 1991, Geostrophic vortices. In: non-linear Topics in Ocean Physics, Proceedings of the International School of Physics Enrico Fermi. *Course CIX, North Holland.* 550.

Molemaker M.J., Mcwilliams J.C., Dewar W.K. (2015), Submesoscale Instability and Generation of Mesoscale Anticyclones near a Separation of the California Undercurrent. *J Phys Oceanogr.* 45:613-629.

Morrow, R., F. Birol, D. Griffin, and J. Sudre (2004), Divergent pathways of cyclonic and anti-cyclonic ocean eddies, *Geophys. Res. Lett., 31, L24311,* doi:10.1029/2004GL020974.

Pascual, A., Faugre, Y., Larnicol, G., Le Traon, P., (2006). Improved description of the ocean mesoscale variability by combining four satellite altimeters. *Geophysical Research Letters.* 33 (2).

Pegliasco, C., A. Chaigneau, and R. Morrow, (2015), Main eddy vertical structures observed in the four major Eastern Boundary Upwelling Systems. *J. Geophys. Res. Oceans.* 120, doi:10.1002/2015JC010950.

Peliz A., Boutov D., Aguiar A.B., Carton X. (2014), The Gulf of Cadiz Gap wind anticyclones. *Continental Shelf Research.* 91:171-191.

Piola, A. R., and A. L. Gordon (1989), Intermediate waters in the southwest South Atlantic. *Deep Sea Res.* Part A, 36(1), 116, doi:10.1016/0198- 0149(89)90015-0.

Reid, J. L. (1989), On the total geostrophic circulation of the South Atlantic Ocean: Flow patterns, tracers, and transports. *Prog. Oceanogr.* 23, 149244, doi:10.1016/0079-6611(89)900013.

Richardson, P. L., and S. L. Garzoli (2003), Characteristics of intermediate water flow in the Benguela Current as measured with RAFOS floats. *Deep Sea Res.* Part II, 50, 87118, doi:10.1016/S0967-0645(02)00380-6.

Rhines, P. B. (1975), Waves and turbulence on a b plane, *J. Fluid Mech.*, 69, 417 443.

Rimaud, J., S. Speich, B. Blanke, and N. Nicolas (2012), The exchange of Intermediate Water in the southeast Atlantic: Water mass transformations diagnosed from the Lagrangian analysis of a regional ocean model. *J. Geophys. Res.* 117, C08034, doi:10.1029/2012JC008059.

Rosso I., Hogg McC. A., Strutton P. G., Kiss A. E., Matear R., Klocker A., van Sebille E. (2014), Vertical transport in the ocean due to sub-mesoscale structures: Impacts in the Kerguelen region. *Ocean Modell.* http://dx.doi.org/10.1016/j.ocemod.2014.05.001.

Roullet G. and Klein P. (2010), Cyclone-Anticyclone Asymmetry in Geophysical Turbulence. *DOI: 10.1103/Phys. Rev. Lett.* 104, 218501.

Roullet G., Capet X., Maze G. (2014), Global interior eddy available potential energy diagnosed from Argo floats. *J. Geophys. Res.* 1651-1656, 10.1002/2013GL059004.

Rubio, A.,Blanke B., Speich S., Grima N., Roy C. (2009), Mesoscale eddy activity in the southern Benguela upwelling System from satellite altimetry and model data. *Prog. Oceanogr.* , doi:10.1016/j.pocean.2009.07.029.

Rusciano, E., S. Speich, and M. Ollitrault (2012), Interocean exchanges and the spreading of Antarctic Intermediate Water south of Africa. *J. Geophys. Res.* 117, C10010, doi:10.1029/2012JC008266.

Schmid, C., O. Boebel, W. Zenk, J. R. E. Lutjeharms, S. L. Garzoli, P. L. Richardson, and C. Barron (2003), Early evolution of an Agulhas Ring, *Deep Sea Res. Part II, 50(1), 141 166.*

Schouten, M. W., de Ruijter, W. P. M., van Leeuwen, P. J. and Ridderinkhof, H. (2003). Eddies and variability in the Mozambique Channel. *Deep Sea Research Part II: Topical Studies in Oceanography, 50, (12-13), 1987-2003*.

Shchepetkin, A. F., and J. C. McWilliams (2003), A method for computing horizontal pressure-gradient force in an oceanic model with a nonaligned vertical coordinate. *J. Geophys. Res.* 108(C3), 3090, doi:10.1029/ 2001JC001047.

Shchepetkin, A. F., and J. C. McWilliams (2005), The regional oceanic modeling System (ROMS): A split-explicit, free-surface, topography-following-coordinate oceanic model. *Ocean Modell.* 9, 304 347, doi:10.1016/j.ocemod.2004.08.002.

Smith, K. S., (2007). The geography of linear baroclinic instability in Earths oceans. *Journal of Marine Research, 65, 655683*.

Smith, W., and D. Sandwell (1997), Global sea floor topography from satellite altimetry and ship depth soundings. *Science* 277 (5334), 19561962, doi:10.1126/science.277.5334.1956.

Soufflet Y., Marchesiello P., Lemarie' F., Jouanno J., Capet X., Debreu L., Benshila R. (2016), On effective resolution in ocean models. *Ocean Modell.* 98 (2016) 3650.

Speich, S., B. Blanke, and W. Cai (2007), Atlantic Meridional Overturning and the Southern Hemisphere Supergyre. *Geophys. Res. Lett.* 34, L23614, doi:10.1029/2007GL031583.

Speich, S., Lutjeharms, J.R.E., Penven, P., Blanke, B. (2006). Role of bathymetry in Agulhas Current configuration and behaviour. *Geophysical Research Letters.* 33, L23611. doi:10.1029/2006GL027157.

Stewart, K.D., A.McC. Hogg, S.M. Griffies, A.P. Heerdegen, M.L. Ward, P. Spence, M.H. England, (2017). Vertical resolution of baroclinic modes in global ocean models, *Ocean modeling, Volume 113, 2017, Pages 50-65, ISSN 1463-5003*, http://dx.doi.org/10.1016/j.ocemod.2017.03.012.

Talley, L. D. (1996), Antarctic Intermediate Water in the South Atlantic. *in The South Atlantic: Present and Past Circulation, edited by G. Wefer et al.* pp. 219238, Springer, Berlin, doi:10.1007/978-3-642-80353-6-11.

.van Leeuwen, P. J. and de Ruijter, W. P. M. (2000). Natal Pulses and the formation of Agulhas Rings. *Journal of Geophysical Research, 105 (C3), 6425-6436*.

Weijer, W., W.P.M. de Ruijter, H.A. Dijkstra and P.J.van Leeuwen (1999), Impact of interbasin exchange on the Atlantic overturning circulation. *J. Phys. Oceanogr.* 29,2266-2284.

Supporting Information for "Indo-Atlantic exchange, mesoscale dynamics and Antarctic Intermediate Waters"

T. A. Capuano,[1] S. Speich,[2] , X. Carton[1] and Remi Laxenaire[3]

Contents of this file

1. Figures S1 to S4

Corresponding author: S. Speich, Laboratoire de Meteorologie Dynamique, LMD-IPSL, Ecole Normale Superieure, Paris, France (speich@lmd.ens.fr)

[1]Laboratoire d'Ocanographie Physique et
Spatiale, LOPS-UBO, Brest.

[2]Laboratoire de Meteorologie Dynamique,
LMD-IPSL, Ecole Normale Superieure,
Paris, France.

[3]Laboratoire de Meteorologie Dynamique,
UMR 8539 Ecole Polytechnique, ENS,
CNRS, Paris, France.

Introduction

This supporting information provides 4 panels of Figures which are described in the main article.

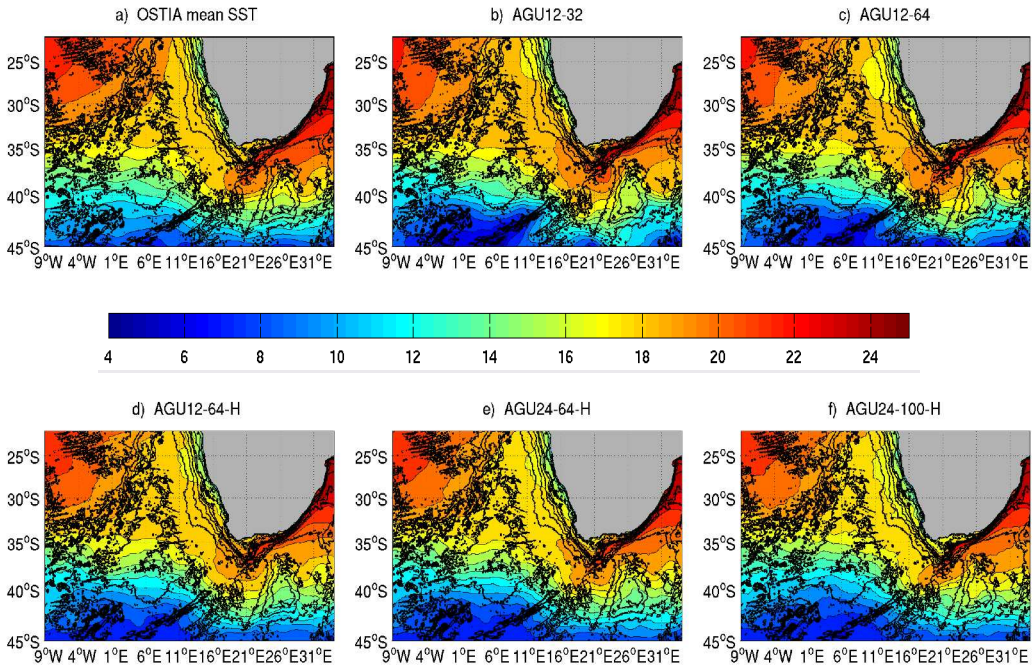

Figure S1. Mean horizontal distributions of Sea Surface Temperature comparing the estimate from OSTIA data (a) with each of our five simulations (b-f). Black lines below the contours are for the -5000,-4000,-3000,-2000,-1000,-500,-200,-100m isobaths from the Etopo2 dataset.

D R A F T October 2, 2017, 7:15pm D R A F T

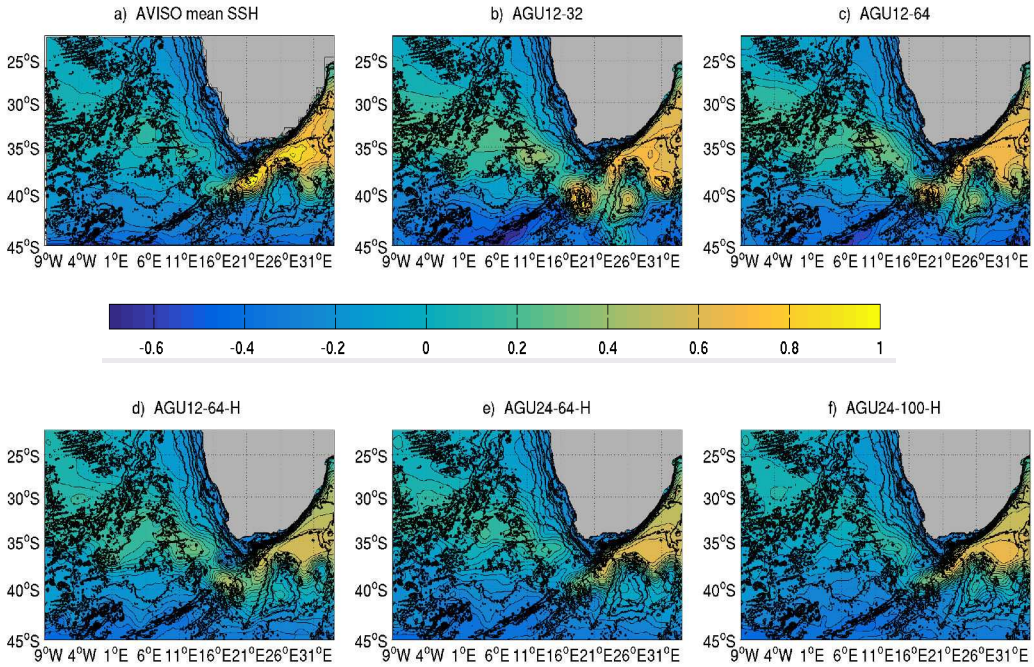

Figure S2. Same as Fig.1 but comparing the mean Sea Surface Height estimated from Aviso data (a) with the one from each of our five simulations (b-f).

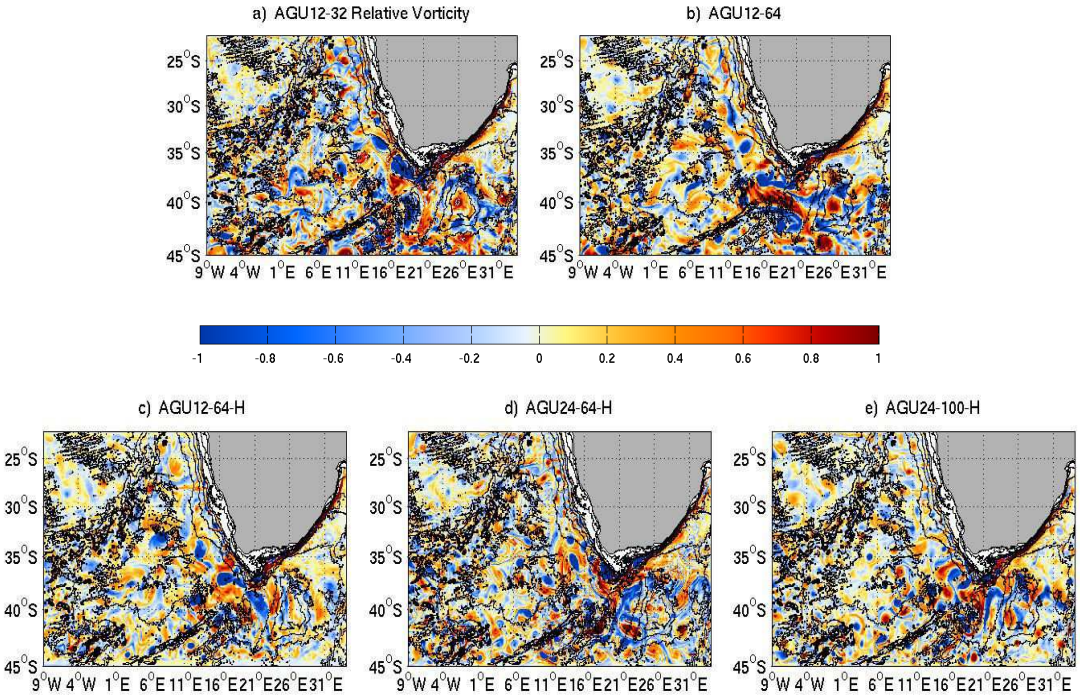

Figure S3. Snapshots of relative vorticity (ω, s^{-1}x 10^{-5}), extracted along the 27.2 isopycnal, from the model month 1 of year 5 for our 5 simulations. Black contours are for the -5000,-4000,-3000,-2000,-1000,-500,-200,-100m isobaths from the Etopo2 dataset.

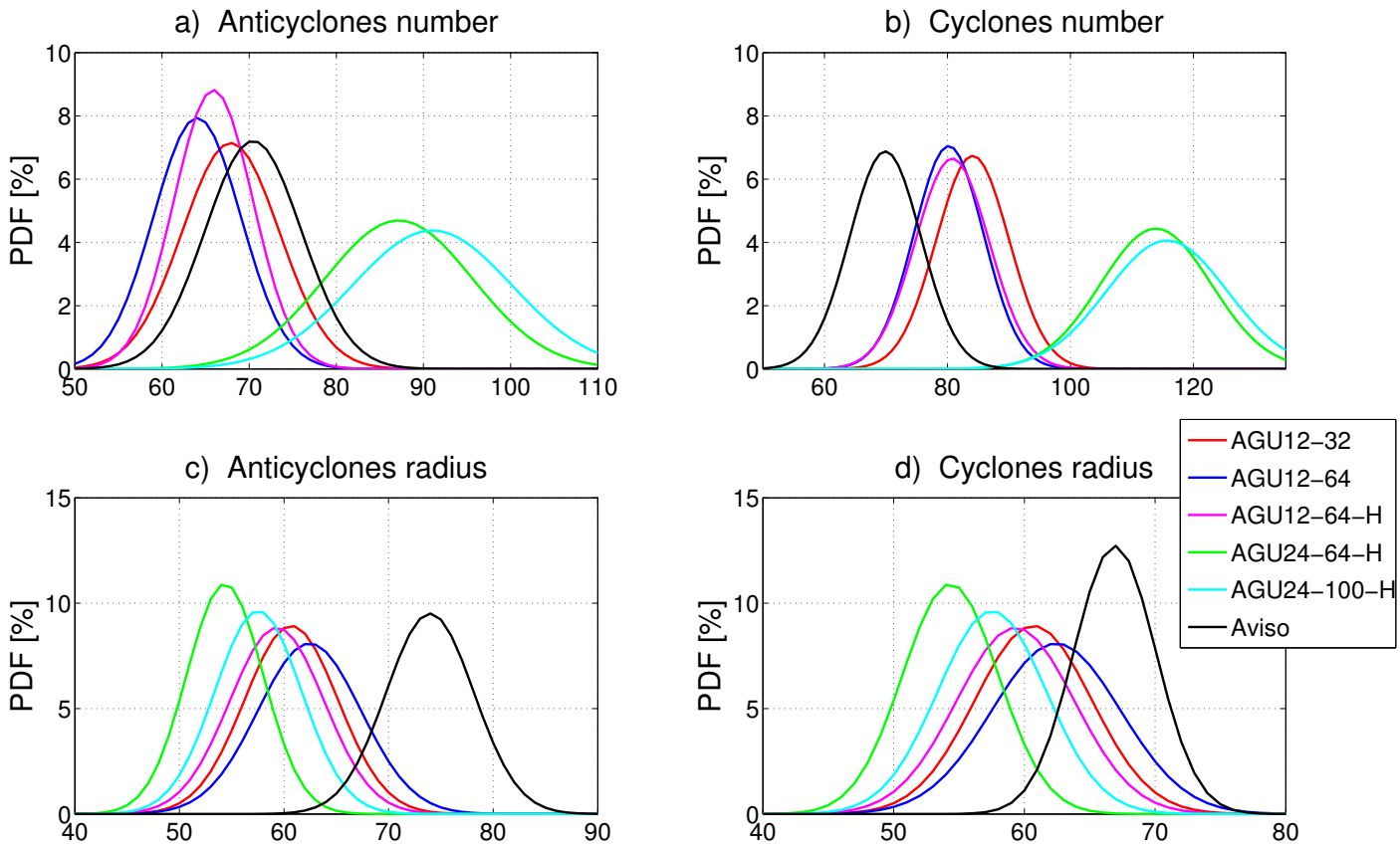

Figure S4. Probability density functions fitted to the time series of the number of (a) anticyclones and (b) cyclones and the mean radius of (c) anticyclones and (d) cyclones detected in each of the five numerical simulations (colored lines) and from AVISO data (black line), without the filtering that removed the modelled eddies whose radius was equal or smaller than 30 km.

4.3 Discussion

In this chapter we presented the results of a series of progressively higher resolutions, regional simulations, focusing on the Cape Basin region, south of the African continent, to assess the role of mesoscale features on the inter-basin exchanges, and the ability of a numerical model to correctly reproduce the observed watermass and eddy characteristics. Specifically, both the horizontal and vertical resolutions were modified, showing that despite the use of increasingly higher horizontal resolution, the model was incapable of representing the observed T-S properties and mesoscale processes unless we augment the number of sigma-levels and we homogeneously distribute them in the vertical. This translated in a vertical grid spacing from about 80 to 50 m, regionally required to adequately resolve the vertical structure of the horizontal flows and its main baroclinic modes. Eddy tracking was then used to study the taxonomy of the mesoscale features in this region, and their role on the exchange of waters between the Indian and Atlantic sectors. We found, as expected, that strong eddies, likely generated through baroclinic processes, are vital for tracer exchange between the basins, and, more surprisingly, that they have a seasonal cycle. This mesoscale variability will be explained in light of the results of the next chapter, which will relate it to the submesoscales seasonality and to the seasonal occurrence of different instabilities originating from the meso-submesoscale interactions.

According to altimeter and in situ observations, the Cape Basin is populated with vortices ranging in diameter from tens of kilometers (eddies) to hundreds of kilometers (rings). The shedding and translation of these vortices influence the inter-oceanic transfers of mass and energy among the South Atlantic, South Indian, and Southern Ocean directly through transient fluxes or indirectly through the mean circulation [*Matano and Beier*, 2003, *Treguier et al.*, 2003]. The grid size of the 5 simulations analysed in this chapter did not allow for the resolution of the full spectrum of oceanic variability, but only that portion with horizontal scales of the order of or slightly smaller than the Rossby radius ($\simeq$30 km at these latitudes). Models at these resolutions are generally regarded as eddy-permitting for the $1/12^\circ$ configurations and eddy-resolving for the ones at $1/24^\circ$. However, it should be noted that the bulk of the Indo-Atlantic inter-ocean exchange is thought to be accomplished by rings with spatial scales much larger than the Rossby radius, ranging from a minimum of 70 km to a maximum of 200. Thus, it is expected that even though our configurations may not contain all the scales of eddy variability, they were still adequate to resolve those that are more relevant to the inter-ocean ex-

change. With these caveats in mind, we have focused our analysis on those aspects of the eddy kinematics that our simulations could properly resolve and pointed out, whenever appropriate, the model's shortcomings, in comparison to the available observations.

At first, we examined the mesoscale eddy field reproduced in our numerical simulations by comparing statistical metrics (polarity, number, amplitude, mean radius) of the modelled structures with the ones estimated from the AVISO gridded data. Considering that the altimetric product has a lower resolution than even our mesoscale-permitting solutions at $1/12°$, all the eddies detected in our simulations were filtered using the criterion of a 30 km radius (all structures with radius equal or lower than this length were removed). This allowed the results of all simulations, especially of the ones at highest resolutions, to become much more comparable to the observational results.
Nonetheless, a reasonable agreement between the unfiltered eddy estimates of AGU24_100_H and the ones of AVISO were obtained in terms of the mean lifetime and pathways of the Agulhas Rings. Their mean radius is usually much larger than 30 km, so we expect them to be correctly sampled in the altimetry product, even if an additional degree of resolution degradation results from the interpolation of the satellites-retrieved observations on an uniform grid. This could partially explain the slight discrepancy that persists in the mean trajectories between the modelled and the observed anticyclones. Other possible sources of this bias are likely related to the model numerics and to a series of physical mechanisms, currently under- or not appropriately resolved, as discussed in more detail in the submitted article (section 4.2) and further tackled in the last chapter of this manuscript.

Despite these limitations, for the modelled Agulhas Rings we also investigated their geometry and verified that their mean profile is quasi-Gaussian, as previously suggested by *Chelton et al.* [2011] on a global scale. In respect to their dynamical interactions with the surrounding environment, the computation of their geometrical moments showed that these anticyclones are interested by different modes of deformation (principally angular mode 2, but also 3 and 4) due to the continuous non-linear exchanges with eddies of opposite sign and with the main, regional currents. This result confirms the highly turbulent nature of the Cape Basin circulation and the existence therein of a milieu of vigorous stirring and mixing [*Boebel et al.*, 1998, 2003].

With the aim to asses how these processes and the behaviour of the modelled eddies

impact the local subsurface water masses, we qualitatively pointed out that the modifications in the T-S properties and spreading of intermediate waters can be mainly related to the dynamical characteristics of the mesoscale eddies in which these waters are trapped. To determine the relative contributions of Cape Basin cyclones and anticyclones to the advection of AAIWs, we separated the T-S curves plotted at the centres of all the eddies detected in each of our simulations according to eddy polarity. We found that, albeit discrepancies exist between our numerical configurations in terms of the simulated AAIWs T-S properties, these appear to be relatively homogeneous in our study region. This implies that cyclones and anticyclones convey the same varieties of AAIWs (i.e. the Indian, the Atlantic and the Indo-Atlantic types, as suggested by *Rusciano et al.* [2012]). Thus, eddies of both signs equally contribute to the AAIWs advection in the Southeast Atlantic, in agreement with what shown in Argo data and in past studies [*Arhan et al.*, 2011, *Boebel et al.*, 2003, *Garzoli and Gordon*, 1996, *Richardson and Garzoli*, 2003, *Rimaud et al.*, 2012]

In relation to the scientific objectives described in Chapter 2, we have thus been able to partially investigate points 1. and 2., namely an assessment of the Cape Basin turbulent field and a description of its dynamical characteristics. The evaluation of both these aspects has been for now restricted to the mesoscale component of the flow. Moreover, we explored point 5. about the impact of the Cape Basin non-linear processes on the water masses exchanges. Indeed, in section 4.2 the eddy detection technique and the EPV budget were used in concert to delineate the role of the mesoscale structures on the water masses advection and mixing and to characterise the eddy temporal variability.
The increased resolutions of the nested configuration (AGU12_36_108) will allow us in the next chapter to better approach points 1. and 2. of our objectives, addressing those questions about the submesoscale contribution to the Cape Basin non-linear dynamics that remained currently unanswered. The analysis of this simulation, in comparison to the one at intermediate horizontal resolution (AGU24_100_H), will also provide qualitative evidence about some of the instabilities deriving from the meso-submesoscale interactions and on their impact on the local water masses. This will alow us to address points 3. and 4. of our study objectives, regarding the energy transfers between different dynamical scales, their seasonal variability and their ultimate effects on the water masses structure.

4.4 Conclusions

At present, models used in climate studies are of coarse resolution (1/8°-1/12°) because of the enormous CPU requirements of long integrations. Hence, differences in the representation of the turbulent processes of the Agulhas Current System, impacting the global MOC, due to model resolution are of great interest to the whole community of climate modellers. During the last decades, there have been many attempts to estimate the Indo-Atlantic interbasin exchanges using numerical simulations (e.g., [*De Ruijter et al.*, 1999] and references therein). Most of those studies have focused on the large-scale aspects of the mass and heat balances and just a few, more recent ones have stressed the attention on the mesoscale processes by which those balances are achieved. Since these estimates are based on coarse, non-eddy-resolving, or barely eddy-permitting, simulations the question remains as to whether their resolution can represent the Indo-Atlantic inter-ocean exchanges. To address this, a better understanding of the mesoscale processes that are unresolved by coarse-resolution models is needed.

In this respect, regional models constitute a powerful and useful tool, since, thanks to their limited cost, they can be run more efficiently than global-scale models. This makes possible to obtain a large number of sensitivity tests on various parametrizations, forcings and processes. For example, through a hierarchy of preliminary experiments run at much lower resolution (1/4°), we investigated the role of the shape and steepness of the bathymetry, as well as the location of the open boundaries and of the diffusion coeffcient. The results were discussed in terms of physical processes inducing or influencing the Agulhas Retroflection, the rings shedding, and the general cyclone genesis and dynamics in the upwelling region. Their analysis helped addressing the choice of the best combination of numerical parameters to use for higher resolution configurations. These tests were also motivated by previous numerical studies [*Doglioli et al.*, 2006, *Matano and Beier*, 2003, *Rubio et al.*, 2009, *Speich et al.*, 2006], who showed how the net Indo-Atlantic inter-ocean exchange is very sensitive to the regional topography and geometry: the steepness of the South-African continental slope; the small radius of deformation of the continental slope at the southern tip of the continent; the presence of a large Agulhas Bank; the narrowing induced by the existence of the Agulhas Plateau, as well as to the specific mid-latitude location of the Agulhas Retroflection. This last point underlines how the inter-ocean exchange can be affected by slight modifications of the mean ocean state and circulation.

In the work presented in this chapter, we offered a qualitative and quantitative description of the Indian/Atlantic interbasin exchange occurring in a sequence of spatially refined numerical experiments. Namely, their horizontal resolution ranged from eddy permitting (1/12°) to mesoscale-resolving (1/24°) and their vertical resolution was gradually modified from 32 to 100, uniformly distributed, sigma-levels, obtaining a homogeneous vertical grid spacing of ∼50 m. Since previous modelling studies [*Marchesiello et al.*, 1998], in line with earlier observational results [*Gordon*, 1985, *Gordon et al.*, 1992, *Lutjeharms*, 1987], suggested the the upper branch of the MOC is composed of intermediate and thermocline waters, we examined with particular attention the AAIWs dynamics and thermoaline structure in the Cape Basin. The latter can be considered a key region for the inter-ocean exchange as it approximately encompasses the area bounded to the northwest by the Walvis Ridge and to the southeast by the Agulhas Ridge; it is thus localised within the Agulhas rings westward path in the South Atlantic (Fig.1 of section 4.2). In light of the main results of this chapter, we believe to have succeded in better detail the crucial role of mesoscale eddies of both polarities in the advection of AAIWs in the Southeast Atlantic. In particular, with our highest eddy-resolving configuration (AGU24_100_H) we managed to reproduce the observed sharp transition of this water mass between the Indian and the South Atlantic ocean along it regional density layer (27.2σ). We modelled indeed how along this isopycnal surface the saltier Indian AAIW is advected within eddies of both signs and mixes with the fresher Atlantic AAIW in the Cape Basin, ultimately leading to the formation of the Indo-Atlantic type of AAIW.

This significant improvement, as any other achieved in the comparison of our high resolutions T-S structure with observations, was obtained by using smoothed climatologies, for the forcing at the surface and at the lateral boundaries, and open boundary conditions [*Marchesiello et al.*, 2001]. The latter are here based on radiation conditions and relaxation to climatology. This choice was motivated by the results of previous modelling studies on the Agulhas circulation [*Barnier et al.*, 1996, 1998] which showed open boundary conditions to be numerically robust and able to bring into the South Atlantic basin the necessary information from the outer oceans. As regards the use of climatological forcing, even though improved accuracy can be expected by the use of more synoptic boundary forcings [*Biastoch et al.*, 2009, *Durgadoo et al.*, 2013, *Loveday et al.*, 2014], the focus of our study is on the intrinsic oceanic turbulent processes, on their variability and impact on the local watermasses when these processes are forced by smoothed climatologies.

Albeit our repeated climatology lacks any high-frequency and inter-annual variability, there are pronounced differences in the simulation outputs between individual years: the thermal structure and the current fields of model year 5 are significantly different from those of year 4 at the same time of year. Intrinsic mesoscale activity is the main contribution to this inter-annual variability, and derives from oceanic instability processes in the absence of added forced variability, as underlined in previous numerical studies on the upwelling regions dynamics [*Marchesiello et al.*, 2003, *Penven et al.*, 2005]. No sensitivity tests have been performed, at present, with more realistic forcing, but their adoption could represent a challenging extension of our work. This would aim to resolve the response of the simulated thermal structure and of the current fields to inter-annual atmospheric fluctuations. In fact, how the inter-year variability observed in the model outputs would compare with that resulting from contrasted atmospheric forcing (such as a relaxed or intensified wind regime) or remote oceanic forcing (such as Rossby waves generated outside the model domain) still remains an open question in the Cape Basin.

Chapter 5

Meso- and Submesoscale Interactions, Air-Sea Exchange and Lateral Mixing

5.1 Introductory Remarks

Having established the instrumental role of the Cape Basin mesoscale eddies in the mixing and advection of intermediate water masses in the Southeast Atlantic, we will in this chapter focus our attention on the submesoscale component of the turbulent field in order to asses if exchanges between the different dynamical scales could as well affect the water masses dynamics. As seen in the satellite images of Figure 1.8 submesoscale fronts seem to widely occur at the surface in the Agulhas Current. Hence, we expect instabilities developing from the interactions between these finescale structures and mesoscale eddies to highly interest the upper layers of the Cape Basin. Here, in addition to the larger vortices and meanders, spawned at the Agulhas Retroflection and locally advected by the main current, significant energy can be transferred into submesoscale fronts, filaments and vortices. As discussed in Chapter 4, this energy derives from the eddy-eddy interaction, the interaction of the eddies with topography and with the current itself. In particular, the submesoscale could arise through surface frontogenesis growing off the interaction of Agulhas Rings with the surrounding Cape Basin eddies. In turn, some submesoscale fronts become unstable and develop submesoscale meanders and fragment into small vortices.

Moreover, previous studies [*Boebel et al.*, 2003, *Rimaud et al.*, 2012, *Rusciano et al.*, 2012, *Schouten et al.*, 2000] have hypothesized filamentogenetic activity also at intermediate depths, particularly along the AAIW layer. This filamentogenesis is manifested by

the presence of anisotropic submesoscale structures. Its origin could be attributed to different processes, among which: mesoscale straining; ageostrophic instabilities; vertical mixing; subduction; non-linear interactions between mesoscale eddies, and eventually (but not yet verified) the vertical influence of near-surface submesoscales through mixing.

According to numerous, numerical studies on this topic [*Callies et al.*, 2015, *Capet et al.*, 2008a,b,c, *Gula et al.*, 2015, *Klein et al.*, 1998, *Molemaker et al.*, 2015, *Rosso et al.*, 2014], the characteristics of submesoscale features are: large Rossby number, vertical velocity and vorticity; relatively flat horizontal velocity spectra; a large vertical buoyancy flux acting to restratify the upper ocean; a submesoscale energy conversion from potential to kinetic; a significant spatial and temporal intermittency in the upper ocean, and material exchanges between the surface boundary layer and the pycnocline. This chapter aims to numerically investigate several of these aspects through the adoption of a series of dedicated diagnostics, carried out over the biggest Agulhas Rings detected in our highest resolution simulations. These diagnostics allowed us to explore the seasonality, the energy transfers and the effects on watermasses of submesoscale processes, whose presence was identified not only at the surface, but also at depth, within the AAIW layer.

5.1.1 Cape Basin water masses formation and transformation

Since our focus is on the impact of meso- and submesoscale processes on the dynamics of the Cape Basin subsurface waters, we selected the main two water masses localised in the upper and intermediate layers: mode waters (Subantarctic Mode Water, SAMW on Fig. 1.8) and AAIWs. Figure 5.1 shows their seasonal vertical distribution within our region of study. These salinity sections come from the KAPEX experiment [*Lutjeharms et al.*, 1997, *Schmid et al.*, 2003], which investigated the thermohaline evolution of an Agulhas ring in the Cape Basin. The sections plotted at the end of the austral summer (March '97) and then at the end of winter (September '97), show how, in 6-months time, the upper layers (from the surface to the 26.5 isopycnal), occupied by SAMW, have become much saltier and thicker, with a mixed layer quite deeper. At depth, instead, AAIW has turned into a thinner and fresher layer within the anticyclone core. In March, we can indeed observe how the Indian variety of AAIW is present along the 27.2 isopycnal, while in September this has been transformed in a less saline variety (the Indo-Atlantic AAIW of *Rusciano et al.* [2012]) likely due to the mixing with the Atlantic AAIW variety.

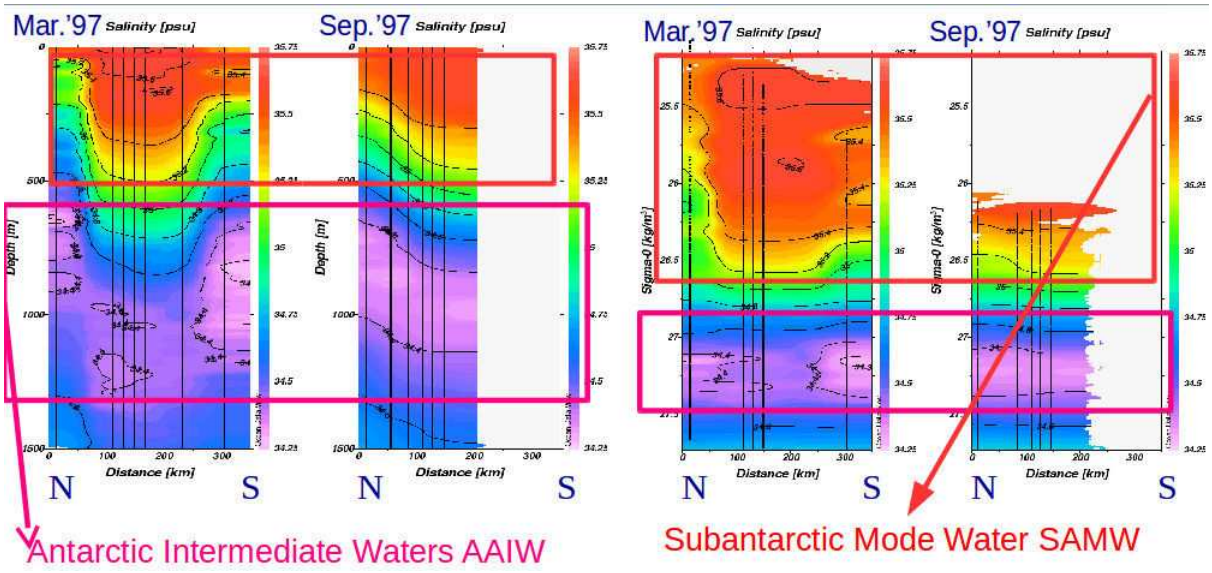

Figure 5.1: Salinity sections from the KAPEX experiment [*Lutjeharms et al.*, 1997], plotted, against pressure on the left and potential density on the right, at the end of summer (March '97) and at the end of winter (September '97) along an Agulhas ring crossing the Cape Basin. Figure adapted from *Schmid et al.* [2003].

In general, SAMW is identified by the 12°C pycnostad within the area of the AC retroflection [*Gordon et al.*, 1987]. Such a distinctive property has been observationally used to localize the presence of this watermass within the Indian Ocean Central Water trapped in the westward-drifting Agulhas rings [*Gladyshev et al.*, 2008]. In the Cape Basin, SAMW is known to flow within the uppermost ocean layers [*Hanawa and Talley*, 2001, *McCartney*, 1977, *Schmid and Garzoli*, 2009, *Talley*, 1996]. More recent observations from the GoodHope project showed, in the winter mixing-layer depth assessed from these profiles, that the rate of formation of SAMW is relatively low in the region [*Arhan et al.*, 2011, *Speich et al.*, 2012]. Nonetheless, observations from the Argo floats and CTD data from the GoodHope cruises suggest strong winter convection in some Agulhas rings. This accounts for a production of a local variety of Mode Water, that is injected in the Atlantic through rings propagation and whose characteristics are different from those of the classic SAMW inflowing from the Indian Ocean and the Agulhas Current [*Arhan et al.*, 2011, *Speich et al.*, 2012]. Indeed, relatively deep convection happens in the Cape Basin within the core of southern advected Agulhas rings [*Speich and Arhan*, 2007] and the results from the GoodHope project confirmed that these events mainly occur in eddies of subtropical water shed from the Agulhas Retroflection [*Arhan et al.*, 2011].

Previous occasional samplings of eddies with a subsurface homogenized core in the Cape

Table 5.1: Agulhas Rings Mode Waters characteristics as referenced by previous authors.

Eddies	Tpot (°C)	S (psu)	Sigma-theta	References
AR B1 B3-1 B2-1	16.2 13.5 13.0	35.42 35.40 35.20		Duncombe-Rae et al. 1996 *Attn : Eddies B3-1 and B2-1 were identified as « Brazil eddies » ... !!*
R1 R2 R3	11.6 17.1 13.6	35.08 35.71 35.34	26.72 26.04 26.53	Arhan et al. 1999
R1 R2	12.0 17	35.2 35.5	26.5 25.8	McDonagh et al. 1999
E1 E2 E3	17.0 17.0 12.5	35.5 35.5 35.2		Gladyshev et al. 2008
M	11.8	35.15	26.75	Arhan et al. 2011
ER Core1 ER Core2	15.5 13.2	35.65 35.35	26.25 26.55	Laxenaire (Personal communication)

Basin suggested a formation of these structures in the subantarctic zone, before their northwestward propagation and subduction beneath lighter Atlantic subtropical waters [*Arhan et al.*, 1999]. Complementary, altimetric tracking of these vortices [*Ducet et al.*, 20010, *Rio and Hernandez*, 2004] pointed out that they originate in the subdivision of newly-spawned Agulhas rings encountering the Agulhas Ridge. Intense cooling and convection of the eddy core waters may occur during the autumn or winter transit through the subantarctic domain, leading to the formation of vertically homogenized water with temperatures that may reach downward to about 12°C [*Speich and Arhan*, 2007]. This locally ventilated water has higher oxygen concentrations than the remotely formed SAMW (of Indian Ocean origin) present in the Agulhas retroflection [*Gordon et al.*, 1987]. Therefore we believe that the water mass visible in the Cape Basin upper layers (between the surface and the 26.5 isopycnal) of Figure 5.1 is not SAMW, but rather represents a modified type of Mode Water, whose formation is directly linked to the meso-submesoscale instabilities happening within the advected Agulhas rings.

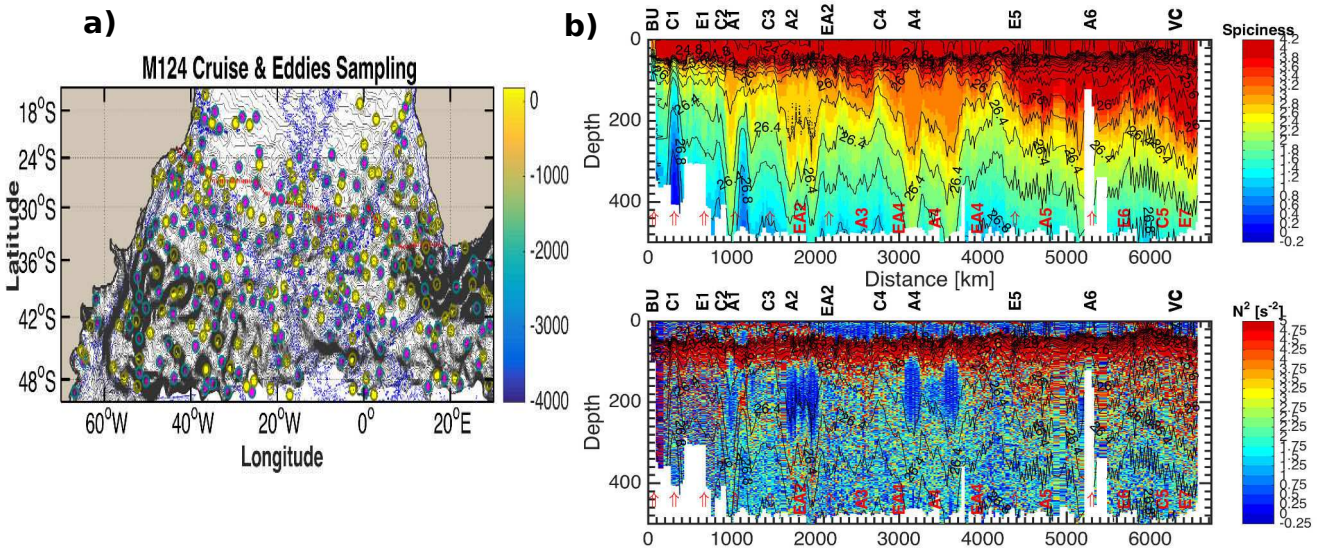

Figure 5.2: (a) Track of the 124 Cruise carried out in the Southeastern Atlantic between February and March 2016 onboard the German RV Meteor. (b) Vertical sections of spiceness (top) and stratification (bottom) along an Agulhas Ring trajectory in the Cape Basin, as sampled during this oceanographic campaign (Courtesy of Sabrina Speich). The bottom section shows homogenized patches of low stratification at around 200 m deep, indicating the subduction of a local variety of mode waters that we defined as Agulhas Ring Mode Water (ARMW).

In our highest resolution, nested configuration, we were able to simulate the presence of this new variety of Mode Water, originating from the trapping and seasonal subduction

of surface waters within the cores of subsurface-intensified rings. That is why we have dubbed this water mass 'Agulhas Ring Mode Water' (ARMW). Its typical T-S properties were previously documented by different authors, who erroneously identified it as SAMW. They provided disparate intervals of potential temperature and salinity, depending on the route undertaken by the sampled Agulhas Ring [*Dencausse et al.*, 2010b]. In the case of the southern, subantarctic pathway this water presented colder and fresher characteristics (11.6°C, 35.08 psu of *Arhan et al.* [1999]), while it appeared warmer and saltier if the ring trajectory was more northward, along the so-called 'warm route' (17°C, 35.5 psu of *Gladyshev et al.* [2008]). Values somewhat intermediate between these two intervals (∼14°C and 35.3 psu) have been lately observed for ARMW by Laxenaire (personal communication) in an ongoing 3-D reconstruction of two Agulhas Rings crossing the Cape Basin, through the colocalisation of Argo profiles within eddies cores detected in altrimetry data. We have summarised these referenced θ-S ranges in Table 5.1, along with the values of potential density that vary between 25.8 and 26.75 σ_{theta} over homogeneous layers 200 to 600 m thick. ARMW has been more recently sampled during an oceanographic cruise crossing the Cape Basin (Fig. 5.2a), where patches of relatively low stratification, hint of local subduction, were observed in the subsurface along an Agulhas Ring passage (Fig. 5.2b). However, up to present, any regional numerical study has been able to reproduce the ARMW formation. We will thus provide in our second submitted manuscript (section 5.2) an unprecedented description of the way this watermass is locally formed, analysing the meso-submesoscale instabilities involved in this process.

Another regional water mass that is of very particular interest for the South Atlantic thermocline ventilation is AAIW. This water mass is found below the seasonal thermocline and is characterized by a salinity minimum along the 27.2 isopycnal [*Talley*, 1996]. The Cape Basin is known not to be a formation region of intermediate waters, hence, the AAIW varieties locally observed are advected by the ocean circulation from different source regions [*Jacobs and Georgi*, 1977]. Once entered into the Cape Basin, observations show that this watermass undergoes drastic transformations of its T-S properties [*Rusciano et al.*, 2012]. These could be partly due to the influence of the strong air-sea interactions [*Sloyan and Rintoul*, 2001]. However, as widely discussed in the previous chapter, these transformations are also related to the intense mixing induced by the local turbulent processes [*Boebel et al.*, 2003], whose effects appear mostly compensated in density [*Rimaud et al.*, 2012, *Rusciano et al.*, 2012]. We have indeed seen how the

Cape Basin cyclones and anticyclones act as very deep-reaching vortices whose turbulent signature extends from the surface down to the base of the thermocline, affecting the mixing and spreading of subsurface waters. In section 5.2, we will demonstrate that the lateral mixing of AAIWs varieties is triggered by the mesoscale stirring of thermohaline fronts, sustaining the production of a conspicous filamentation at intermediate depths and leading to a tracer cascade at submesoscales [*Smith and Ferrari*, 2009].

5.1.2 Meso-submesoscale instabilities at the surface and at depth

We will now introduce the dynamical interactions between the meso- and submesocale processes that we believe having a leading role in the formation and transformation of the Cape Basin subsurface water masses.
Within the upper layers, the main background mechanism responsible for the seasonal subduction of surface waters is frontogenesis, which is an essential ingredient for upper-ocean submesoscale occurrence, as explained in details in *Capet et al.* [2008a,b,c]. Their view on the submesoscale regime (depicted in the diagram of Fig. 5.3) is the one of a middle path between two prevailing theories on their origin, that emphasize either frontogenesis/eddy-stirring [*Lapeyre et al.*, 2006] or surface-layer instability [*Boccaletti et al.*, 2007]. Several studies on the generation and development of upper-ocean submesoscale structures have indeed underlined the existence of a net distinction between two main sources of submesoscale activity: 1) the stirring of surface buoyancy gradients by interior mesoscale eddies [*Lapeyre et al.*, 2006, *Thomas and Ferrari*, 2008]; 2) the growth of mixed layer eddies and fronts through unstable processes [*Capet et al.*, 2008a, *Fox-Kemper et al.*, 2008a,b, *Mahadevan et al.*, 2010, *Mensa et al.*, 2013]. Other studies suggested that both types of processes described above tend to coexist [*Callies et al.*, 2016, *Capet et al.*, 2008c].

Capet et al. [2016] recently proposed another baroclinic instability process as able to couple the unstable behaviors of the ocean surface and interior. Inspired by the work of *Roullet et al.* [2012], they consider a turbulent regime in which the primary instability arises from the joint presence of a surface buoyancy gradient and an interior velocity shear, leading to the so-called 'Charney baroclinic instability' (C-BCI, [*Charney*, 1947]). This type of instability strengthens near-surface frontal activity with important consequences in terms of turbulent energetics for the upper water masses, as C-BCI plays a role in the seasonal restratification of the subsurface ocean. Oceanic regions which are

seasonally destratified and interested by mode water formation, may be conducive to C-BCIs, as we will demonstrate the Cape Basin to be.

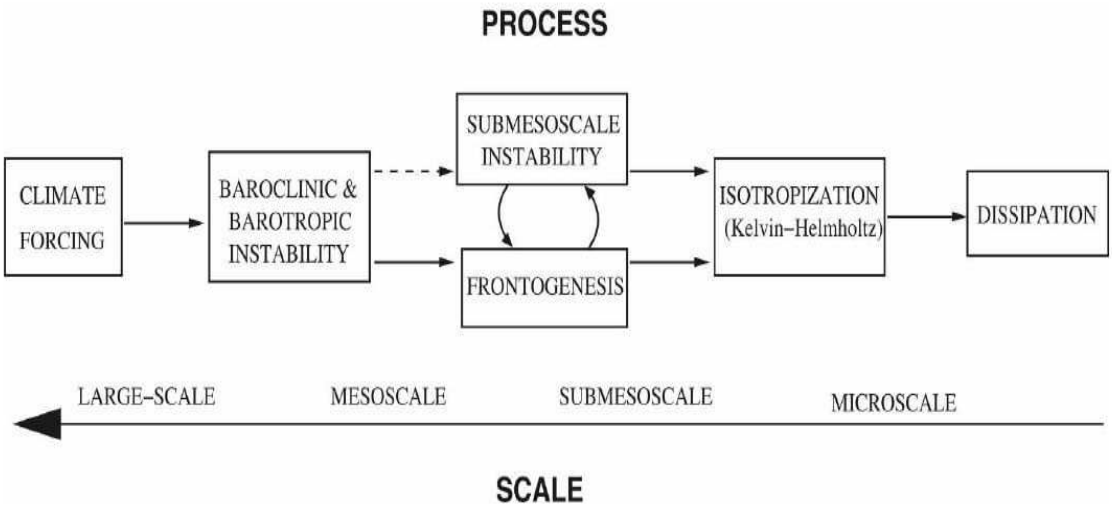

Figure 5.3: Schematic diagram for the main dynamical regimes by scale and their connecting total-energy transformation processes in an equilibrium oceanic circulation [*Capet et al.*, 2008c].

In our study region we overall observed the occurrence of both forms of submesoscale activity, fully captured by the highest resolution simulation (the submesoscale-resolving AGU12_36_108) and partially by the mesoscale-resolving one (AGU24_100_H), depending on the analyzed season. In summer, our region of study is mainly dominated by eddy-stirring and the mesoscale-driven submesoscale activity, triggering, within and around the largest anticyclonic eddies, symmetric instabilities, which are confined in the upper layers. In winter, mixed layer instabilities (MLIs) prevail in the upper ocean. At intermediate depths, instead, both seasons are characterised by the mesoscale stirring of tracers, leading to an abundant filamentogenesis and a density-compensated mixing of AAIWs in local varities. In the submitted manuscript presented in section 5.2 we have reviewed in detail the differences between these two finescales regimes. We found that the development of C-BCIs is the dynamical process able to reconnect them, with robust results for their occurrence in the upper layers, involved in the ARMW formation, and preliminary evidence also for intermediate depths.

For the latter, we mainly provided qualitative arguments to demonstrate that along-isopycnal eddy advection plays a major role in shaping the T-S relationship at the AAIWs level. The T-S structure of thermocline waters is currently understood as being set at

the surface by thermohaline forcing in the form of convective production of mode waters [*McCartney*, 1977] and subduction of winter mixed layers [*Stommel*, 1979]. The water mass properties are then advected into the interior by the mean ocean circulation, dispersed by eddies, and modified by diapycnal mixing [*Ferrari and Polzin*, 2005].
Much has been learned about isopycnal [*Robbins et al.*, 2000] and diapycnal [*Ledwell et al.*, 1998] processes in the past 70 years, but the implications of these observations for the establishment of the T-S relationship have not been fully appreciated. There persists a dichotomy between the effect of stirring and mixing on water mass properties: diapycnal mixing tends to homogenize different water types and consequently tighten the T-S relation; whereas isopycnal stirring creates contrasts between water types and enhances variability in the T-S relation [*McCartney*, 1982]. This is simply the distinction between stirring and mixing of *Eckart* [1948] applied to the T-S diagram.

One of the purposes of the work discussed in the present chapter is to qualify the roles of eddy stirring and diapycnal mixing in creating the T-S relation observed in the Cape Basin within the AAIWs layer from an analysis of the modelled T-S variability, whose effects on density has been observed to be almost completely compensated [*Boebel et al.*, 2003, *Rusciano et al.*, 2012]. Two main mechanisms could be responsible of such a phenomenon: 1) double-diffusive instabilities at molecular scales, as the source of the observed variability [*Schmitt*, 1994]; and 2) mesoscale stirring of large-scale temperature and salinity gradients by geostrophic turbulence, resulting in a direct cascade of thermoaline variance to small scales [*Smith and Ferrari*, 2009]. We rather support the idea that the second type of process is at play in our region of study. On one hand, because the first mechanism has been shown to be limitedly effective in a region closed to our area of interest [*Craneguy*, 1999], where double diffusive processes have been extensively studied to assess their importance in driving AAIWs intrusions in the ACC. *Craneguy* [1999] demonstrated that the intensity of vertical diffusivity in salt-fingers profiles was not sufficient to explain the strong cross-frontal injections of AAIWs observed in his study region.

On the other hand, because *Ferrari and Polzin* [2005] showed convincing evidence that mesoscale stirring is at work in the generation of T-S variability in the eastern North Atlantic, where very different subsurface water masses (i.e. the salty Mediterranean Outflow Water and the fresher North Atlantic Central Waters) converge. This oceanic region has strong similarities to the Cape Basin, where saltier Indian waters meet and mix with

the fresher waters of Atlantic origin [*Rusciano et al.*, 2012]. Moreover, using numerical simulations of a fully turbulent, time-evolving quasi-geostrophic flow, *Klein et al.* [1998] argued that mesoscale stirring occurs generically in regions where baroclinic eddies coincide with mean lateral gradients of temperature or salinity. In chapter 4, we showed that the Cape Basin could be one of these regions, since baroclinic instabilities were identified as the primary candidate for the eddies generation, and the basin is characterized by important T-S horizontal gradients, particularly at the AAIWs level [*Boebel et al.*, 2003, *Matano and Beier*, 2003].

The occurrence of tracer variance cascade within an Agulhas Ring had been already numerically explored by *Drijfhout et al.* [2001]. They suggested, as the most likely mechanism to affect the SSH decay of Agulhas rings, the interleaving by thermohaline intrusions, due to a double-diffusive origin. Later findings of *Beal* [2007] pointed out that the Agulhas interleaving intrusions would be rather linked to advective processes, being initially forced by rotating inertial velocities, and with subsequent growth possibly driven by small-scale baroclinic instabilities. According to their in-situ observations, the properties of these intrusions indicated that double diffusion was not essential for their development. In baroclinic fronts, that is, fronts with vertical and/or horizontal velocity shear, as in the Agulhas Current, twisting can also alter the slope of the isopycnal layers [*May and Kelley*, 1997]. In these cases, vertical shear becomes an important driving mechanism.

Therefore, we do not discard the hypothesis that our region of study constitutes an hybrid case where both types of density-compensation mechanisms coexist. However, our present numerical resolution does not allow us to investigate the presence of thermohaline intrusions. We have consequently restricted our analysis to the tracers variance and mixing driven by mesoscale stirring. We found that such a process is particularly efficient at the AAIWs level, where the generation of compensated T-S gradients by lateral eddy stirring can overcome the generation of T-S variance by vertical turbulence.

5.2 Article "Mesoscale and submesoscale processes in the southeast Atlantic and their impact on the regional thermohaline structure"

Mesoscale and submesoscale processes in the southeast Atlantic and their impact on the regional thermohaline structure.

Tonia Astrid Capuano[1], Sabrina Speich[2], Xavier Carton[1], Bruno Blanke[1]

[1]Laboratoire d'Oceanographie Physique et Spatiale, LOPS-UBO, Brest, France

[2]Laboratoire de Meteorologie Dynamique, LMD-IPSL, Ecole Normale Superieure, Paris, France

Key Points:

- Mesoscale spatio-temporal variability in the Cape Basin is also influenced by submesoscale mechanisms
- Seasonality of the flow instabilities highly affects the dynamics of the upper and lower thermocline water masses
- Small scale processes strongly impacts the Indo-Atlantic transports of heat and salt

Corresponding author: Sabrina Speich, speich@lmd.ens.fr

Abstract

The turbulent processes in the Cape Basin, the southeasternmost gate of the Atlantic Ocean, play a key role in the transport and mixing of upper to intermediate water masses entering the area from the Indian Ocean, making them especially relevant for the Indo-Atlantic transfer of heat and salt. In this paper, two numerical simulations at different horizontal resolutions are used to study meso- and submesoscale dynamics, their phenomenology, their evolution and their impact on the local water masses. Submesoscale processes seasonally affect both, the upper and intermediate layers, but there are clear dynamical differences between the two layers. Several types of instabilities underline this spatial and temporal variability. Near the surface, mixed-layer instabilities occur during winter, while mesoscale-driven instabilities, as the symmetric type, prevail in summer. The connection between these two seasonal regimes is ensured, in anticyclonic eddies and within the mixed layers, by Charney baroclinic instabilities, involved in the local formation and subduction of Mode Water, that we have dubbed as Agulhas Rings Mode Water. Intermediate depths are instead characterized by mesoscale mechanisms of density-compensation and lateral stirring of the tracer variance, triggering a significant filamentogenesis whose vertical scales are comparable to those mentioned in previous studies. This leads to a particularly efficient mixing of Antarctic Intermediate Waters of Indian and Atlantic origins. Lagrangian estimates highlight the new and significant role of fine scale structures in setting the water masses properties of upper and lower thermocline waters materializing the Indo-Atlantic exchange and therefore potentially affecting the global ocean circulation.

1 Introduction

1.1 The Indo-Atlantic interocean exchange

The Agulhas Current (AC) is the western boundary current of the southern Indian Ocean subtropical gyre and is primarily driven by the large-scale pattern of wind stress curl between the southeast trade winds and the Southern Hemisphere westerlies [*Beal et al.*, 2011]. South of the Agulhas Bank, at the outer edge of the continental shelf, the AC retroflects sharply, and continues eastwards as the Agulhas Return Current (ARC, *Lutjeharms et al.* [1992]). At the Agulhas Retroflection (AR) the current regularly loops back upon itself, and large anticyclonic eddies (known as 'Agulhas rings') are shed in the Cape Basin, and, from there, they move into the South-Atlantic Ocean [*Lutjeharms and Gordon*, 1987; *Ou and de Ruijter*, 1986].

The transport of water from the South-Indian to the South-Atlantic oceans has substantial implications for the convective circulation of the Atlantic Ocean as a whole [*Gordon*, 1985].

Weijer et al. [1999] and *Biastoch et al.* [2008] have demonstrated that these inter-basin fluxes of heat and salt are important for maintaining the strength and operation of the Atlantic Meridional Overturning Circulation (AMOC). Past descriptions of the Indo-Atlantic exchange suggested that this transport is mainly dominated by the migration of Agulhas rings from the AR through the Cape Basin into the western South-Atlantic (see *Lutjeharms* [1996] for a summary of observational studies). Other numerical experiments have focused on the turbulent activity of this oceanic basin [*Drijfhout et al.*, 2001; *Reason*, 2001; *You et al.*, 2003; *Matano and Beier*, 2003; *Treguier et al.*, 2003; *Biastoch et al.*, 2008], underlining how Agulhas eddies influence not only the transient transports, but also fluxes associated with the mean circulation (eddy fluxes, for example, supply most of the energy of the Benguela Current; *Veitch et al.* [2009]).

In particular, the work of *Matano and Beier* [2003] indicated that a distinctive characteristic of the eddy variability within the Cape Basin is the co-existence of cyclonic and anticyclonic vortices in dipole structures that resemble the Heton model [*Hogg and Stommel*, 1985]. The same authors pointed out that the momentum fluxes, essential to the kinetic energy balance of the Cape Basin, are primarily driven by baroclinic and barotropic eddies, with negligible contributions from the mean circulation. In support to the latter, Lagrangian studies suggested that the transfer of properties and their mixing, rather than being uniformly distributed across the entire subtropical gyre, appears to be concentrated in some small regions [*Boebel et al.*, 1998]. The Cape Basin is one of them, characterized as the highest world ocean spot of eddy kinetic energy [*Boebel et al.*, 2003]. This implies that the mesoscale details of the inter-basin exchanges are extremely important and cannot be simply represented by some constant mixing coefficient in diagnostic, large-scale, model simulations [*Gordon et al.*, 1992].

In summary, the Indo-Atlantic interocean exchange is currently thought to consist of three major parts [*Lutjeharms*, 1996; *De Ruijter et al.*, 1999]: 1) the advection of Agulhas filaments, 2) the shedding of Agulhas rings [*Lutjeharms et al.*, 1992], and 3) the transport and mixing of intermediate water between the two southern hemisphere subtropical gyres of the Indian and Atlantic Ocean [*Speich and Arhan*, 2007; *Speich et al.*, 2007; *Rusciano et al.*, 2012]. Since the contribution of Agulhas filaments is thought to be significantly smaller than that of Agulhas rings [*Schmid et al.*, 2003], this paper will mainly focus on the last two components of this exchange. Eddies of both signs are indeed fundamental for the advection of the local watermasses and the transfer of the related T-S anomalies in the Cape Basin, as already suggested in earlier observational studies [*Lutjeharms et al.*, 2003; *Boebel et al.*, 2003; *Giulivi and Gordon*, 2006; *Arhan et al.*, 2011]. In this context we will mainly focus on the analysis of anti-

cyclones since they have a much longer lifetime than cyclones [*Dencausse et al.*, 2010; *Laxenaire et al.*, Submitted] and also because the targeted instabilities at mesoscale are better resolved within the largest Agulhas rings detected in our simulated domain.

1.2 The role of Agulhas rings

Several studies, based on satellite-altimetry data, have led to a general agreement on the way Agulhas rings cross the South-Atlantic Ocean [*Gordon and Haxby*, 1990; *Byrne et al.*, 1995; *Schouten et al.*, 2000; *Laxenaire et al.*, Submitted]. They showed that once these eddies have escaped the southeastern Cape Basin, they propagate north-westward as isolated structures at latitudes of 20°S-35°S, generally slowing down at the approach of bathymetric ridges. The Agulhas rings move partly due to β-induced motion and partly due to advection by the background currents [*De Ruijter et al.*, 1999]. Their speed and tracks are influenced by bottom topography and interaction with other eddies [*Byrne et al.*, 1995; *Schouten et al.*, 2000; *Laxenaire et al.*, Submitted]. Ring translation speeds have been reported to vary between 3 and 16 km/day [*McDonagh et al.*, 1999; *Goni et al.*, 1997] and within 10 months after their formation most rings have reached the Walvis Ridge [*Schouten et al.*, 2000]. However, the behavior of Agulhas rings in the southeastern Cape Basin, closer to their formation region, is more complex, and was at times presented in contrasted manners.

Garzoli and Gordon [1996]; *Garzoli et al.* [1996] and *Goni et al.* [1997], emphasizing the net north-westward translation of the rings in the Cape Basin, defined a relatively narrow ring corridor in which they would propagate and where Atlantic water from the west and Indian water from the east would mix. *Boebel et al.* [2003], on the other hand, stressed the attention on the turbulent character of the southeastern Cape Basin and the ensuing intense water mass mixing. *Schouten et al.* [2000] have pointed out that shear diffusion, due to small-scale dispersion and large-scale deformation of the rings, may be an important decay mechanism in the Cape Basin, together with convective modification and double diffusive interleaving. Overall, the shedding of large Agulhas eddies and rings certainly play a key role for the entrainment of Indian Ocean waters into the South Atlantic, even if it still remains unclear how these transient fluxes are ultimately driven into the North Atlantic basin [*Treguier et al.*, 2003].

1.3 Cape Basin watermasses

Hydrographic and tracer data show that the westward transfer of Indian Ocean water into the Southeast Atlantic is limited to waters with potential densities, with respect to the sea sur-

face, lower than 27.5 σ_{theta} and shallower than 1500 -2000 m [*Gordon et al.*, 1992]. The Indian water masses involved in this exchange are those advected by the Agulhas Current: South Indian Central Water, Subtropical Mode Water, Indian Antarctic Intermediate Water and, eventually, Red Sea Water. These waters meet and partially mix with Central and Intermediate waters of the South Atlantic as well as Subantarctic Surface Waters [*Gordon et al.*, 1992; *Giulivi and Gordon*, 2006; *Rusciano et al.*, 2012].

Recent studies have pointed out that the Cape Basin is a key region for the global MOC but also in terms of water masses modifications. This is partly due to the intense air-sea interactions that transform the upper Indian Ocean water core of Agulhas Rings, made of South Indian Central Waters and Subtropical Mode Waters, in different varieties of what we can call Agulhas Rings "mode water" (ARMW). The latter are characterized by homogeneous layers 200 to 600 m thick and potential densities varying from 26.0 to 26.8 σ_{theta} [*Arhan et al.*, 1999; *Gladyshev et al.*, 2008; *Arhan et al.*, 2011]. While ARMW has been accounted from in-situ data, ocean models are unable to represent it: modelled Agulhas Rings are characterized by a stably stratified structure [*Rimaud et al.*, 2012].

Another important water mass that takes part in the Indo-Atlantic exchange and is modified in the Cape Basin is Antarctic Intermediate Water (AAIW). In this region, the fresh South Atlantic AAIW (A-AAIW) converges with the saltier and older Indian AAIW (I-AAIW) [*Jacobs and Georgi*, 1977]. Their mixing gives rise to the Indo-Atlantic AAIW (IA-AAIW) having an intermediate minimum value of salinitity [*Rusciano et al.*, 2012], and this happens isopycnally as I-AAIW and A-AAIW have comparable densities (27.2 σ_{theta}). It has been observed that I-AAIW advected in the Cape Basin within Agulhas Rings undergoes to modifications (freshening by mixing with A-AAIW) rapidly after the rings have entered our study region [*Schmid et al.*, 2003]. Again, numerical models are currently not able to realistically reproduce the physical processes driving this regional transformation of AAIW in the ocean interior [*Rimaud et al.*, 2012]. Hence, they do not simulate correctly the transport and properties fluxes into the South Atlantic associated with these water masses [*Rimaud et al.*, 2012].

1.4 Objectives and outline of the study

In the present work, we will mainly focus on the 3D-structure, variability and dynamical characteristics of the Cape Basin mesoscale eddies, with a particular emphasis on anticyclones. In parallel, we will numerically explore the nature and origin of submesoscale processes and diagnose the different types of instabilities that may derive from them. An addi-

tional goal of this study will be to assess the impact of these meso- and submesoscale processes on the dynamics and on the formation and transformation of the upper 1500 m water masses, in order to better understand they role in the Indo-Atlantic interocean exchange.

In light of the above-mentioned objectives, the paper is organized as follows. In section 2, the numerical framework is described: the model setup is briefly presented and some technical characteristics of the two analyzed configurations are provided. In this section, we also introduce the diagnostics used to investigate the different types of instabilities that could characterize the interactions between the meso- and submesoscales. The principal differences between the horizontal resolutions of the two simulations are presented in section 3, principally in terms of energetics. This section closes up with a discussion on the emerging evidence of a separation, in distinct dynamical regimes, between the upper layers and those at intermediate depths, at the base of the thermocline. Section 4 focuses on the turbulent activity within the upper layers: the instabilities at play, the energy transfers associated with them and the seasonality of the interactions between the meso- and submesoscale. An assessment of the impact of these turbulent structures on the thermohaline properties of the local mode waters is also presented at the end of this section, where we address the possible occurrence of Charney Baroclinic Instabilities (C-BCIs) within the mixed layer and their implication in the formation and subduction of a local variety of mode waters (ARMW), as we have previously defined them. In section 5, we firstly provide some general remarks on the effects of the density-compensation mechanism on AAIW dynamics and then discuss the plausibility that the mesoscale stirring of tracers is responsible for mixing different types of AAIWs within the Cape Basin. Lastly, in section 6 we present preliminary Lagrangian results on the role played by small scale processes in the Indo-Atlantic exchange of thermocline waters, before offering a summary of the main results, together with some prospectives and conclusions of this work, in section 7.

2 Methods

2.1 The numerical model

The study is carried out using the IRD-UCLA version of the Regional Ocean Modeling System (ROMS) [*Shchepetkin and McWilliams*, 2003, 2005], which has been extensively and successfully tested in the Cape Basin region [*Speich et al.*, 2006; *Rubio et al.*, 2009; *Veitch et al.*, 2009; *Rimaud et al.*, 2012]. This circulation model is a split-explicit and free-surface model that makes the Boussinesq and hydrostatic assumptions when solving the primitive equa-

tions. The code uses a third-order up-stream biased scheme for advection, which provides lateral diffusivity/viscosity [*Shchepetkin and McWilliams*, 2009].

In the vertical the model is discretized on a sigma, or topography-following, stretched coordinate system. The grid is isotropic and does not introduce any asymmetry in the horizontal dissipation of turbulence, allowing a fair representation of mesoscale dynamics [*Penven et al.*, 2006]. The bottom topography is derived from the ETOPO2 (2' resolution) database [*Smith and Sandwell*, 1997]. Although the latest version of the model includes a pressure gradient scheme associated with a specific equation of state to limit errors in the computation of the pressure gradient [*Shchepetkin and McWilliams*, 2009], the bathymetry has been filtered in order to keep the 'slope parameter' r $<$0.25. The model has 100 vertical levels and the vertical sigma-coordinate is homogeneously distributed along the water column. In our configurations, we also activated the optimizing function of the vertical coordinate system that ensures an increased resolution in the subsurface and a fair smoothing of the tracer fields [*Lemarie et al.*, 2012]. This numerical choice has shown to be very influential for a 'realistic' representation of the watermasses characteristics of our study region.

All the model external forcing functions are derived from climatologies. At the surface, the model heat and fresh water fluxes are extracted from the COADS climatology [*Da Silva et al.*, 1994]. The initial conditions of the model is an ocean at rest with temperature and salinities from the World Ocean Atlas (WOA) for the month of January. For the wind stress, a monthly mean climatology is computed from QuikSCAT scatterometer data [*Bentamy et al.*, 2003; *Ayina et al.*, 2006]. The deliberate choice of using a climatological wind forcing for a simulation that is forced for multiple years, is in accordance with the focus on equilibrium dynamics. Moreover, it allows for an investigation of intrinsic, or unforced, system variability. At the four lateral boundaries an active, implicit, upstream-biased, radiation condition [*Marchesiello et al.*, 2001] connects the model solution to the monthly means of forcings extracted from the WOA climatology. The vertical mixing scheme is based on the K-profile parametrization (KPP) of *Large et al.* [1994], while the horizontal mixing is parametrized as a linear combination of Laplacian and biharmonic mixing, scaled with the grid size [*Lemarie et al.*, 2012].

Our model is integrated for 5 years and the output fields are stored and daily averaged everyday. Two horizontal resolutions are set: a high-resolution simulation (AGU12_36_108) at 1/12° horizontal resolution nested with a 1/36° and 1/108°, that is fully meso- and submesoscale resolving; and a medium-resolution simulation (AGU24_100_H) at 1/24° horizontal resolution, that partly permits submesoscale dynamics, but completely resolves mesoscale fea-

tures. Results presented in this paper come from the analysis of the last four years of each simulation. The first year is discarded as a spin-up period required to reach statistical equilibrium and for eddy kinetic energy (EKE=1/2 ((u_std)^2+(v_std)^2], where u and v are the zonal and meridional velocity components, and 'std' designates the standard deviation of their instantaneous values) to reach a plateau. In these two simulations we also make use of the tracking methodology of [*Chaigneau et al.*, 2008] to detect eddies for: discriminating between anticyclones (ACes) and cyclones (Ces); tracing their contours over horizontal maps; and localizing their centers for computing specific diagnostics. We refer to [*Laxenaire et al.*, Submitted] for an exhaustive description of the algorithm latest version.

2.2 The two model configurations

Analysis of the high-resolution simulation and comparison between the two simulations allow us to isolate processes that are directly linked to submesoscales. But before proceeding in this direction, we briefly present each of the two simulations. Our lowest resolution simulation, AGU24_100_H, is a fully mesoscale-resolving, submesoscale-permitting configuration, characterized by a horizontal grid-spacing, Δx, equal to $\sim$3.6 km and 100 sigma-levels, homogeneously distributed, in the vertical. Our highest resolution solution, AGU12_36_108, consists of a double-way nested configuration with two child grids embedded within a parent domain (Fig. 1a). The latter represents a 1/12°(Δx$\simeq$ 8 km) run with 100, homogeneously distributed, vertical levels, forcing a first child domain at 1/36° (Δx$\simeq$ 2.7 km), placed just after the Agulhas Retroflection and, embedded into it, a second child domain at 1/108° (Δx$\simeq$ 0.8 km), centered on the area of the Cape Basin. Figure 1a shows the geographical extensions of the three domains of our nested solution. This simulation employs the two-way AGRIF embedding capability of ROMS [*Debreu and Mazauric*, 2006], which is designed such that the output from the lower resolution parent domain provides boundary conditions for the higher resolution child domains nested within it and the child domains in turn feed the parent domain. This technique allows for more consistent boundary conditions, and is far less costly than running the parent domain at the resolution of either one of the two child domains. The parent domain has exactly the same extension of the one covered by AGU24_100_H (Fig. 1b), going from 10°W to 34°E and from 22°S to 45°S; the one of the first child is placed just after that the AC curls back eastward, spawning its rings westward (26-38°S, 3°W-15°E). The second child is then centered on the Cape Basin (30-37°S, 5-12°E), in an area intentionally chosen to be weakly affected by the complex topography of this region, in order to better iso-

late those physical processes directly related to the intrinsic ocean dynamics. As previously mentioned, all the simulations presented here are based on the same depth dataset, parameters, and forcing. Hereafter we will refer to the nested and higher resolution simulation (AGU12_36_108) as HR (for High Resolution), and to the lower resolution one (AGU24_100_H) as LR.

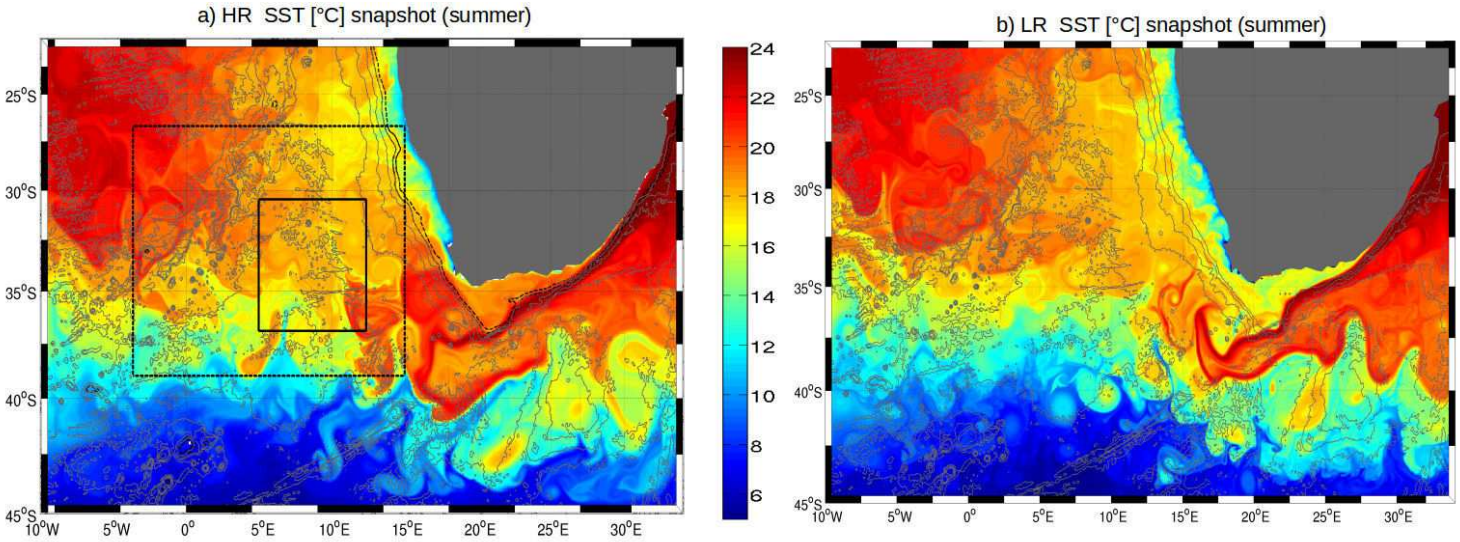

Figure 1. Instantaneous maps of Sea Surface Temperature showing the geographical extensions of the two numerical simulations analyzed in this paper: the three domains of the nested, HR solution (a) and the one of the mesoscale-resolving, LR simulation (b). Black contours are for the -5000,-4000,-3000,-2000,-1000,-500,-200,-100m isobaths from the Etopo2 dataset [*Smith and Sandwell*, 1997].

2.3 Diagnostics for the instabilities analysis

The submesoscale regime is characterized by the ability to transfer energy from the available potential energy (APE) and the KE of the mesoscale to smaller scales, opening the road toward the dissipative scales [*McWilliams*, 2008; *Molemaker et al.*, 2010]. Thus, we will primarily focus on the EKE release from different types of instabilities that can occur once ocean fronts intensify [*Haine and Marshall*, 1998]. The first type we will consider is the general class of baroclinic MLIs, and we propose to quantify them through their direct expression, i.e., the conversion rate of APE to EKE [*Boccaletti et al.*, 2007; *Fox-Kemper et al.*, 2008; *Capet et al.*, 2008c]. This conversion is common to all baroclinic instabilities and can be evaluated in terms of eddy vertical buoyancy flux (VBF):

$$VBF = < W'b' > \tag{1}$$

where W is the vertical velocity and b the buoyancy anomaly (b= - (g/ρ_0) ρ), while brackets denote a time average and the prime denotes fluctuations relative to this average. Then we quantify the conversion from mean KE (MKE) to EKE due the horizontal and vertical shear (HRS and VRS), calculated following the mathematical expressions given in *Gula et al.* [2015]:

$$HRS = - < u'u' > \frac{\partial < u >}{\partial x} - < u'v' > [\frac{\partial < u >}{\partial y} + \frac{\partial < v >}{\partial x}] - < v'v' > \frac{\partial < v >}{\partial y} \quad (2)$$

$$VRS = - < u'w' > \frac{\partial < u >}{\partial z} - < v'w' > \frac{\partial < v >}{\partial z} \quad (3)$$

These diagnostics quantify the horizontal and vertical exchange of KE between the MKE and EKE components. In particular, a conversion of MKE to EKE (HRS >0) may be interpreted as representing barotropic instability. Conversely, if there is a non-linear exchange from EKE to MKE (HRS <0), the eddies act to strengthen the mean flow [*Wells et al.*, 2000]. Positive values of VRS could instead indicate the presence of Kelvin-Helmholtz instabilities. The predominance of one of the two source terms, VBF or HRS >0, indicates that the eddy generation mechanism is primarly a baroclinic instability (VBF >0) or a barotropic instability (HRS>0).

The Okubo-Weiss (OW) is a metric used to identify elliptic (vorticity-dominated) and hyperbolic (strain-dominated) regions, which has been often applied to 2D or quasi-geostrophic, quasi-non-divergent flows [*Okubo*, 1970; *Weiss*, 1991]. For the general case of a non-null horizontal divergence field, OW can be written as:

$$OW = \sigma^2 - \omega^2 \quad (4)$$

where σ= (σ_n^2+σ_s^2)$^{1/2}$ is the strain rate of the horizontal (u, v) velocity field, with its normal, σ_n= $\frac{\partial u}{\partial x}$ - $\frac{\partial v}{\partial y}$, and shear, σ_s= $\frac{\partial u}{\partial y}$ + $\frac{\partial v}{\partial x}$, components, and where ω= $\frac{\partial v}{\partial x}$ - $\frac{\partial u}{\partial y}$ is the vertical component of relative vorticity (RV). For positive values of OW, the strain prevails, whereas negative values correspond to a dominant vorticity-based dynamics, usually associated with vortex cores. This parameter can be used to characterize regions of concentrated vorticity, and thus of coherent eddies, in a given two-dimensional velocity field.

The structure and evolution of the Ertel potential vorticity (Q, *Ertel* [1942]) can be used as a means to help interpreting submesoscale physics, since their dynamics are intimately linked with processes that modify the potential vorticity (PV) field, such as the forcing by wind stress, the buoyancy fluxes and the advection of PV by eddies [*Thomas*, 2005]. The mathematical form we have used here comes from *Peliz et al.* [2014]:

$$Q = -\frac{1}{\rho}\left((f+\omega)\frac{\partial \rho}{\partial z} - (\frac{\partial v}{\partial z}\frac{\partial \rho}{\partial x}) + (\frac{\partial u}{\partial z}\frac{\partial \rho}{\partial y})\right) \quad (5)$$

When Q is multiplied by the Coriolis parameter (f= $2\Omega\sin\phi$), we theoretically expect negative values to appear in regions where symmetric instabilities could be at play, corresponding as well to areas where the gradient Richardson number (Ri) is <1. Ri can be defined as follows [*Thomas et al.*, 2016]:

$$Ri = \frac{N^2}{S^2} \tag{6}$$

where $N^2 = \frac{\partial b}{\partial z}$ and $S^2 = \frac{\partial u}{\partial z}^2 + \frac{\partial v}{\partial z}^2$. N^2 is the stratification and S^2 is the squared shear. According to theory, a stratified, actively mixing boundary layer (i.e. here in summer) with Ri close to 1 is consistent with fronts that are symmetrically unstable [*Thomas et al.*, 2013], whereas for values less than 0.25 Kelvin-Helmholtz instabilities could be expected [*Bruggemann, and Eden*, 2015]. In section 4.2 we will verify the first possibility by analyising surface maps and vertical sections of these three diagnostics for the two model resolutions.

A last diagnostic used to quantify the turbulence due to submesoscales and hence discriminate the capability of our two numerical resolutions to resolve them consists in estimating the frontogenetic tendency. Frontogenetic activity mostly develops near the ocean surface, where the absence of vertical velocities allows straining from mesoscale eddies to increase density variance, thus leading to an effective sharpening of existing density fronts [*Lapeyre et al.*, 2006; *McWilliams and Molemaker*, 2011]. Frontogenesis is commonly studied in terms of the frontal tendency function F_{sh} and we make use of its definition by *Giordani and Caniaux* [2001]:

$$F_{sh} = -\overline{< (\frac{\partial \rho}{\partial x})^2 \frac{\partial u}{\partial x} + (\frac{\partial \rho}{\partial y})^2 \frac{\partial v}{\partial y} + \frac{\partial \rho}{\partial x}\frac{\partial \rho}{\partial y}(\frac{\partial u}{\partial y} + \frac{\partial v}{\partial x}) >} \tag{7}$$

where potential density ρ is related to buoyancy 'b', as seen in the VBF definition. A positive sign of F_{sh} represents an increase in the magnitude of the density gradient (i.e. frontogenesis), while a negative sign indicates frontolysis or weakening of this density gradient.

In Section 5.1, devoted to the processes of AAIW density compensation, we calculated the spiciness, here defined as in *Smith and Ferrari* [2009]:

$$\gamma = \beta_t(T - T_0) + \beta_s(S - S_0) \tag{8}$$

where β_t and β_s respectively represent the coefficients of thermal expansion and haline contraction and T_0 and S_0 are reference values of temperature and salinity. Being spiceness a measure of the passive spatial variations of watermass properties in density units, the net discrepancy between its spatial variability in HR and LR will highlight how the two resolutions reproduce a very dissimilar type of lateral mixing.

3 Energetics

3.1 Horizontal and Vertical Submesoscale Signature

Before proceeding to the analysis of the diagnostics presented above, we will examine the differences between the two numerical experiments and the impacts that the small-scale features present in the high resolution solution have on the simulated energetics. We firstly calculated the total KE spectra within the second child domain of HR, at different depths (near surface -5 m, -100, 500 and 800 m), by taking the instantaneous values of horizontal velocities and averaging them by season. In Figure 2 we show the spectra extracted for the summer (model year 5, month 1; i.e. Y5M1, panel 'a') and winter (Y5M8, panel 'b') seasons.

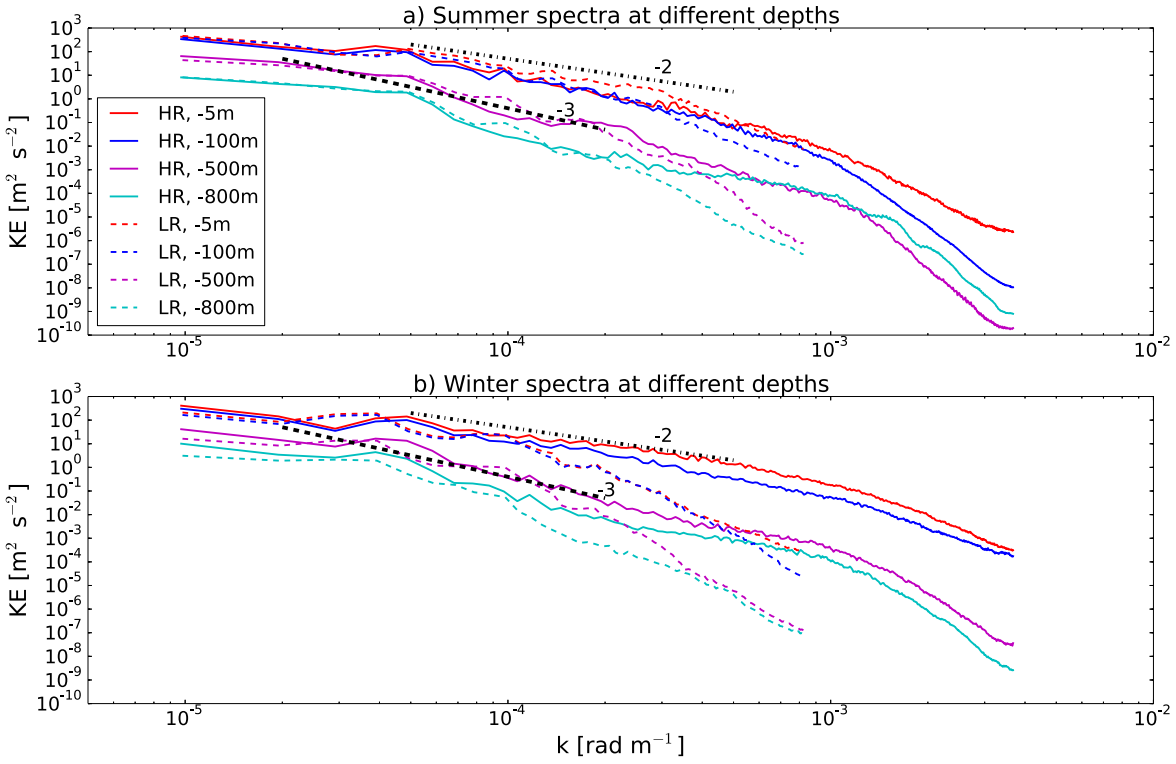

Figure 2. Kinetic energy spectra computed at different depths from istantaneous values of horizontal velocities for the HR (continuous lines) and the LR (dashed) and averaged over summer (a) and winter (b).

For both seasons, the spectral curves of HR (continuous line in all the curves of Fig. 2) exhibit, at all depths, very energetic small-scales. In winter the spectral curve has, near the surface, a typical slope of k^{-2}, in agreement with previous findings on the submesoscales cas-

cade of energy [*Capet et al.*, 2008a; *Klein et al.*, 2008]. The curves at intermediate depths (500 and 800 m, cyan and magenta, continuous lines in Fig. 2) present a slope close to -3 and show a weaker seasonal variability compared to the upper layers curves (red and blue, continuous lines in Fig. 2), indicating how the dynamics of these intermediate layers are less affected by the seasonality of the surface forcing. The spectral curves of LR (dashed line in all the curves of Fig. 2) have a slope close to -3 both in summer and winter, showing a negligible, seasonal difference at all depths, and a lack of submesoscale processes.

We use the vertical profiles of the root mean square (rms) of W for each resolution as a diagnostic to further discriminate the two simulations analysed in this manuscript. Following the methodology detailed in [*Capet et al.*, 2008a]), we decompose the total field into the temporal mean (W_{mean}), mesoscale (W_{ME}) and submesoscale (W_{SME}) components: W_{Total}= W_{mean}+W_{ME}+W_{SME}, in order to highlight the vertical contribution of the simulated, different spatial structures.

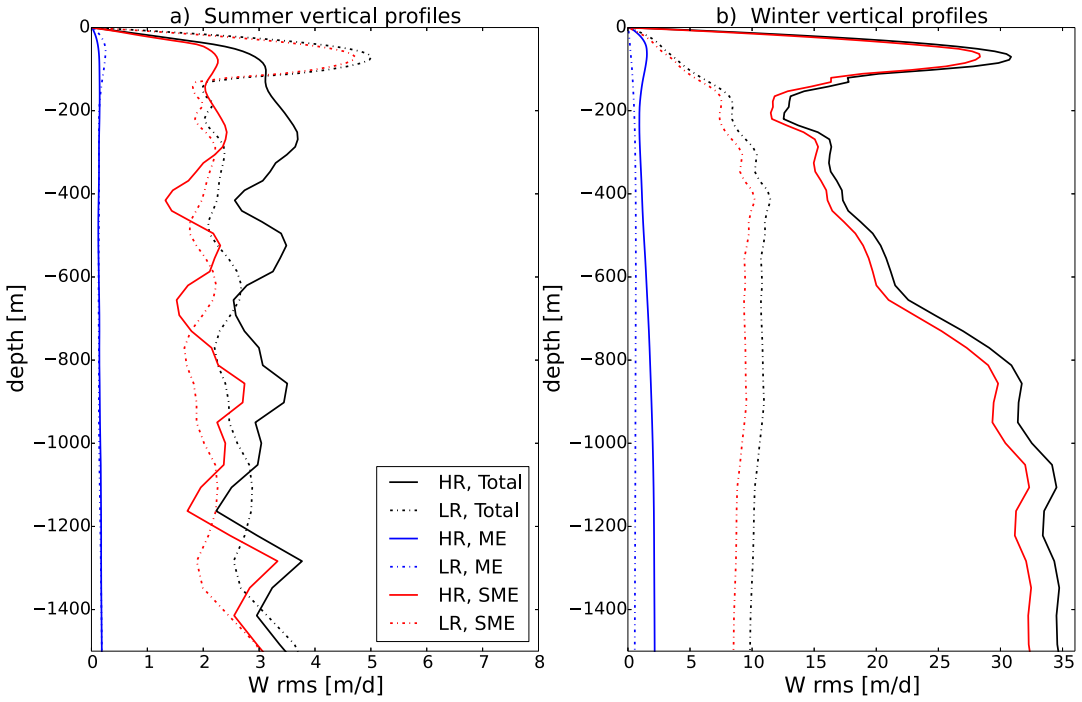

Figure 3. Root-mean-square (rms) profiles of the different componenents (total, meso- and sub-mesoscale) of vertical velocity (W), extracted in summer (a) and winter (b) along the first 1500 m of the water column, for the HR (continuous lines) and the LR (dashed lines).

The horizontal spatial rms metrics were computed at each sigma-level, and then temporally averaged over the summer (Fig. 3a) and winter (Fig. 3b). Given our focus on the watermass dynamics of the upper to intermediate depth layers, without considering the impact of topographic effects, results are plotted here from the surface down to 1500m. The HR rms profiles of W present the most elevated magnitudes, where the total W_{rms} (i.e. $W_{rms}= \overline{\sqrt{< W^2 >}}$) is 4-fold higher than the LR profile in summer and up to 20-fold higher in its winter maximum peaks. This increase in magnitude is particularly significant in the submesoscale component of the velocity field, which is strongly enhanced close to the surface at both seasons. The surface signature is dominated by submesoscale activity, while mesoscale-induced vertical velocities are almost independent of depth. On the other hand, the submesoscale component in LR shows only minimal surface enhancement in winter, even if it intensifies in summer. At both resolutions the mesoscale and the submesoscale velocities are similar in structure, although the magnitudes are larger at HR, as it will be further investigated looking at vertical sections of VRS and VBF in section 4.1. Another important difference between the two simulations is the marked seasonal variability of all the W_{rms} components of HR, showing a dramatic change with seasons. In particular, the submesoscales winter values for HR are almost one order of magnitude higher than the summer ones, while only a negligible variation can be percieved for LR. We have observed, in experiments preparatory to this study (results not shown), that our model captures a seasonal cycle at increasing horizontal resolution. This seasonality will be explored in more details in section 4.3, by analyzing the seasonal behavior of the mixed layer depth (MLD) as reproduced in each of the two simulations.

3.2 Vertical distinction of dynamical regimes

In Figure 4 we present zonal sections of temperature (T, 'a'), salinity (S, 'b'), potential density (σ_{theta}, 'c') and meridional velocity (v, 'd') of HR at Y5M1. They show the presence of an Agulhas ring between 7.5 and 11°E, and also a layering of very different water masses between the surface and the intermediate depths. At the surface, a shallow mixed layer caps, within the Agulhas ring, a homogeneous layer of ARMW 300 m thick. At greater depth, we note an intense stratification above the AAIW layer, characterized by a salinity minimum, and a quasi-homogeneous layer, centered between 700 and 1200 m and extending between the 27 and 27.4 isopycnals, with higher values of salinity (i.e. compared to the environment) found at the vertical of the eddy core.

Given the differences seen in the vertical distributions of W and v (respectively Figs. 3b and 4d) between the upper layers (i.e. from the surface to the base of the mixed layer) and the AAIW depths of our study region, confirmed by the spectral results of Figure 2, we further investigate this vertical distinction in dynamical regimes. The meridional velocity exhibits, for instance, higher magnitudes in the upper layers than at greater depth, which could be due to the influence of the surface forcing more efficient in the near-surface than at depth.

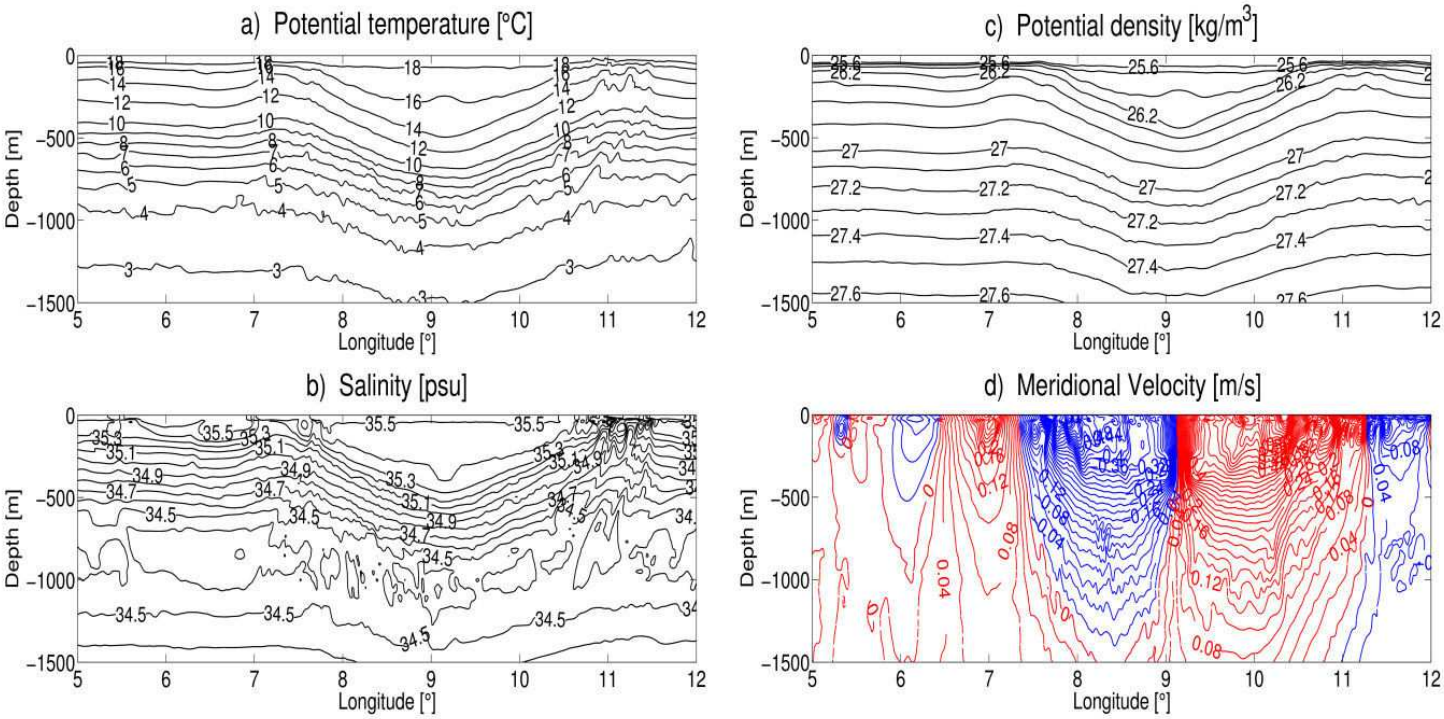

Figure 4. Zonal, instantaneous sections of temperature (T, 'a'), salinity (S, 'b'), potential density ('c') and meridional velocity ('d') plotted at 34°S along a summer anticyclone detected within the HR. In subplot 'd', red contours are for positive values of velocity and blue for negative.

In this regard, the diagnostics presented in the following sections will support the hypothesis initially proposed by *Boebel et al.* [2003] on the coexistence of two dynamical regimes between the upper and the intermediate layers of the Cape Basin, describing a 'stirring' regime near the surface and a 'blender' regime at greater depth. This was proven to be true by the observational work of *Rusciano et al.* [2012] and the numerical study of *Rimaud et al.* [2012], where Lagrangian integration of particles showed how both the vertical mixing and lateral stirring of AAIWs within the Cape Basin lead to the formation of new varieties of this watermass.

Our results will confirm their findings investigating the different instabilities and the meso-submesoscales interactions that play a key role as triggering mechanisms of these processes.

To do so, we firstly focus on the energetic signature discriminating the upper and intermediate layers of our study region, looking at vertical profiles of EKE, VBF (Eq. 1) and frontogenetic tendency (F_{sh}, Eq. 6), extracted by spatially and temporally averaging their seasonal values for the two simulations and seasons contrasted in this paper (Figs. 5 a-c).

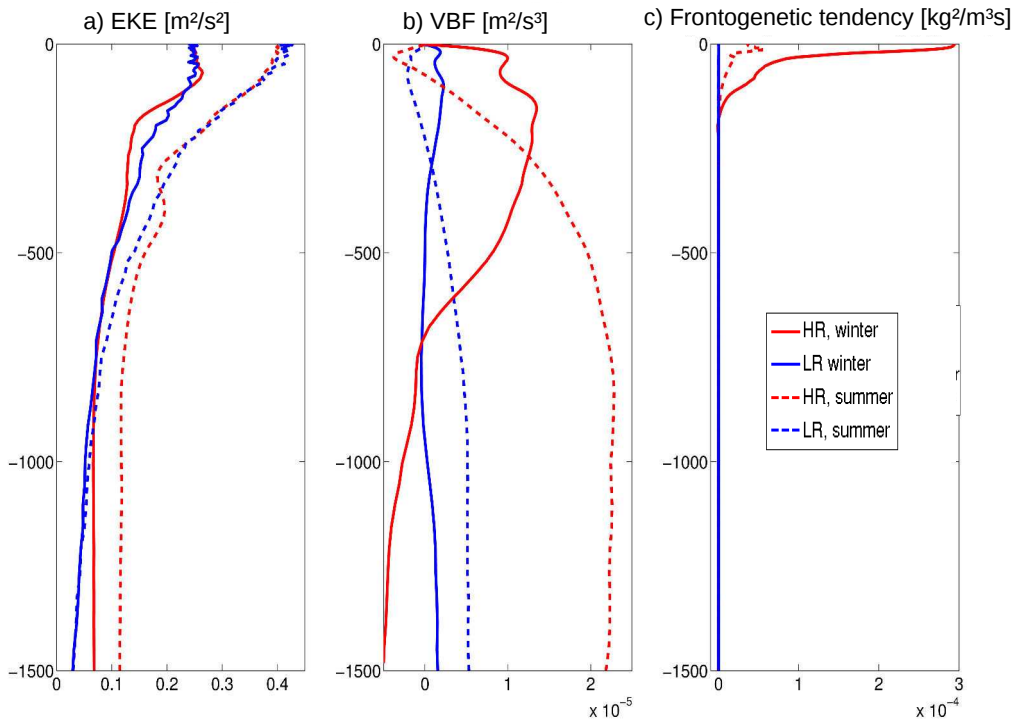

Figure 5. Vertical profiles of eddy kinetic energy (EKE, a), vertical buoyancy flux (VBF, b) and frontogenetic tendency (F_{sh}, c) at HR (in red) and LR (in blue) for summer (dashed lines) and winter (continuous).

Looking at the profiles of Figure 5, LR (blue lines) exhibits, in comparison to the HR curves (red lines), minor seasonal fluctuations in terms of the VBF depth-distribution (Fig. 5b), and even smaller for F_{sh} (Fig. 5c), while it shows greater seasonal variability in the EKE distributions (Fig. 5a). The latter is indeed characterized at LR by higher values in summer than in winter, suggesting a predominance of mesoscale dynamics in our region of study during the former season, as visible also at HR. At certain depths ($\sim$50 m in summer and $\sim$250 m in win-

ter), the EKE at LR is more important in magnitude than at HR (for ex. at the surface in winter and below, at about 250 m, in summer), probably due to the lack of finer scales instabilities able to modify and eventually drain the EKE reservoir of the flow as it occurs in HR.

Concerning the VBF vertical distribution, the two resolutions show a similar patterns for both seasons, even though the amplitude of HR values is considerably larger than for LR (respectively red and blue lines in Fig. 5b), and this is particularly true in winter. During this season we observe, for both resolutions, an enhancement in VBF just below the surface and a decrease just below the mean MLD and again an increase coincident with the MLD maximum. At greater depths, VBF decreases at both resolutions and in HR it becomes negative below 1000 m. On the other hand, in summer at HR, the vertical maximum of VBF is reached at the level of the AAIW layer. Hence, this vertical distribution of VBF clearly underlines the separation between the dynamical regimes of the upper and intermediate layers.

The LR limits in resolving the presence of submesoscales and their seasonal intensification clearly emerge in the profiles of F_{sh} (Fig. 5c), characterized by very low values, barely oscillating around the zero-baseline, for both seasons. The HR simulation shows, instead, considerable values of F_{sh} within the upper 300 m of the water column and they are particularly high in winter, being about one order of magnitude larger than in summer. This suggests that near-surface frontogenesis, likely resulting from the stirring of mean buoyancy gradients by the mesoscales, is in our region of study more active in winter, within a depth extending from the surface down to the ML base. We find that this layer could be also affected by C-BCIs and this possibility is more extensively discussed in the next section, where we separately present, for the upper and AAIW layers, specific diagnostics on the instabilities at play in each layer. For this analysis, we will restrict our discussion on the results obtained for two ACes, one for summer and one for winter, detected at HR and chosen as representative of the average, dynamical behaviour of Agulhas Rings in the Cape Basin.

4 Upper Layers Dynamics

4.1 Mixed Layer Instabilities

Figures 3 and 5 have shown that the upper ocean dynamics at HR is dominated by an important submesoscale activity. We seek to understand its origin. Firstly, we look for the occurrence of baroclinic MLIs, consisting of thermocline shear-driven instabilities that play a crucial part in the submesoscale dynamics of the surface ML [*Boccaletti et al.*, 2007]. To verify that our chosen ACes are generated through barotropic rather than baroclinic instabilities ,

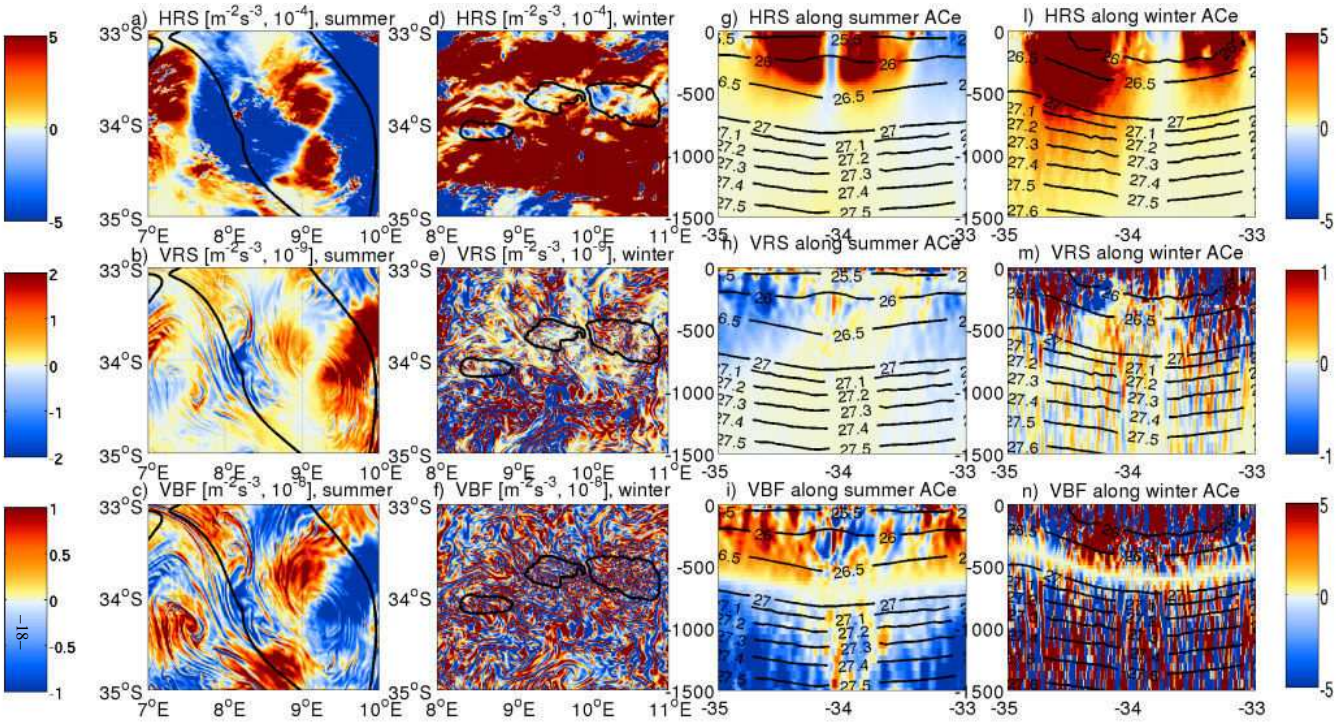

Figure 6. Left panel: Snapshots of horizontal and vertical shear (HRS and VRS, [$m^{-2}s^{-3}$]) and vertical buoyancy flux (VBF, [$m^{-2}s^{-3}$]) plotted along an ACe detected within the HR simulation in summer (on the left) and winter (on the right). Black contours define the outer limits of the detected eddy. Right panel: meridional sections of the same metrics, extracted at 9.2°E with black contours for isopycnals ranging from 26 to 28 kg/m^3. Note that the maps of the left panel (a-f) share the colorbars on the left, while the ones on the right are for the sections of the right panel (g-n).

Confidential manuscript submitted to *JGR-Oceans*

435 we analyse the surface and vertical distributions of HRS (Eq. 2), VRS (Eq. 3) and VBF
436 for the summer and winter seasons (Figs. 6 a-n) . Positive and negative values are present at
437 the two sides of the front localized along the eddy main axis, extending from 8 to 9.5°E. Larger
438 values of VBF are found in winter due to the more intense vertical velocities found in this sea-
439 son (Fig. 3b), responsible for driving larger buoyancy fluxes. For the summer ACe, being ge-
440 ometrically close to an elliptic eddy with a Gaussian shape, we observe a quadripolar struc-
441 ture of HRS [*Hua et al.*, 2013] (Fig. 6 a), where the alternation of opposite sign values is re-
442 lated to the eddy deformation. The analyzed ACe is surrounded by two smaller Ces, exerting
443 a shear on it and visible also in the HRS section (Fig. 6g), where the isopycnals doming and
444 diving characterize the interacting eddies of opposite signs and mainly happen in summer.
445 In winter instead, the HRS surface map (Fig. 6d) presents the highest positive values at
446 the centers of the multiple, smaller vortices and filaments making up the ACe center (between
447 9.5 and 10.5°E). Its spatial distribution is however much smoother than those of VRS and VBF
448 (Figs. 6e and f), strongly dominated by the occurrence of very fine scales, both within the con-
449 tours of the ACe and at its surroundings. This suggests that weaker energy transfers due to
450 the horizontal shear take place in winter, when submesoscales prevail, and that shear instabil-
451 ities, like the barotropic ones, are mainly confined at the periphery of the summer eddies. More-
452 over, in the winter section of VBF (Fig. 6n) the subduction of filaments, laterally generated
453 by the shear between the ACe and the nearby Ces, indicates how the fine structures are mainly
454 marked in VBF at depth, while more in HRS and VRS at the surface (Figs. 6l and m).
455 Overall, VRS is more intense in winter than in summer, while HRS remains pronounced
456 also in summer, even though more enhanced in winter, especially in terms of its vertical ex-
457 tension. VBF, in particular, shows a net contrast between the upper 300 m and the interme-
458 diate levels, being clearly separated by a layer in which VBF=0, corresponding to the AAIW
459 layer of low salinity (Fig. 4b). This underlines the transition between the two different dynam-
460 ical regimes (i.e. highly ageostrophic at the surface versus quasi-geostrophic at depth) intro-
461 duced in section 3.3. We conclude this analysis by mentioning that the vertical separation be-
462 tween these two regimes is completely absent in the LR sections (not shown), where all the
463 variables have a barotropic behavior at depth, confirming for LR a more diffusive dynamics.

464 **4.2 Symmetric Instabilities**

465 To assess if symmetric instabilities [*Thomas et al.*, 2013, 2016] play a role in the sim-
466 ulated dynamics of the Cape Basin, we computed the OW parameter (Eq. 3), the Ertel PV (Q,

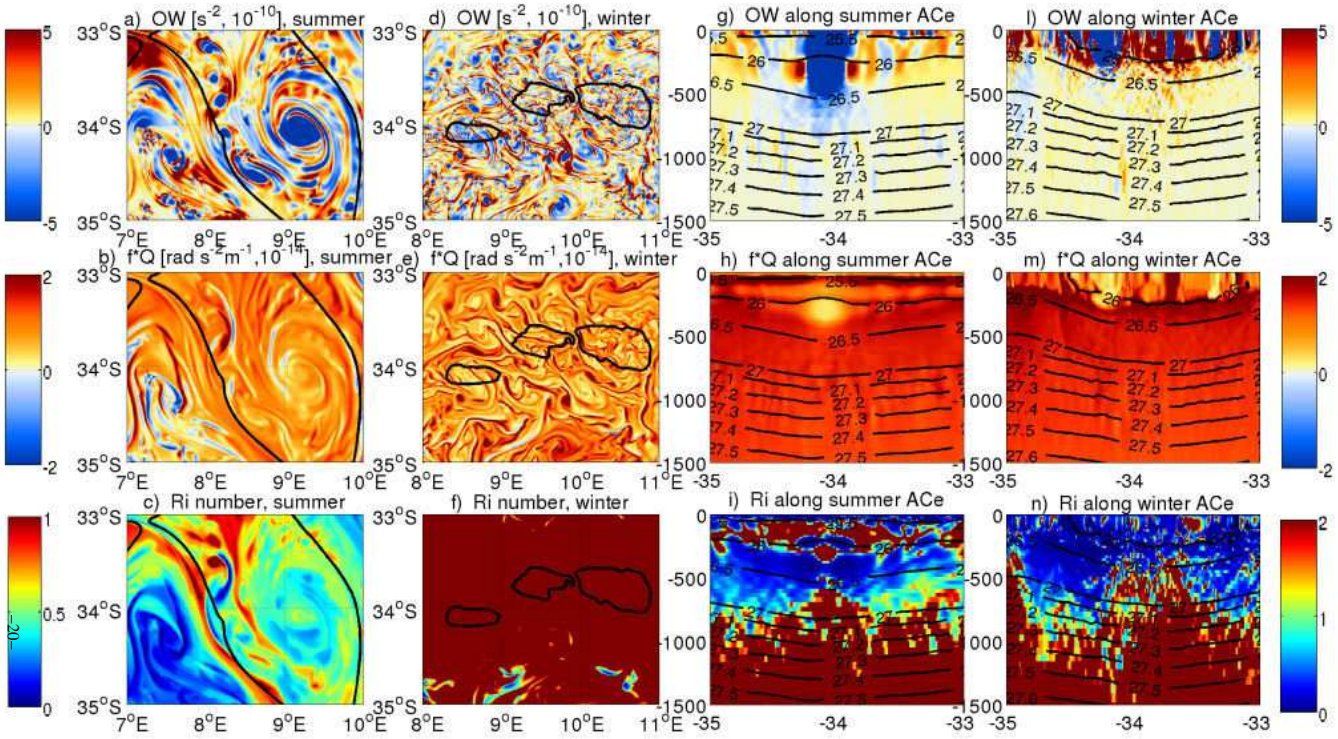

Figure 7. Left panel: Same as Figure 7 but showing the instanataneous maps of the Okubo-Weiss parameter (OW, [s^{-2}]), the Ertel potential vorticity multiplied by the Coriolis parameter (f*Q, [rad s^{-2} m^{-1}]) and the Richardson number (Ri). Right panel: meridional sections of the same metrics, extracted at 9.2°E with black contours for isopycnals (26 to 28 kg/m^3). Note that the maps of the left panel (a-f) share the colorbars on the left, while the ones on the right are for the sections of the right panel (g-n).

Confidential manuscript submitted to *JGR-Oceans*

Eq. 4) multiplied by the Coriolis parameter (f∗Q) and the gradient Richardson number (Ri, Eq. 5). Figures 7 (a and d) show two typical snapshots of OW extracted near the surface at both seasons for HR. The σ^2 term appears to be dominant in winter (positive OW), indicating a direct connection with the submesoscale field, since it represents a signature not only of strain but also of divergence/convergence. The latter is strongly increased when frontogenesis and MLIs are more active [*Mensa et al.*, 2013], as it happens during winter in our study region. The surface map of f∗Q over the summer HR ACe (Fig. 7b) shows filaments of negative values around the center of the eddy and at the periphery of it, corresponding to the same locations where Ri $<$1 (Fig. 7c). In LR (not shown here), filaments remain positive even when Ri $<$1 (a necessary but not sufficient condition), confirming that LR is not able to capture the development of symmetric instabilities. As expected, at both resolutions the cores of the eddies are characterized by negative values of OW (Figs. 7a and d).

In the summer sections of OW and f∗Q (Figs. 7d and e) we observe winter water isolation below the ML and the seasonal thermocline, identified by a core of negative values for these two variables. Here the eddy core is surrounded by filamentary structures, indicative of subduction (see section 4.4), as shown in an animation of PV and W sections, extracted at each time step from spring Y4M10- to the next summer- Y5M1- of our HR simulation (Supplemental Material 1). These filaments are not well resolved by LR, neither are any of the other fine scales visible in the OW and f∗Q maps of HR. Smaller vortices and filaments emerge in the winter maps of LR (not shown), even though they do not attain the HR fine scales (Figs. 7 d-f), where the surface maps of the three quantities seem to be definitively dominated by the so-called 'soup of submesoscales' [*Capet et al.*, 2008a]. The latter extends vertically down to 500 m of depth, and produces a thick, homogeneous band between the 26 and 26.5 isopycnals (Figs. 7 l-n), creating a typical layer of mode waters within the Cape Basin, the ARMW. During winter, we observe in the upper layers fewer filaments where f∗Q $<$0 and Ri $<$1, suggesting that symmetric instabilities take place mostly in summer, in the HR simulation.

4.3 Seasonality of the meso-submesoscale interactions

Overall, the regional dynamics in the Cape Basin is governed by mesoscale structures, triggering submesoscale instabilities in the shallow mixer layer, in summer, at the frontal edge of the mesoscale eddies. In winter smaller submesoscales, driven by the stronger atmospheric forcing, prevail and affect the entire region, and, in particular the interior of mesoscale eddies, extending from the surface to the deepest eddy layers. This is in agreement with the results

initially shown in the KE spectra of Figure 2. In summer, the local dynamics is essentially characterized by mesoscale barotropic instabilities, leading to surface structures (filaments, fronts, smaller vortices), whose interaction can trigger submesoscale shear instabilities, as the symmetric type. Instead, in winter, shallower baroclinic instabilities, like MLIs, forced by the action of the wind and the passage of seasonal storms, or induced by strong lateral gradients of density, dominate the upper layers. Below the thermocline, frontal instabilities develop during both seasons, due to the interaction between adjacent eddies of opposite signs, as observable in the animation of the PV and W sections (Supplementary Material 1).

This indicates how the portion of submesoscales captured by HR is marked by a strong seasonality, as documented in previous numerical studies at comparable resolutions [*Callies et al.*, 2015; *Brannigan et al.*, 2015; *Brannigan*, 2016] and explained by the two main mechanisms identified by *Callies et al.* [2015]. In summer, with a prevailing presence of mesoscale structures, submesoscale flows are energized by mesoscale-driven frontogenesis, where strain fields, at the edge of mesoscale eddies, sharpen surface buoyancy gradients. This clearly appears in the summer map of the OW surface distribution (Fig. 7a), where the highest positive values, indicative of a strain predominance, can be found along submesoscale filaments and around the centers of the smaller vortices. Additionally, in the summer OW section (Fig. 7g), we observe the density gradient sharpening at the edges of the core of the subsurface-intensified ACe, above which a thin layer of much finer scales develops close to the surface. These submesoscale flows are confined in the shallow surface layer, as shown in the VRS and VBF summer sections (Figs. 6 h-i), where very small scales are visible only in the first 50 m of the water column and correspond to the HR surface spectra of KE (Fig. 2). From the same figure note also that the degree of geostrophic balance changes as the resolution increases with evidence for stronger, non-linear processes becoming more important during the winter season, when the ML deepens [*Brannigan et al.*, 2015]. This is consistent with stronger instabilities developing within the ML as it thickens. They energize the submesoscales via baroclinic instability (the second mechanism of *Callies et al.* [2015], as was shown in the VBF surface map and vertical section for the winter ACe (Figs. 6f and i). That is why HR, which reproduces a seasonal cycle, with a much thicker ML in winter than in summer and very pronounced compared to LR (see Table 1), captures the formation of such ML instabilities, as shown in the winter sectons of OW and f*Q (Figs. 7g and h). The MLD is here computed as the depth at which the density difference with respect to the surface is equivalent to a 0.03 density change.

Concerning its seasonal cycle, given that lateral buoyancy gradients are fairly constant throughout the year, the KE generated by finescale instabilities peaks in winter, when the ML is the deepest. In summer, with shallower ML, these instabilities are damped, as it appears from the HR horizontal and vertical distributions of energy transfers (Figs. 6). Hence HR, resolving a portion of submesoscale processes, captures the non-linear processes affecting the mixing layer and inducing a large seasonal variation that is not represented in LR (Table 1). This aspect will be further detailed in the next section.

Table 1. Table listing the mean values of mixed layer depth (MLD), averaged over the summer and winter seasons within all the anticyclones and cyclones detected in the HR simulation and in the LR solution.

Mean MLD (m)	Summer	Winter
ACes	HR= 30 LR=36	HR= 105 LR=54
Ces	HR= 30 LR=35	HR= 107 LR=45

4.4 Charney Baroclinic Instability and Mode Waters subduction

Charney baroclinic instability (C-BCI, *Charney* [1947]) arises from the co-existence of a surface buoyancy gradient and an interior PV gradient, of opposite signs, and is able to couple the unstable evolutions of the ocean surface and interior, at meso- and submesoscale [*Capet et al.*, 2016]. A necessary and most frequently sufficient condition for C-BCI is that the vertical gradient of buoyancy frequency (dN^2/dz) changes sign [*Charney*, 1947]. This can be achieved in layers of mode water [*Capet et al.*, 2016], as those present in Agulhas rings (ARMW) and observed from in-situ data to be located between the 26 and 26.8 isopycnals [*Arhan et al.*, 1999; *Gladyshev et al.*, 2008; *Arhan et al.*, 2011]. Figure 4 shows that the lighter variety of ARMW (occupying the 25.8-26.2 isopycnals range) is well represented in HR (despite it experiences only a smooth winter forcing). The vertical seasonal distribution of dN^2/dz at HR reaches values of about -3, -4 x 10^{-7} $s^{-2}m^{-1}$ and in some locations even lower than -5 x $10^{-7}s^{-2}m^{-1}$ (Fig. 8), both in winter and summer ACes (Figs. 9 a and b, respectively).

At places and times where mode waters are actively formed through convection, we expect more energetic instabilities (such as convective, symmetric or MLIs) to dominate the upper-ocean dynamics over a depth range comparable to that of negative dN^2/dz [*Capet et al.*, 2016].

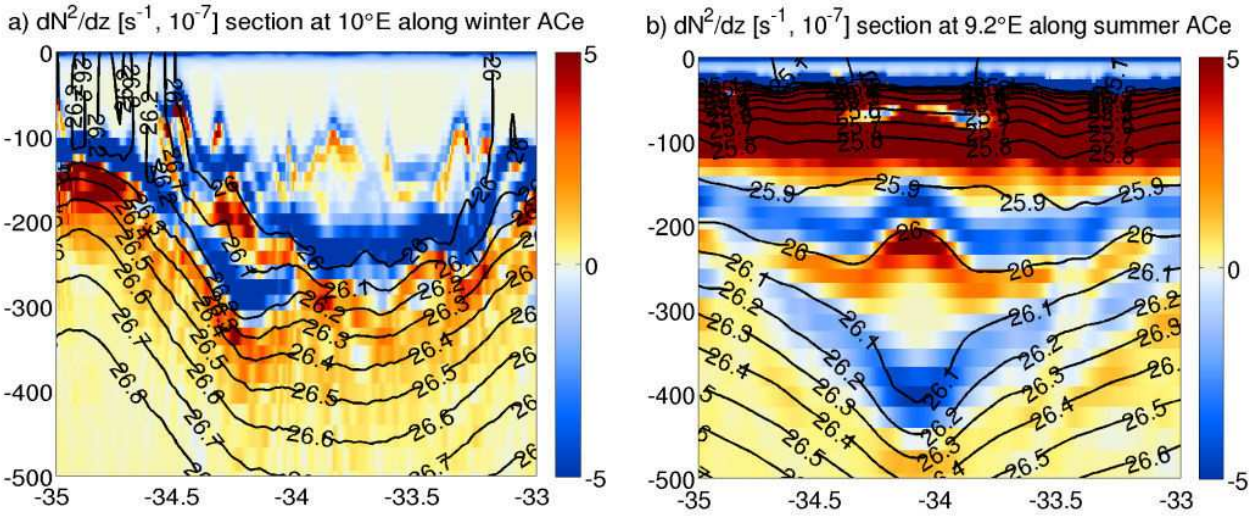

Figure 8. Meridional sections of the vertical gradient of stratification (dN^2/dz) plotted at 10°E along a winter anticyclone (a) and at 9.2°E along a summer anticyclone (b) for the first 500 m of the water column. Black contours are for isopycnals ranging from 25 to 26.8 kg/m^3.

The same authors hypothesize that C-BCI may impact mode water dynamics either through wintertime convection/subduction or due to calm weather conditions that render the surface mixed layer relatively shallow. Our case would rather be the first one since we observe hints of the ML subduction in the animation of the PV and W (Supplemental Material 1). Meridionally and seasonally averaged profiles of W skewness also show in winter downward velocities greater than upward velocities in the near-surface (Supplemental Material 2).

In our study region, the primary mechanism triggering subduction is likely frontogenesis, highly enhanced during winter in the upper 300 m of the water column (see the results for HR in Fig. 6c). Subduction at upper ocean fronts is often driven by internal instabilities (mostly baroclinic, see *Spall* [1995]), where frontogenesis forces the water parcels below and across the front. Intense ageostrophic cross-front and vertical velocities (O(30 m/d), see Fig. 3b for the HR winter profiles) may then take place, leading to the formation of deep ACes and shallow Ces during the subduction process. Here, the subsurface intensified ACes have their core below the ML base (see the dN^2/dz minimum in Figs. 8), as seen in the HR summer sections of OW, f*Q and Ri (Figs. 7 d-f). These ACes are mainly biconvex lenses, often axisymmetric, below which the isopycnals deflection, quantified by $d\rho/dz$, is of the order of 10^{-3} kg/m^4. An analysis of several model runs (not shown here) indicates that most of the simulated ACes are close to Gaussian in profile and elliptical in shape. Thus, HRS is quadripolar (Fig. 6 a),

whose mode 2 deformation is due to the shear of neighboring currents and eddies [*Hua et al.*, 2013]. These elements support our interpretation that subduction is important in creating the minimum stratification layers conducting to C-BCIs at the mode waters depths.

To summarize, our results on the ARMW seasonal formation and subduction suggest that, in winter, the more intense atmospheric air-sea interactions deepen the MLD by destratifing the water column and enhancing frontogenesis within this layer. This leads to the generation of submesoscale internal instabilities, mainly represented by baroclinic instabilities, as the Charney type. The latter trigger the subduction of surface winter waters below the ML, injecting in the ocean interior a mode waters core (i.e. the ARMWs), that remains thereafter isolated from the ML and the atmosphere. Agulhas rings with such ARMW core become subsurface-intensified ACes, marked by a layer of low dN^2/dz (and thus low PV). As the submesoscale frontogenesis is not resolved in LR, we observe the development of ARMW only at HR.

5 Intermediate Depths Dynamics

5.1 Mesoscale stirring of AAIWs

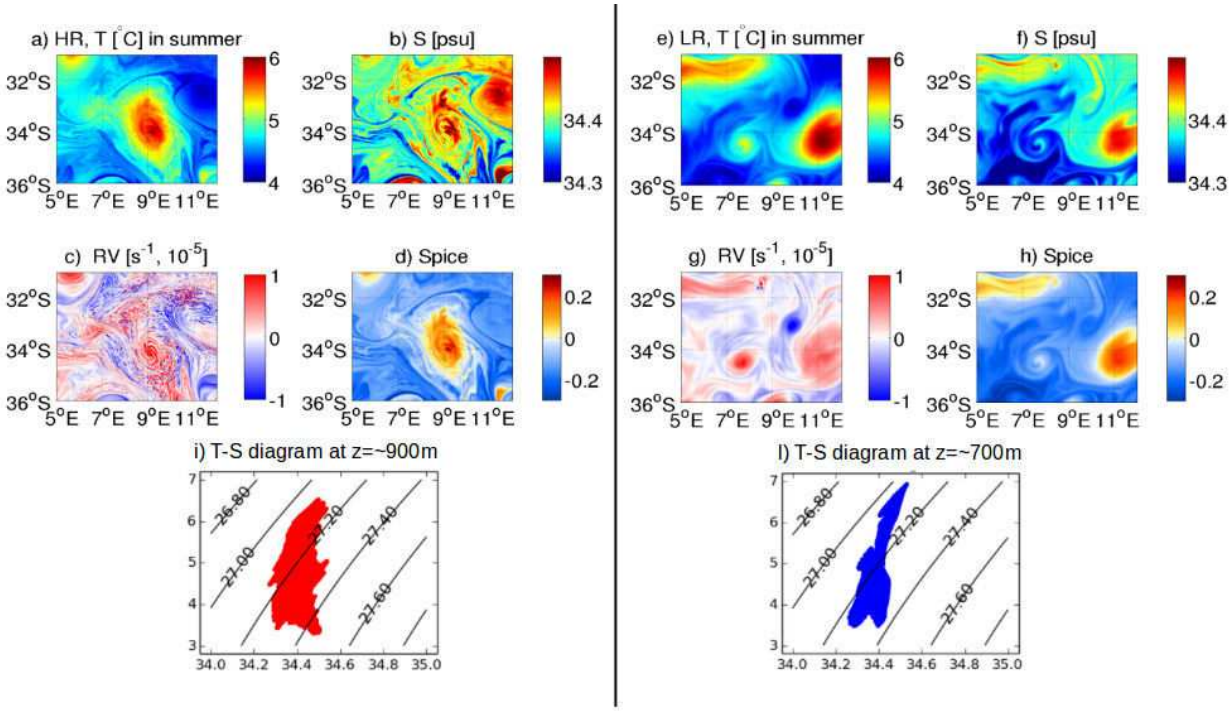

Figure 9. Top panels: snapshots of temperature (T), salinity (S), relative vorticity (RV) and spice extracted along the 27.2 isopycnal over a summer ACe of the HR (a-d) and the same for the LR (e-h). Bottom panels: T-S diagrams showing the same thermo-haline distributions of the top panels, for HR (i) and the LR (l).

Here we focus on the dynamics at intermediate depths, which in our study region are occupied by AAIWs. Previous numerical and observational studies [*Schouten et al.*, 2000; *Boebel et al.*, 2003; *Rusciano et al.*, 2012; *Rimaud et al.*, 2012] have hypothesized that the regional AAIW dynamics and properties are governed by lateral mesoscale stirring giving rise to strong density compensated submesoscale thermohaline fronts few kilometers wide. In the 27.2 isopycnal distribution of T, S spiciness and RV, extracted for the same model timestep at LR and HR (Figs. 9a-d and 9e-h, respectively), it is evident that both resolutions exhibit such sharp fronts. This is particularly true for HR, where their distributions show intense finescale structures and filaments. The 27.2 isopycnal represents the regional core of AAIW as observed by in-situ data [*Talley*, 1996] and in our simulations (Fig. 4 for the HR). Indeed, in the T-S diagrams of Figure 9 ('i' for HR and 'l' for LR, correspondent to the T-S distributions of Figs. 9a-d and 9e-h), the T-S variability is almost completely compensated in its effect on sigma, as highlighted by the noticeable spreading of the T-S values concentrated along the 27.2 σ.

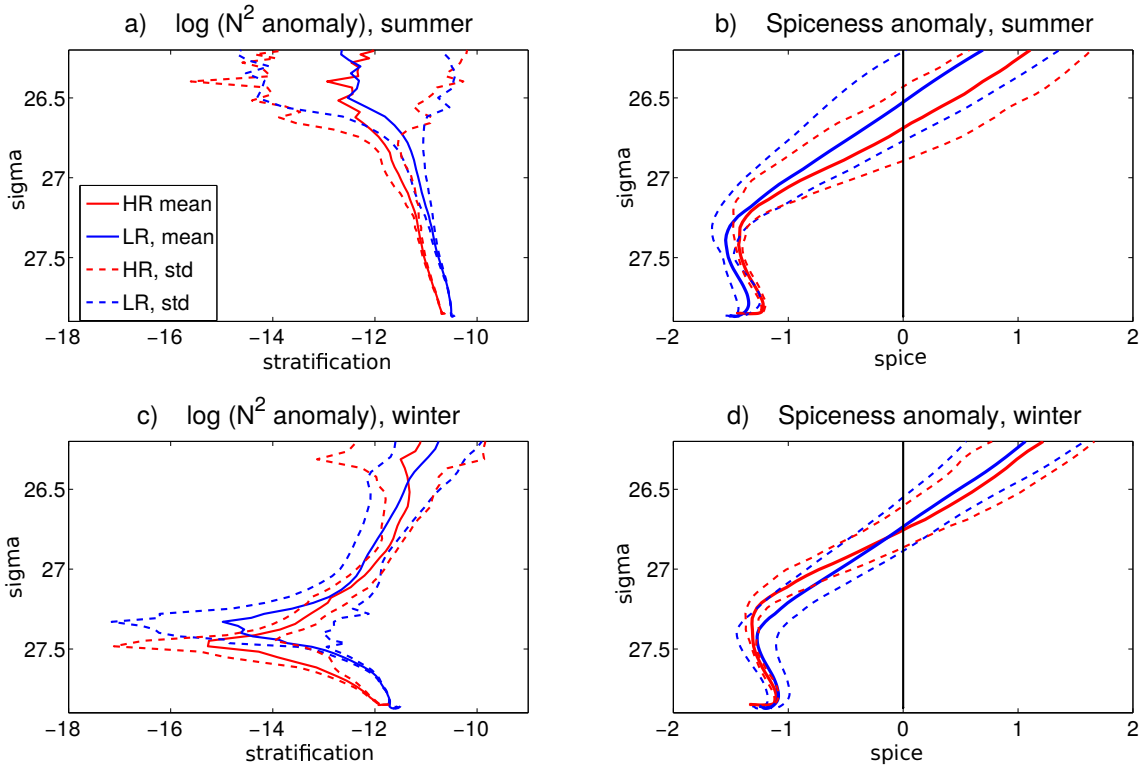

Figure 10. Vertical profiles of the anomaly of stratification (N^2, [s^{-2}]) and spice, against potential density [kg/m^3], extracted in summer (top plots) and winter (bottom) for the HR simulation (in red) and the LR solution (in blue). Continuous lines are for the mean values and dashed lines are for the standard deviation.

The contrast in the spatial variability of spiciness between HR and LR (Figs. 9d and h) show how the two resolutions reproduce different mechanisms of lateral mixing, as further highlighted in section 5.2. This difference is confirmed in the vertical profiles of stratification and spiceness for the two resolutions and seasons (Figs. 10): both resolutions are characterized by a positive anomaly of spiciness in the upper layers and negative at depth, but the LR curves of standard deviation are not as tight and close to the mean within the AAIW layer (between 27.2-27.6σ) as in the HR. This confirms that the LR does not fully capture the separation between the surface and subsurface dynamical regimes. Moreover, the strongest stratification anomalies, approximately located along the 25.7 and the 26.5σ in summer (Fig. 10a) and along the 26.4 and the 27.4 isopycnals in winter (Fig. 10c), are always shallower in LR than in HR. This is particularly true in winter, probably due to the large difference in the value of the MLD at this season, between the two model resolutions. This difference has an impact also on the depth of the density compensated layer: they are always observed at much shallower levels in LR compared to HR (with a vertical difference of about 100 m).

Two main mechanisms have been proposed in the literature to explain the generation of thermohaline structures with weak density signature in the ocean interior: double diffusive instabilities (or lateral intrusions via thermohaline front instabilities), and lateral stirring by mesoscale vortices. It must be first recalled that the former can occur in dynamically quiet regions (e.g. for drifting meddies in the open ocean, [*Ruddick et al.*, 2010]) whereas the latter always requires a substantial degree of mesoscale turbulence. In our simulations we did not prescribe different heat and salt diffusivities in the model, thus precluding double diffusion processes. In addition, our study region being a very energetic spot, due to the co-existence of baroclinic eddies with intense lateral gradients of temperature and salinity, the second process is favored (see *Klein et al.* [1998]); this was also found true for AAIW in the Antarctic Circumpolar Current, by *Craneguy* [1999]. Note that though double diffusion may impact filamentogenesis, it is not a necessary condition for its onset as well as for the vertical cascade of tracer variance to occur (see also [*Meunier et al.*, 2015]. The contrasted structure of spice, showing intense filaments along the 27.2 isopycnal (Fig. 9d and h) while density is homogeneous (Fig. 9i and l), indicates that stirring has likely triggered filamentogenesis here.

In terms of orders of magnitude, microstructure intrusions cause lateral fluxes of salt and heat that are often comparable to those by more dynamic, larger scale processes, such as mesoscale eddy stirring or barotropic/baroclinic instability [*Ruddick and Richards*, 2003]. In several locations, like for example within Mediterranean salt lenses, they have been associated to eddy

diffusivities of O(3-6 x 10^3 m^2 s^{-1}) [*Ruddick*, 2003]. Measurements of isopycnal dispersion due to mesoscale stirring, reported in *Ferrari and Polzin* [2005], indicate rates somewhat smaller than 1 x 10^3 m^2 s^{-1}. Hybrid cases, where lateral fluxes can lead to the decay of rings and Meddies, have also been observed. *Garrett* [1983] showed how fronts can be sharpened by eddy stirring and smoothed by intrusions. In HR, the mean value of horizontal diffusivity along the 27.2 isopycnal is about 3.3 x 10^3 m^2 s^{-1}, indicating that our study region could also represent a hybrid case. But, since the vertical resolution of our nested solution is, at intermediate depths, about 45 m, we are currently not able to resolve the scales of intrusions typical of diapycnal mixing, so we have restricted our analysis to the isopycnal stirring mechanism.

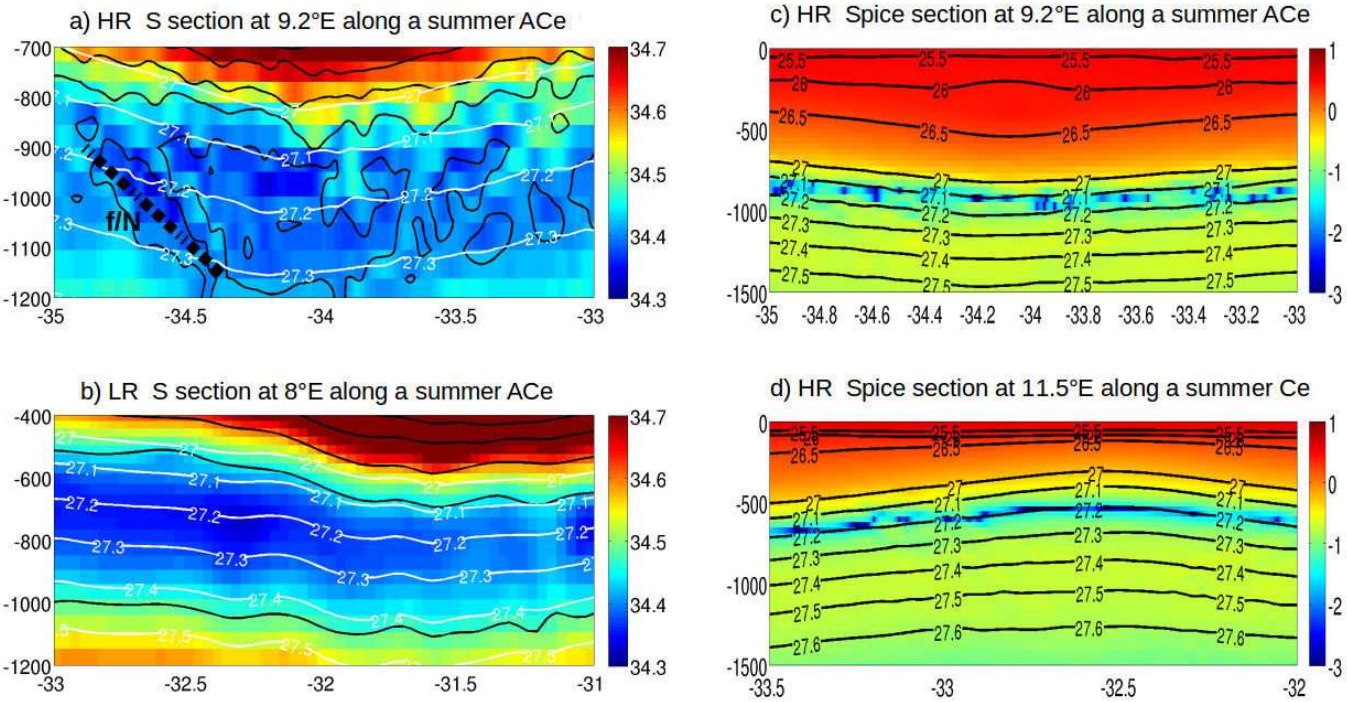

Figure 11. Left panel: meridional sections of salinity [psu] plotted at intermediate depths along a summer ACe detected in the HR (a) and in the LR (b). Colour and black contours are for salinity values, while white contours are for isopycnals ranging from 26 to 28 kg/m^3. In 'a', the f/N slope of the tracer filaments is marked by a black, dashed line. Right panel: meridional sections of spiciness plotted in summer along an ACe at 9.2°E (c) and a Ce at 11.5°E (d) detected in the HR. Black contours are for isopycnals (26 to 28 kg/m^3).

Figure 11a shows a zonal section of S for HR in correspondance of a summer ACe. Between the 27.1 and 27.4 isopycnals, interleaving filaments of low S appear and have a vertical extension of about 200-300 m, comparable to the observations of *Ledwell et al.* [1998], and

are thus much steeper than the background isopcynals. Their slope is consistent with the f/N ratio calculated for submesoscale turbulence and the isotropic forward cascade of tracer variance [*Smith and Ferrari*, 2009]. These low salinities can also be observed at intermediate depths in the LR section (Fig. 11b)but here they tend to form uniform layers instead of filaments as in HR. Indeed, only HR is characterized by a layer of negative spiciness below the 27.0 isopycnal, as shown in summer sections below eddies of both polarities (Figs. 11c and d).

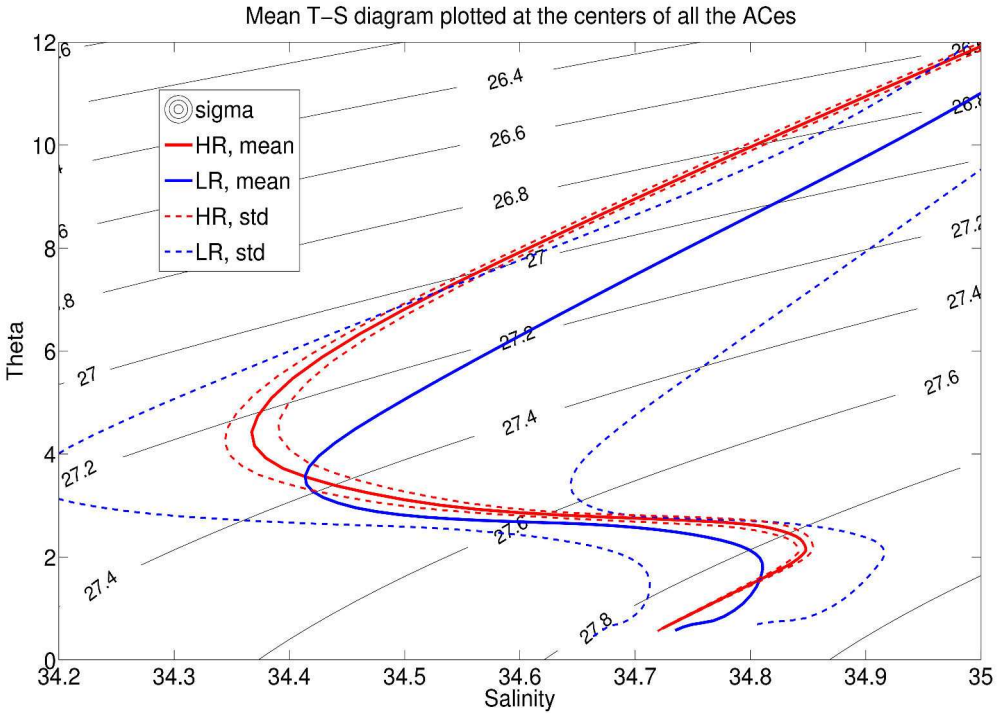

Figure 12. T-S diagram showing mean (continuous lines) and standard deviation (dashed) values extracted at AAIW depths at the centers of all the ACes detected in the HR (in red) and in the LR (in blue).

The spiciness is particularly negative along the 27.2 isopycnal. This spiciness minimum layer appears no matter the sign of the eddy and seems to spread across the entire section. The submesoscale, density-compensated thermohaline fronts, arising from the lateral eddy stirring, contribute at these intermediate depths to the vigorous generation of spiceness (Fig. 9d) and increased tracer variance in the AAIW layer as shown by the T-S diagram of Figure 12. Here the HR T-S dispersion (red curves) is high within the AAIW layer, and weak above and be-

low it, in relation with large isopycnal gradients of T and S. On the contrary, the dispersion is uniform over depth for LR (blue curves in Fig. 12). We thus conclude that lateral stirring of tracers by eddies of both signs, in HR, is effective and leads to density-compensated T and S submesoscale filaments within the AAIWs layer of the Cape Basin. These filaments have scales that cannot be resolved by LR.

5.2 Which instabilities at depth?

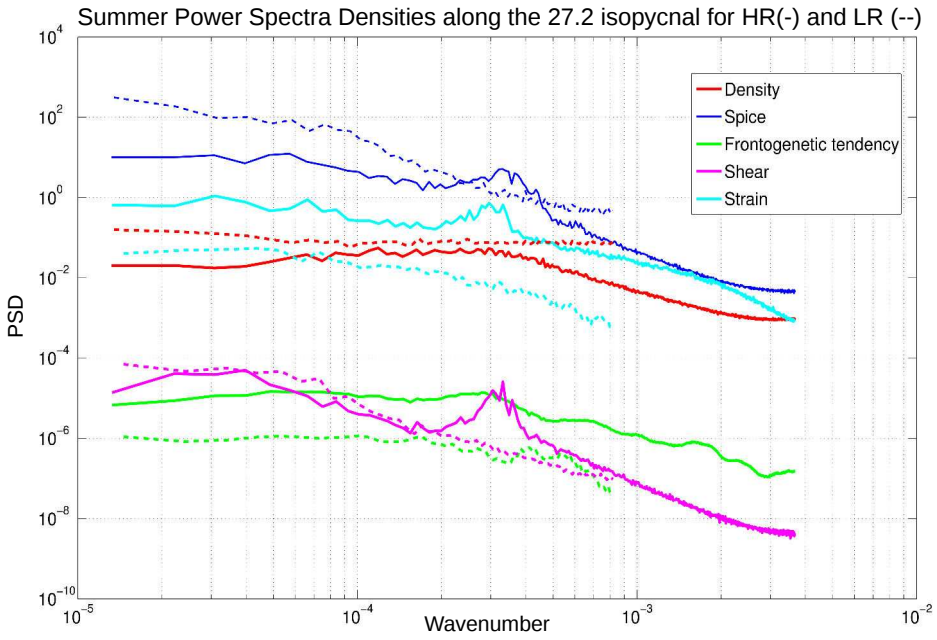

Figure 13. Power spectra densities curves of density, spice, frontogenetice tendency, shear and strain computed in summer along the 27.2 isopycnal for the HR (continuous lines) and the LR (dashed lines).

In an attempt to investigate the types of instabilities involved in the mechanisms of mesoscale lateral stirring at intermediate depths, we looked at power spectra density (PSD) curves of density, spice (Eq. 8), frontogenetic tendency (Eq. 7), shear and strain (Eq. 4), computed at σ=27.2 for the two model resolutions (Fig. 13) during the summer season. Here, besides the expected result that LR curves (dashed lines in Fig. 13) are flatter and do not reproduce the smaller scales as does HR (continuous lines in the same figure), we observe for HR two peaks: one at k= 3 x 10^{-4}m^{-1} ($\sim$3 km), which corresponds to the limit between the meso- and the submesoscale;

and a second peak at k= 5 x 10^{-5}m^{-1} ($\sim$20 km), that coincides with the mesoscales. These peaks are well marked for spice, but also for shear and strain. The latter represent the gradients of the velocity field, thus these peaks should be expected also in the PSD of RV.

On the other hand, the density field is smoother; as a consequence, the frontogenetic tendency, which combines the velocity and density gradients, shows a more attenuated peak at the meso/submeso-scale transition. At these scales, filamentary and frontal structures are formed in spice and not in density, and are well visible in the HR distributions of shear and strain extracted for summer, at the same time-step, along the 27.2 isopycnal (Fig. 14 a and b). Both of them display a clear interweaving of meso- and submesoscales, with submesoscale filaments overlaying the eddies; this is particular true for strain (Fig. 14b).

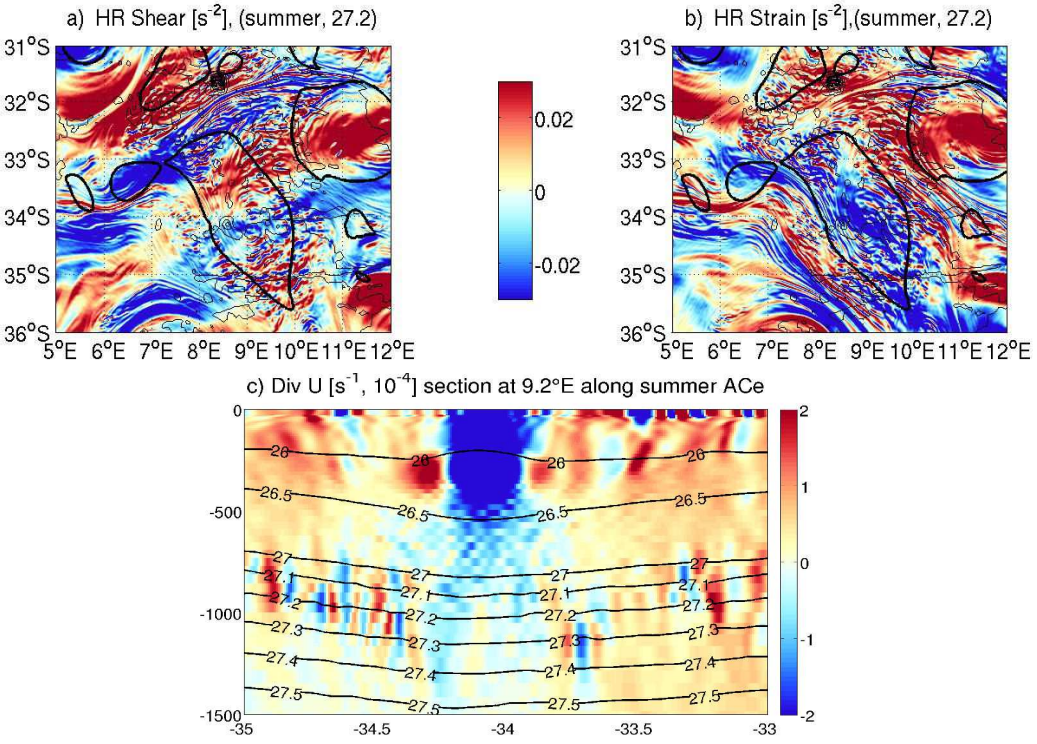

Figure 14. Summer snapshots of shear (a) and strain (b) extracted at σ=27.2 in the HR. Black contours define the outer limits of the detected eddies. (c), meridional section of the horizontal divergence of velocity, plotted along a summer ACe of the HR with black contours for isopycnals ranging from 26 to 28 kg/m^3.

Here the sign of its magnitude is positive if the eddy stretches along the x-axis, as for the Ce centered at 11.5°E- 32.5°S, and negative when the eddy is more deformed along the y-axis, like for the large ACe centered at 9.2°E- 34°S that we discussed more in detail in this

work. For this ACe, the shear (Fig. 14a) shows alternating sign along its largest, meridional axis, mainly driven by the distribution of the 'dU/dy' component (not shown here). Thus, a clear dipolar structure, as the one visible for the eddies centered at 6°E- 32.5°S and at 11.5°E-32.5°S, cannot be identified for this ACe, characterized by a highly turbulent pattern of interior shear, driven by very fine scales and possibly by internal gravity waves.

This hypothesis is supported by a vertical section of the horizontal divergence of velocity, plotted along the same ACe (Fig. 14c), where alternating, positive and negative, values propagate between the 27 and 27.5 isopycnals. If we reconnect these internal waves and the fine-scale, shear structures to the abundant presence of small features and filaments seen in the HR RV snapshot of Figure 10c, different instabilities (C-BCIs, shear or frontal) may be responsible of this turbulent distribution.

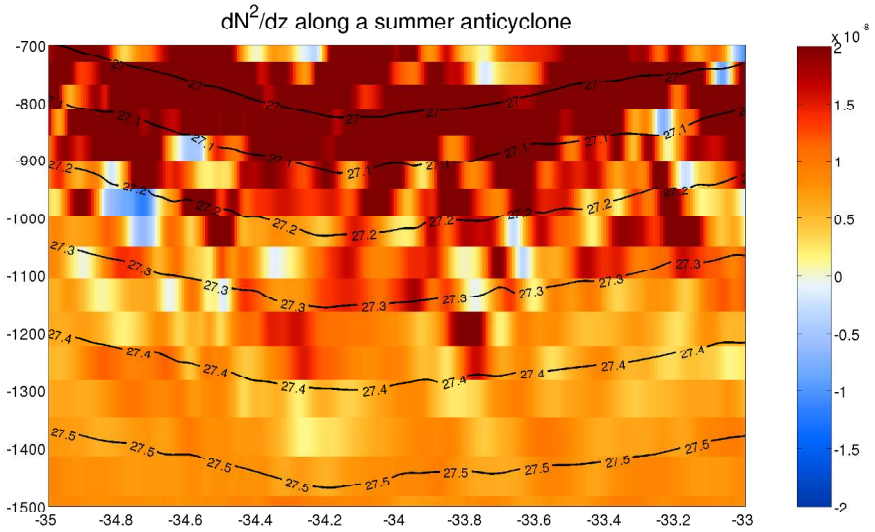

Figure 15. Meridional section of the vertical gradient of stratification (dN^2/dz, [s^{-1}]) plotted at 9.2°E along a summer anticyclone for the intermediate depths of the water column ($\sim$ 700-1500 m). Black contours are for isopycnals ranging from 27 to 27.5 kg/m^3.

To verify if the C-BCI could take place also at greater depths than the base of the ML, and in particular within the AAIW layers, we look at the meridional section of dN^2/dz along the same anticyclone analysed up to now. In Figure 15 we observe that filaments of negative values of this metric can be actually identified within the 27 and 27.3 isopycnals and therefore these layers could be conducive to this kind of baroclinic instability. However the generation of these filaments could also be related to other unstable mechanisms, like a barotropic

instability, their own coiling within the eddy core, after interaction with a neighboring structure, or finescale shear and strain. In the latter case, the ratio of vertical shear to horizontal strain would be proportional to N/f [*Charney*, 1971] and the tracer filaments slope would be much steeper than the typical isopycnal slopes, as seen in our S sections of Figure 11a. We then suggest that C-BCI could develop in the Cape Basin AAIW layer, even though further ad-hoc diagnostics would be required to confirm this preliminary evidence.

6 Impact of Smaller-scales on the Indo-Atlantic Exchange

In this section we use a Lagrangian approach to quantify the impact of smaller-scales dynamics in the Indo-Atlantic transport of thermocline watermasses. Integration of particles trajectories were performed for the two simulations analyzed in this work (HR and LR) using the offline mass-preserving algorithm ARIANE [*Blanke et Raynaud*, 1997; *Blanke et al.*, 1999] applied to daily archives of the multiyear, three-dimensional velocity field. This methodology allows the full description of individual trajectories as well as volume transport estimates based on the tiny weight allotted to each particle and transported without alteration along its trajectory. The volume of water transported from an initial to a final geographical section is computed by summing the transport of the particles achieving the connection that is being considered. Default information interpolated along individual trajectories includes salinity, temperature, depth, and density.

Our Lagrangian experiments were conducted over the control domain corresponding to the geographical extension of the HR solution, as shown in the transport streamfunction map of Figure 16. The particles were initialized at the initial sections located at the eastern and southern boundaries and intercepted at the western and northern boundaries of this control domain (respectively traced in red and black in Fig. 16). Over these geographical sections where millions of particles were spread (to account for an inward velocity), we kept only the particles associated with relevant salinity and density values typical of thermocline waters in the Cape Basin, meaning using their values from the surface to the 27.6 isopycnal. Each particle was associated with an individual weight related to the local magnitude of the incoming transport (expressed here in sverdrups, with 1 Sv = $10^6 m^3 s^{-1}$). All particles were integrated backward in time and the starting dates were sequentially taken during the last four years of the available archive, giving a total transport of about 30 SV for HR (Fig. 16) and of $\sim$20 SV for LR. We then plotted histogram bars of the difference between the final and the initial transports, computed as the number of particles normalised by their total transport and binned by poten-

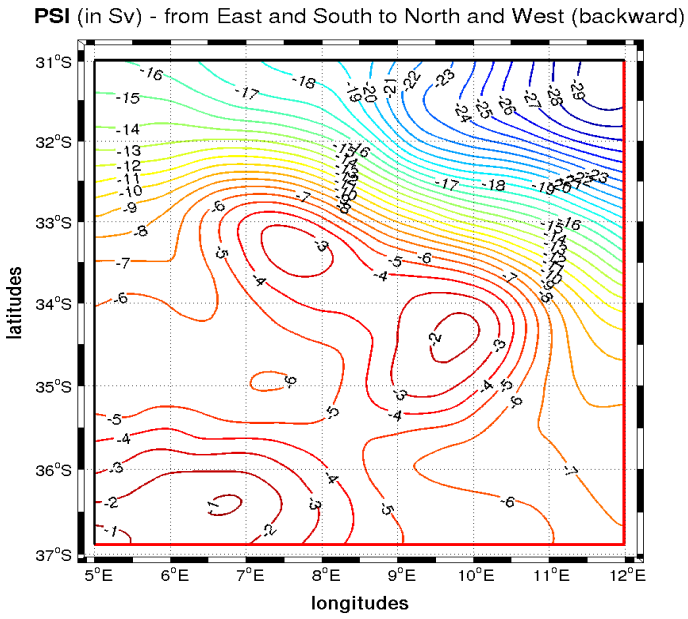

746 **Figure 16.** Lagrangian transport streamfunction estimated within the domain of the second child
747 of the HR (Nested-child2), with the initial sections coloured in red and the final sections in black.

762 tial density classes (Fig. 17a). We verified that the highest resolutions simulation (in red in
763 Fig. 17a) is the only one able to capture a prominent, net transport, from the Indian to the At-
764 lantic oceans, of thermocline waters, mainly consisting of the lighter (σ = 25.6- 25.8) and denser
765 (σ = 26.4- 26.6) varieties of mode water, and to a lesser extent of intermediate waters (σ =
766 27.2). If we plot the same Lagrangian estimates binned by salinity classes (Fig. 17b), we ob-
767 serve for intermediate waters a net transport in correspondence of the IA-AAIW salinity class
768 (S = 34.4 psu), which results from the lateral mixing of the Indian and Atlantic AAIWs. Both
769 of these figures show that small-scale dynamics strongly influence mode and intermediate wa-
770 ter properties by efficiently forming and transforming water masses. These ”in route” trans-
771 formations affect the water properties of the Indo-Atlantic transport, acting on the interocean
772 fluxes of heat and freshwater and therefore on the AMOC.

775 ## 7 Summary and Conclusions

776 The Indo-Atlantic exchange of thermocline and intermediate waters is essential in main-
777 taining the AMOC, by providing the return flow to the North Atlantic and compensating the
778 North Atlantic Deep Water outflow to the Southern Ocean [*Gordon et al.*, 1992; *Speich et al.*,
779 2007]. This mainly happens through Agulhas rings injected into the Cape Basin, in the south-

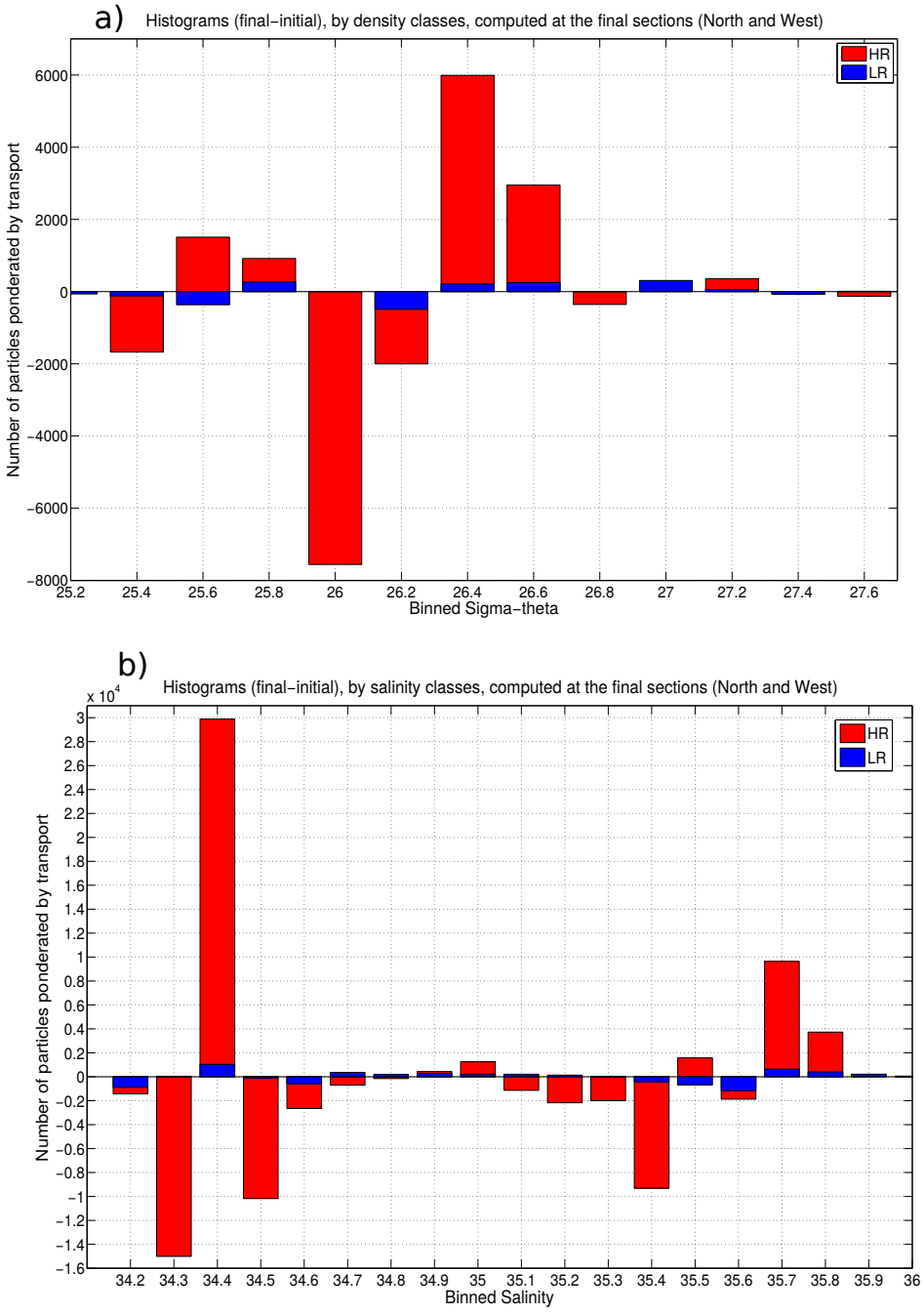

773 **Figure 17.** Histograms of the differences between the final and initial Lagrangian transports [Sv],

774 binned by density (a) and salinity (b) classes, for the HR simulation (in red) and for the LR (in blue).

easternmost corner of the Atlantic, after detachment from the AC at the AR, thus representing the major cause of current variability in this region [*Garzoli et al.*, 1996].

Several issues are important to assess more accurately how Agulhas rings contribute to inter-ocean fluxes [*Lutjeharms et al.*, 2003]. These naturally include their horizontal and vertical dimensions, as well as their anomalous heat and salt contents soon after having been spawned [*Schmid et al.*, 2003]. In this paper, we analyzed some of these aspects, investigating the geometry of the simulated ACes and their thermohaline structure, as well as the impact that these turbulent features have on the local water masses properties and advection. We have also pointed out that different types of instabilities develop within these rings during their journey in the Cape Basin, where they interact among themselves and with eddies of opposite sign.

Previuos numerical studies [*Wells et al.*, 2000; *Matano and Beier*, 2003; *Weijer et al.*, 2013] have shown that both barotropic and baroclinic processes play a major role as triggering mechanisms of eddies generation in the greater Agulhas Current System. In our work, we have further investigated the relative importance of these two main mechanisms of eddies interactions within the Cape Basin, underlining their role in producing finer scales turbulence. We used two regional numerical simulations, run respectively at mesoscale and submesocale-resolving resolutions. We firstly discriminated the range of scales and turbulent processes that each of these simulations is able to resolve. Then, by the analysis of specific diagnostics, applied to the eddies detected within our study region, we have quantified the energy contents and transfers at different scales and assessed their effects on the formation and transformation of the local watermasses. The results were here discussed for a summer and a winter ACes, chosen, in each of the two simulations, to represent the mean behavior of the simulated Agulhas rings.

Our main finding consisted in demonstrating a clear vertical separation between the dynamical regimes prevailing in the upper and intermediate depth layers. At the surface and down to the base of the ML, enhanced values of EKE, VBF and frontogenesis are related to the seasonal development of different instabilities: MLIs, symmetric and C-BCIs. MLIs mainly dominate in winter, when the action of the atmospheric forcing is more important and leads to a significant deepening of the ML. Because these instabilities are at a submesoscale exclusively solved by HR, only this simulation captured a correct seasonal cycle of the MLD. The same result holds for symmetric and shear instabilities, triggered by the interaction of mesoscale barotropic instabilities and mainly active, in our study region, during summer, when small meanders and filaments appear around and within mesoscale eddies.

We have also shown that these two seasonal, dynamical regimes are involved, *via* C-BCIs, in the formation of a local variety of mode waters, ARMW, commonly found in the core of Agulhas rings. C-BCIs are triggered in winter, engendering the subduction of surface waters below the ML where they form thick homogeneous layers of mode waters. Below the thermocline, frontal instabilities seem to develop, at both seasons, due to the interaction between adjacent eddies of opposite signs, leading to deformations of the eddy geometry and likely affecting its 3-D structure and thermohaline content.

For intermediate depths, we have provided evidence of relevant mechanisms of density compensation and lateral stirring of thermohaline fronts, driven by the intense meso- and submesoscale fields. In fact, similarly to the intrusions of the Mediterranean Water Overflow into the intermediate layers of the North Atlantic [*Smith and Ferrari*, 2009], a vigorous geostrophic eddy field, developed through baroclinic instability of the mean flow, has been documented in the literature within the Cape Basin [*Boebel et al.*, 2003; *Matano and Beier*, 2003; *Treguier et al.*, 2003]. Here, the mesoscale eddies stretch and twist the intense T-S gradients and produce sharp submesoscale T-S filaments along isopycnals. The eddy generation of submesoscale T-S variance is particularly effective at the depth of AAIWs, where salty and warm Indian AAIW converges and mixes with the fresher and colder Atlantic AAIW variety [*Rusciano et al.*, 2012; *Rimaud et al.*, 2012]. Therefore, our work endorses the assumption of *Smith and Ferrari* [2009] that in regions characterized by large watermass contrasts, the generation of compensated submesoscale T-S gradients by lateral mesoscale eddy stirring can overcome the generation of T-S variance by vertical turbulence. This hypothesis could be further investigated through the adoption of a more idealized, numerical approach. Here, by taking a S-QG approach, we only explored the possibility that C-BCIs can dynamically couple layers within the ocean interior characterized by marked changes in stratification.

By using Lagrangian diagnostics, we finally showed the impact of resolving smaller-scale processes assumes on the simulated Indo-Atlantic exchange of subsurface watermasses. These transports estimates indicate that only at HR the model can depict the interocean transfer of upper and lower thermocline waters, by capturing the formation and advection of different types of mode waters (ARMW) and the AAIW transformation in its regional varieties. Although more experimental studies are needed to corroborate the generality of the present results, we conclude by reiterating the key role of meso- and submesoscale processes in driving and structuring the advection of subsurface watermasses in the Cape Basin. These water masses materialize the Indo-Atlantic exchange, and thus rule the related heat and salt anomalies pene-

trating into the Atlantic Ocean and ultimately influencing the AMOC. The two configurations, run at different horizontal resolutions in our study, highlight that, in order to correctly represent the observed transport and water masses properties involved in this exchange, the simulated scales need to include a large portion of the submesoscale spectrum.

Acknowledgments

The authors greatly appreciate discussions with Xavier Capet, Gildas Cambon, Guillaume Lapeyre, Guillaume Roullet, Bernard Barnier, Arne Biastoch and Jeroen Molemaker. This work was supported by the "Laboratoire d'Excellence" LabexMER (ANR-10-LABX-19) and co-funded by a grant from the French government under the program "Investissements d'Avenir", and by a grant from the Regional Council of Brittany. This work was also supported by the European Union Horizon 2020 research and innovation programme under grant agreement no. 633211 (AtlantOS), and by the 11-ANR-56-004 SAMOC research grant. This study is part of the CLIVAR-SAMOC international initiative. We also acknowledge funding from the ANR/DGA program DYNED ATLAS and the French CNRS computer centre IDRIS for technical and computational support. We thank both reviewers who helped us to improve this manuscript.

References

Arhan, M., H. Mercier, and J. R. E. Lutjeharms (1999), The disparate evolution of three Agulhas rings in the South Atlantic Ocean. *J. Geophys. Res.* 104, C9, 2098721005, doi:10.1029/1998JC900047.

Arhan, M., S. Speich, C. Messager, G. Dencausse, R. Fine, and M. Boye (2011), Anticyclonic and cyclonic eddies of subtropical origin in the subantarctic zone south of Africa. *J. Geophys. Res.* 116, C11004, doi:10.1029/2011JC007140.

Ayina, H.-L., A. Bentamy, A. M. Mestas-Nuez, and G. Madec (2006), Theimpact of satellite winds and latent heat fluxes in a numerical simulation of the tropical Pacific Ocean,*J. Clim., 19, 58895902, doi:10.1175/ JCLI3939.1*.

Beal, L. M., W. P. M. de Ruijter, A. Biastoch, R. Zahn, and SCOR/IAPSO/WCRP Working Group 136 (2011), On the role of the Agulhas System in Ocean Circulation and Climate, *Nature* 472, 429-436, doi:10.1038/nature09983.

Bentamy, A., K. B. Katsaros, M. Alberto, W. M. Drennan, E. B. Forde, and H. Roquet (2003), Satellite estimates of wind speed and latent heat flux over the global oceans, *J. Clim., 16, 637656, doi:10.1175/1520-0442 (2003)016¡0637:SEOWSA¿2.0.CO;2*.

876 Biastoch, A., C. W. Boning, and J. R. E. Lutjeharms (2008), Agulhas leakage dynam-
877 ics affects decadal variability in Atlantic overturning circulation. *Nature* 456, 489 492
878 doi:10.1038/nature07426.

879 Blanke, B., and S. Raynaud (1997), Kinematics of the Pacific Equatorial Undercurrent: An
880 Eulerian and Lagrangian approach from GCM results, *J. Phys. Oceanogr., 27, 10381053*,
881 doi:10.1175/1520-0485(1997) 027¡1038:KOTPEU¿2.0.CO;2.

882 Blanke, B., M. Arhan, G. Madec, and S. Roche (1999), Warm water paths in the Equa-
883 torial Atlantic as diagnosed with a general circulation model, *J. Phys. Oceanogr., 29,*
884 *27532768*, doi:10.1175/1520-0485(1999) 029¡2753:WWPITE¿2.0.CO;2.

885 Boccaletti, G., Ferrari, R., Fox-Kemper, B., 2007. Mixed layer instabilities and
886 restratification.*J. Phys. Oceanogr. 37 (9), 22282250.* doi:10.1175/JPO3101.1.
887 http://journals.ametsoc.org/doi/abs/10.1175/JPO31011.

888 Boebel, O., Duncombe Rae, C., Garzoli, S., Lutjeharms, J., Richardson, P., Rossby, T.,
889 Schmid, C., Zenk, W., (1998). Float experiment studies interocean exchanges at the tip
890 of Africa. *EOS 79 (1), 68*.

891 Boebel, O., J. R. E. Lutjeharms, C. Schmid, C. Zenk, T. Rossby, and C. Barron (2003),
892 The Cape Cauldron: A regime of turbulent inter-ocean exchange. *Deep Sea Res., Part I,*
893 *50, 5786* doi:10.1016/S0967-0645.

894 Brannigan, L., D. Marshall, A. Naveira-Garabato, and G. Nurser (2015), The seasonal
895 cycle of submesoscale flows, *Ocean Modell., 92, 6984.*

896 Brannigan L. (2016), Intense submesoscale upwelling in anticyclonic eddies. *Geophys.*
897 *Res. Lett., 43, 33603369* doi:10.1002/2016GL067926.

898 Bruggemann, N.; Eden, C. (2015), Routes to Dissipation under Different Dynamical
899 Conditions. *Journal of Physical Oceanography 45. : S. 21492168.* doi: 10.1175/JPO-D-
900 14-0205.1

901 Byrne, D. A., A. L. Gordon, and W. F. Haxby (1995), Agulhas eddies: a synoptic view
902 using Geosat ERM data, *J. Phys. Oceanogr, 25, 902-917.*

903 J. Callies, R. Ferrari, J. M. Klymak, and J. Gula (2015), Seasonality in submesoscale
904 turbulence, *Nat. Commun., 6*.

905 Capet X., McWilliams J. C., Molemaker M. J., Shchepetkin A. F. (2008a), Mesoscale to
906 submesoscale transition in the California Current System. Part I: Flow structure, eddy
907 flux, and observational tests. *J. Phys. Oceanogr.* 38, 2943.

908 Capet, X., McWilliams, J., Molemaker, M., Shchepetkin, A. (2008c), Mesoscale to subme-
909 soscale transition in the California current system. Part III: energy balance and flux. *J.*
910 *Phys. Oceanogr. 38 (10), 22562269*.

911 Capet, X., G. Roullet, P. Klein, and G. Maze (2016), Intensification of Upper-Ocean Sub-
912 mesoscale Turbulence through Charney Baroclinic Instability. J. Phys. Oceanogr., 46,
913 33653384, https://doi.org/10.1175/JPO-D-16-0050.1

914 Chaigneau, A., Gizolme, A., Grados, C., (2008), Mesoscale eddies off Peru' in altime-
915 ter records: Identification algorithms and eddy spatio-temporal patterns. *Progress in*
916 *Oceanography.* 79 (2), 106119.

917 Charney, J. G. (1947), The dynamics of long waves in a baro- clinic westerly current. *J.*
918 *Meteor., 4, 136162, doi:10.1175/1520-0469(1947)004,0136:TDOLWI.2.0.CO;2.*

919 Charney, J. G. (1971), Geostrophic turbulence. *J. Atmos. Sci. 28, 10871095*.

920 Chelton, D. B., R. A. deSzoeke, M. G. Schlax, K. E. Naggar, and N. Siwertz (1998),
921 Geographical variability of the first-baroclinic rossby radius of deformation. *J. Phys.*
922 *Oceanogr.* 28, 433 460.

923 Craneguy P., (1999), Mecanismes d'intrusion de l'eau antarctique intermediaire antarctique
924 a travers le courant circumpolaire antarctique. *PhD thesis.*

925 Da Silva, A.M., Young-Molling, C.C., Levitus, S. (1994), Atlas of Surface Marine Data
926 1994, vol. 1. *Algorithms and Procedures, NOAA Atlas NESDIS, vol. 6, NOAA, Silver*
927 *Spring.*

928 Debreu, L., Mazauric, C. (2006), Adaptive Grid Refinement (AGRIF) in Fortran 90: Users
929 Guide Version 1.3. ¡http://www-lmc.imag.fr/IDOPT/AGRIF/index.html¿.

930 De Ruijter, W. P. M., Biastoch, A., Drijfhout, S. S., Lutjeharms, J. R. E., Matano, R. P.,
931 Pichevin, T., van Leeuwen, P. J., and Weijer, W. (1999), Indian-Atlantic inter-ocean
932 exchange: dynamics, estimation and impact, *J. Geophys. Res., 104, 20 88520 911*.

933 Dencausse, G., M. Arhan, and S. Speich (2010), Spatio temporal characteristics
934 of the Agulhas Current retroflection, *Deep Sea Res., Part I, 57(11), 13921405,*
935 *doi:10.1016/j.dsr.2010.07.004*.

936 Drijfhout S. S., Kattenberg, A., Haarsma, R. J., and Selten, F. M. (2001), The role of the
937 ocean in midlatitude, interannual-to-decadal-timescale climate variability of a coupled
938 model. *J. Climate, 14(17), 3617-3630* doi: 10.1175/1520-0442.

939 Duncombe Rae, C. M., F. A. Shillington, J. J. Agenbag, J. Taunton-Clark, and M. L.
940 Grtindlingh (1992), An Agulhas Ring in the South Atlantic Ocean and its interaction

941 with the Benguela upwelling frontal system, *Deep- Sea Res., 39, 2009-2027.*

942 Duncombe Rae, C. M., S. L. Garzoli, and A. L. Gordon (1996), The eddy field of the
943 southeast Atlantic Ocean: a statistical census from the Benguela Sources and Transport
944 project. *J. Geophys. Res., 101,11949-11964*.

945 Ertel, H. (1942), Ein neuer hydrodynamischer Erhaltungssatz. *Naturwiss.* 30, 543544.

946 Ferrari, R., and K. Polzin (2005), Finescale structure of the TS relation in the eastern
947 North Atlantic.*J. Phys. Oceanogr., 35, 14371454.*

948 Fox-Kemper, B., Ferrari, R., Hallberg, R. (2008), Parameterization of mixed
949 layer Eddies. Part I: theory and diagnosis. *J. Phys. Oceanogr. 38 (6), 11451165.*
950 doi:10.1175/2007JPO3792.1.

951 Garrett, C. (1983), On the initial streakiness of a dispersing tracer in two- and three-
952 dimensional turbulence. *Dyn. Atmos. Oceans, 7, 265277*.

953 Garzoli, S. L., A. L. Gordon, V. Kamenkovich, D. Pillsbury, and C. Duncombe Rae
954 (1996), Variability and sources of the southeastern Atlantic circulation, *J. Mar. Res., 54,*
955 *1039-1071*.

956 Garzoli, S. L., and A. L. Gordon (1996), Origins and variability of the Benguela Current,
957 *J. Geophys. Res., 101,897-906.*

958 Giordani, H., and G. Caniaux (2001): Sensitivity of cyclogenesis to sea surface tem-
959 perature in the Northwestern Atlantic. Monthly Weather Review, vol 129, n 6, pp
960 1273-1295.

961 Gladyshev, S., M. Arhan, A. Sokov, and S. Speich (2008), A hydrographic section from
962 South Africa to the southern limit of the Antarctic Circum- polar Current at the Green-
963 wich meridian, *Deep Sea Res., Part I, 55(10), 12841303*, doi:10.1016/j.dsr.2008.05.009.

964 Goni, G.J., S.L. Garzoli, A.J. Roubicek, D.B. Olson, and O.B. Brown (1997), Agulhas
965 ring dynamics from TOPEX/POSEIDON satellite altimeter data, *J. Mar. Res., 55, 861-*
966 *883*.

967 Gordon, A. L. (1985), Indian-Atlantic transfer of thermocline water at the Agulhas
968 retroflection, *Science, 227, 10301033*.

969 Gordon, A. L., and W. F. Haxby (1990), Agulhas eddies invade the South Atlantic: ev-
970 idence from Geosat altimeter and shipboard CTD survey, *J. Geophys. Res., 95, 3117-*
971 *3125.*

972 Gordon, A. L., J. R. E. Lutjeharms, and M. L. Grtindlingh (1987), Stratification and circu-
973 lation at the Agulhas Retroflection, *Deep-Sea Res. 34, 565- 599.*

Gordon, A. L., R. F. Weiss, W. M. Smethie Jr. and M. J. Warner (1992), Thermocline and intermediate water communication between the South Atlantic and Indian Oceans,*J. Geophys. Res., 97, 72237240*, doi:10.1029/92JC00485.

Giulivi, C. F. and A. L. Gordon, (2006), Isopycnal displacements within the Cape Basin thermocline as revealed by the Hydrographic Data Archive. *Deep-Sea Research Part I-Oceanographic Research Papers.* 53(8): 1285-1300.

Gula, J., M. J. Molemaker, and J. C. McWilliams (2015), Topographic vorticity generation, submesoscale instability and vortex street formation in the Gulf Stream. *Geophys. Res. Lett., 42, 40544062*. doi: 10.1002/2015GL063731.

Hanawa, K., and L. D. Talley (2001), Mode water, in *Ocean Circulation and Climate, Int. Geophys. Ser.,* vol. 77, edited by G. Siedler, J. Church, and J. Gould, chap. 5.4, pp. 373386, Academic, San Diego, doi:10.1016/S0074-6142(01)80129-7.

Haine, T.W.N., Marshall, J. (1998), Gravitational, symmetric, and baroclinic instability of the ocean mixed layer. *J. Phys. Oceanogr. 28 (4), 634658.*

Hogg, N.G., Stommel, H.M. (1985), The heton, an elementary interaction between discrete baroclinic geostrophic vortices, and its implications concerning heat-flow. *Proceedings of the Royal Society of London, A 397, 120.*

Hoskins, B.J. and Bretherton F. P., 1972. Atmospheric frontogenesis models -Mathematical formulation and solution. *J. Atmos. Sci. 29 (1), 1137.*

Hua Bach-Lien, Menesguen Claire, Le Gentil Sylvie, Schopp Richard, Marsset Bruno, Aiki Hidenori (2013), Layering and turbulence surrounding an anticyclonic oceanic vortex: in situ observations and quasi-geostrophic numerical simulations. *Journal Of Fluid Mechanics, 731, 418-442.*

Jacobs, S. S., and D. T. Georgi (1977), Observations on the southwest Indian/Antarctic Ocean, in *A Voyage of Discovery, edited by M. Angel, pp. 4384, Pergamon, Oxford, UK*.

Klein, P., Treguier, A.M., Hua, B.L. (1998), Three-dimensional stirring of thermohaline fronts. *Journal of Marine Research 56, 589612.*

Klein P, Lien Hua B, Lapeyre G, Capet X, LeGentil S, Sasaki H (2008) Upper Ocean Turbulence from High-Resolution 3D Simulations. *J Phys Oceanogr 38:1748-1763*.

Lapeyre, G., Klein, P. and Hua, B. L. (2006), Oceanic restratification forced by surface frontogenesis. *J. Phys. Oceanogr. 36 (8), 15771590*.

Large, W. G., J. C. McWilliams, and S. C. Doney (1994), Oceanic vertical mixing: A review and a model with a nonlocal boundary layer parameterization, *Rev. Geophys., 32,*

363 403.

Laxenaire R., Speich S., Blanke B., Chaigneau A. and Pegliasco C. (Accepted), New insights on Agulhas rings dynamics as inferred from altimetry.

Ledwell, J. R., A. J. Watson, and C. S. Law (1998), Mixing of a tracer in the pycnocline. *J. Geophys. Res., 103, 21 49921 529.*

Lemarie F., Kurian, J., Shchepetkin, A.F., Molemaker, M.J., Colas, F., McWilliams, J.C. (2012), Are There Inescapable Issues Prohibiting the use of Terrain-Following Coordinates in Climate Models? *Ocean Modell.* doi:10.1016/j.ocemod.2011.11.007.

Lutjeharms, J. R. E. and Gordon, A. L. (1987), Shedding of an Agulhas Ring observed at sea, *Nature.* 325, 138140.

Lutjeharms, J. R. E., de Ruijter, W. P. M., and Peterson, R. G (1992), Inter-basin exchange and the Agulhas retroflection; the development of some oceanographic concepts. *Deep Sea Res., 39, 17911807.*

Lutjeharms, J. R. E. (1996), The exchange of water between the south Indian and south Atlantic oceans, in The South Atlantic: Present and Past Circulation, *edited by G. Wefer et al., pp. 125-162, Springer Verlag, New York.*

Lutjeharms J. R. E., Penven P., and Roy C. (2003), Modelling the shear-edge eddies of the southern Agulhas Current, *Cont. Shelf Res., 23, 10991115.*

Marchesiello P., McWilliams J.C., Shchepetkin A.F. (2001), Open boundary conditions for long-term integration of regional oceanic models. *Ocean Modelling.* 3,121.10.1016/S1463-5003(00)00013-5.

Matano, R., Beier, E.J. (2003), A kinematic analysis of the Indian/Atlantic interocean exchange. *Deep Sea Res. II, this issue (PII:S0967-0645(02)00395-8).*

Mensa, J.A., Garraffo, Z., Griffa, A., Ozgokmen, T.M., Haza, A., Veneziani, M. (2013), Seasonality of the submesoscale dynamics in the Gulf stream region.*Ocean Dyn. 63 (8), 923941.* doi:10.1007/s10236-013-0633-1.

McCartney, M. S. (1977), Subantarctic Mode Water, in *A Voyage of Discovery: George Deacon 70th Anniversary Volume,* edited by M. V. Angel, pp. 103119, Pergamon, Oxford, UK

McDonagh, E. L., K. J. Heywood, and M. P. Meredith (1999), On the structure, paths, and fluxes associated with Agulhas rings, *J. Geophys. Res., 104(C9), 2100721020, doi:10.1029/1998JC900131.*

McWilliams, J.C. (2008), The nature and consequences of oceanic eddies. In: *Eddy-Resolving Ocean Modeling*, M. Hecht and H. Hasumi, eds., AGU Monograph, 5-15.

McWilliams, J.C., Molemaker, M.J. (2011), Baroclinic frontal arrest: a sequel to unstable frontogenesis. *J. Phys. Oceanogr. 41 (3), 601619.* doi:10.1175/2010JPO4493.1.

Meunier, T., C. Mnesguen, R. Schopp, and S. Le Gentil (2015), Tracer Stirring around a Meddy: The Formation of Layering. *J. Phys. Oceanogr., 45, 407423*.

Molemaker, M. J., J. C. McWilliams, and X. Capet (2010), Balanced and unbalanced routes to dissipation in an equilibrated Eady flow. *J. Fluid Mech., 654, 35 63,* doi:10.1017/S0022112009993272.

Molemaker M.J., Mcwilliams J.C., Dewar W.K. (2015), Submesoscale Instability and Generation of Mesoscale Anticyclones near a Separation of the California Undercurrent. *J Phys Oceanogr.* 45:613-629.

Okubo, A. (1970), Horizontal dispersion of floatable particles in the vicinity of velocity singularities such as convergences, *Deep Sea Res., 17, 445454*.

Ou, H. W., and W. P. M. de Ruijter (1986)eparation of an inertial boundary current from a curved coastline, *J. Phys. Oceanogr., 26, 22672279.*

Peliz A., Boutov D., Aguiar A.B., Carton X. (2014), The Gulf of Cadiz Gap wind anticyclones. *Continental Shelf Research.* 91:171-191.

Penven, P., C. Roy, J. R. E. Lutjeharms, A. Colin de Verdie‘re, A. Johnson, F. Shillington, P. Freon, and G. Brundrit (2001), A regional hydrodynamic model of the Southern Benguela, *S. Afr. J. Sci., 97, 472 476*.

Penven, P., Chang, N., Shillington, F. (2006), Modelling the Agulhas Current using SAfE (Southern African experiment). *Geophysical Research Abstracts 8 (04225).*

Reason, C. J. C. (2001), Evidence for the influence of the Agulhas Cur- rent on regional atmospheric circulation patterns, *J. Climate, 14,27692778, 2001.*

Rimaud, J., S. Speich, B. Blanke, and N. Nicolas (2012), The exchange of Intermediate Water in the southeast Atlantic: Water mass transformations diagnosed from the Lagrangian analysis of a regional ocean model. *J. Geophys. Res.* 117, C08034, doi:10.1029/2012JC008059.

Rosso I., Hogg McC. A., Strutton P. G., Kiss A. E., Matear R., Klocker A., van Sebille E. (2014), Vertical transport in the ocean due to sub-mesoscale structures: Impacts in the Kerguelen region. *Ocean Modell.* http://dx.doi.org/10.1016/j.ocemod.2014.05.001.

Roullet G. and Klein P. (2010), Cyclone-Anticyclone Asymmetry in Geophysical Turbulence. *DOI: 10.1103/Phys. Rev. Lett.* 104, 218501.

Rubio, A.,Blanke B., Speich S., Grima N., Roy C. (2009), Mesoscale eddy activity in the southern Benguela upwelling system from satellite altimetry and model data. *Prog. Oceanogr.* , doi:10.1016/j.pocean.2009.07.029.

Ruddick, B. R. (1992), Intrusive mixing in a Mediterranean salt lensintrusion slopes and dynamical mechanisms. *J. Phys. Oceanogr., 22, 1274 1285*.

Ruddick, B. and K. Richards (2003), Oceanic thermohaline intrusions: observations. *Prog. Oceanogr., 56 (3 4), 499 527.*

Ruddick, B. R., Oakey, N. S. and Hebert, D. (2010), Measuring lateral heat flux across a thermohaline front: A model and observational test. *Journal of Marine Research, vol. 68, no. 3-4, pp. 523-539.*

Rusciano, E., S. Speich, and M. Ollitrault (2012), Interocean exchanges and the spreading of Antarctic Intermediate Water south of Africa. *J. Geophys. Res.* 117, C10010, doi:10.1029/2012JC008266.

Schmid, C., O. Boebel, W. Zenk, J. R. E. Lutjeharms, S. L. Garzoli, P. L. Richardson, and C. Barron (2003), Early evolution of an Agulhas Ring, *Deep Sea Res. Part II, 50(1), 141 166.*

Schmid, C., and S. L. Garzoli (2009), New observations of the spreading and variability of the Antarctic Intermediate Water in the Atlantic, *J. Mar. Res., 67, 815843*, doi:10.1357/002224009792006151.

Schouten, M. W., de Ruijter, W. P. M., van Leeuwen, P. J., and Lutjeharms, J. R. E. (2000), Translation, decay and splitting of Agulhas rings in the south-eastern Atlantic ocean, *J. Geophys. Res., 105, 21 91321 925.*

Shchepetkin, A. F., and J. C. McWilliams (2003), A method for computing horizontal pressure-gradient force in an oceanic model with a nonaligned vertical coordinate. *J. Geophys. Res.* 108(C3), 3090, doi:10.1029/ 2001JC001047.

Shchepetkin, A. F., and J. C. McWilliams (2005), The regional oceanic modeling system (ROMS): A split-explicit, free-surface, topography-following-coordinate oceanic model. *Ocean Modell.* 9, 304 347, doi:10.1016/j.ocemod.2004.08.002.

Shchepetkin, A. F., and J. C. McWilliams (2009), Correction and commentary for Ocean forecasting in terrain-following coordinates: Formulation and skill assessment of the regional ocean modeling system by Haidvogel et al., *J. Comput. Phys., 227, 35953624.*

1104 Sloyan, B. M., and S. R. Rintoul (2001), Circulation, renewal and modification of Antarc-
1105 tic Mode and Intermediate Water, *J. Phys. Oceanogr., 31, 10051030*.
1106 Smith, K. S. and E. Bernard, (2013), Geostrophic turbulence near rapid changes in stratifi-
1107 cation. *Physics of Fluid 25, 046601*. doi: http://dx.doi.org/10.1063/1.4799470
1108 Smith, K.S. and R. Ferrari, (2009), The Production and Dissipation of Compensated
1109 Thermohaline Variance by Mesoscale Stirring. *J. Phys. Oceanogr., 39, 24772501*,
1110 https://doi.org/10.1175/2009JPO4103.1
1111 Smith, W., and D. Sandwell (1997), Global sea floor topography from satel-
1112 lite altimetry and ship depth soundings. *Science* 277 (5334), 19561962,
1113 doi:10.1126/science.277.5334.1956.
1114 Soufflet Y., Marchesiello P., Lemarie F., Jouanno J., Capet X., Debreu L., Benshila R.
1115 (2016), On effective resolution in ocean models. *Ocean Modell.* 98 (2016) 3650.
1116 Spall, M. A. (1995), Frontogenesis, subduction, and cross-front exchange at upper ocean
1117 fronts, *J. Geophys. Res., 100(C2), 25432557, doi:10.1029/94JC02860.*
1118 Speich, S., Lutjeharms, J.R.E., Penven, P., Blanke, B. (2006), Role of bathymetry in Ag-
1119 ulhas Current configuration and behaviour. *Geophysical Research Letters.* 33, L23611.
1120 doi:10.1029/2006GL027157.
1121 Speich, S., B. Blanke, and W. Cai (2007), Atlantic Meridional Overturning
1122 and the Southern Hemisphere Supergyre. *Geophys. Res. Lett.* 34, L23614,
1123 doi:10.1029/2007GL031583.
1124 Speich, S., and M. Arhan (2007), GOODHOPE/Southern Ocean: A study and monitoring
1125 of the Indo-Atlantic connections. *Mercator Newsl.* 27, 2941.
1126 Stone, P.H. (1966), On non-geostrophic baroclinic stability. *J. Atmos. Sci. 23 (4), 390400*.
1127 Talley, L. D. (1996), Antarctic Intermediate Water in the South Atlantic. *in The South*
1128 *Atlantic: Present and Past Circulation, edited by G. Wefer et al.* pp. 219238, Springer,
1129 Berlin, doi:10.1007/978-3-642-80353-6-11.
1130 Thomas, L.N., (2005), Destruction of potential vorticity by winds. *J. Phys. Oceanogr. 35*
1131 *(12), 24572466.*
1132 Thomas, L., Ferrari, R., (2008), Friction, frontogenesis, and the stratification of the surface
1133 mixed layer. *J. Phys. Oceanogr. 38 (11), 25012518. doi:10.1175/2008JPO3797.1*.
1134 Thomas, L.N., Taylor, J.R., Ferrari, R., Joyce, T.M., (2013), Symmetric instabil-
1135 ity in the gulf stream. *Deep Sea Res. Part II: Top. Stud. Oceanogr. 91, 96110.*
1136 doi:10.1016/j.dsr2.2013.02.025.

Thomas, L.N., J.R. Taylor, E.A. DAsaro, C.M. Lee, J.M. Klymak, and A. Shcherbina (2016), Symmetric Instability, Inertial Oscillations, and Turbulence at the Gulf Stream Front. *J. Phys. Oceanogr., 46, 197217.* https://doi.org/10.1175/JPO-D-15-0008.1

Treguier, A.-M., Boebel, O., Barnier, B., Madec, G. (2003), Agulhas eddy fluxes in a 1/6° Atlantic model. *Deep Sea Res. II, this issue (PII:S0967-0645(02)00396-X).*

Vallis, G. K. (2006), Atmospheric and Oceanic Fluid Dynamics. *Cambridge University Press, 745 pp.*

Van Aken H. M., A.K. van Veldhoven, C. Veth, W.P.M. de Ruijter, P.J. van Leeuwen, S.S. Drijfhout, C.P. Whittle, M. Rouault (2003), Observations of a young Agulhas ring, Astrid, during MARE in March 2000, *Deep Sea Research Part II: Volume 50, Issue 1, p. 167-195, ISSN 0967-0645.* http://dx.doi.org/10.1016/S0967-0645(02)00383-1.

Veitch, J., Penven P., Shillington F. (2009), The Benguela: A laboratory for comparative modeling studies. *Prog. Oceanogr., doi:10.1016/ j.pocean.2009.07.008.*

Weijer, W., W.P.M. de Ruijter, H.A. Dijkstra and P.J.van Leeuwen (1999), Impact of interbasin exchange on the Atlantic overturning circulation. *J. Phys. Oceanogr.* 29,2266-2284.

Weijer, W., V. Zharkov, D. Nof, H. A. Dijkstra, W. P. M. de Ruijter, A. Terwisscha van Scheltinga, and F. Wubs (2013), Agulhas ring formation as a barotropic instability of the retroflection, *Geophys. Res. Lett., 40, 54355438,* doi:10.1002/2013GL057751.

Weiss, J. (1991), The dynamics of enstrophy transfer in two-dimensional hydrodynamics, *Physica D, 48(23), 273294, doi:10.1016/0167-2789(91)90088-Q*.

Wells, N. C., V. O. Ivchenko, and S. E. Best (2000), Instabilities in the Agulhas Retroflection Current system: A comparative model study, *J. Geophys. Res., 105(C2), 32333241.*

You, Y., Lutjeharms, J., Boebel, O., de Ruijter, W.P.M. (2003), Quantification of the interocean exchange of intermediate water masses around the Cape of Good Hope. *Deep Sea Res. II, this issue (PII:S0967-0645(02)00384-3.*

Supporting Information for "Mesoscale and submesoscale processes in the southeast Atlantic and their impact on the regional thermohaline structure."

T. A. Capuano,[1] S. Speich,[2] , X. Carton[1] and Bruno Blanke[1]

1. Figures S1 and S2.

2. Caption for Movies S1 (File uploaded separately): animation of zonal sections of Potential Vorticity (PV) and vertical velocity (W), extracted at each timestep (daily) from spring- Y4M10- to the next summer- Y5M1- within the domain of our HR simulation.

Introduction

This supporting information provides two figures and one animation which are described in the main article.

Corresponding author: S. Speich Laboratoire de Meteorologie Dynamique, LMD-IPSL, Ecole Normale Superieure, Paris, France (speich@lmd.ens.fr)

[1]Laboratoire d'Ocanographie Physique et
Spatiale, LOPS-UBO, Brest.

[2]Laboratoire de Meteorologie Dynamique,
LMD-IPSL, Ecole Normale Superieure,
Paris, France.

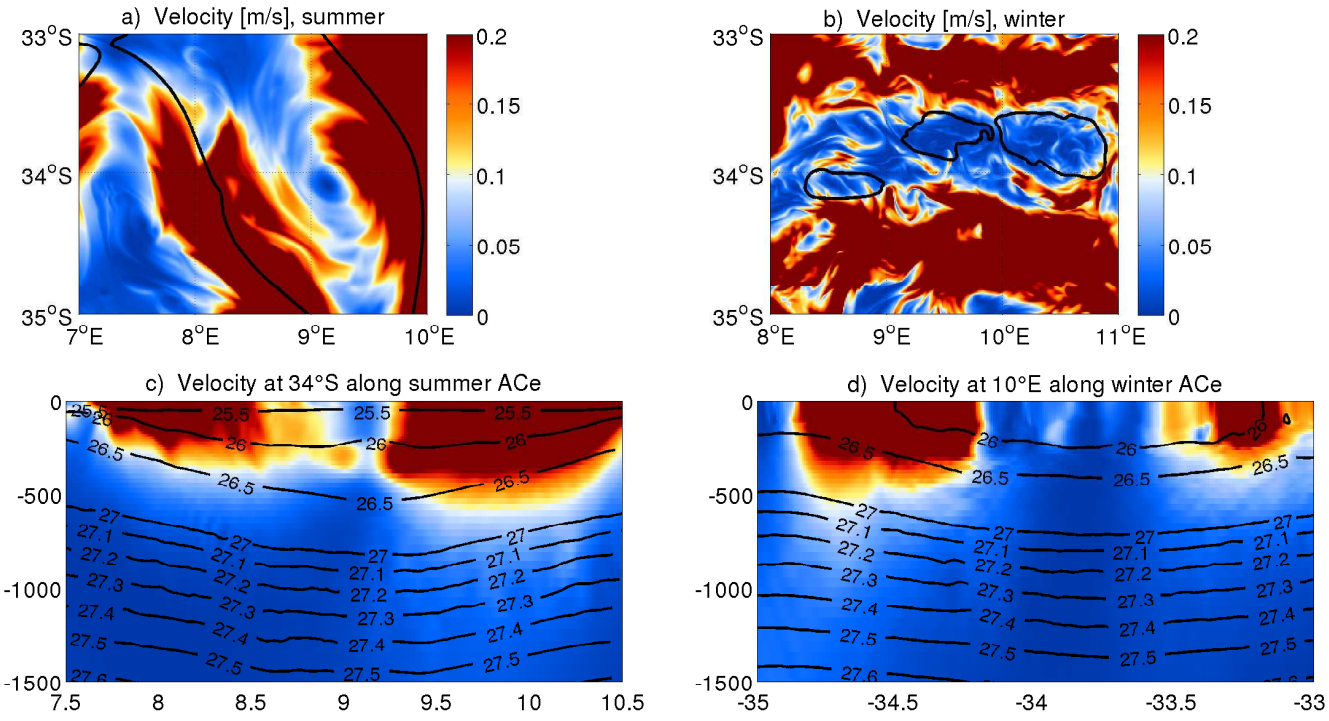

Figure S1. Seasonal maps and sections of the horizontal velocity (u^2+v^2) within the HR simulation, correspondent to the energy transfers plots of Figure 6.

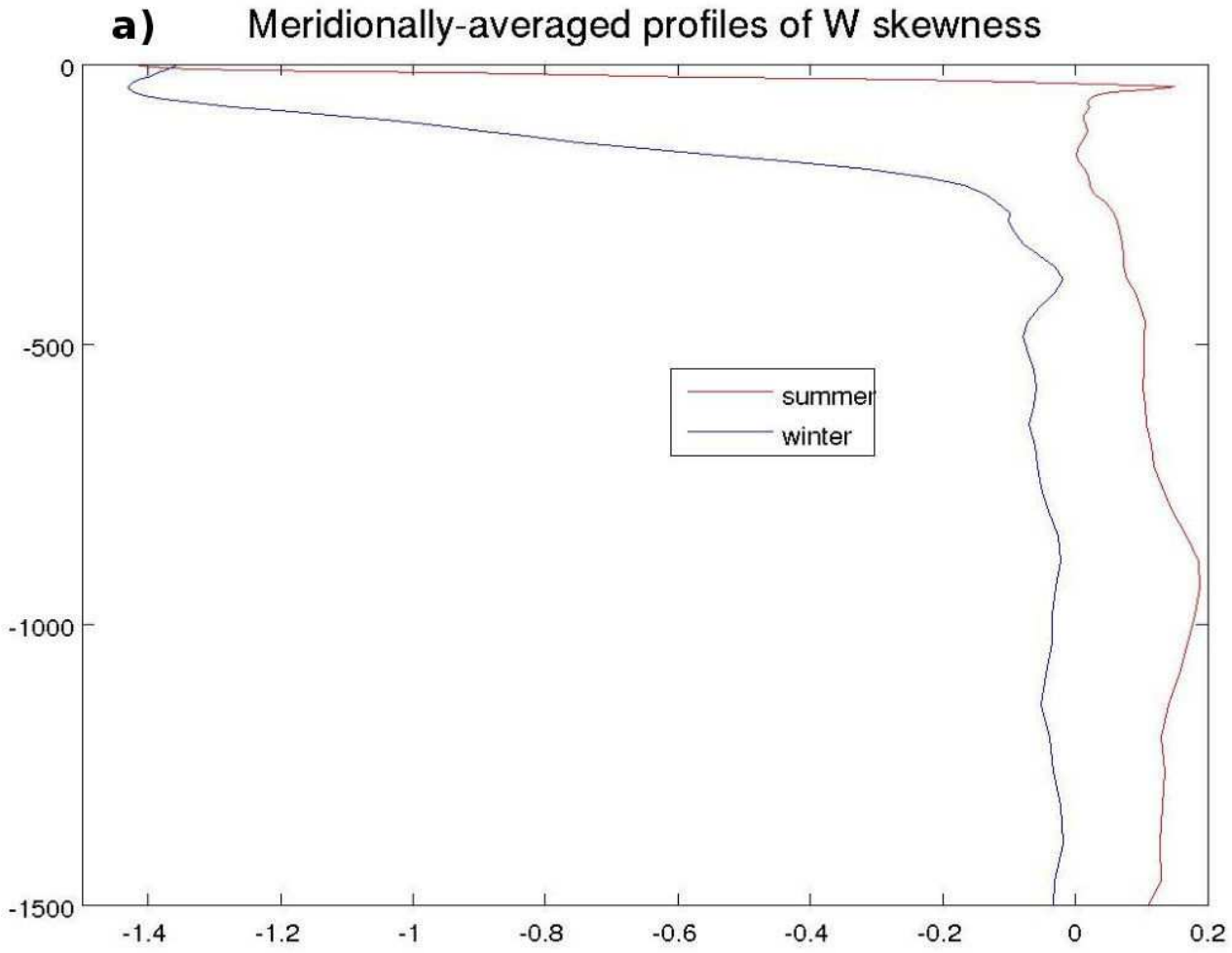

Figure S2. Meridionally and temporally averaged profiles of the skweness of vertical velocity (W, [m/d]), for the summer (in red) and the winter (in blue) seasons, within the HR simulation.

5.3 Discussion

In a submesoscale-resolving nested simulation, which correctly captures these finescale processes in the upper layers but also at depth, we were able to address the formation and transformation of the local water masses down to the base of the main thermocline. By contrasting the analysis of this simulation with a mesoscale-resolving one, we investigated how several meso-submesoscale interactions taking place in the Cape Basin are responsible of such water masses variations. In particular, our results amplify the suggestions of *Boebel et al.* [2003] on the existence of two distinct dynamical regimes influencing the upper-ocean and intermediate depth water masses in the Cape Basin: a predominance of ageostrophic flow in the near-surface, whereas prevailing quasi-gesotrophic dynamics within the AAIWs layer.

5.3.1 Upper layers instabilties

The near-surface, down to the base of the mixed layer, is characterised by the seasonal enhancement in the values of vertical velocity, eddy kinetic energy, vertical buoyancy flux and frontogenetic tendency, related to the presence of submesoscale structures and the development, in summer and winter, of different instabilities. The latter sustain a highly ageostrophic flow, whose energetic, finer scales (Fig. 2 of the submitted manuscript presented in section 5.2 of this chapter) have a direct impact on the formation and advection of the upper layers watermasses. In particular, we provide qualitative evidence that C-BCIs are at play in the Cape Basin and directly related to the winter subduction of a local type of mode waters (ARMW) within the anticyclones detected in the nested simulation. By definition, mode water regions are characterized by the presence of pycnostads, that is, weak upper-ocean stratification (N^2) and deep N^2 maximal with negative dN^2/dz over the depth range of the pycnostad [*Capet et al.*, 2016]. C-BCIs can thus be important in such regions as the Cape Basin.

Furthermore, we demonstrated that in our study region mixed-layer instabilities mainly occur within Agulhas Rings in winter. During this season, we assist to the restratification of the surface mixed layer by submesoscales, triggering the slumping of lateral buoyancy gradients within mixed layer eddies, as previuosly shown in other studies [*Boccaletti et al.*, 2007, *Capet et al.*, 2008a, *Molemaker et al.*, 2005]. Observational studies have confirmed that the lateral density gradients associated with this type of eddies reach scales as small

as a localized internal Rossby radius [*Hosegood et al.*, 2006], with typical values of a few kilometers. The latter is an order of magnitude smaller than the previously suggested smallest scales of variability [*Ferrari and Rudnick*, 2000] and far below the horizontal resolution of mesoscale-resolving numerical models. That is why the analysis of the energy transfers, performed over the Agulhas rings crossing the Cape Basin, showed the occurrence of mixed layer instabilities only in our nested configuration.

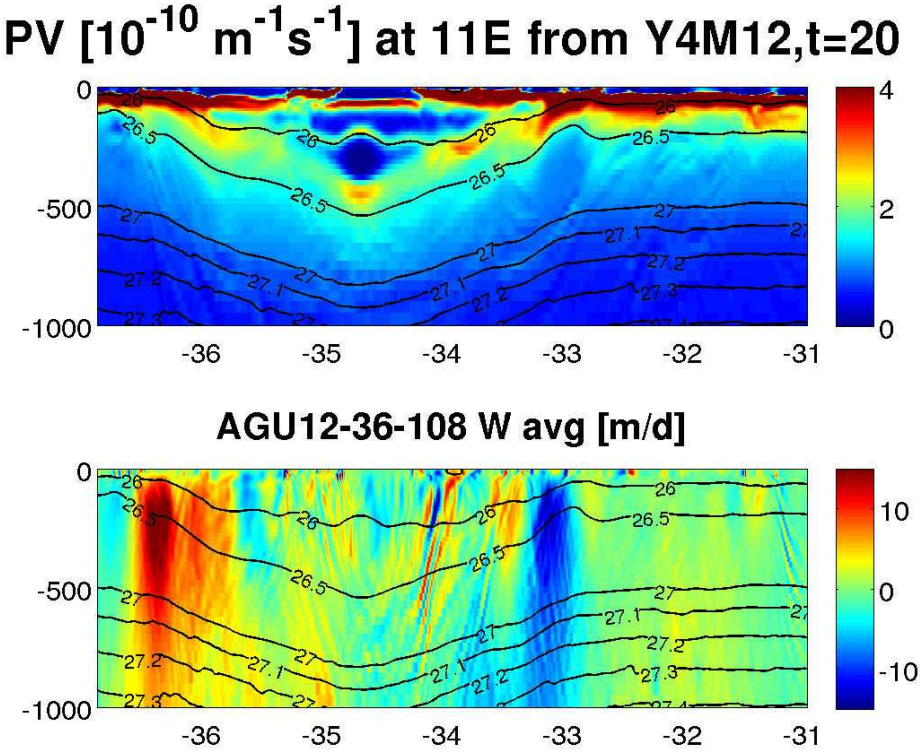

Figure 5.4: Instantaneous sections of potential vorticity (top) and vertical velocity (bottom), along a summer anticyclone crossing the domain of our nested configuration (AGU12_36_108).

We also pointed out that in summer, where negative potential vorticity occurs, a net subduction of surface waters is triggered by a flux of PV across the base of the mixed layer, accompanied by enhanced gradients of vertical velocity (Fig. 5.4), in line with previously published work [*Brannigan*, 2016, *Taylor and Ferrari*, 2009, *Thomas*, 2005]. This happens in correspondence of upper-layers filaments where the Richardson number attained values <1, showing symmetric instability. No such advective response develops where positive potential vorticity occurs. In our submesoscale-resolving simulation, we observed negative values of the product of the Ertel PV by the Coriolis parameter (fQ, Fig. 8b of the submitted manuscript presented in section 5.2) within narrow filaments of width O(10 km) surrounding the outer and inner limits of summer anticyclones. Here

symmetric instability drives slantwise convection along isopycnals throughout a stratified but turbulent surface mixed layer (Figs. 8g, h, i and Fig. 9b of the submitted manuscript presented in section 5.2). This result is in agreement with the findings of previous studies [*D'Asaro et al.*, 2011, *Taylor and Ferrari*, 2010].

Thus, we confirm the hypothesis of previous studies [*Drijfhout et al.*, 2001, *Matano and Beier*, 2003, *You et al.*, 2003] on the Agulhas Rings being a class of subsurface-intensified eddies able to isolate the T-S properties of newly formed water masses trapped within their cores and advect them across the Cape Basin, as it happens for ARMW. This class of anticyclones corresponds to the nearly zonal belt of subsurface eddies described by *Zhang et al.* [2017], as located around 30°S and the western tip of the Agulhas Current system and presenting shallower core depths compared to those in the deep convection regions of the North-Atlantic.
In fact, the vertical distribution of PV, in sections traced along our summer anticyclones (example in Fig. 5.4), is not only characterized by a central minimum. It is also marked by a high-low-high structure, consistent with the vertical deformations of isopycnals (i.e. stretching in the middle and squeezing above and below). This three-compartment structure can be related to the vertical distribution of the stratification in the section of dN^2/dz along the HR summer ACe (Fig. 9 of the second article), where we saw a minimum of stratification at the core of the eddy and higher values of N^2 below and above it. This vertical distribution of N^2 corresponds to the one theoretically expected under lenticular eddies being statically stable [*Meunier et al.*, 2015]. In particular, between the 26 and the 26.5 isopycnals we can locate a minimum of N^2 over a ring, having a local maximum just below the eddy core, and forming with it a 'hat-like' structure. The latter has been observed under intra-thermocline eddies and Meddies [*Hua et al.*, 2013], where a breaking of the potential vorticity pole takes place due to local instabilities.

In addition to the aforementioned mechanism of C-BCIs, the filamentary structures seen at the base of the mixed layer in the high resolution section of PV and vertical velocity (Fig. 5.4), may have also been created by symmetric instability. This could arise in the subsurface from the interaction of the Agulhas ring with the atmospheric forcing, as in the idealized context investigated by *Brannigan* [2016]. But since our current surface forcing is very smoothed, we were unable to verify this possibility. An alternative hypothesis is that these filaments have originated due to the straining of tracer fields along isopycnals by

the mesoscale quasi-geostrophic type flow [*Smith and Ferrari*, 2009]. However, the slope of these filaments is much shallower than the f/N slope predicted by theory, contrary to similar structures observed at intermediate depths.

5.3.2 Eddy stirring and mixing at intermediate depth

Deeper in the water column, along the AAIW layer, we indeed observed, within both cyclones and anticyclones detected in the nested simulation, interleaving filaments of temperature and salinity much steeper than the background isopcynals. Their slope is consistent with the theoretically expected f/N scaling of the isotropic forward cascade of tracer variance by submesoscales [*Charney*, 1971].
Here, the key assumption is that the interior ocean dynamics on scales of 1–500 km can be described by the quasi-geostrophic (QG) approximation. This allows us to explain the structure of the thermohaline anomalies in terms of well-known properties of forced QG turbulence, as underlined by *Klein et al.* [1998]. At intermediate levels, the simulated mesoscale structures stir the large-scale T and S gradients, leading to forward cascade of T-S variance at submesoscales, whose effects on AAIWs local varieties are completely density-compensated, as shown by *Rusciano et al.* [2012] and *Rimaud et al.* [2012]. We thus suggest that in the Cape Basin QG dynamics predominates at intermediate depth.

This clearly appears in the spectral curves of kinetic energy (Fig. 2 of the submitted manuscript presented in section 5.2 of this chapter) and in those of the vertical diffusion coefficients (Fig. 14 of the submitted manuscript presented in section 4.2 of chapter 4). This quasi-geostrophic flow advects salt and temperature gradients within the AAIWs layer, which is thus characterised by large fluctations in T-S properties compared to the much tighter relationship observed in the upper thermocline (Fig. 13 of the submitted manuscript presented in section 5.2). Due to the local convergence of Indian and Atlantic AAIW varieties, submesoscale filaments, arising along the 27.2 isopycnal (Fig. 5.5), produce compensated T-S fine-structure through the stirring of the mesoscale field. This implies strong mechanisms of homogenization and lateral mixing, as previously documented in the literature [*Arhan et al.*, 2011, *Gladyshev et al.*, 2008, *Piola and Georgi*, 1982], which drive the ultimate transformation of AAIW into its Indo-Atlantic variety.

We thus demonstrated that in the Cape Basin the enhanced strain rate of the mesoscale dynamics leads to the formation, along the AAIWs level, of narrow filaments and fronts

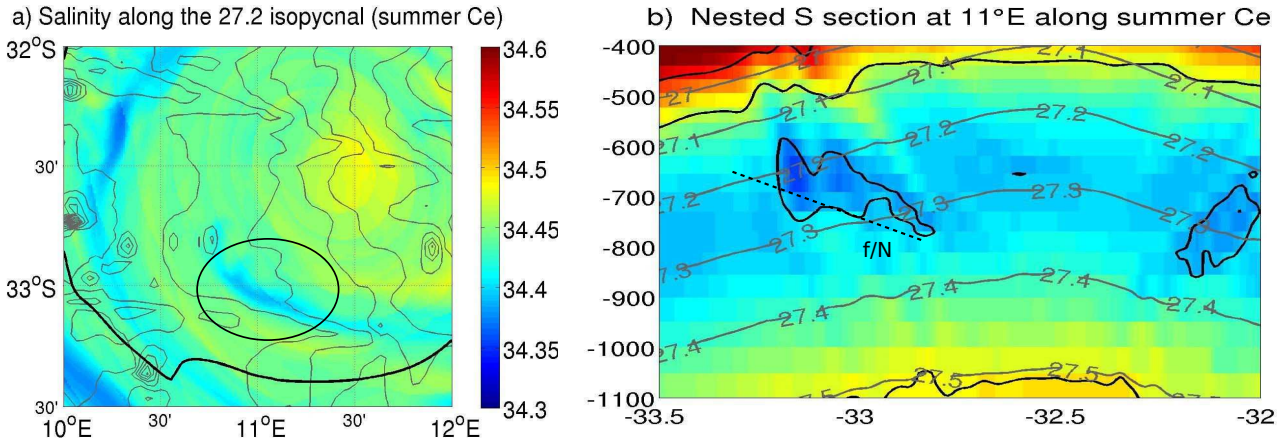

Figure 5.5: Salinity snapshots at intermediate depths showing the horizontal (a) and vertical (b) localisation of a submesoscale filament within a cyclone detected in AGU12_36_108.

that arise through cascades of mesoscale energy and tracer variance into the submesoscale range. The mechanisms that could be responsible of halting this forward cascade of T-S variance at the submesoscales, have not been explicitly addressed in this work. One possibility is that the formation of isopycnal T-S gradients is arrested in the horizontal by three-dimensional turbulence as a result of internal wave breaking [*Ledwell et al.*, 1998]; hints of internal waves have been observed to propagate along the 27.2 isopycnal (Fig. 15c of the submitted manuscript presented in section 5.2). However, this scenario would lead to quite small T-S features (O(10m)), that we are currently not able to capture with a vertical resolution of ~ 50 m. The filaments that we resolve at present are O(10km) and higher. The ratio of horizontal-to-vertical scales of the tracer filaments has been shown to be proportional to the ratio of shear over strain [*Smith and Ferrari*, 2009]. Thus, when the shear is much larger than the strain, the vertical scale of the tracer will be much smaller than its horizontal scale. This explains why the tracer filaments are much thinner in the vertical than in the horizontal (Fig. 5.5), and how the cascade of tracer variance is arrested once the thickness of the filaments becomes of the same order as the scale of the isotropic turbulence characterizing internal wave breaking [*Klein et al.*, 1998].

5.4 Conclusions

The results of this chapter enabled us to complement our picture of the Cape Basin turbulent dynamics, acquiring some insight on the submesoscale component of these processes and on the instabilities originating from its interactions with the mesoscales. Hence, we

believe to have satisfactorily addressed points 1. and 2. of our objectives, regarding the qualitative and quantitative description of the Cape Basin turbulent field, of its characteristic scales and of the energy transfers between them. This evaluation was undertaken at different depths (upper vs intermediate layers), but also at specific locations of the study region. The nested approach allowed us, indeed, to focus our attention on the nonlinear interactions between the disparate dynamical scales occurring within the biggest eddies crossing the second child domain of this simulation. The latter was intentionally centered within the Agulhas rings pathway in the South Atlantic, away from the continental slope and prominent topographic features, in accordance with our main interest in the meso-submesoscale interactions. By investigating the marked seasonality of these processes and their associated instabilities within the detected Agulhas rings, we also tackled point 3 of our objectives, concerning the temporal variability of the turbulent field.

However, still much remains to investigate about the globality of the instabilities at play in the Cape Basin and about their triggering mechanisms. Our analysis of the energy transfers between the different dynamical scales indicate that a part of these instabilites, which appear to be related to the mesoscale in an 'eddy-resolving' simulation, are substantially submesoscale-driven when resolved with a finer computational grid. We thus expect that the application of the nested approach to wider areas than our current domains, including a greater portion of the Agulhas Current System, to shed further light on the role of these meso-submesoscale interactions in the generation and advection of the Agulhas eddies and filaments in the South-Atlantic.

What clearly stems out at present is the importance that these meso-submesoscale nonlinear processes have in the Cape Basin for the formation, transformation and transport of the upper and subsurface waters, down to the base of the pycnocline. These findings fully answer points 4. and 5. of our study objectives on the impact of the meso-submesoscale interactions on the regional water masses strucuture, mixing and advection. In fact, we provided robust evidence that the seasonal occurrence of different types of upper-ocean instabilities trigger the formation and subduction, within Agulhas Rings, of a newly identified type of mode water, that we defined as Agulhas Ring Mode Water (ARMW). In parallel, we showed that intense mesoscale stirring is at play at intermediate depths, generating a forward cascade of tracer variance at submesoscale and driving the AAIWs

lateral mixing in its regional varieties. Since these results regard the dynamics of two subsurface watermasses taking part in the Indo-Atlantic inter-ocean exchange, we show that mesoscale and submesoscale processes play a key role in this interbasin transfer.

Investigating the physical processes that could be responsible to halt the foward cascade of tracer variance in the Cape Basin goes beyond the objectives of our study, therefore it will be left to future research. Furthermore, our present simulations are too limited in resolution to directly characterize the expected 3D isotropization process [*Capet et al.*, 2008c]. However, both frontogenesis in the upper layers and submesoscale filamentogenesis at intermediate depths should provide a route to dissipation. Sorting out the energetic functioning of a regional simulation at higher resolution and exploring its sensitivity vis-a-vis vertical dissipation parameterization and the usage of synoptic scales in the forcing (as a source of inertial oscillations, inertial gravity waves, but also as a way to let frontal processes produce net restratification) open interesting follow-ups to this work.

Chapter 6

Final Conclusions and Perspectives

6.1 General overview

The quantification of inter-ocean leakage from the South Indian to the South Atlantic Ocean is an important measure for the role of the Agulhas system in the global MOC. *Thompson et al.* [1997], in an inter-comparative study between numerical simulations of the Southern Ocean circulation, run at different resolutions, pointed out that their highest resolution model presented a transfer of heat into the South Atlantic through the Agulhas Retroflection region, which had a major impact on the amount of heat transport in the Atlantic MOC. In their case, decreasing the resolution of the model led to a near extinction of this inter-ocean transfer and consequently to a lower equilibrium temperature in the South Atlantic. That is why the dependence of the strength of the meridional heat transport in the South Atlantic on model resolution is of particular concern in the use of ocean models for climate studies.

Mesoscale and submesoscale structures- such as Agulhas rings, Mozambique eddies, coastal and offshore filaments of temperature and salinity, small vortices, meanders and fronts- have been largely observed and modelled in the Agulhas Current System. To explore the specific influence of these meso-submesoscale variabilities in the Indo-Atlantic exchange, a set of regional numerical simulations, run at increasingly higher resolutions, were designed in this study, focusing on the Cape Basin area. This oceanic region is indeed a key hotspot for investigating such processes and their impact on both water masses transformations and air-sea exchanges. The aims of this work were to resolve a gradually higher portion of the energy spectrum scales and, in doing so, to diagnose their effect on

the structure and dynamics of the local circulation and watermasses.

While great progress has been made in the last two decades in characterizing and analyzing the ocean mesoscale field, our understanding of smaller scale dynamics remains fundamentally incomplete, and the associated practical problem of understanding and predicting lateral eddy fluxes of heat and material properties remains unsolved [*Boccaletti et al.*, 2007]. Numerical simulations indicate that these fluxes are an essential link in the oceans large-scale circulation and have therefore a crucial influence on the ocean role in the Earth climate system [*Biastoch et al.*, 2008, 2009, *Durgadoo et al.*, 2013].

New insights into the dynamics controlling vertical exchanges in the upper ocean have come from high-resolution satellite products and numerical models conducted in large domains over the past decade, since the increase of spatial and temporal resolution naturally leads to the representation of a wider energy spectrum [*Soufflet et al.*, 2016]. Some of these numerical experiments also suggest that vertical exchanges in the upper ocean occurs principally at wavelength scales smaller than 100 km, and that motions at these scales may have a large impact on physical-biological coupling and on the lateral dispersion of natural and anthropogenic tracers [*Klein and Lapeyre*, 2009, *Mahadevan*, 2016].

As a result, in the last decade the understanding of oceanic submesoscale dynamics has greatly been improved [*Capet et al.*, 2008a,b,c, *Klein et al.*, 2008, *Molemaker et al.*, 2010, *Thomas and Ferrari*, 2008] and the ubiquity of upper ocean frontal dynamics is now acknowledged. In addition, more recent studies [*Haza et al.*, 2012, *Mensa et al.*, 2013] indicate that submesoscale motions may have a strong impact on mesoscale variability. Their results point out towards the existence of a much richer variety of dynamical regimes, and associated spectral energy transfer mechanisms and pathways, than were apparent before, through which submesoscale motions are coupled to mesoscale motions.

Nonetheless, evidence for such flows in the real ocean remains limited. This is why one of the intentions of our work was to use a realistic numerical approach to shed more light on these small scale dynamics and their triggering mechanisms in a climatically crucial area as the Cape Basin. Achieving an insight on these processes, that could serve as the basis for reliably predicting their response to a variable ocean state and their evolution in the Earth's changing climate, is currently one of the key challenges in physical oceanography.

6.2 Main results

We summarise here the most prominent findings of our study by addressing the key questions outlined in Chapter 2 and offering, for each of these objectives, a synthesis of the pertinent results.

In relation to point 1. concerning the quantification of the Cape Basin turbulent field, our work provided a detailed examination of the regional meso and submesoscale dynamics. In Chapter 4 we mainly quantified them in a statistical way through the analysis of eddy-resolving simulations aimed at describing the mesoscale structures. From the latter it emerged that the simulation at $1/24°$ with 100 vertical levels, homogeneuosly distributed, was the most energetic, with more and smaller eddies of both signs detected here than in the lower resolution solutions and in satellite data. However, the results of AGU24_100_H in terms of the Agulhas Rings mean pathway and lifetime are closely comparable to the same estimates from AVISO. The simulations intercomparison also highlighted the importance that an adequate vertical resolution assumes in our model in order to progressively resolve higher baroclinic modes in the vertical, and, in doing so, allows to correctly represent the watermasses structure at the surface and at depth.
In Chapter 5, we then qualified the submesoscale component of the flow, using the output of a finer resolution simulation. Its analysis revealed a recurrent presence in the Cape Basin of small scales features, submesoscale wiggles and fronts, between and within the large mesoscale eddies, with which they continuously interact in the upper layers, but also down to the main pycnocline. Hence, in both the previous chapters, the emerging picture is that of a highly energetic environment, characterised by strongly non-linear processes and exchanges between different dynamical scales.

This partially tackled also the objectives of point 2. on the characteristics of the regional mesoscale and submesoscale processes and their relations, in terms of energetics and scales. To complement this view, we investigated their temporal dependence, revealing that the marked seasonality of the eddy field is actually due to the occurrence of several types of instabilities driven by the meso-submesoscale interactions at different times of the year. These interactions were explored both in the upper and intermediate layers, following the Agulhas Rings passage in the Cape Basin, as reprodcued in our highest resolution simulation. Here we also evaluated the effects of their temporal variability on the Mixed Layer Depth and on the thermoaline fluxes, showing that the seasonal vari-

ations of the latter are directly linked to the submesoscales action through mixing and destratification/restratification mechanisms of the water column.

We were also able to provide a detailed description of some of the distinct instabilities that characterise the Cape Basin dynamics in relation to the different seasons, addressing the objectives of point 3. on the local meso-submesoscale instabilities, their variability and triggering factors. Previous studies [*Biastoch and Krauss*, 1999] suggested that for the formation of Agulhas mesoscale structures the barotropic instability mechanism seemed to be minor, whereas baroclinic instabilities were more likely involved in their generation. Our results strongly support this hypothesis. In Chapter 4 we showed how the seasonal cycle of the eddies number was closely related to that of the first Rossby radius of deformation, indicating baroclinic processes as essential for these eddies generation. In Chapter 5 we confirmed and further investigated these preliminary findings, examining the different classes of baroclinic instabilities (mixed-layer, symmetric, Charney type) originating from the meso-submesoscale interactions.
We found indeed that the upper ocean mainly experiences baroclinic shear instabilities, with a predominance of mixed-layer instabilities in winter and symmetric instabilities in summer. We also showed that the type of instability able to reconnect these two fine-scale regimes is the Charney-baroclinic instability, relating the surface dynamics with that in the ocean interior. The divergent motions associated to the seasonal development of these meso-submesoscale instabilities indicated that ageostrophic dynamics prevail in the Cape Basin upper layers. Conversely, the intermediate depths dynamics were shown to be more quasi-geostrophic and characterised by a conspicuous filamentogenesis and lateral mixing. Both these processes are driven by the horizontal stirring of the mesoscale straining field, leading to a submesoscale cascade of tracer variance and to the formation of isopycnally compensated T-S fronts.
Given the smoothed forcings used in our simulations and their limited length, we currently explained the physics behind the generation and evolution of these meso-submesoscale instabilities through the analysis of local and instantaneous, oceanic mechanisms. But we do not exclude that more remote factors (both oceanic and atmospheric) could also affect their variability and the use of a longer numerical integration, in concert with the adoption of more realistic forcings, would give some insight on these aspects.

In particular, we have focused our attention on the impact that the meso-submesoscale

processes have on the local watermasses in terms of their formation, spreading and transformation, aiming to answer point 4. of our objectives on the influence of the turbulent scales interactions on the regional waters dynamics. In this respect, the findings of Chapter 4 pointed out that both cyclones and anticyclones convey the same varieties of AAIWs in the Cape Basin and thus equally contribute to their advection in the South-Atlantic. In Chapter 5, we then detailed how their homogenization takes place at intermediate depths. Here the enhanced straining of the mesoscale field isopycnally stirs and mixes the AAIWs T-S properties in its local varieties, giving rise to submesoscales filamentary structures whose slope is much steeper than the background isopycnals.
In the upper layers, the submesoscale-induced frontogenesis triggers the winter subduction of surface waters within Agulhas rings crossing the Cape Basin, where these waters remain isolated, conserving their T-S characteristics, until at least the following summer. This leads to the formation of a new type of mode waters, ARMW, which had been in the last years sampled during oceanographic cruises and by Argo floats, but it had never been modelled before. Hence, promising results can be expected by the use of higher numerical simulations on the investigation of the Cape Basin water masses structure and dynamics. In particular, more dedicated studies on the ARMW fate and advection are advisable in order to better evaluate the amount and role of this water in the ventilation of the Atlantic Ocean thermocline and understand the behaviour of the eddies that convey it.

These different analyses enabled us to show how the non-linear dynamics of the Cape Basin affect the Indo-Atlantic watermasses exchange and transformation, and, in doing so, to provide an answer to the questions of point 5. on the adoptions of specific diagnostics to assess this influence. The use of the eddy detection algorithm for the quantification of the meso- submesoscale field, of the EPV budget for looking at their temporal variability and of the energy conversion metrics for investigating their instabilities, allowed us to actually identify two dynamical regimes (ageostrophic vs quasi-geostrophic) between the upper and intermediate layers of the Cape Basin. In this regard, the analysis of the nested simulation clearly suggests a close interaction between the surface and the interior dynamics for which the contribution of the submesoscales is essential. On one hand, these submesoscales are produced by the horizontal stirring of density anomalies by mesoscale eddies, both in the upper and intermediate layers. In turn, the divergent motions associated with these submesoscales impact the mesoscale eddy dynamics, enhancing the kinetic energy content due to ocean turbulence in simulations at higher resolution.

6.3 Model resolution and energy convergence

Our numerical choice of using both a nested and non-nested configuration was aimed to evaluate how important would be modelling the whole domain of the Agulhas Current System at very high resolution, being this latter option computationally very demanding. In addition, the nesting approach not only allows the study of the influence of external perturbations on Cape Basin dynamics, but also the feedback of local meso-submesoscale processes on the larger-scale circulation, a characteristic that is not feasible with global high-resolution models [*Maltrud and McClean*, 2005]. Comparison of the inter-ocean exchange in the high-resolution nested simulation with its coarser resolution counterpart (at $1/24°$) reveals that the latter significantly over-estimates the amount of water flowing into the Atlantic Ocean, similarly to the other lower resolution simulations reviewed in chapter 4.

We also demonstrated the need to explicitly simulate not only the mesoscale but also the regional submesoscale processes that interest the Cape Basin circulation. The submesoscale field that we achieved to resolve in our highest resolution simulation underlines a marked transition from meso- to submesocale regimes, although it does not significantly alter the dominant mesoscale flow structures and their lateral material eddy fluxes. It rather adds a new component to the flow with sharp near-surface density fronts and associated submesoscale instabilities and vortices, which in our study were observed both at the upper and intermediate layers. The emergent submesoscale currents are spawned and sustained from the mesoscale eddy field that has its own origin in the instabilities, barotropic and baroclinic, of the Agulhas Current System. The consequences of resolving submesoscale processes are modest for the mean fields, but significant for the kinetic energy budget, the associated tracer fluctuation spectra and their dynamical balances, as documented in previuos studies [*Capet et al.*, 2008b,c]. We therefore emphasize the importance of taking into account explicitly these small-scale frontogenesis mechanisms, and the related divergent motions, in order to represent the full non-linear interactions and thus the properties of the oceanic turbulence, that strongly impact the Indo-Atlantic exchange and the water masses formation and transformation. High spatial resolution, consistent in both horizontal and vertical directions is a prerequisite to correctly represent these processes in the Cape Basin, as in any other highly turbulent oceanic region.

In terms of numerical convergence, based on the change in spectrum slopes with numer-

ical resolution, the transition from vigorous mesoscale field to an energetic submesoscale activity seems essentially completed at the highest resolutions simulation we have run (1/108° for the nested solution). Although further resolution increases would theoretically push the dissipation range- where the spectra steepen from their submesoscale range- toward even higher wavenumber (k) [*Capet et al.*, 2008a], we do not expect significant further slope changes. This remark, however, overlooks any additional regime changes that must somehow occur between submesoscale and microscale flows; but these are outside the scope of the present study.

Nevertheless, we need to take into account that dissipation in present submesoscale models remains dominated by numerical constraints rather than physical. In *Marchesiello et al.* [2011], model convergence at submesoscale is controlled by numerical dissipation, which overpowers submesoscale energy production and transfer. Effective resolution can thus be defined as the dissipation wavelength marking the start of dissipation range, below which model dynamics become unphysical. This dissipation range is a function of the model numerical filters, that make the energy spectrum very sensitive at submesoscale to the orientation of mixing [*Soufflet et al.*, 2016].

It is generally assumed that eddy-resolving models have only small spurious diapycnal mixing (Veronis effect) associated to numerical needs. This argument has been opposed by *Roberts and Marshall* [1998] and is confirmed by the latest work of *Soufflet et al.* [2016]. These authors found that the effect of spurious diapycnal mixing is to suppress submesoscale KE injection by draining the supply of APE required to sustain frontal processes. This argues in favour of third-order rotated diffusion schemes such as the RSUP3 [*Marchesiello et al.*, 2009] used in our simulations. Moreover, effective resolution in models using high-order advection/diffusion schemes, as ROMS, follows a linear function of grid spacing: $\sim 7\Delta x$ [*Marchesiello et al.*, 2011]. Thus, lots of cautious was adopted when analysing the output of our nested simulation to make sure that the dissipation obtained in this case was essentially numerical instead of physical.

The model convergence becomes a delicate topic especially when treating turbulent motions in the mixed layer and in the interior layer below, where they can couple to produce eddy fluxes differing from those that would be found without such an interaction [*Ramachandran et al.*, 2014]. According to these authors, mixed layer and subsurface flows in

weakly stratified environments combine to enhance mixed layer restratification. Although the tendency to intensify the interior baroclinic instability with increased resolution may be physical, the smoothed forcing used in our simulations likely amplifies this tendency in a way that is not. Hence, more theoretical and modelling studies on the eddies energy injection in the ocean interior would be advisable to further investigate these aspects.

6.4 Limitations due to boundary conditions, surface forcing and topography

As observed in other upwelling system numerical studies (see for example *Marchesiello et al.* [2003] for the California Current System and *Penven et al.* [2001] for the Benguela Current System), in the absence of synoptic and interannual variability in the surface fluxes, ROMS is able to generate an intense mesoscale activity through oceanic instability processes. After a relatively short spin-up of one year, our numerical solutions do not present any significant temporal drift and are representative of the known Cape Basin dynamics, as shown in the validation sections of our model output against observations. Since our configurations do not represent operational simulations, the evaluation of the model skills was carried out by a general comparison of the averaged circulation, the mean baroclinic structure and T-S contents with what has been published in literature and with annual or seasonal climatologies. This comparison proved the variuos degree of realism of the simulations.

However, our model presents some weaknesses. Firstly, due to limitations in domain size or boundary conditions, it fails to produce the observed position of the Agulhas Retroflection, impacting the modelled energy content both at the surface (EKE) and in the ocean interior (EAPE). Secondly, a discrepancy persists between the structure of the subsurface thermocline reproduced in our numerical solutions and the one observed by in-situ data. Thirdly, our modelled Agulhas rings show mean trajectories which are slightly shifted more north-westward compared to what retrieved in AVISO data.

The last two points could be related to the large scale structure of the COADS climatology employed for the initial and boundary conditions. But an important role is surely played also by the surface forcing, since *Capet et al.* [2004] demonstrated that the near shore structure of the wind stress might be preponderant in oceanic regions characterised

by seasonal upwelling. The Cape Basin dynamics are in fact largely influenced by the southern Benguela Current, which is one of the world's largest upwelling systems. Hence, to address the last two points, it will be necessary to have access to the fine structure of the wind stress in a band of 50 km close to the shore. Indeed, because of its smoothness, the wind is not a significant source of energy in our simulations, except for the mean flow. Thus, we expect more synoptic wind products to allow the reproduction of more realistic, coastal processes, as well as to incite an even greater range of fine scales. The latter are directly affected by the depth of the mixed layer, who mainly depends on the seasonal intensity and variability of the atmospheric forcing [*Callies et al.*, 2015, *Mensa et al.*, 2013].

Another limiting factor for the development of a 'realistic' submesoscale field in our present numerical configurations is likely represented by the degree of bathymetry smoothing operated in our model. *Gula et al.* [2015b] have recently shown in a ROMS high resolution simulation of the Gulf Stream, that substantial vorticity is generated in the turbulent bottom boundary layer, due to the topographic drag along the continental slope and leading to the formation of submesoscale vortices. In sigma-coordinate models, the realism of topography can be considered a compromise between the desired steepness of the terrain and a spurious pressure gradient force generated over very steep slopes [*Marchesiello et al.*, 2009]. To reduce the latter effect, a substantial amount of filtering is required unless the resolution is very high. In our case, even with the 0.8 km resolution of the nested solution, the topography had to be smoothed. Although the relevant details of the topography such as promontories, canyons and seamounts are preserved here, future simulations should consider higher resolutions run with an improved bathymetry.

The sensitivity of the local circulation to the complex regional topography has been indeed tested in preliminary numerical experiments. It has been also widely documented in previous studies [*Boebel et al.*, 2003, *Lutjeharms and van Ballegooyen*, 1984, *Matano and Beier*, 2003, *Schouten et al.*, 2002, *Speich et al.*, 2006], linking the variability of the stream to the topographic features. Therefore we presume that the role of the bathymetry, and in particular of the Vema Seamount, would be not simply to steer the flow but to have a broader indirect dynamical influence. Similarly to what observed in other western boundary currents topographically-controlled [*Gula et al.*, 2015], mean-to-eddy and eddy-to-mean energy conversions, induced by the bathymetric gradients, can be expected to alter the path and velocity of the Agulhas turbulent structures crossing the Cape Basin.

6.5 Outlook

The different sections of this manuscript have demonstrated that the answers to the initial scientific questions of our study are far from straightforward. Many issues are still open and await further dedicated observations, modelling and theoretical studies.
The degree to which the Indo-Atlantic inter-ocean exchange is determined by or determines the Atlantic MOC still represents a matter of debate. Global scale, ocean-only model studies [*Shriver and Hurlbutt*, 1997] suggest that the rate of NADW exchange has a direct impact on the Indonesian Passages throughflow and the Indian to Atlantic Ocean flow. *Weijer et al.* [1999] and *Biastoch et al.* [2008] showed that the shape and strength of lateral fluxes prescribed at 30°S directly impact the Atlantic MOC strength. These topics could only be addressed by coupled ocean-atmosphere modeling studies that involve realistic feedbacks between varying inter-ocean exchanges and changing global-scale buoyancy fluxes across the air-sea interface. On a regional scale, a related question is whether varying Agulhas leakage is due to intrinsic ocean-only variability, in which also the interaction with the Antarctic Circumpolar Current may be important, or whether there are coupled modes of varying inter-ocean exchange and associated atmospheric pressure field responses [*Biastoch et al.*, 2009, *Durgadoo et al.*, 2013, *Loveday et al.*, 2014].

Hence, although this dissertation has shed some light on several aspects of the Indo-Atlantic exchange in the Cape Basin, even more new questions seem to have been raised. We will here discuss some of the topics that may become the subject of further research. To begin with, modeling studies are not more than a theoretical exercise if they are not supported by observations. Thus, our first perspectives point towards in-situ measurements of submesoscale fronts, at the surface and at intermediate depths of the Cape Basin, that would corroborate our numerical findings on their occurrence and variability. For example, high resolution, in-situ sampling of thermoaline tracers would provide some observational hints of the filamentogenetic activity shown in our simulations.
Additional venues can be contemplated for the extension/ application of this work:

- Integration of a longer numerical solution, of at least 10 years, in conjunction with the use of more realistic surface forcing, in order to explore more in details the temporal dependence observed in the number and mean radius of the modelled eddies. Oceanic inter-annual disturbances, originating from the equatorial regime in the form of Kelvin waves, seem to highly affect the Southern Benguela region [*Veitch et al.*, 2009]. Thus

they are likely to have an impact also on the Cape Basin seasonal dynamics. A dedicated model study could greatly improve our understanding of this interaction process;

- The use of the Lagrangian integration of particles, at higher numerical resolutions than what had previously been done [*Doglioli et al.*, 2006, *Rimaud et al.*, 2012], to quantify, in the horizontal, the lateral mixing and spreading of thermocline and intermediate Cape Basin waters, and, in the vertical, their diapycnal mixing and ventilation;

- The coupling of our highest mesoscale-resolving configuration (AGU24_100_H) with an atmospheric model would better the solution, especially in coastal regions where the wind drop-off is under-estimated in satellite products and results in a cool, coastal bias;

- A submesocale nesting at higher resolution ($\simeq$ 500m) than currently would provide further insight on the large vertical velocities that occur at frontal zones, on the influence of submesoscale processes on the advection of the local watermasses and on the interactions between Agulhas eddies and finer structures. A higher resolution would also enable us to examine the presence, within the AAIWs layer, of interleaving, thermohaline intrusions due to diapycnal mixing, whose vertical scales are usually smaller than 50m;

- Explicitly resolving the details of the vertical mixing processes, presently parametrised with the non-local K-profile (KPP) boundary layer scheme [*Large et al.*, 1994], implemented for both surface and bottom boundary layers, would allow us to thoroughly describe the formation, advection and transformation of the local water masses;

- Idealised and simplified model experiments to set up a process study for investigating the entrainment of water masses within two merging vortices and the possible formation of horizontal fronts due to their fusion, probably leading to the occurrence of shear instabilities along these fronts;

- The results of our simulations have been extensively verified and are therefore ready to be used in biological numerical frameworks, such as biogeochemical and ecosystem models. For instance, by using the configuration of our nested solution, the role of submesoscales in the vertical flux of nutrients and other biological parameters could be quantified and correlated to the distribution of different species within the Cape Basin.

Bibliography

Arakawa, A., Lamb, V. (1977), Computational Design of the Basic Dynamical Processes of the UCLA General Circulation Model. *Methods Computational Physics, 17, 173-265.*

Arhan, M., H. Mercier, and J. R. E. Lutjeharms (1999), The disparate evolution of three Agulhas rings in the South Atlantic Ocean. *J. Geophys. Res.* 104, C9, 20987-21005, doi:10.1029/1998JC900047.

Arhan, M., H. Mercier, and Y. Park (2003), On the deep water circulation of the eastern South Atlantic Ocean. *Deep-Sea Research I 50 (2003) 889–916.*

Arhan, M., S. Speich, C. Messager, G. Dencausse, R. Fine, and M. Boye (2011), Anticyclonic and cyclonic eddies of subtropical origin in the subantarctic zone south of Africa. *J. Geophys. Res.* 116, C11004, doi:10.1029/2011JC007140.

Armstrong, E. M., and J. Vazquez-Cuervo (2001), "A New Global Satellite-Based Sea Surface Temperature Climatology",*Geophys. Res. Lett., 28(22), 4199–4202.*

Ayina, L., A. Bentamy, A.M. Mestas-Nuñez, and G. Madec, (2006): The Impact of Satellite Winds and Latent Heat Fluxes in a Numerical Simulation of the Tropical Pacific Ocean. *J. Climate, 19, 5889–5902*, https://doi.org/10.1175/JCLI3939.1.

Backeberg, B. C., P. Penven, and M. Rouault (2012), Impact of intensified Indian Ocean winds on the mesoscale variability of the Agulhas system, *Nat. Clim. Change, 2, 608–612.*

Barnier, B.; Siefridt, L.; Marchesiello, P. (1995), Thermal forcing for a global ocean circulation model using a three-year climatology of ECMWF analyses. *J. of Marine Systems, Volume 6, Issue 4, p. 363-380.*

Barnier, B., Marchesiello, P., De Miranda, A.P., (1996). Modelling the ocean circulation in the South Atlantic: A strategy for dealing with open boundaries. In *The South*

Atlantic: Present and Past Circulation, eds. G. Wefer, W.H. Berger, G. Siedler and D. Webb, pp. 289-304. Springer, Berlin.

Barnier, B., Marchesiello, P., Pimenta de Miranda, A., Coulibaly, M. Molines, J.M., (1998). A sigma-coordinate primitive equation model for studying the circulation in the South Atlantic. Part I: model configuration with error estimates. *Deep-Sea Research I 45, 543-572.*

Beal, L. M. and H. L. Bryden, (1997). Observations of an Agulhas Undercurrent, *Deep-Sea Res., 44, 1715-1724.*

Beal, L. M., T. K. Chereskin, Y. D. Lenn, and S. Elipot, (2006). The sources and mixing characteristics of the Agulhas Current.*J. Phys. Oceanogr., 36, 2060–2074*, doi:10.1175/JPO2964.1.

Beal, L.M., (2007). Is Interleaving in the Agulhas Current Driven by Near-Inertial Velocity Perturbations?. *J. Phys. Oceanogr., 37, 932–945*, https://doi.org/10.1175/JPO3040.1

Beal, L. M., (2009). A time series of Agulhas Undercurrent transport.*J. Phys. Oceanogr., 39, 2436–2450*, doi:10.1175/2009JPO4195.1.

Beal, L. M., W. P. M. de Ruijter, A. Biastoch, R. Zahn, and SCOR/IAPSO/WCRP Working Group 136 (2011), On the role of the Agulhas System in Ocean Circulation and Climate, *Nature* 472, 429-436, doi:10.1038/nature09983.

Beal, L.M., S. Elipot, A. Houk, and G.M. Leber, (2015). Capturing the Transport Variability of a Western Boundary Jet: Results from the Agulhas Current Time-Series Experiment (ACT). *J. Phys. Oceanogr., 45, 1302–1324*, https://doi.org/10.1175/JPO-D-14-0119.1

Bentamy, A., K. B. Katsaros, M. Alberto, W. M. Drennan, and E. B. Forde (2003), Daily surface wind fields produced by merged satellite data, in Gas Transfer at Water Surfaces,*Geophys. Monogr. Ser., vol. 127, edited by M. A. Donelan et al., pp. 343-349, AGU, Washington, D. C.*, doi:10.1029/GM127p0343

Berger, W. H,. and G. Wefer, (1996). Expeditions into the past: Paleoceanographic studies in the South Atlantic, in The South Atlantic: present and past circulation. *Eds. Wefer, G., W. H. Berger, G. Siedler, D. J. Webb, Springer-Verlag, Berlin Heidelberg, 363-410.*

Biastoch, A., Krauss, W., (1999). The role of mesoscale eddies in the source regions of the Agulhas Current. *Journal of Physical Oceanography 29, 2303–2317.*

Biastoch, A., , C. Reason, J. Lutjeharms, and O. Boebel, (1999). The importance of flow in the Mozambique Channel to seasonality in the greater Agulhas Current system. *Geophys. Res. Lett., 26, 3321–3324*, doi:10.1029/1999GL002349.

Biastoch, A., C. W. Boning, and J. R. E. Lutjeharms (2008), Agulhas leakage dynamics affects decadal variability in Atlantic overturning circulation. *Nature* 456, 489 492 doi:10.1038/nature07426.

Biastoch, A., J. R. E. Lutjeharms, C. W. Boning, and M. Scheinert (2008b), Mesoscale perturbations control inter-ocean exchange south of Africa,*Geophys. Res. Lett., 35, L20602*, doi:10.1029/2008GL035132.

Biastoch, A., C. W. Boning, F. Schwarzkopf, and J. Lutjeharms, (2009). Increase in Agulhas leakage due to poleward shift of Southern Hemisphere westerlies.*Nature, 462, 495–498*, doi:10.1038/nature08519.

Biastoch, A., and C. W. Boning, (2013). Anthropogenic impact on Agulhas leakage.*Geophys. Res. Lett., 40, 1138–1143*, doi:10.1002/grl.50243.

Blanke, B., M. Arhan, G. Madec, and S. Roche (1999), Warm water paths in the Equatorial Atlantic as diagnosed with a general circulation model, *J. Phys. Oceanogr., 29, 2753–2768, doi:10.1175/1520-0485(1999) 029<2753:WWPITE>2.0.CO;2.*

Blayo, E., Debreu, L., (1999). Adaptive mesh refinement for finite-difference ocean models: First experiments. *Journal of Physical Oceanography 29, 1239-1250.*

Bleck, R., and B. Boudra, (1986). Wind-driven spin-up eddy-resolving ocean models formulated in isopycnic and isobaric coordinates. *J. Geophys. Res.,* 91 (C6), 7611-7621

Boccaletti, G., Ferrari, R., Fox-Kemper, B., 2007. Mixed layer instabilities and restratification.*J. Phys. Oceanogr. 37 (9), 2228-2250.* doi:10.1175/JPO3101.1. http://journals.ametsoc.org/doi/abs/10.1175/JPO3101.1

Boebel, O., Duncombe Rae, C., Garzoli, S., Lutjeharms, J., Richardson, P., Rossby, T., Schmid, C., Zenk, W., (1998). Float experiment studies inter-ocean exchanges at the tip of Africa. *EOS 79 (1), 6–8.*

Boebel, O., Davis, R.E., Ollitrault, M., Peterson, R.G., Richardson, P.L., Schmid, C., Zenk, W., (1999). The intermediate depth circulation of the western South Atlantic. *Geographical Research Letters 26, 3329–3332.*

Boebel, O., J. R. E. Lutjeharms, C. Schmid, C. Zenk, T. Rossby, and C. Barron (2003), The Cape Cauldron: A regime of turbulent inter-ocean exchange. *Deep Sea Res., Part I, 50, 5786* doi:10.1016/S0967-0645.

Brannigan, L., D. Marshall, A. Naveira-Garabato, and G. Nurser (2015), The seasonal cycle of submesoscale flows, *Ocean Modell., 92, 69-84.*

Brannigan L. (2016), Intense submesoscale upwelling in anticyclonic eddies. *Geophys. Res. Lett., 43, 3360-3369* doi:10.1002/2016GL067926.

Bryden, H., L. Beal, and L. Duncan (2005), Structure and transport of the Agulhas Current and its temporal variability,*J. Oceanogr., 61, 479 – 492.*

Bruggemann, N.; Eden, C. (2015), Routes to Dissipation under Different Dynamical Conditions. *Journal of Physical Oceanography 45. : S. 2149-2168.* doi: 10.1175/JPO-D-14-0205.1.

Bunker, A.F., (1988).Surface energy fluxes of the South Atlantic Ocean, *Month. Weath. Rev., 116, 809-823.*

Byrne, D. A., A. L. Gordon, and W. F. Haxby (1995), Agulhas eddies: a synoptic view using Geosat ERM data, *J. Phys. Oceanogr, 25, 902-917.*

Cabanes, C., Grouazel, A., von Schuckmann, K., Hamon, M., Turpin, V., Coatanoan, C., Paris, F., Guinehut, S., Boone, C., Ferry, N., de Boyer Montégut, C., Carval, T., Reverdin, G., Pouliquen, S., and Le Traon, P.-Y., (2013). The CORA dataset: validation and diagnostics of in-situ ocean temperature and salinity measurements, *Ocean Sci., 9, 1–18, doi:10.5194/os-9-1-2013.*

Callies G., R. Ferrari, J. M. Klymak, and J. Gula (2015), Seasonality in submesoscale turbulence, *Nat. Commun., 6.*

Callies G. Flierl, R. Ferrari, and B. Fox-Kemper, (2016). The role of mixed-layer instabilities in submesoscale turbulence. *J. Fluid Mech., 788, 5-41,* doi:10.1017/jfm.2015.700.

Capet, X. J., P. Marchesiello, and J. C. McWilliams (2004), Upwelling response to coastal wind profiles, *Geophys. Res. Lett., 31, L13311*, doi:10.1029/2004GL020123.

Capet X., McWilliams J. C., Molemaker M. J., Shchepetkin A. F. (2008a), Mesoscale to submesoscale transition in the California Current System. Part I: Flow structure, eddy flux, and observational tests. *J. Phys. Oceanogr.* 38, 2943.

Capet X., McWilliams J. C., Molemaker M. J., Shchepetkin A. F. (2008b), Mesoscale to submesoscale transition in the California Current System. Part II: Frontal processes. *J. Phys. Oceanogr.*, 38, 44-64.

Capet, X., McWilliams, J., Molemaker, M., Shchepetkin, A. (2008c), Mesoscale to submesoscale transition in the California current system. Part III: energy balance and flux. *J. Phys. Oceanogr. 38 (10), 2256-2269.*

Capet, X., G. Roullet, P. Klein, and G. Maze (2016), Intensification of Upper-Ocean Submesoscale Turbulence through Charney Baroclinic Instability. *J. Phys. Oceanogr., 46, 3365-3384.* https://doi.org/10.1175/JPO-D-16-0050.1

Carton, X. (2001), Hydrodynamical modeling of oceanic vortices. *Surveys in Geophysics 22: 179.* https://doi.org/10.1023/A:1013779219578.

Chaigneau, A., Gizolme, A., Grados, C., (2008), Mesoscale eddies off Peru' in altimeter records: Identification algorithms and eddy spatio-temporal patterns. *Progress in Oceanography.* 79 (2), 106-119.

Chaigneau, A., Marie, L. T., Gérard, E., Carmen, G., Oscar, P., (2011). Vertical structure of mesoscale eddies in the eastern south pacific ocean: A composite analysis from altimetry and argo profiling floats. *Journal of Geophysical Research: Oceans.* 116 (C11).

Charney, J. G. (1947), The dynamics of long waves in a baro- clinic westerly current. *J. Meteor., 4, 136-162, doi:10.1175/1520-0469(1947)004,0136:TDOLWI.2.0.CO;2.*

Charney, J. G. (1971), Geostrophic turbulence. *J. Atmos. Sci. 28, 1087-1095.*

Chassignet, E.P., D.B. Olson, andD.B. Boudra, (1989). Evolution of rings in numerical models and observations.in: J.C.J. Nihoul, B.M. Jamart (eds.)*Mesoscale/Syn Coherent Structures in Geophysical Turbulence. Elsevier, 337-357.*

Chassignet, E.P., (1992). Rings in numerical models of ocean general circulation: A statistical study. *J.Geophys. Res.97, 9479-9492.*

Chelton, D. B., R. A. deSzoeke, M. G. Schlax, K. E. Naggar, and N. Siwertz (1998), Geographical variability of the first-baroclinic rossby radius of deformation. *J. Phys. Oceanogr.* 28, 433 - 460.

Chelton, D. B., Schlax, M. G., Samelson, R. M., (2011), Global observations of non-linear mesoscale eddies. *Progress in Oceanography.* 91 (2), 167–216.

Craneguy P., (1999), Mecanismes d'intrusion de l'eau antarctique intermediaire antarctique a travers le courant circumpolaire antarctique. *PhD thesis.*

D'Asaro, E., C. Lee, L. Rainville, R. Harcourt, and L. Thomas (2011), Enhanced turbulence and energy dissipation at ocean fronts, *Science, 332(6027), 318–22.* doi:10.1126/science.1201515.

Da Silva, A.M., Young-Molling, C.C., Levitus, S. (1994), Atlas of Surface Marine Data 1994, vol. 1. *Algorithms and Procedures, NOAA Atlas NESDIS, vol. 6, NOAA, Silver Spring.*

Debreu, L., Blayo, E., (2003). AGRIF: Adaptive Grid Refinement In Fortran. *Submitted to ACM Transactions on Mathematical Software—TOMS.*

Debreu, L., Vouland, C., (2003). AGRIF: Adaptive Grid Refinement in Fortran. *[Available online http://www-lmc.imag.fr/IDOPT/AGRIF/index.html].*

Debreu, L., Mazauric, C. (2006), Adaptive Grid Refinement (AGRIF) in Fortran 90: Users Guide Version 1.3. <http://www-lmc.imag.fr/IDOPT/AGRIF/index.html>.

Debreu, L., Blayo, E., (2008). Two-way embedding algorithms: a review. *Ocean Dyn. 58, 415–428.*

Debreu L., Marchesiello P., Penven P., Cambon G. (2012). Two-way nesting in split-explicit ocean models: Algorithms, implementation and validation. *Ocean Modelling, Elsevier, 2012, 49-50, pp.1-21.*

De Ruijter, W. P.M., (1982) Asymptotic analysis of the Agulhas and Brazil Current systems. *J. Phys. Ocenogr. 12, 361-373.*

De Ruijter, W. P. M., Biastoch, A., Drijfhout, S. S., Lutjeharms, J. R. E., Matano, R. P., Pichevin, T., van Leeuwen, P. J., and Weijer, W. (1999), Indian-Atlantic inter-ocean exchange: dynamics, estimation and impact, *J. Geophys. Res., 104, 20 885-20 911.*

Dencausse, G., M. Arhan, and S. Speich (2010), Spatio-temporal characteristics of the Agulhas Current retroflection, *Deep Sea Res., Part I, 57(11), 1392-1405, doi:10.1016/j.dsr.2010.07.004.*

Dencausse, G., Arhan, M., Speich, S., (2010b). Routes of agulhas rings in the southeastern Cape Basin.*Deep Sea Research Part I: Oceanographic Research Papers 57 (11), 1406–1421.*

Dencausse, G., M. Arhan, and S. Speich (2011), Is there a continuous Subtropical Front south of Africa?,*J. Geophys. Res., 116, C02027*, doi:10.1029/2010JC006587.

Di Marco, S.F., W.D. Nowlin Jr., and P. Chapman, (1998). Properties and transport of the Mozambique Channel, *1998 US WOCE Report 34- 35.*

Doglioli, A. M., M. Veneziani, B. Blanke, S. Speich, and A. Griffa (2006), A Lagrangian analysis of the Indian-Atlantic inter-ocean exchange in a regional model, *Geophys. Res. Lett., 33, L14611, doi:10.1029/ 2006GL026498.*

Doglioli, A. M., B. Blanke, S. Speich, and G. Lapeyre (2007), Tracking coherent structures in a regional ocean model with wavelet analysis: Application to cape basin eddies, *Journal of Geophysical Research: Oceans, 112(C5)*, n/a–n/a, doi:10.1029/2006JC003952, c05043.

Drijfhout S. S., Kattenberg, A., Haarsma, R. J., and Selten, F. M. (2001), The role of the ocean in midlatitude, interannual-to-decadal-timescale climate variability of a coupled model. *J. Climate, 14(17), 3617-3630* doi: 10.1175/1520-0442.

Duacs/AVISO, A new version of ssalto/duacs products available in April 2014. version 1.1, CNES,*http://www.Aviso.altimetry.fr/fileadmin/documents/data/duacs/Duacs2014.pdf.*

Ducet N., P.Y. Le Traon and G. Reverdin, (2000). Global high-resolution mapping of ocean circulation from TOPEX/Poseidon and ERS-1 and –2. J. *Geophys. Res., 105, 19477-19498.*

Duncombe Rae, C. M., F. A. Shillington, J. J. Agenbag, J. Taunton-Clark, and M. L. Grtindlingh (1992), An Agulhas Ring in the South Atlantic Ocean and its interaction with the Benguela upwelling frontal system, *Deep- Sea Res., 39, 2009-2027.*

Duncombe Rae, C. M., S. L. Garzoli, and A. L. Gordon (1996), The eddy field of the southeast Atlantic Ocean: a statistical census from the Benguela Sources and Transport project. *J. Geophys. Res., 101,11949-11964.*

Durgadoo, J. V., B. R. Loveday, C. J. C. Reason, P. Penven, and A. Biastoch, (2013). Agulhas leakage predominantly responds to the Southern Hemisphere westerlies. *J. Phys. Oceanogr., 43, 2113–2131, doi:10.1175/JPO-D-13-047.1.*

Eckart, C., (1948). An analysis of stirring and mixing processes in incompressible fluids.*J. Mar. Res., 7, 265–275.*

Ertel, H. (1942), Ein neuer hydrodynamischer Erhaltungssatz. *Naturwiss.* 30, 543-544.

Faure, V., M. Arhan, S. Speich and S. Gladyshev (2011), Heat budget of the surface mixed layer south of Africa, *Ocean Dyn., 61(10), 1441–1458*, doi:10.1007/s10236-011-0444-1.

Feron, R. C. V., W.P.M. de Ruijter, and D. Oskam, (1992). Ring-shedding in the Agulhas Current system, *J. Geophys. Res., 97, 9467-9477.*

Feron, R.C.V., (1994). Eddies and mean flow in the ocean: applications of satellite altimetry, *Ph.D. dissertation, 125 pp, Utrecht University, Utrecht, Netherlands.*

Feron, R.C.V., W.P.M. de Ruijter, and P.J. van Leeuwen,(1998). New method to determine the mean ocean circulation from satellite altimetry, *J. Geophys. Res., 103, 1343-1362.*

Ferrari, R., and K. Polzin (2005), Finescale structure of the T-S relation in the eastern North Atlantic.*J. Phys. Oceanogr., 35, 1437-1454.*

Ferrari, R., and D. L. Rudnick (2000), Thermohaline variability in the upper ocean, *J. Geophys. Res., 105(C7), 16,857–16,883.*

Fine, R.A., (1993). Circulation of Antarctic Intermediate Water in the South Indian Ocean, *Deep-Sea Res., 40, 2021-2042.*

Fox-Kemper, B., R. Ferrari, and R. Hallberg, (2008a). Parameterization of Mixed Layer Eddies. Part I: Theory and Diagnosis. *J. Phys. Oceanogr. 38, 1145-1165,.* https://doi.org/10.1175/2007JPO3792.1

Fox-Kemper, B., Ferrari, R., Hallberg, R. (2008b), Parameterization of mixed layer Eddies. Part II: Prognosis and Impact. *J. Phys. Oceanogr., 38, 1166–1179*, https://doi.org/10.1175/2007JPO3788.1.

Garrett, C. (1983), On the initial streakiness of a dispersing tracer in two- and three-dimensional turbulence. *Dyn. Atmos. Oceans, 7, 265-277.*

Garzoli, S. L. and Goni, (2000). Combining altimeter observations and oceanographic data for ocean circulation and climate studies, in: *Satellites, Oceanography and Society, edited by: Halpern, D., Elsevier Oceanography Series 63, Elsevier, Amsterdam, pp. 79-97.*

Garzoli, S. L., A. L. Gordon, V. Kamenkovich, D. Pillsbury, and C. Duncombe Rae (1996), Variability and sources of the southeastern Atlantic circulation, *J. Mar. Res., 54, 1039-1071.*

Garzoli, S. L., and A. L. Gordon (1996), Origins and variability of the Benguela Current, *J. Geophys. Res., 101,897-906.*

Garzoli, S. L., and R. Matano (2011), The South Atlantic and the Atlantic meridional overturning circulation,*Deep Sea Res., Part II, 58 (17–18), 1837–1847*, doi:10.1016/j.dsr2.2010.10.063

Giordani, H., and G. Caniaux (2001): Sensitivity of cyclogenesis to sea surface temperature in the Northwestern Atlantic. Monthly Weather Review, vol 129, n6°, pp 1273-1295.

Giulivi, C. F. and A. L. Gordon, (2006), Isopycnal displacements within the Cape Basin thermocline as revealed by the Hydrographic Data Archive. *Deep-Sea Research Part I-Oceanographic Research Papers.* 53(8): 1285-1300.

Gladyshev, S., M. Arhan, A. Sokov, and S. Speich (2008), A hydrographic section from South Africa to the southern limit of the Antarctic Circum- polar Current at the Greenwich meridian, *Deep Sea Res., Part I, 55(10), 1284-1303*, doi:10.1016/j.dsr.2008.05.009.

Goni, G.J., S.L. Garzoli, A.J. Roubicek, D.B. Olson, and O.B. Brown (1997), Agulhas ring dynamics from TOPEX/POSEIDON satellite altimeter data, *J. Mar. Res., 55, 861-883.*

Gordon, A. L. (1985), Indian-Atlantic transfer of thermocline water at the Agulhas retroflection, *Science, 227, 1030-1033.*

Gordon, A. L. (1986), inter-ocean exchange of thermocline water, *J. Geophys. Res., 91, 5037-5046.*

Gordon, A. L., J. R. E. Lutjeharms, and M. L. Grtindlingh (1987), Stratification and circulation at the Agulhas Retroflection, *Deep-Sea Res. 34, 565- 599.*

Gordon, A. L., and W. F. Haxby (1990), Agulhas eddies invade the South Atlantic: evidence from Geosat altimeter and shipboard CTD survey, *J. Geophys. Res., 95, 3117-3125.*

Gordon, A. L., R. F. Weiss, W. M. Smethie Jr. and M. J. Warner (1992), Thermocline and intermediate water communication between the South Atlantic and Indian Oceans,*J. Geophys. Res., 97, 72237240*, doi:10.1029/92JC00485.

Gordon, A. L. (2001), inter-ocean exchange, in *Ocean Circulation and Climate, Int. Geophys. Ser., vol. 77, edited by G. Siedler, J. Church, and J. Gould, chap. 4.7, pp. 303–314, Academic, San Diego, Calif.*

Gordon, A. L. (2003), The brawniest retroflection, *Nature, 421(6926), 904–905, doi:10.1038/421904a.*

Gordon, A.L., Sprintall, J., Wijffels, S., Susanto, D., Molcard, R., Van Aken, H., Ffield, A.L., de Ruijter, W., Lutjeharms, J., Speich, S., Beal, L. (2010), inter-ocean exchange of thermocline water: Indonesian Throughflow; 'Tassie' Lekage; Agulhas Leakage. *Proceedings of OceanObs'09: Sustained Ocean Observations and Information for Society.* (Vol. 2).

Grutindlingh, M. L.,(1980).On the volume transport of the Agulhas Current, *Deep-Sea Res., 27, 557-563.*

Grutindlingh, M. L.,(1983). On the course of the Agulhas Current,*S. Afr. geogr. J., 65, 49-57.*

Grundlingh, M. L. (1988). Altimetry in the southwest Indian Ocean, S. Afr. *J. Sci., 84, 568–573.*

Grundlingh, M. L. and Pearce, A. F. (1990). Frontal features of the Agulhas Current in the Natal Bight, *S. Afr. Geogr. J., 72, 11–14.*

Grundlingh, M. L. (1992). Agulhas Current meanders: review and a case study,*S. Afr. Geogr. J., 74, 19–28.*

Grutindlingh, M. L., (1995). Tracking eddies in the southeast Atlantic and southwest Indian oceans with TOPEX/POSEIDON, *J. Geophys. Res., 100, 24977-24986.*

Gula, J., M. Molemaker, and J. McWilliams (2015), Gulf Stream dynamics along the Southeastern U.S. Seaboard, *J. Phys. Oceanogr., 45(3), 690–715.*

Gula, J., M. J. Molemaker, and J. C. McWilliams (2015b), Topographic vorticity generation, submesoscale instability and vortex street formation in the Gulf Stream. *Geophys. Res. Lett., 42, 4054-4062.* doi: 10.1002/2015GL063731.

Halo, I., B. Backeberg, P. Penven, I. Ansorge, C. Reason, and J. Ullgren (2014), Eddy properties in the Mozambique Channel: A comparison between observations and two numerical ocean circulation models, *Deep Sea Res., Part II*, doi:10.1016/j.dsr2.2013.10.015,

Hanawa, K., and L. D. Talley (2001), Mode water, in *Ocean Circulation and Climate, Int. Geophys. Ser.,* vol. 77, edited by G. Siedler, J. Church, and J. Gould, chap. 5.4, pp. 373-386, Academic, San Diego, doi:10.1016/S0074-6142(01)80129-7.

Haine, T.W.N., Marshall, J. (1998), Gravitational, symmetric, and baroclinic instability of the ocean mixed layer. *J. Phys. Oceanogr. 28 (4), 634-658.*

Harris, T. F. W., (1972). Sources of the Agulhas Current in the spring of 1964, *Deep-Sea Res., 19, 633-650.*

Haza A, Ozgokmen TM, Griffa A, Garraffo ZD, Piterbarg L (2012). Parameterization of particle transport at submesoscales in the Gulf Stream region using Lagrangian subgridscale models. *Ocean Model 42:31–49.*

Hoflich, O., (1994). Climate of the South Atlantic Ocean, in World Survey of Climatology, vol. 15, Climates of the Oceans, *edited by H. van Loon, pp. 1-191, Elsevier, New York.*

Hogg, N.G., Stommel, H.M. (1985), The heton, an elementary interaction between discrete baroclinic geostrophic vortices, and its implications concerning heat-flow. *Proceedings of the Royal Society of London, A 397, 1-20.*

Hosegood, P., M. C. Gregg, and M. H. Alford (2006), Sub-mesoscale lateral density structure in the oceanic surface mixed layer, *Geophys. Res. Lett., 33, L22604, 1–6.* doi:10.1029/2006GL026797. doi:10.1175/JPO2770.1

Hoskins, B.J. and Bretherton F. P., (1972). Atmospheric frontogenesis models - Mathematical formulation and solution. *J. Atmos. Sci. 29 (1), 11-37.*

Hoskins, B.J., (1982). The mathematical theory of frontogenesis.*Annu. Rev. Fluid Mech., 14, 131-151.*

Howard, W. R., and W. L. Prell, (1992). Late quaternary surface circulation of the southern Indian Ocean and its relationship to orbital variation.*Paleoceanography, 7, 79-117.*

Hua Bach-Lien, Menesguen Claire, Le Gentil Sylvie, Schopp Richard, Marsset Bruno, Aiki Hidenori (2013), Layering and turbulence surrounding an anticyclonic oceanic vortex: in situ observations and quasi-geostrophic numerical simulations. *Journal Of Fluid Mechanics, 731, 418-442.*

Jacobs, S. S., and D. T. Georgi (1977), Observations on the southwest Indian/Antarctic Ocean, in *A Voyage of Discovery, edited by M. Angel, pp. 43-84, Pergamon, Oxford, UK.*

Jayne, S. R., L. C. St. Laurent, and S. T. Gille (2004), Connections between ocean bottom topography and Earth's climate, *Oceanography, 17(1), 65–74*, doi:10.5670/oceanog.2004.68.

Klein, P., Treguier, A.M., Hua, B.L. (1998), Three-dimensional stirring of thermohaline fronts. *Journal of Marine Research 56, 589-612.*

Klein, P., B. Hua, G. Lapeyre, X. Capet, S. L. Gentil, and H. Sasaki (2008), Upper ocean turbulence from high 3-D resolution simulations,*J. Phys. Oceanogr., 38, 1748 - 1763.*

Klein P. and Lapeyre G. (2009), The Oceanic Vertical Pump Induced by Mesoscale and Submesoscale Turbulence.*Annu. Rev. Mar. Sci. 2009. 1:351–75.*

Klein P., Lapeyre G., Roullet G., Le Gentil S., Sasaki H. (2011). Ocean turbulence at meso and submesoscales: connection between surface and interior dynamics. *Geophysical And Astrophysical Fluid Dynamics , 105(4-5), 421-437.* http://doi.org/10.1080/03091929.2010.532498

Krug, M., S. Swart, and J. Gula (2017), Submesoscale cyclones in the Agulhas current, *Geophys. Res. Lett., 44, 346–354*, doi:10.1002/2016GL071006.

Lapeyre, G., Klein, P. and Hua, B. L. (2006), Oceanic restratification forced by surface frontogenesis. *J. Phys. Oceanogr. 36 (8), 1577-1590.*

Lapeyre G. and Klein P. (2006). Impact of the small-scale elongated filaments on the oceanic vertical pump. *Journal of Marine Research.* 64, 835-851.

Large, W. G., J. C. McWilliams, and S. C. Doney (1994), Oceanic vertical mixing: A review and a model with a nonlocal boundary layer parameterization, *Rev. Geophys., 32, 363 - 403.*

Laxenaire R., Speich S., Blanke B., Chaigneau A. and Pegliasco C. (Submitted), New insights on Agulhas rings dynamics as inferred from altimetry.

Ledwell, J. R., A. J. Watson, and C. S. Law (1998), Mixing of a tracer in the pycnocline. *J. Geophys. Res., 103, 21 499-21 529.*

Lemarie F., Kurian, J., Shchepetkin, A.F., Molemaker, M.J., Colas, F., McWilliams, J.C. (2012), Are There Inescapable Issues Prohibiting the use of Terrain-Following Coordinates in Climate Models? *Ocean Modell.* doi:10.1016/j.ocemod.2011.11.007.

Locarnini, R., A. Mishonov, J. Antonov, T. Boyer, H. Garcia, O. Baranova, M. Zweng, and D. Johnson (2010), World Ocean Atlas 2009, vol. 1, Temperature, *US Gov. Print. Off., Washington, DC.*

Loveday, B.R., J.V. Durgadoo, C.J. Reason, A. Biastoch, and P. Penven, (2014). Decoupling of the Agulhas Leakage from the Agulhas Current. *J. Phys. Oceanogr., 44, 1776–1797, https://doi.org/10.1175/JPO-D-13-093.1.*

Lumpkin, R., and K. Speer (2007), Global ocean meridional overturning, *J. Phys. Oceanogr., 37 (10), 2550–2562, doi:10.1175/JPO3130.1.*

Lutjeharms, J. R. E. and Valentine, H. R., (1984). Southern Ocean thermal fronts south of Africa, *Deep-Sea Res., 31, 1461–1476.*

Lutjeharms, J. R. E. and van Ballegooyen, R. C. (1984). Topographic control in the Agulhas Current system, *Deep-Sea Res., 31, 1321-1337.*

Lutjeharms, J. R. E., (1987). Meridional heat transport across the Subtropical Convergence by a warm eddy, *Nature, 331, 251-253.*

Lutjeharms, J. R. E. and Gordon, A. L. (1987), Shedding of an Agulhas Ring observed at sea, *Nature.* 325, 138-140.

Lutjeharms, J. R. E. , (1988a). Examples of extreme circulation events of the Agulhas Retroflection, *S. Afr. J. Sci., 84, 584–586.*

Lutjeharms, J. R. E., (1988) Remote sensing corroboration of the retroflection of the East Madagascar Current, *Deep-Sea Res., 35, 2045-2050.*

Lutjeharms, J. R. E. and Roberts, H. R. (1988). The Natal pulse; an extreme transient on the Agulhas Current, *J. Geophys. Res., 93, 631–645.*

Lutjeharms, J. R. E. and van Ballegooyen, R. C., (1988a). Anomalous upstream retroflection in the Agulhas Current, *Science, 240, 1770–1772.*

Lutjeharms, R. C. , J. R. E. and van Ballegooyen (1988b). The retroflection of the Agulhas Current. *Journal of physical Oceanography,* 18 (11), 1570-1583.

Lutjeharms, J. R. E. and Valentine, H. R., (1988a). Eddies at the Sub-Tropical Convergence south of Africa,*J. Phys. Oceanogr., 18, 761–774.*

Lutjeharms, J. R. E., Catzel, R., and Valentine, H. R. (1989). Eddies and other border phenomena of the Agulhas Current, *Cont. Shelf Res., 9, 597–616.*

Lutjeharms, J. R. E. and Connell, A. D. (1989). The Natal Pulse and inshore countercurrents off the South African east coast. *South African Journal of Science*, 85, 533-535.

Lutjeharms, J. R. E., de Ruijter, W. P. M., and Peterson, R. G (1992), Inter-basin exchange and the Agulhas retroflection; the development of some oceanographic concepts. *Deep Sea Res., 39, 1791-1807.*

Lutjeharms, J. R. E., and J. Cooper, (1996) Inter-basin leakage through Agulhas current filaments,*Deep-Sea Res., 43, 213-238.*

Lutjeharms, J. R. E. and de Ruijter, W. P. M. (1996). The influence of the Agulhas Current on the adjacent coastal ocean: possible impacts of climate change. *Journal of Marine Systems, 7, 321-336.*

Lutjeharms, J. R. E. (1996), The exchange of water between the south Indian and south Atlantic oceans, in The South Atlantic: Present and Past Circulation, *edited by G. Weferet al., pp. 125-162, Springer Verlag, New York.*

Lutjeharms, J.R.E., Boebel, O., Rossby, T., (1997). KAPEX: an international experiment to study deep water movement around southern Africa.*South African Journal of Science 93 (9), 377–388.*

Lutjeharms, J. R. E. and Ansorge, I., (2001). The Agulhas Return Current, *J. Mar. Syst., 30, 115–138.*

Lutjeharms, J. R. E. (2001), The Agulhas Current, in *Encyclopedia of Ocean Sciences, edited by J. H. Steele, S. A. Thorpe, and K. K. Turekian, pp. 104–113, Academic, San Diego, doi:10.1006/rwos.2001.0365.*

Lutjeharms, J. R. E. (2006), The Agulhas Current, *329 pp., Springer, Heidelberg, Germany.*

Lutjeharms, J. R. E. (2007), Three decades of research on the greater Agulhas Current, *Ocean Sci. 3(1): 129-147.*

Lutjeharms J. R. E., Penven P., and Roy C. (2003a), Modelling the shear-edge eddies of the southern Agulhas Current, *Cont. Shelf Res., 23, 1099-1115.*

Mahadevan, A., A. Tandon, and R. Ferrari (2010), Rapid changes in mixed layer stratification driven by submesoscale instabilities and winds,*J. Geophys. Res., 115, C03017*, doi:10.1029/2008JC005203.

Mahadevan A., (2016). The impact of submesoscale physics on primary productivity of plankton. *Ann. Rev. Mar. Sci. 8, 161–184.* (doi:10.1146/annurev-marine-010814-015912)

Maltrud, M. E., and J. McClean (2005), An eddy resolving global 1/10 deg ocean simulation, *Ocean Modell., 8, 31- 54.*

Marchesiello P., B. Barnier, and A. Pimenta de Miranda, (1998). A sigma-coordinate primitive-equation model for studying the circulation in the South Atlantic. Part II: Meridional transports and seasonal variability. *Deep-Sea Res., 45A, 573–608.*

Marchesiello P., McWilliams J.C., Shchepetkin A.F. (2001), Open boundary conditions for long-term integration of regional oceanic models. *Ocean Modelling.* 3,121.10.1016/S1463-5003(00)00013-5.

Marchesiello, P., McWilliams, J., Schepetkin, A. (2003), Equilibrium structure and dynamics of the California Current system. *Journal of Physical Oceanography.* 33, 753783.

Marchesiello P., Debreu L., and Couvelard X. (2009), Spurious diapycnal mixing in terrain-following coordinate models: The problem and a solution. *Ocean Modell.* 26,156169, doi:10.1016/j.ocemod.2008.09.004.

Marchesiello, P., Capet, X., Menkes, C., Kennan, S.C., (2011). Submesoscale dynamics in tropical instability waves. *Ocean Modell. 39 (1–2), 31–46. doi:10.1016/j.ocemod. 2011.04.011.*

Martin, M. J., A. Hines, and M. J. Bell, (2007). Data assimilation in the FOAM operational short-range ocean forecasting system: A description of the scheme and its impact. *Quart. J. Roy. Meteor. Soc., 133, 981–995.*

Matano, R. P. (1996). A numerical study of the Agulhas retroflection: the role of bottom topography, *J. Phys. Oceanogr., 26, 2267–2279.*

Matano, R., Beier, E.J. (2003), A kinematic analysis of the Indian/Atlantic inter-ocean exchange. *Deep Sea Res. II, this issue (PII:S0967-0645(02)00395-8).*

Mauritzen, C., K. L. Polzin, M. S. McCartney, R. C. Millard, and D. E. West-Mack (2002), Evidence in hydrography and density fine structure for enhanced vertical mixing over the Mid-Atlantic Ridge in the western Atlantic, *J. Geophys. Res., 107(C10), 3147, doi:10.1029/2001JC001114.*

May, B. D., and D. E. Kelley, (1997). Effect of baroclinicity on double-diffusive interleaving. *J. Phys. Oceanogr., 27, 1997-2008.*

Mensa, J.A., Garraffo, Z., Griffa, A., Ozgokmen, T.M., Haza, A., Veneziani, M. (2013), Seasonality of the submesoscale dynamics in the Gulf stream region.*Ocean Dyn. 63 (8), 923-941.* doi:10.1007/s10236-013-0633-1.

Mey, R. D., N. D. Walker, and M. R. Jury (1990), Surface heat fluxes and marine boundary layer modification in the Agulhas Retroflection region, *J. Geophys. Res., 95(C9), 15997–16015*, doi:10.1029/JC095iC09p15997

McCartney, M. S. (1977), Subantarctic Mode Water, in *A Voyage of Discovery: George Deacon 70th Anniversary Volume,* edited by M. V. Angel, pp. 103-119, Pergamon, Oxford, UK.

McCartney, M. S. (1982). The subtropical recirculation of Mode Waters. *J. Mar. Res., 40, 427–464.*

McCartney, M. S, and M. E. Woodgate-Jones, (1991). A deep-reaching anticyclonic eddy in the subtropical gyre of the eastern South Atlantic, *Deep-Sea Res., 38, S411-S443.*

McDonagh, E. L., K. J. Heywood, and M. P. Meredith (1999), On the structure, paths, and fluxes associated with Agulhas rings, *J. Geophys. Res., 104(C9), 21007-21020, doi:10.1029/1998JC900131.*

McWilliams, J.C. (2008), The nature and consequences of oceanic eddies. In: *Eddy-Resolving Ocean Modeling*, M. Hecht and H. Hasumi, eds., AGU Monograph, 5-15.

McWilliams, J.C. (2016). Submesoscale currents in the ocean. *Proc. R. Soc. Lond. A 472, 20160117,1–32.*

McWilliams, J.C., Molemaker, M.J. (2011), Baroclinic frontal arrest: a sequel to unstable frontogenesis. *J. Phys. Oceanogr. 41 (3), 601-619.* doi:10.1175/2010JPO4493.1.

Meunier, T., C. Ménesguen, R. Schopp, and S. Le Gentil (2015), Tracer Stirring around a Meddy: The Formation of Layering. *J. Phys. Oceanogr., 45, 407-423.*

Miller, P., (2004). Multi-spectral front maps for automatic detection of ocean colour features from SeaWiFS.*Int. J. Remote Sens., 25, 1437–1442.*

Mohrholz, V., M. Schmidt and J. R. E. Lutjeharms (2001). The hydrography and dynamics of the Angola-Benguela frontal zone and environment in April 1999. *JSouth Afr. j. mar. sc. 97: 199-208.*

Molemaker, M. J., J. C. McWilliams, and I. Yavneh (2005), Baroclinic instability and loss of balance, *J. Phys. Oceanogr., 35(9), 1505–1517,.*

Molemaker, M. J., J. C. McWilliams, and X. Capet (2010), Balanced and unbalanced routes to dissipation in an equilibrated Eady flow. *J. Fluid Mech., 654, 35 63,* doi:10.1017/S0022112009993272.

Molemaker M.J., Mcwilliams J.C., Dewar W.K. (2015), Submesoscale Instability and Generation of Mesoscale Anticyclones near a Separation of the California Undercurrent. *J Phys Oceanogr.* 45:613-629.

Nelson, G., (1989). Poleward motion in the Benguela area, In *Coastal and Estuarine Studies, Vol. 34, Poleward Flows along Eastern Ocean Boundaries, edited by Neshyba, S. J., C. N. K. Mooers, R. L. Smith, and R. T. Barber, pp. 110-130, Springer, New York.*

Okubo, A. (1970), Horizontal dispersion of floatable particles in the vicinity of velocity singularities such as convergences, *Deep Sea Res., 17, 445-454.*

Olson, D. B., Fine, R. A., and Gordon, A. L., (1992). Convective modifications of water masses in the Agulhas, *Deep-Sea Res., 39 (Supplement 1): s163–s181.*

Olson, D. B. and Evans, R. H. (1986). Rings of the Agulhas Current, *Deep-Sea Res., 33, 27–42.*

Ou, H. W., and W. P. M. de Ruijter (1986)eparation of an inertial boundary current from a curved coastline, *J. Phys. Oceanogr., 26, 2267-2279.*

Owens W.B., Wong A.P.S., (2009). An improved calibration method for the drift of the conductivity sensor on autonomous CTD profiling floats by theta-s climatology,*Deep-Sea Research Part I: Oceanographic Research Papers, 56(3), 450-457.*

Peeters, F. J. C., R. Acheson, G.-J. A. Brummer, W. P. M. de Ruijter, G. G. Ganssen, R. R. Schneider, E. Ufkes, and D. Kroon (2004), Vigorous exchange between Indian and Atlantic Ocean at the end of the last five glacial periods, *Nature, 400, 661 – 665.*

Pegliasco, C., A. Chaigneau, and R. Morrow, (2015), Main eddy vertical structures observed in the four major Eastern Boundary Upwelling Systems. *J. Geophys. Res. Oceans.* 120, doi:10.1002/2015JC010950.

Penven, P., Lutjeharms, J. R. E., Marchesiello, P., Weeks, S. J., and Roy, C. (2001). Generation of cyclonic eddies by the Agulhas Current in the lee of the Agulhas Bank, *Geophys. Res. Lett., 28, 1055–1058.*

Penven, P., V. Echevin, J. Pasapera, F. Colas, and J. Tam (2005), Average circulation, seasonal cycle, and mesoscale dynamics of the Peru Current System: A modeling approach, *J. Geophys. Res., 110, C10021*, doi:10.1029/2005JC002945.

Penven, P., Chang, N., Shillington, F. (2006), Modelling the Agulhas Current using SAfE (Southern African experiment). *Geophysical Research Abstracts 8 (04225).*

Penven, P., Debreu, L., Marchesiello, P., McWilliams, J.C., (2006c). Application of the ROMS embedding procedure for the central California upwelling system.*Ocean Model. 12, 157–187.*

Penven, P., Marchesiello, P., Debreu, L., Lefevre, J., (2008). Software tools for pre- and post-processing of oceanic regional simulations.*Environ. Model. Soft. 23, 660-662.* http://dx.doi.org/10.1016/j.envsoft.2007.07.004.

Penven, P., I. Halo, S. Pous, and L. Marie (2014), Cyclogeostrophic balance in the Mozambique Channel, *J. Geophys. Res. Oceans, 119*, doi:10.1002/2013JC009528.

Pichevin, T., Nof, D. and Lutjeharms, J. R. E. (1999). Why are there Agulhas rings? *Journal of Physical Oceanography*, 29, 693-707.

Peterson, R. G., and L. Stramma, (1991).Upper-level circulation in the South Atlantic ocean, *Prog. Oceanogr., 26, 1-73.*

Piola, A. R., and D. T. Georgi (1982), Circumpolar properties of Antarctic Intermediate Water and Subantarctic Mode Water,*Deep Sea Res., 29, 687–711, doi:10.1016/0198-0149(82)90002-4.*

Piola, A. R., and A. L. Gordon, (1989). Intermediate waters in the uthwest South Atlantic, *Deep-Sea Res., 36, 1-16.*

Rahmstorff, S., (1996).On the freshwater forcing and transport of the Atlantic thermohaline circulation. *Climate Dyn, 12,799-811.*

Ramachandran, S., A. Tandon, and A. Mahadevan, (2014). Enhancement in vertical fluxes at a front by mesoscale-submesoscale coupling. *J. Geophys. Res. Oceans, 119, 8495–8511*, doi:10.1002/2014JC010211.

Reason, C.J.C., R. J. Allan, and J. A. Lindsay,(1996a). Dynamical response of the oceanic circulation and temperature to interdecadal variability in the surface winds over the Indian Ocean, *J. Climate, 9, 97-114.*

Reason, C.J.C., R. J. Allan, and J. A. Lindsay,(1996b). Evidence for the influence of remote forcing on interdecadal variability in the southern Indian Ocean.*J. Geoph. Res. 101, 11867-11882.*

Reason, C. J. C. (2001), Evidence for the influence of the Agulhas Cur- rent on regional atmospheric circulation patterns, *J. Climate, 14,2769-2778, 2001.*

Richardson, P. L., (2007). Agulhas leakage into the Atlantic estimated with subsurface floats and surface drifters.*Deep-Sea Res. I, 54, 1361–1389, doi:10.1016/j.dsr.2007.04.010.*

Richardson, P. L., and S. L. Garzoli (2003), Characteristics of intermediate water flow in the Benguela Current as measured with RAFOS floats. *Deep Sea Res.* Part II, 50, 87–118, doi:10.1016/S0967-0645(02)00380-6.

Rimaud, J., S. Speich, B. Blanke, and N. Nicolas (2012), The exchange of Intermediate Water in the southeast Atlantic: Water mass transformations diagnosed from the Lagrangian analysis of a regional ocean model. *J. Geophys. Res.* 117, C08034, doi:10.1029/2012JC008059.

Rintoul, S. R. (1991), South Atlantic interbasin exchange, *J. Geophys. Res., 96, 2675–2692, doi:10.1029/90JC02422.*

Rio M.H. and F. Hernandez, (2004). A mean dynamic topography computed over the world ocean from altimetry, in situ measurements, and geoïd model. *J. Geophys. Res., 109, C12032*, doi: 10.1029/2003JC002226.

Robbins, P. E., J. F. Price, W. B. Owens, and W. J. Jenkins, (2000): The importance of lateral diffusion for the ventilation of the lower thermocline in the subtropical North Atlantic. *J. Phys. Oceanogr., 30, 67–89.*

Roberts, M., Marshall, D., (1998). Do we require adiabatic dissipation schemes in eddy-resolving ocean models?*J. Phys. Oceanogr. 28, 2050–2063.*

Rosso I., Hogg McC. A., Strutton P. G., Kiss A. E., Matear R., Klocker A., van Sebille E. (2014), Vertical transport in the ocean due to sub-mesoscale structures: Impacts in the Kerguelen region. *Ocean Modell.* http://dx.doi.org/10.1016/j.ocemod.2014.05.001.

Rouault, M., and J.R.E.Lutjeharms, (1994). Air-sea interaction in the marine atmosphere boundary layer: a new South African research venture, *S. Afr. J. Sci., 90, 11-12.*

Rouault, M. and Lutjeharms, J. R. E., (2000). Air-sea exchange over an Agulhas eddy at the Subtropical Convergence,*Global Atmos. Ocean Syst., 7, 125–150.*

Rouault, M., Lee-Thorp, A. M., and Lutjeharms, J. R. E., (2000) The atmospheric boundary layer above the Agulhas Current during alongcurrent winds, *J. Phys. Oceanogr., 30, 40–50.*

Rouault, M., White, S. A., Reason, C. J. C., Lutjeharms J. R. E., and Jobard, I., (2002). Ocean-atmosphere interaction in the Agulhas Current and a South African extreme weather event, *Weather Forecast.,17, 655–669.*

Rouault, M. and Lutjeharms, J. R. E., (2003). Estimation of sea-surface temperature around southern Africa from satellite-derived microwave observations, *S. Afr. J. Sci., 99, 489–494.*

Roullet G. and Klein P. (2010), Cyclone-Anticyclone Asymmetry in Geophysical Turbulence. *DOI: 10.1103/Phys. Rev. Lett.* 104, 218501.

Roullet, G., J. C. McWilliams, X. Capet, and M. J. Molemaker, (2012). Properties of steady geostrophic turbulence with isopycnal outcropping. *J. Phys. Oceanogr.,* 42, 18-38, doi:10.1175/JPO-D-11-09.1.

Roullet G., Capet X., Maze G. (2014), Global interior eddy available potential energy diagnosed from Argo floats. *J. Geophys. Res.* 1651-1656, 10.1002/2013GL059004.

Rubio, A.,Blanke B., Speich S., Grima N., Roy C. (2009), Mesoscale eddy activity in the southern Benguela upwelling system from satellite altimetry and model data. *Prog. Oceanogr.* , doi:10.1016/j.pocean.2009.07.029.

Ruddick, B. R. (1992), Intrusive mixing in a Mediterranean salt lens—intrusion slopes and dynamical mechanisms. *J. Phys. Oceanogr., 22, 1274 -1285.*

Ruddick, B. and K. Richards (2003), Oceanic thermohaline intrusions: observations. *Prog. Oceanogr., 56 (3- 4), 499 -527.*

Ruddick, B. R., Oakey, N. S. and Hebert, D. (2010), Measuring lateral heat flux across a thermohaline front: A model and observational test. *Journal of Marine Research, vol. 68, no. 3-4, pp. 523-539.*

Rusciano, E., S. Speich, and M. Ollitrault (2012), inter-ocean exchanges and the spreading of Antarctic Intermediate Water south of Africa. *J. Geophys. Res.* 117, C10010, doi:10.1029/2012JC008266.

Saetre, R., and J. Da Silva, (1984). The circulation of the Mozambique Channel, *Deep-Sea Res., 31, 485-508.*

Sarmiento, J. L., N. Gruber, M. A. Brzezinksi, and J. P. Dunne (2004). High latitude controls of thermocline nutrients and low latitude biological productivity, *Nature, 426, 56-60*, doi:10.1038/nature02127

Schmid, C., Siedler, G., Zenk, W., (2000). Dynamics of intermediate water circulation in the subtropical South Atlantic. *Journal of Physical Oceanography 30, 3191–3211.*

Schmid, C., O. Boebel, W. Zenk, J. R. E. Lutjeharms, S. L. Garzoli, P. L. Richardson, and C. Barron (2003), Early evolution of an Agulhas Ring, *Deep Sea Res. Part II, 50(1), 141 - 166.*

Schmid, C., and S. L. Garzoli (2009), New observations of the spreading and variability of the Antarctic Intermediate Water in the Atlantic, *J. Mar. Res., 67, 815-843*, doi:10.1357/002224009792006151.

Schmitt, R. W., (1994) Double diffusion in oceanography. *Annu. Rev. Fluid Mech., 26, 255–285.*

Schouten, M. W., de Ruijter, W. P. M., van Leeuwen, P. J., and Lutjeharms, J. R. E. (2000), Translation, decay and splitting of Agulhas rings in the south-eastern Atlantic ocean, *J. Geophys. Res., 105, 21 913-21 925.*

Schouten, M.W., De Ruijter, W.P.M., van Leeuwen, P.J., (2002). Upstream control of the Agulhas ring shedding.*Journal of Geophysical Research, 10.1029/2001JC000804.*

Shakespeare, C.J., Taylor, J.R., (2013). A generalised mathematical model of geostrophic adjustment and frontogenesis: uniform potential vorticity. *J. Fluid Mech. 736, 366–413.*

Shannon, L. V. (1979).The Cape Nimbus-7 CZCS programme: An overview and preliminary results, *S. Afr. J. Sci., 75, 564.*

Shannon, L. V., and D. Hunter, (1988). Notes on Antarctic Intermediate Water around Southern Africa, *S. Aft. J. Mar. Sci., 6, 107-117.*

Shannon, L. V., Lutjeharms, J. R. E., and Agenbag, J. J. (1989). Episodic input of Subantarctic water into the Benguela region, *S. Afr. J. Sci., 85, 317–332.*

Shannon, L. V., and G. Nelson (1996), The Benguela: Large scale features and processes and system variability, in *The South Atlantic Past and Present Circulation, edited by G. Wefer et al., pp. 163–210, Springer, New York.*

Shchepetkin, A.F. and J.C. McWilliams, (1998). Quasi-Monotone Advection Schemes Based on Explicit Locally Adaptive Dissipation.*Mon. Wea. Rev., 126, 1541-1580.*

Shchepetkin, A. F., and J. C. McWilliams (2003), A method for computing horizontal pressure-gradient force in an oceanic model with a nonaligned vertical coordinate. *J. Geophys. Res.* 108(C3), 3090, doi:10.1029/ 2001JC001047.

Shchepetkin, A. F., and J. C. McWilliams (2005), The regional oceanic modeling system (ROMS): A split-explicit, free-surface, topography-following-coordinate oceanic model. *Ocean Modell.* 9, 304 347, doi:10.1016/j.ocemod.2004.08.002.

Shchepetkin, A. F., and J. C. McWilliams (2009), Correction and commentary for "Ocean forecasting in terrain-following coordinates: Formulation and skill assessment of the regional ocean modeling system" by Haidvogel et al., *J. Comput. Phys., 227, 3595-3624.*

Shriver, J. F., and H. E. Hurlbutt, (1997). The contribution of the global thermohaline circulation to the Pacific to Indian Ocean throughflow via Indonesia. *J. Geophys. Res., 102, 5491-5511.*

Siedler, G., Muller, T.J., Onken, R., Arhan, M., Mercier, H., King, B.A., Saunders, P.M., (1996). The zonal WOCE sections in the South Atlantic. In: Wefer, G., Berger, W.H., Siedler, G., Webb, D.J. (Eds.), *The South Atlantic. Springer, Berlin-Heidelberg, pp. 83–104.*

Sloyan, B. M., and S. R. Rintoul (2001), Circulation, renewal and modification of Antarctic Mode and Intermediate Water, *J. Phys. Oceanogr., 31, 1005-1030.*

Smith, K. S. and E. Bernard, (2013), Geostrophic turbulence near rapid changes in stratification. *Physics of Fluid 25, 046601.* doi: http://dx.doi.org/10.1063/1.4799470

Smith, K.S. and R. Ferrari, (2009). The Production and Dissipation of Compensated Thermohaline Variance by Mesoscale Stirring. *J. Phys. Oceanogr., 39, 2477-2501*, https://doi.org/10.1175/2009JPO4103.1

Smith, W., and D. Sandwell (1997). Global sea floor topography from satellite altimetry and ship depth soundings. *Science* 277 (5334), 19561962, doi:10.1126/science.277.5334.1956.

Song, Y. and D. B. Haidvogel (1994), A semi-implicit ocean circulation model using a generalized topography-following coordinate system. *J. Comp. Phys., 115(1), 228-244.*

Soufflet Y., Marchesiello P., Lemarie F., Jouanno J., Capet X., Debreu L., Benshila R. (2016), On effective resolution in ocean models. *Ocean Modell.* 98 (2016) 36-50.

Souza, J. M. A. C., C. de Boyer Montegut, and P. Y. Le Traon (2011), Comparison between three implementations of automatic identification algorithms for the quantification and characterization of mesoscale eddies in the South Atlantic Ocean, *Ocean Sci. Discuss., 8(2), 483-531, doi:10.5194/osd-8–483-2011.*

Spall, M. A. (1995), Frontogenesis, subduction, and cross-front exchange at upper ocean fronts, *J. Geophys. Res., 100(C2), 2543-2557, doi:10.1029/94JC02860.*

Speich, S., B. Blanke, and G. Madec, (2001). Warm and cold water routes of an OGCM thermohaline conveyor belt. *Geophys. Res. Lett., 28, 311–314*, doi:10.1029/2000GL011748.

Speich, S., Lutjeharms, J.R.E., Penven, P., Blanke, B. (2006), Role of bathymetry in Agulhas Current configuration and behaviour. *Geophysical Research Letters.* 33, L23611. doi:10.1029/2006GL027157.

Speich, S. and M. Arhan, (2007). ARGO floats sample vertically homogeneized in Agulhas Rings, *Coriolis Newsletter, 4, 15-16.*

Speich, S., B. Blanke, and W. Cai (2007), Atlantic Meridional Overturning and the Southern Hemisphere Supergyre. *Geophys. Res. Lett.* 34, L23614, doi:10.1029/2007GL031583.

Speich, S., M. Arhan, E. Rusciano, V. Faure, M. Ollitrault, A. Prigent, and S. Swart (2012), Use of ARGO floats to study the ocean dynamics south of Africa: What we have learned from the GoodHope project and what we plan within the SAMOC International Programme, *Joint Coriolis Mercator Ocean Q. Newsl., 45, 21–27.*

Stommel, H., (1979). Determination of water mass properties pumped down from the Ekman layer to the geostrophic flow below. *Proc. Natl. Acad. Sci. U.S.A., 76, 3051–3055.*

Stone, P.H. (1966), On non-geostrophic baroclinic stability. *J. Atmos. Sci. 23 (4), 390-400.*

Stramma, L. and Lutjeharms, J. R. E., (1997). The flow field of the sub-tropical gyre of the South Indian Ocean, *J. Geophys. Res., 102, 5513–5530.*

Stramma, L. and England, M., (1999). On the water masses and mean circulation of the South Atlantic Ocean. *Journal of Geophysical Research 104, 20863–20883.*

Stramma, L., and R. G. Peterson, (1989) Geostrophic transport in the Benguela Current region, *J. Phys.Oceanogr.,19, 1440-1448.*

Sutyrin, G., S. Herbette, and X. Carton (2011), Deformation and splitting of baroclinic eddies encountering a tall seamount, *Geophys. Astrophys. Fluid Dyn., 105(4–5), 478–505*, doi:10.1080/03091929.2011.566566.

Talley, L. D. (1996), Antarctic Intermediate Water in the South Atlantic. *in The South Atlantic: Present and Past Circulation, edited by G. Wefer et al.* pp. 219-238, Springer, Berlin, doi:10.1007/978-3-642-80353-6-11.

Taylor, J. R., and R. Ferrari (2009), On the equilibration of a symmetrically unstable front via a secondary shear instability,*J. Fluid Mech., 622, 103*, doi:10.1017/S0022112008005272.

Taylor, J. R., and R. Ferrari (2010), Buoyancy and wind-driven convection at mixed layer density fronts, *J. Phys. Oceanogr., 40, 1222–1242.*

Thomas, L.N., (2005), Destruction of potential vorticity by winds. *J. Phys. Oceanogr. 35 (12), 2457-2466.*

Thomas LN, Tandon A, Mahadevan A. (2008). Submesoscale processes and dynamics. In Ocean Modeling in an Eddying Regime, *ed. MW Hecht, H Hasumi, pp. 17–38. Geophys. Monogr. Vol. 177. Washington, DC: Am. Geophys. Union.*

Thomas, L., Ferrari, R., (2008), Friction, frontogenesis, and the stratification of the surface mixed layer. *J. Phys. Oceanogr. 38 (11), 2501-2518. doi:10.1175/2008JPO3797.1.*

Thomas, L.N., Taylor, J.R., Ferrari, R., Joyce, T.M., (2013), Symmetric instability in the gulf stream. *Deep Sea Res. Part II: Top. Stud. Oceanogr. 91, 96-110.* doi:10.1016/j.dsr2.2013.02.025.

Thomas, L.N., J.R. Taylor, E.A. D'Asaro, C.M. Lee, J.M. Klymak, and A. Shcherbina (2016), Symmetric Instability, Inertial Oscillations, and Turbulence at the Gulf Stream Front. *J. Phys. Oceanogr., 46, 197-217.* https://doi.org/10.1175/JPO-D-15-0008.1

Thompson, S. R., D. P. Stevens, and K. Doos, (1997). The importance of inter-ocean exchange south of Africa in a numerical model, *J. of Geophys. Res., 102 (C2), 3303-3315.*

Treguier, A.-M., Boebel, O., Barnier, B., Madec, G. (2003), Agulhas eddy fluxes in a 1/6° Atlantic model. *Deep Sea Res. II, this issue (PII:S0967-0645(02)00396-X).*

Ullman, D. S., and P. C. Cornillon, (2000). Evaluation of front detection methods for satellite-derived SST data using in situ observations. *J. Atmos. Oceanic Technol., 17, 1667–1675.*

Ullman, D. S., and Z. Shan, (2007) On the characteristics of subtropical fronts in the North Atlantic. *J. Geophys. Res., 112, C01010,* doi:10.1029/2006JC003601.

Valentine, H. R., J. R. E. Lutjeharms, and G. B. Brundrit, (1993). The water masses and volumetry of the southern Agulhas Current region, *Deep-Sea Res., 40, 1285-1305.*

Van Aken H. M., A.K. van Veldhoven, C. Veth, W.P.M. de Ruijter, P.J. van Leeuwen, S.S. Drijfhout, C.P. Whittle, M. Rouault (2003), Observations of a young Agulhas ring, Astrid, during MARE in March 2000, *Deep Sea Research Part II: Volume 50, Issue 1, p. 167-195, ISSN 0967-0645.* http://dx.doi.org/10.1016/S0967-0645(02)00383-1.

Van Ballegooyen, R. C., Grundlingh, M. L., and Lutjeharms, J. R. E., (1994). Eddy fluxes of heat and salt from the southwest Indian Ocean into the southeast Atlantic Ocean: a case study,*J. Geophys. Res., 99, 14 053–14 070.*

Van Leeuwen, P. J. and de Ruijter, W. P. M. (2000). Natal Pulses and the formation of Agulhas Rings. *Journal of Geophysical Research, 105 (C3), 6425-6436.*

Veitch, J., Penven P., Shillington F. (2009), The Benguela: A laboratory for comparative modeling studies. *Prog. Oceanogr., doi:10.1016/ j.pocean.2009.07.008.*

Walker, N. D. and Mey, R. D. (1988). Ocean/atmosphere heat fluxes within the Agulhas Retroflection region, *J. Geophys. Res., 93, 15 473-15 483.*

Warner, M. J., and R. F. Weiss, (1992).Chlorofluormethanes in South Atlantic Antarctic Intermediate Water. *Deep-Sea Res., 39, 2053-2075.*

Wakker, K.F., R.C.A. Zandbergen, M.C. Naeije, and B.A.C. Ambrosius, (1990). GEOSAT altimeter data analysis for the oceans around South Africa, *J. Geophys. Res., 95, 2991-3006.*

Weijer, W., W.P.M. de Ruijter, H.A. Dijkstra and P.J.van Leeuwen (1999), Impact of interbasin exchange on the Atlantic overturning circulation. *J. Phys. Oceanogr.* 29,2266-2284.

Weijer, W., de Ruijter, W. P. M., Sterl, A., and Drijfhout, S. S., (2003). Response of the Atlantic overturning circulation to South Atlantic sources of buoyancy, *Global Planet. Change, 34, 293–311.*

Weijer, W., V. Zharkov, D. Nof, H. A. Dijkstra, W. P. M. de Ruijter, A. Terwisscha van Scheltinga, and F. Wubs (2013), Agulhas ring formation as a barotropic instability of the retroflection, *Geophys. Res. Lett., 40, 5435-5438,* doi:10.1002/2013GL057751.

Weiss, J. (1991), The dynamics of enstrophy transfer in two-dimensional hydrodynamics, *Physica D, 48(2-3), 273-294, doi:10.1016/0167-2789(91)90088-Q.*

Wells, N. C., V. O. Ivchenko, and S. E. Best (2000), Instabilities in the Agulhas Retroflection Current system: A comparative model study, *J. Geophys. Res., 105(C2), 3233-3241.*

Whittle, C., Lutjeharms, J.R.E., Duncombe Rae, C.M., and Shillington, F.A.. (2008). Interaction of Agulhas filaments with mesoscale turbulence: a case study. *South African Journal of Science, 104(3-4), 135-139.*

Yi, J., Y. Du, Z. He, and C. Zhou (2014), Enhancing the accuracy of automatic eddy detection and the capability of recognizing the multicore structures from maps of sea level anomaly, *Ocean Sci, 10(1), 39–48,* doi:10.5194/os-10-39-2014.

You, Y. , (1998). Rain-formed barrier layer of the western equatorial Pacific warm pool: A case study, *Journal of Geophysical Research, 103(C3), 5361-5378.*

You, Y., (2002). Quantitative estimate of Antarctic Intermediate Water contributions from the Drake Passage and the southwest Indian Ocean to the South Atlantic, *Journal of Geophysical Research, 107(C4), 10.1029/2001JC000880.*

You, Y., Lutjeharms, J., Boebel, O., de Ruijter, W.P.M. (2003), Quantification of the inter-ocean exchange of intermediate water masses around southern Africa. *Deep Sea Res. II, this issue (PII:S0967-0645(02)00384-3.*

Zhang, Z., Y. Zhang, and W. Wang (2017), Three-compartment structure of subsurface-intensified mesoscale eddies in the ocean, *J. Geophys. Res. Oceans, 122, 1653–1664,* doi:10.1002/2016JC012376.

Dynamiques océaniques à petite échelle dans le Bassin du Cap et leur impact sur la circulation régionale

RESUMÉ

Nous étudions le rôle des processus océaniques à petite échelle dans la formation et transformation des eaux de surface et intermédiaires qui participent à l'échange Indo- Atlantique à travers le Bassin du Cap. La dynamique de cette région est caractérisée par une forte turbulence et nous montrons l'impact que les structures de méso- ou de sous-méso- échelle, leur interactions dynamiques et leur variabilité saisonnière ont sur les eaux locales de la thermocline. Une série des simulations numériques, allant de 'eddypermitting' a 'submesoscale resolving', souligne l'importance d'une résolution verticale adéquate pour bien représenter les propriétés des masses d'eau.

Les tourbillons de Aiguilles sont principalement générés par des instabilités baroclines, et sont caractérisés par une saisonnalité, liée aux différentes instabilités dans les couches supérieures. En été, les instabilités symétriques sont plutôt en jeu, tandis qu'en hiver les instabilités de la couche de mélange prédominent. L'instabilité barocline de Charney connecte ces deux régimes de la sous-méso-échelle et joue un rôle majeur dans la formation saisonnière d'un nouveau type d'eaux modales : l'Agulhas Rings Mode Water.

Enfin, on montre que tant les cyclones que les anticyclones transportent et mélangent l'Antarctic Intermediate Water, l'étirement de la méso-échelle produisant des filaments et structures thermohalines très fines.

Nos résultats suggèrent l'existence des deux régimes dynamiques qui affectent les couches supérieures et intermédiaires du Bassin du Cap. Près de la surface, la frontogenèse et une énergique sous-méso-échelle conduisent à un régime agéostrophique. Les profondeurs intermédiaires sont caractérisées par un régime quasi-géostrophique due à l'action prédominante de la méso-échelle.

Mots clés : processus de méso- et sous-méso- échelle, échange Indo-Atlantique, dynamiques des masses d'eau.

Small-scale ocean dynamics in the Cape Basin and its impact on the regional circulation

ABSTRACT

This study addresses the role of oceanic small-scale processes in the formation and transformation of subsurface waters that participate in the Indo-Atlantic interocean exchange.

We focus on the Cape Basin dynamics, characterized by a highly non-linear turbulence.

We provide qualitative and quantitative evidence of the direct impact that meso- and submesoscale structures, their dynamical interactions and their seasonal variability have on the local thermocline and intermediate waters. A sequence of numerical simulations, ranging from 'eddy-permitting' to 'submesoscale resolving', underlines the importance of an adequate vertical resolution to correctly depict the water masses properties.

We point out that Agulhas eddies are mainly generated through baroclinic instabilities and are marked by a clear seasonality. This is linked to the seasonal occurrence of distinct meso-submesoscale instabilities in the upper layers: symmetric instabilities are at play during summer, while mixed-layer instabilities prevail in winter. We also found that Charney baroclinic instability connects these two submesoscale regimes and plays a major role in the seasonal formation of a newly-identified type of mode waters: Agulhas Rings Mode Water. Finally, we show that eddies of both polarity advect, stir and mix Antarctic Intermediate Water, via the mesoscale strain field producing filaments and T-S fine-scale structures.

Our results suggest the existence of two dynamical regimes affecting the upper and intermediate layers of the Cape Basin. Near the surface, the submesoscale-driven frontogenesis and their enhanced energetics lead to a predominance of ageostrophic dynamics. The intermediate depths are, instead, characterised by a quasi-gesotrophic regime due to the prevailing mesoscale effects.

Keywords : meso- and submesoscale processes, Indo-Atlantic exchange, water masses dynamics.